E-577

LARGE MOMENTUM TRANSFER ANTIPROTON-PROTON AND PROTON-PROTON ELASTIC SCATTERING AT 100 AND 200 GeV/c

A Thesis

Presented to the Faculty of the Graduate School

of Cornell University

in Partial Fulfillment of the Requirements for the Degree of

Doctor of Philosophy

by

David Howard Kaplan

August 1983

AAB1875

Biographical Sketch

The author [redacted] and attended Greenwich Village's New York University where he majored in physics, received the B.A. degree summa cum laude in 1973, and became a member of Phi Beta Kappa and Blue Key National Honor Fraternity. He also holds an M.S. degree in theoretical physics from Cornell University.

He had a very enjoyable time being a teaching assistant in the Cornell University Physics Department, and in this regard he thanks especially Cornell Professor R. O. Pohl. He also held appointment as a research assistant through Cornell's Newman Laboratory of Nuclear Studies while at Fermilab. In 1982 he joined the faculty at Colgate University.

Acknowledgements

It is always a pleasure to thank those from whom one has learned or from whom help and encouragement have been received. Accordingly, I express my deep appreciation to:

Professor Jay Orear, my thesis advisor, for making it possible for me to continue at Cornell by allowing me to work on the experiment reported on in this thesis, for encouragement at some crucial points, for arranging for my financial support while I was at Fermilab, for advice about this thesis and for letting me use his neat computer to make the histograms;

Professor John Kogut, teacher and friend, for his constant encouragement, time, support, defense and open-mindedness, for generally being a nice guy and a "mensch", for a ride on the truck, for a trip to the Truck and Warehouse Theater and Divine, for pointin' out de shoe shiner guy and for being on "our side"; Hi, fella!;

Dr. Paul Karchin, the author's fellow graduate student, for many valuable discussions about physics and other things and for leading the way;

Keith Krueger and Sean McHugh, the author's other fellow graduate students, for many useful discussions and for their parts in the work reported here;

Professors David Cassel and Peter Lepage for serving on my special committee;

Mrs. Velma Ray, without whose incredible speed in turning a handwritten pile of pages into final typed form this thesis would have been

considerably delayed, for her sense of humor and perspective;
The Draftspeople--Tom Madison, Don Miller, Gretchen Doolittle, and Barbara Lang--for doing an admirable job on such short notice;
Professor Robert O. Pohl, for whom it was a pleasure to work in Physics 218, for giving me both encouragement and freedom of presentation;
Professor Hans Bethe, for early encouragement that I will always remember;
Joan, for listening to politics "with a cast of thousands".

This thesis reports results of an experiment done in collaboration at Fermilab; the names of the collaborators are listed in reference 101.

Table of Contents

Table of Contents (continued)

ued)

Page

196
196
196
196
196
200
201
201
201
201
205
207
207
207
208
209
210
210
214
217
217
218
218
219
220
221
221
221
223
223
226

the Target

List of Tables

Page

134

150

153

ıys

172

227

228

230

235

238

241

244

246

248

250

List of Figures

List of Figures (continued)

List of Figures (continued)

List of Figures (continued)

Page

251

253

255

256

258

I. PREVIOUS DATA AND THOUGHTS ABOUT ELASTIC SCATTERING

A. Notation, Metric and Some General Definitions

Any two body scattering reaction can be written symbolically as

$$a + b \rightarrow c + d$$

where the letters denote particle species. In this thesis we report certain differential cross sections for the elastic scattering reactions

$$pp \rightarrow pp$$

and

$$\bar{p}p \rightarrow \bar{p}p \ .$$

"p" will denote either a proton or a four momentum; the context will always be clear. Three momenta will be written as, e.g., $\vec{p}$. "$\bar{p}$" will always denote an antiproton. Some further definitions:

$p_{cm}, \vec{p}_{cm}$ ≡ the center of mass four, three momentum of a particle,

p_{lab} ≡ the magnitude of the three momentum of incident particle "a" in the laboratory frame,

m ≡ the proton (or antiproton) mass,

θ_f, θ_{lab} ≡ the laboratory scattering angle of outgoing particle "c" with respect to the incident direction of "a",

θ_{cm} ≡ the center of mass scattering angle,

$p_{a,b,c,d}$ ≡ four momentum of a, b, c or d,

$q \equiv p_c - p_a$,

$s \equiv (p_a + p_b)^2$,

$t \equiv -q^2$.

Definition of metric: $p^2 = m^2$.

We will generally set $\hbar = c = 1$.

B. Previous Data and a Bit of Phenomenology

1. The pp Situation Before the I.S.R. and Fermilab

a. Data

Long ago, low (by today's standards) energy elastic cross sections were plotted as a function of $\cos\theta_{lab}$. The first observations for pp elastic scattering were: a) the general existence of a spectacular forward peak, and b) a generally increasing concentration of cross section in the forward direction. In particular, $\frac{d\sigma}{d\Omega}(0^\circ)$ went approximately like p_{lab}^2.

Probably around 1965 someone noticed that things would be much neater if differential cross sections were plotted against the Lorentz scalar t.

$$t \equiv (p_a - p_c)^2 = -2p_{cm}^2(1 - \cos\theta_{cm})$$
$$\approx -p_{lab}^2\theta_{lab}^2 \quad \text{at high energy and small } \theta_{lab}.$$

In Figure I-1 we show the elastic p-p situation as it was around 1970. The following observations were made:

(i) The value of $\frac{d\sigma}{dt}$ at $t \approx 0$ is approximately independent of the incident momentum (since $-t \sim p_{lab}^2$ at fixed $\theta_f \to 0$).

(ii) For fixed t the cross section decreases until it appeared to "stabilize" at high energy where, at least crudely, $\frac{d\sigma}{dt}$ depended on -t alone.

(iii) However, the approach to stabilization was not uniform. For "low" $|t|$, $\frac{d\sigma}{dt}$ depending on only -t was achieved by $p_{lab} \sim 10$ GeV/c. At higher -t, apparently higher incident energy was needed for this.

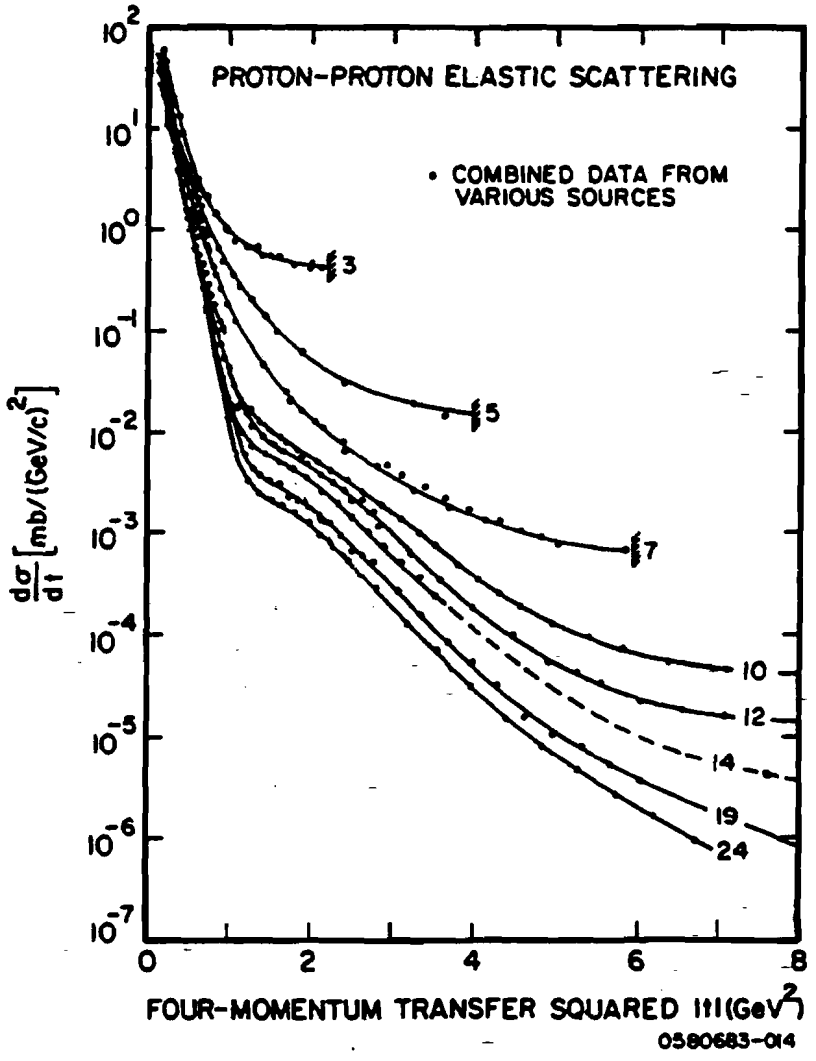

Figure I-1. The proton-proton elastic scattering situation around 1970 (figure adapted from ref. 11).

(iv) For "low" $|t|$, i.e., $0 \leq t \leq 0.5$ $(GeV/c)^2$,

$$\frac{d\sigma}{dt} = Ae^{-b|t|}$$

was a pretty good fit covering about four decades of drop!

It was noticed that for pp scattering b was increasing slowly with s. To set the scale we note that it was later found that at

$p_{lab} = 200$ GeV/c $b \approx 10$ $(GeV/c)^{-2}$ for pp, 11 for $\bar{p}p$,

8 for $\pi^{\pm}p$, $K^{-}p$ and about 7 but increasing rapidly for $K^{+}p$.

At the highest momenta available around 1970 there were signs of a developing "shoulder" at $-t \sim 1$ $(GeV/c)^2$ but otherwise the cross sections seemed very smooth. However, from another point of view, J. Orear noticed in 1964[1] that the p-p elastic scattering data were fit well by the empirical formula

$$\frac{d\sigma}{d\Omega} = Ae^{-p_\perp/p_o}$$

where $p_\perp = p_{cm}\sin\theta_{cm}$, and p_o and A were fitted constants. At that time no theoretical reason was known for the appearance of $p_\perp$ in the fit.

In Figure I-2 we show some low energy $\bar{p}p$ data.

b. Early Thoughts on This Data

(i) Simple Optical Models

(α) Motivation and Black Disc Model

The early p-p data, especially the low -t elastic data, reminds one very much of optical diffraction. Some of the reasons for this are the existence of the elastic forward peaks, the general approximate energy independence (especially in the forward peaks) of elastic scattering, the fact that the $t \to 0$ differential elastic cross sections are almost completely imaginary (absorptive), and the (historical) early

observation that the p-p <u>total</u> cross section seemed to be asymptotically independent of energy. Indeed, one "expects" that elastic scattering <u>should</u> be diffractive--$\lambda \approx 0.2$ fermi/p_{lab} for the incident particle so $p_{lab} > 1$ GeV/c implies $\lambda < R$ (R = proton radius). Simple diffraction models have also had much success in nuclear physics.[2] So one imagines, then, a simple model in which the De Broglie waves of the incident projectile strike a stationary target particle (in the lab frame) and are partially diffracted and partially absorbed. The absorption then represents scattering into inelastic channels. The diffraction represents elastic scattering (i.e., elastic scattering is the "shadow" of absorption). These very simple ideas form the basis of the optical model. If the target is considered as a completely "opaque" obstacle of radius R the simple model is called the "black disc" model. In the black disc model one would have

$$\frac{d\sigma}{dt} = \pi R^4 \frac{J_1\sqrt{-tR^2}}{tR^2} ,$$

$$\frac{d\sigma}{dt}(t=0) = \frac{\pi R_o^4}{4} , \quad \text{and}$$

$$\sigma_{el} \equiv \int \frac{d\sigma_{el}}{d\Omega} d \approx \pi R^2$$

$$\frac{\sigma_{el}}{\sigma_{tot}} = \frac{1}{2}$$

Note that these formulae imply the existence of zeros in $\frac{d\sigma}{dt}$ (familiar, of course, from optics). Using $R \approx 1$ fm, it is found that the first zero should be near $-t \approx 0.6$ (GeV/c)^2. Thus, an obvious problem with the model is that there is no zero (or even dip) in $\bar{p}$-p elastic scattering near this value of -t (at least as of 1982).

However, the reader can see from Figure I-2 that there is a dip in 5 GeV/c $\bar{p}p$ elastic scattering somewhat near there. As the energy is raised from 5 to 30 GeV/c it seems to go away. Thinking about this, we note that the $\bar{p}p$ total cross section is very high at 5 GeV/c compared to the pp total cross section. A large inelastic cross section means high absorption--i.e., great "blackness". As the energy increases from 5 GeV/c the total $\bar{p}p$ cross section falls. We could suggest, then, that the 5 GeV/c $\bar{p}p$ dip is a "black-disc dip" which washes out with increasing energy because of the fall of σ_{tot}. Since $\sigma_{tot}(pp)$ is so small at low energy, in this simple model we "expect" no pp dip at low energy. We could suggest this, but we are not sure if we'd be taken seriously!

The black disk model has problems besides the absence of a $-t \approx 0.8$ GeV/c pp dip anyway--no exponential behavior at low $|t|$ (in a wide enough range), etc. These problems are well known.

(β) Grey Disc Model[2]

One obvious way to modify the black disc model is to model the proton as a grey disc. "In the lab frame" one imagines de Broglie waves incident on a disc (or sphere) whose (integrated along beam direction) absorption "Γ" is a function of impact parameter b. That's like shining light through a smudgy microscope slide or something. Then taking a well-known result straight from optics one has

$$f(q^2) = \frac{ik}{2\pi}\int d^2b\, e^{i\vec{q}\cdot\vec{b}}\Gamma(b)$$

$$\equiv ik\,\langle\Gamma(b)\rangle$$

where $f(q^2)$ is the scattering amplitude and $\langle\ \rangle$ means "Fourier transform".

It's easy to get rid of the dip and reproduce an exponential behavior

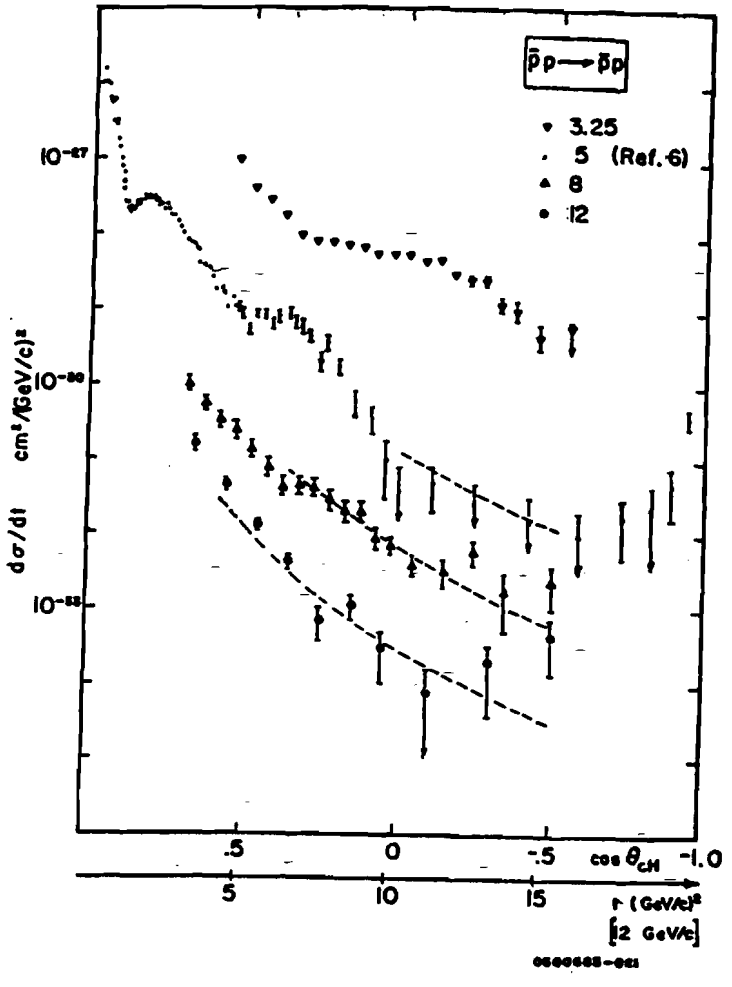

Figure I-2. The low energy $\bar{p}p$ elastic scattering situation (figure adapted from ref. 18).

for the cross section--just take

$$\Gamma(b) = \Gamma(0)e^{-(b/b_o)^2}$$

then since the transform of a Gaussian in b is a Gaussian in q, and since $-t \equiv q^2$, one has

$$\frac{d\sigma}{dt} \propto \Gamma^2(0)b_o^4\, e^{-b_o|t|/2}$$

Comparing this to the parametrization of the data $\frac{d\sigma}{d\Omega} = A\,e^{-Bt}$ one finds

$$b_o = \sqrt{2B}\ .$$

Then $B \approx 10\ (\text{GeV/c})^{-2}$ gives $b_o \approx 0.9$ fm. For purposes of comparison we note that the electromagnetic radius of the proton (from e-p scattering) is about 0.8 fm r.m.s. But at large -t, especially at higher energy, this method has problems. Also, one does not see where "shrinkage" comes in.

(γ) Simple Regge Pole Model[3]

The basic Regge pole model also dates from about twenty years ago. Its natural domain of application is large s, low $|t|$. The basic prediction is

$$\frac{d\sigma}{dt}(\text{elastic}) = D_1(t)\left(\frac{s}{s_o}\right)^{2\alpha_1(t)-2},$$

where D is a function of t only. Use of the optical theorem and the assumption of a constant total cross section implies $\alpha_1(0) = 1$. The resulting exchange trajectory, having the quantum numbers of the vacuum, is commonly known as the "Pomeron". If the trajectory is linear at large s, low $|t|$, i.e., if

$$\alpha_p(t) = 1 + at\ ,$$

one has

$$\frac{d\sigma}{dt}(\text{elastic}) = \left(\frac{d\sigma}{dt}\right)_{t=0} \exp[2b \log(\frac{s}{s_0})]t \ .$$

Thus the exponential behavior of the cross section is duplicated and shrinkage is predicted. But there are problems--especially at high -t. One possible problem is the prediction that asymptotically the total cross section should be constant and that σ_{el} should approach zero logarithmically with s. [Experimentally σ_{el}/σ_{tot} seems to be holding constant at about 18% for $s \geq 100$ GeV^2.]

It is interesting to note[3] that the linearity of the Pomeron trajectory can be at least qualitatively accounted for in the "string model" of Quantum Chromodynamics (QCD). Much work has been done lately on deriving Regge theory from QCD, but it is not our purpose to discuss this in this thesis. We refer the reader to some very interesting papers by Alan White on this.[4,5]

(δ) s-Channel Versus t-Channel and the Purpose of this Chapter

At least superficially the Regge model is more in line with modern field theory ideas because it involves t-channel exchanges. The simple optical model begun above corresponds to an s channel ("annihilation") picture. Unfortunately, this seems to have led, in the late 1960s and 1970s, to two different camps of physicists. s-channel models which are generally simpler, developed most notably to the Chou-Yang mode, the Glauber expansion models, and powerful general techniques of "impact parameter analysis". Development of the t-channel idea led to Reggeon Field Theory (RFT). In general t-channel models give a better prediction of the s-dependence of elastic scattering and s-channel models give a better prediction of the t-dependence.

Nowadays we hope that the good features of both models can be derived from QCD. If this is so (and perhaps if it is not so) it is possible that "diffraction" could be an important testing ground for QCD. (Perhaps more work should be done on this.) We had originally intended, in this chapter, to survey some of the connections between the older s and t channel models and QCD. But time considerations stood in the way of this. However, the author wonders if these models, though phenomenological, could be at least useful guides in the techniques of forming the proper approximations fo QCD in the "diffractive" limit, especially since this is apparently not the regime of perturbation theory. (Indeed it has been noted that the problems of low |t| diffraction and confinement are probably closely related (since "low |t| scattering includes contribution from large impact parameter. "Dips" in the mid |t| range could be due to interference "between different limits of QCD." We shall remark more about this later.)

Years ago elastic scattering was considered important because it was considered "simple" and hence "fundamental". Now many feel that elastic scattering is complicated but not fundamental, and hence unimportant. Elastic scattering does indeed seem to be complicated, if not completely intractable, in perturbative QCD. Perhaps that is only because the proper theoretical techniques have not yet been realized.

Whether this is true or not remains to be seen. At any rate, in this chapter we will at least outline some of the successes and failures of some of the s-channel "optical" models. The t-channel models (especially RFT) are more complicated (at least in appearance), hence we shall not say very much about them.

(ε) Some Elementary Connections

A formal connection between the optical models and the t channel models has been made by series expansion. The reader is referred to the excellent articles by Amaldi et al.[6] and Zachariasen[7] for this. However, in a slightly different vein, an early conjecture, bridging the two points of view at least vaguely, was made by Wu and Yang (called the "Wu-Yang conjecture").[8] This was the conjecture that p-p elastic scattering might go like $F^4(q^2)$, where $F(q^2)$ is the proton (e.g., electric) form factor. For now we note that some well known elementary justification may be given for it by noting that in field theory (e.g., QCD), loosely, $F(q^2)$ is the amplitude for a proton to absorb (or give up) transverse momentum q^2. Then $[F(q^2)]^2$ is the amplitude for one proton to send off q^2 and another to absorb it. Forgetting, for the time being, propagators for exchanged particles, convergence problems, etc., etc., (i.e., short circuiting the t-channel) the scattering cross section is then F^4. It's actually not a bad fit to the data at low $|t|$. It will also form part of the basis for things to come in later pages.

One could even continue this very vague bridging of the s channel and t-channel models by assuming that the exchange "propagator" is, in fact, the pomeron, and then writing[9] "for first order" (i.e., low $|t|$),

$$\frac{d\sigma}{dt}(a+b\to a+b) \sim F_a^2(t)F_b^2(t)\ \exp[2\alpha_p' t\, \ell n\,(\tfrac{p}{p_o})]$$

In this sort of picture it has been argued[9] that, just as the $F_a^2F_b^2$ factor characterizes the dimensions of the colliding hadrons a and b, so does the "exp" term characterize the intrinsic dimensions of the (presumably valence) quarks inside the hadrons. [Indeed, in ref. 9, it is argued

that $r^2_{quark} \approx 3a'_p \approx 0.9$ GeV^{-2} from this!]

This, of course, is kind of artificial. In "purer" optical models one might replace the "exp" term with quark-quark scattering amplitudes that depend, e.g., on q^2 only, etc. (denoted by "$t_{qq}(q^2)$"). One could then fit quark-quark amplitudes with the low -t data and <u>then</u> use these <u>set</u> t_{qq}'s to predict the high -t data. (This is the general scheme in a class of "Glauber expansion" models). In the process one may be able to make meaningful statements about "the sizes of quarks", etc. We shall discuss these things later. For now we want to discuss more data that is relevant to understand where our experiment fits into the scheme of things. This will also put the development of the basic models in perspective.

2. <u>Higher Energy pp Data from CERN and Fermilab</u>

Throughout the 1970s elastic scattering was done at both the CERN I.S.R. (Intersecting Storage Rings) and at Fermilab. The low |t| data we will discuss later only insofar as it affects theories pertaining to the data reported in this thesis. The mid and high -t data we discuss now.

a. <u>Mid [1 ≤ -t ≤ 5 (GeV/c)^2] t Data</u>

The major discovery here was first made at CERN[10] with the I.S.R. around 1972 or so--the discovery of an apparent dip in the elastic $\frac{d\sigma}{dt}$ for p-p near -t = 1.4 (GeV/c)^2, for the four energies that were studied--$\sqrt{s}$ = 23.5, 30.7, 44.9 and 53 GeV. In Figure I-3 [11] we show some of this newer CERN data together with some of the older lower energy p-p data we've already referred to. Also in the figure, for comparison, is a plot of $G^4(t)$, where G(t) is the dipole formula for the proton form factor.

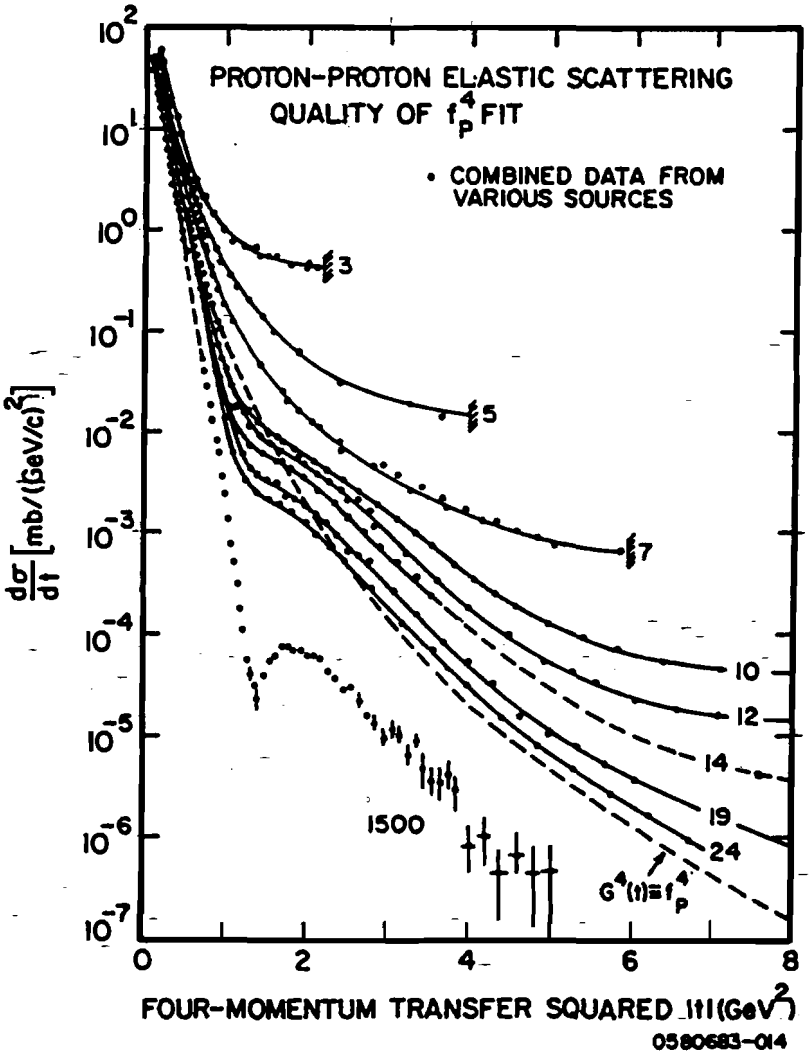

Figure I-3. Early CERN data at p_L = 1500 GeV/c together with older elastic scattering data. Also shown is $G^4(t)$ where G(t) is the dipole form factor formula for the proton. (Figure adapted from ref. 11.)

This discovery excited some interest at Fermilab where a study was soon undertaken by Akerlof and collaborators[12] to see if the dip would persist down in energy to p_{lab} = 200 and 100 GeV/c. Their results are shown in Figure I-4a --apparently there is a dip at 200 GeV/c and apparently there isn't one at 100 GeV/c. Thus it appeared that the onset of the dip occurred at any energy between these two values.

Later on an attempt was made at Fermilab to pin this down using an internal gas-jet target (by a Rochester-Imperial College-Fermilab collaboration[13]). The results of this are shown in Figure I-4b. From this "high resolution" (in -t) experiment we see evidence that there is no dip at 100 GeV/c and just a hint of one at 150 GeV/c.

Meanwhile (1974-78) the people at CERN made another[14], more precise investigation of $\frac{d\sigma}{dt}$ for pp at center-of-mass energies of about 23.5, 30.5, 44.6, 52.8 and 62.1 GeV using the "split field magnet" technique. The data from this is shown in Figure I-5. The following important features can be noted immediately:

(i) The position of the dip apparently moves "backward" toward decreasing-t as the energy is increased from $\sqrt{s}$ = 23.5 GeV to $\sqrt{s}$ = 62.1 GeV.

(ii) The deep seems to become shallower with increasing energy in this range.

(iii) There is a pronounced second maximum which also seems to move backward with energy.

We describe some of the results found by Nagy et al.[14] in a bit more detail as they will concern us:

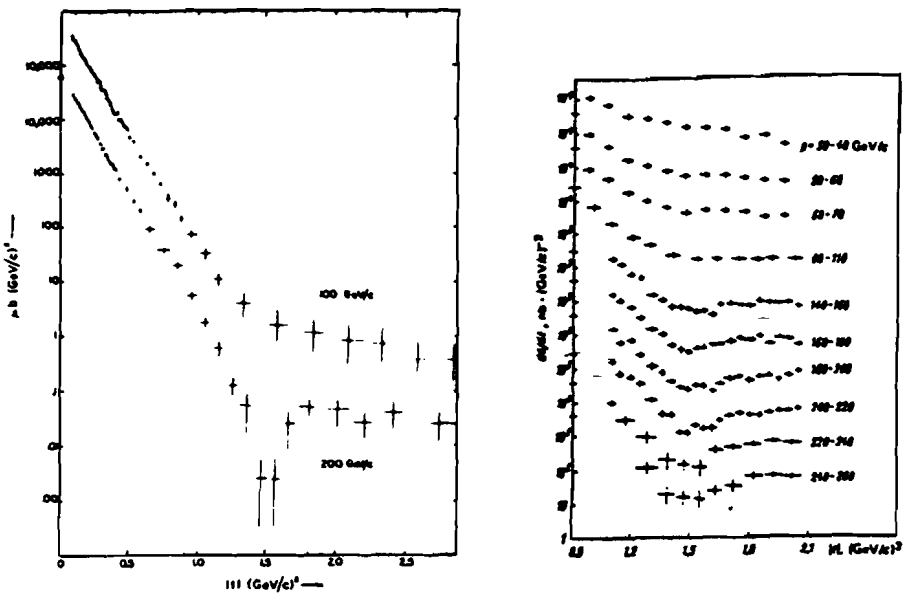

(a) (b)

Figure 1.4. (a) pp elastic scattering at 100 and 200 GeV/c (from ref. 12).

(b) pp elastic scattering at a variety of energies between 30 and 260 GeV/c (from ref. 13).

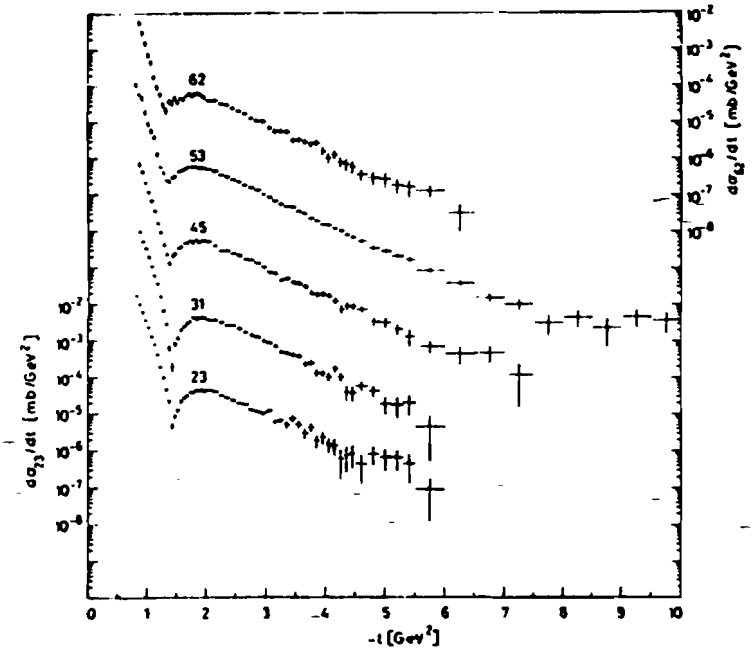

Figure I-5. Elastic scattering at the I.S.R. Numbers on data curves are center-of-mass energies. Curves are artificially displaced from each other by factors of ten for clarity. (Figure from ref. 14.)

(α) Following an earlier parameterization by Phillips and Barger[15] the cross section was parametrized by two (destructively) interfering amplitudes near the dip:

$$\frac{d\sigma}{dt} = A\left|e^{b(t-t_0)/2} + e^{d(t-t_0)/2 + i\phi}\right|^2$$

where the values of the five parameters depend on energy. The fit was found to be good in the region $1.05 \leq -t \leq 2.5$ GeV^2, thus demonstrating that five parameters seem to be enough to cover the t-dependence in this region. $\phi = \pi$ gives both amplitudes completely imaginary and a zero instead of a dip. For $\phi = \pi + \varepsilon$, $\frac{d\sigma}{dt}$ at the minimum is $\approx A\varepsilon^2$. (Real part fills in dip.)

The s dependence of $\frac{d\sigma}{dt}$ at the minimum is shown in Figure I-6a and seems to behave similarly to the s-dependence of $\rho^2\sigma_{tot}^2$, where ρ is the ratio of the real to imaginary part of the $t = 0$ scattering amplitude. This similarity will be seen to be of theoretical interest. It is of the type predicted by simple "geometrical scaling" ("G.S."). [From the figure note that the similarity improves when $\sqrt{s} \geq 30$ GeV. This provides early evidence for an apparent energy threshold for geometrical scaling. We shall discuss G.S. later.] It is seen in Figure I-6b that the position of the dip behaves about like σ_{tot}^{-1} with energy. This is also interesting and important. Position and height of the second max are s-dependent also. For details on that, see Nagy et al.[14]

(β) - Beyond the Second Max. At each energy in the range from $2.3 \leq -t \leq 5.1$ GeV/c the parametrization

$$\frac{d\sigma}{dt} = C\exp[-D(|t| - 3\ \text{GeV}^2)]$$

gave good results with C and D energy independent. "D" was about

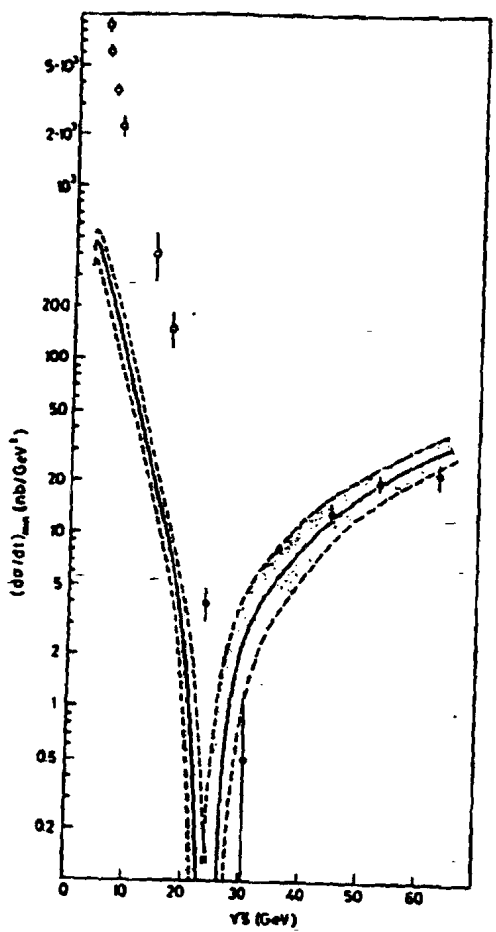

Figure I-6a. Energy dependence of the differential cross section at the minimum. The dashed band is proportional to $\rho^2\sigma_{tot}^2$ normalized to the data at $\sqrt{s}$ = 53 GeV. (From ref. 14.)

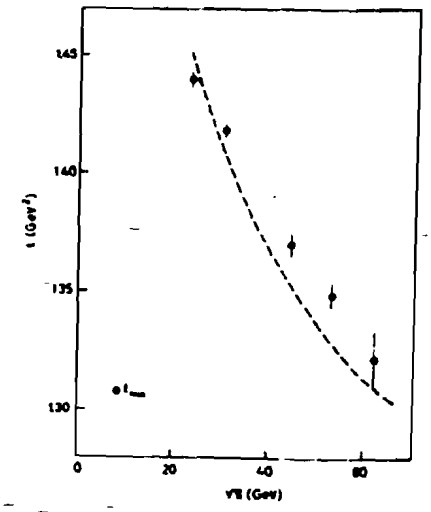

Figure I-6b. Energy dependence of the position of the minimum in the ISR energy range. (From ref. 14.)

1.8 $(GeV/c)^{-2}$.

(γ) - $-t \geq 5\ (GeV/c)^2$. Here the only CERN data was the $\sqrt{s} = 53$ GeV data. It appeared that there was a definite decrease in the exponential slope beyond $-t \approx 5\ (GeV/c)^2$.

b. Higher -t Data

An experimental study was undertaken at Fermilab in the late 1970s to measure pp elastic scattering in the higher -t range by a Cornell-Lebedev-McGill-Northeastern group[16,17] at 200 and 400 GeV/c. When the cross sections were plotted against -t smooth variations of exponential slope were found. (At 200 GeV/c for $5.0 \leq -t \leq 6.2$ exp. slope was about 1.5 (average), by the range $9 \leq -t \leq 12$ it dropped to about 0.9 $(GeV/c)^{-2}$. At 400 GeV similar results were found. However, in the t ranges of this experiment ($5 \leq -t \leq 12$) Orear and Hojvat found that they could get very good fits at both energies with the simple exponentials

$$\frac{d\sigma}{dt} = A e^{-bp_\perp}, \quad p_\perp \equiv p \sin\theta \approx \sqrt{-t}$$

with b values 6-7 $(GeV/c)^{-1}$ ("Orear fall-off"). (Thus perhaps $p_\perp$ is the natural variable.)

3. 50 GeV/c CERN $\bar{p}p$ Data

In the mid-summer of 1980 a CERN group first reported[18] observation of a dip near $-t = 1.4$ GeV/c for elastic $\bar{p}p$ scattering at 50 GeV/c. This 50 GeV/c $\bar{p}p$ data seemed very similar in the details to the $\sqrt{s} \approx 45$ GeV pp data of Nagy et al. (It should be noted that $\sigma_{tot}(pp)$ at $\sqrt{s} \approx 45$ GeV is not too different from $\sigma_{tot}(\bar{p}p)$ at 50 GeV/c.)

C. Development of the Phenomenology and Theory

1. Comment About t-Channel Models (following Nagy et al.[14])

Since the p-p dip position is energy dependent the simple model with the exchange of a single Regge pole (e.g., Pomeron) is ruled out (since the residue function only depends on t in the model). The trial superposition of two Regge poles for the elastic amplitude by Nagy et al. failed with linear trajectories (again due to poor fit of s-dependence of dip position). A superposition of three poles worked well but needed 8 parameters.

Collins and Gault[19] have proposed a model with a single pomeron pole and a two pomeron cut which agrees excellently with the $\sqrt{s}$ = 53 GeV data; however, there are theoretical problems as the Froissart bound is is violated. Attempts to fix this seem to lead either to disagreement with the data or to RFT. But, as we have already remarked, RFT is very complicated and we do not wish to discuss it.

2. The Model of Chou and Yang[20]

a. Formulation of the Basic Model and Comparison to Data

(i) Formulation

One of the problems with the simple grey disc optical model lies in the ambiguity in the choice of the absorption function $\Gamma(b)$. The Chou-Yang model removes much of this amgibuity while at the same time keeping the spirit of and improving on the already mentioned Wu-Yang conjecture.

First, some notation: $S(b) \equiv 1 - \Gamma(b)$ = "transmission" (recall b is impact parameter). $S(b) \equiv e^{-\Omega(b)}$; $\Omega(b)$ is called the "opacity". The exponential form is reminiscent of the depletion of a beam in passing

through a slab if Ω is proportional to the thickness of the slab. The reasoning of the model is roughly as follows:

Pretend that the two hadrons approaching each other in the c.m. are "like" two three-dimensional "droplets" that will pass through each other. Even the solution to the resulting classical scattering problem is difficult to attain. So idealize the problem:

(i) For de Broglie waves "shining" on a stationary "target" hadron the opacity should be

$$D(x,y) = \int_{-\infty}^{\infty} \rho(x,y,z)dz \ ,$$

where z is the beam direction and where $\rho(x,y,z)$ is a measure of the hadronic matter density at a point.

(ii) Now in any frame make the elementary observation that the instantaneous amount of scattering at a point should be proportional to the product of the densities there. This implies that the individual hadron opacities should be multiplied somehow (note: opacities are multiplied, not absorptions).

(iii) Then pretend that the total depletion of probability amplitude for two hadrons passing through each other is the same as that for a "structureless" wave passing through a single disc of the "product" opacity. $(s(b) = e^{-\Omega(b)})$.

By referring to Figure I-7 the reader will see that a "reasonable product" opacity is found by convolution:

$$\Omega(b) = \mu_{12} \iint d^2b' D_1(b-b')D_2(b')$$

where subscripts 1,2 refer to the identities of the hadrons and

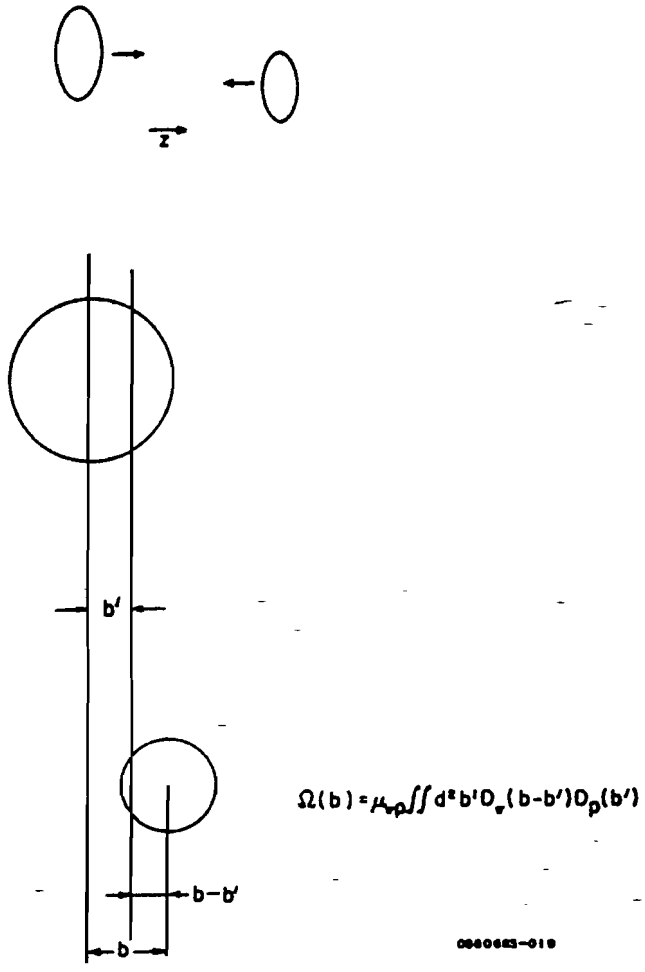

$$\Omega(b) = \mu_{vp} \iint d^2b' D_v(b-b') D_p(b')$$

0000685-010

Figure I-7. Illustrating the integrand of $\Omega(b)$ (see text).

where μ_{12} is a constant.

(iv) At this point Chou and Yang guessed that the hadronic matter distribution (in the proton) is proportional to the electric charge distribution as measured by elastic e-p scattering. Thus, if $\langle\rho(x,y,z)\rangle$ denotes the Fourier transform (the result of which is in momentum transfer space),

$$\langle\rho(x,y,z)\rangle = F_E(q^2)$$

where $F_E(q^2)$ is the hadron form factor. Converting to two-dimensional impact parameter space one has, then

$$\langle\Omega(b)\rangle = \mu_{12}\langle D_1 \circledast D_2\rangle = \mu_{12}\,\langle D_1\rangle\,\langle D_2\rangle \ ,$$

where $\circledast$ refers to convolution and where the convolution theorem of Fourier transforms has been used. Then

$$\langle\Omega(b)\rangle = \mu_{12}F_1(q^2)F_2(q^2)$$

where the subscript "E" is assumed.

(v) The parameter μ_{12} is not arbitrary--it may be set by using the optical theorem

$$\sigma_{tot} \propto 4\sqrt{\pi}\, f(0) \ , \qquad \text{where } |f(t)|^2 = \frac{d\sigma}{dt} \ ,$$

where <u>it is assumed that a(t) is purely imaginary at all t.</u> Then using the basic optical model result that

$$f(q^2) = ik\,\langle\Gamma(b)\rangle \quad \text{with } \Gamma(b) = 1 - s(b),$$

one has

$$\frac{d\sigma}{dt} = \pi\left|\left\langle 1 - e^{-\mu_{12}\langle F_1(q^2)F_2(q^2)\rangle}\right\rangle\right|^2$$

where $\langle\!\langle\ \rangle\!\rangle$ also denotes Fourier transform. This is the basic Chou-Yang result. Note that there are <u>no</u> free parameters.

(ii) Comparison with pp Data

The original Chou-Yang model was proposed around 1968. At that time $-t \approx 1.4$ (GeV/c)^2 dip in p-p scattering was unknown. Chou and Yang used the dipole formula for $F_p(q^2)$. Their results disagreed strongly with the data known at that time. They also predicted a dip near $-t \approx 1.5$ (GeV/c)^2. So many people scoffed. Then the dip was found.

Kac[21] has obtained a good fit of the Chou-Yang model to the $\sqrt{s} = 53$ GeV data (see Figure I-8a). We see that the behavior of the cross section out to the dip is extremely well predicted (we do not look into the χ^2 of the fit to the extreme low -t data here--see later)--remarkably the cross sections hugs the model curve for over six decades of drop! The position in -t of the dip seems to be also accurately predicted. These features certainly suggest that the model should be taken seriously. In obtaining this fit he has used Shaw's[22] empirical "two pole" fit to $G_m^p(q^2)$,

$$G_m^p(q^2)/\mu_p = (1 + q^2/m^2)^{-1}(1 + q^2/m'^2)^{-1} \quad ,$$

with $m_p = .656$ and $m' \equiv m + 1$, rather than the simple dipole formula. This two-pole formula seems a better fit to $G_m^p(q^2)$ than the dipole formula does, out to $t \approx 2$ (GeV/c)^2 (just past the second max.). (With the dipole formula one gets a much lower quality fit (including a slightly different dip position)--see ref. 21). It is seen from the figure that beyond $t \approx 2$ (GeV/c)^2 the Kac fit increasingly underestimates the data. This has been the cause of much speculation, some of which we feel is nonsense.

In any case, there is a bit more to be said about the Kac fit. The

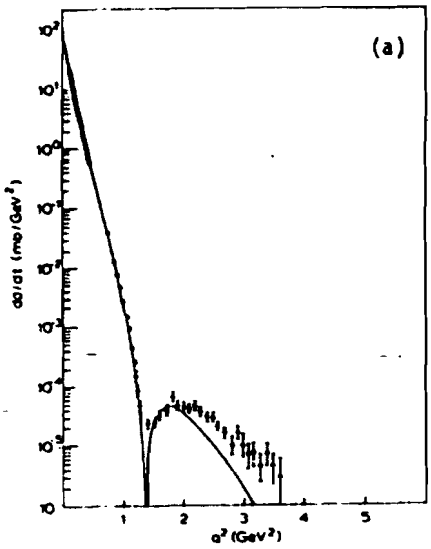

Figure I-8.
Fits of Chou-Yang model to $\sqrt{s}$ = 53 GeV CERN data.

(a) The fit of Maxwell Kac with extrapolated σ_T = 45.1 mb (see text) (from ref. 21).

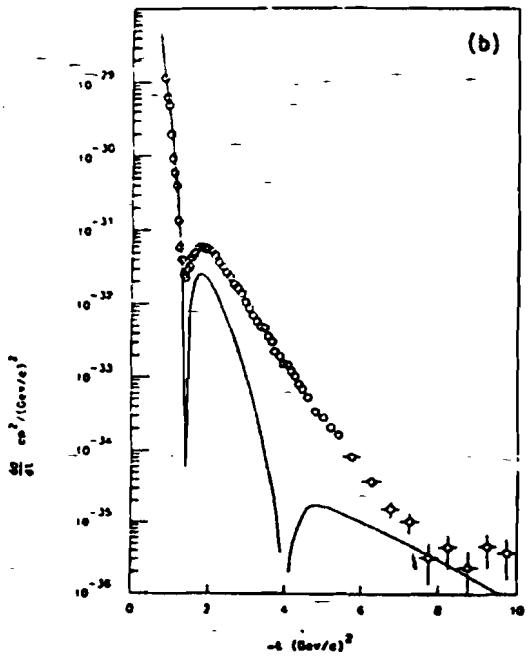

(b) A fit with extrapolated σ_T = 43.2 mb, closer to the "true" value of σ_T. Note the difference at the second maximum as compared to Kac's fit (from ref. 24).

reader may be wondering why we keep referring to it as a "fit" when the Chou-Yang model is supposed to have no free parameters. That is because Kac fit the value of the parameter μ_{12} to the height of the second maximum. The fit value of μ_{pp} for this ($\sqrt{s}$ = 53 GeV) data translates into an equivalent value of 45 mb for σ_{tot}.

The measured value of σ_{tot}, however, is about 42.3 mb at this energy. The reader might think that his ~5% difference in the σ_{tot}'s would have only a small effect. However, it has been pointed out by Nina Byers[23] that the height of the second maximum in the model is very sensitive to small changes in parameters. She states, for example, that a 5% change in σ_{tot} causes a 250% change in $\frac{d\sigma}{dt}$ at $t \approx 1.8$ (GeV/c)^2! [The dip <u>position</u> however is relatively insensitive to small changes.] An example of a calculation[24] with σ_{tot} = 43.2 mb is shown in Figure I-8b. Note the difference at the second maximum!

Another problem common to the use of both the Shaw formula and the dipole formula in the Chou-Yang model is the prediction of a second dip somewhere near $-t \approx 5$ (GeV/c)^2. No such dip is observed at p_L = 200 GeV/c, p_L = 400 GeV/c or at $\sqrt{s}$ = 53 GeV. This has caused some[25] to practically rule out the Chou-Yang model. However, as noted by Kac himself[21], since the Shaw two pole fit to the form factor is inaccurate for $-t \geq 2$ (GeV/c)^2, one does not expect the Chou-Yang model to work well with it beyond this value of -t.

Byers[23] has pointed out that the three pole formula

$$G_m^p(q^2) = [(1 - t/0.382)(1 - t/2.1)(1 - t/14.0)]^{-1}$$

is a better fit to the data[26] on G_m^p than is Shaw's formula, out to

$-t \sim 6$ (GeV/c)^2. Indeed, she has indicated that with this the predicted second dip moves out to $-t \approx 6$ (GeV/c)^2. [The change in the prediction of $\frac{d\sigma}{dt}$ for $0 \lesssim t \leq 2$ is essentially negligible between the two- and three-pole formulas.] Thus, it is entirely plausible that the prediction of a second minimum would go away altogether with the use of the "correct" $q^2 \gtrsim 6$ (GeV/c)^2 form factor, and hence perhaps some of the despair about the high q^2 behavior of the model is premature.

(iii) Energy Dependence and Comparison of Predictions for $\bar{p}p$ and pp Scattering in the Basic Chou-Yang Model

(α) Energy Thresholds for and Depth of Dips I--Simple Analysis

To the extent of the author's knowledge the form factor of the anti-proton has not been measured directly. However, it is certainly not unreasonable to assume that it is the same as that of the proton. Indeed, if one believes the Chou-Yang model, the existence of the $\bar{p}p$ dip could be interpreted evidence for this! On the other hand, one could take the attitude that any differences between the pp and $\bar{p}p$ elastic cross sections, at least asymptotically in energy, would be due to form factor differences.* One certainly does not expect this. But perhaps the most valuable experiments are those that check the "obvious" and lead to surprises.

In any case, there certainly are differences in pp and $\bar{p}p$ elastic scattering at nonasymptotic energies--e.g., the pp dip near $-t \approx 1.4$ (GeV/c)^2 seems to come in at about 150 GeV/c whereas the corresponding $\bar{p}p$ dip comes in at much lower energy. However, the only energy dependence

*I.e., in the framework of the model [as $s \to \infty$ it appears that $\sigma_{tot}(\bar{p}p)\, \sigma_{tot}(pp) \to 1$.] In the framework of QCD, ultimately, of course, this would mean differences in the quark-gluon structures of the p and $\bar{p}$.

in the model comes from the parameter μ, which in turn depends only on σ_{tot}. The dip depth in the model is insensitive to σ_{tot}--that's because the dip is a <u>zero</u> in the model. This follows from the assumption that the amplitude is completely imaginary.

We've already remarked how the addition of a small real part to the amplitude can affect $\frac{d\sigma}{dt}$ at the minimum. So to understand the dip depth we should look, perhaps, at data on the ratio of the real to imaginary part of the amplitude. Chou and Yang seem, on the other hand, to be of the opinion that the energy dependence for the appearance and disappearance of dips is due instead to some sort of unspecified "low energy effects" which are cancelled somehow (<u>although not explicitly in the basic model</u>) by a large σ_{tot}. They state: "Why does $p\bar{p}$ exhibit the first dip at lower energies than pp? The answer is probably: [the] $p\bar{p}$ [total] cross section is much larger than [the] pp [total cross section] at low energies, and pure geometrical scattering is therefore not so easily overwhelmed by low energy effects."[27] There may be truth in this; however, it seems less vague to the author to simply note that [Re f/Im f at $t = 0$] for $\bar{p}p$ is very close to zero at 50 GeV/c, whereas for pp at this energy $\rho < -0.1$!

With this train of thought, looking at the Fajardo et al.[28] results for ρ (see Figure I-9) we can entertain some interesting conjectures: For example, we see that at low energy (5 or 10 GeV/c) $|\rho_{pp}|$ is relatively large ($\sim$0.3 or 0.4) whereas $\rho_{\bar{p}p}$ is close to zero. This could be why the low energy pp cross section is smooth while the low energy $\bar{p}p$ cross section shows a dip at $t \approx 0.7$.

We also see that ρ_{pp} grows increasingly positive above $p_{lab} \approx 200$

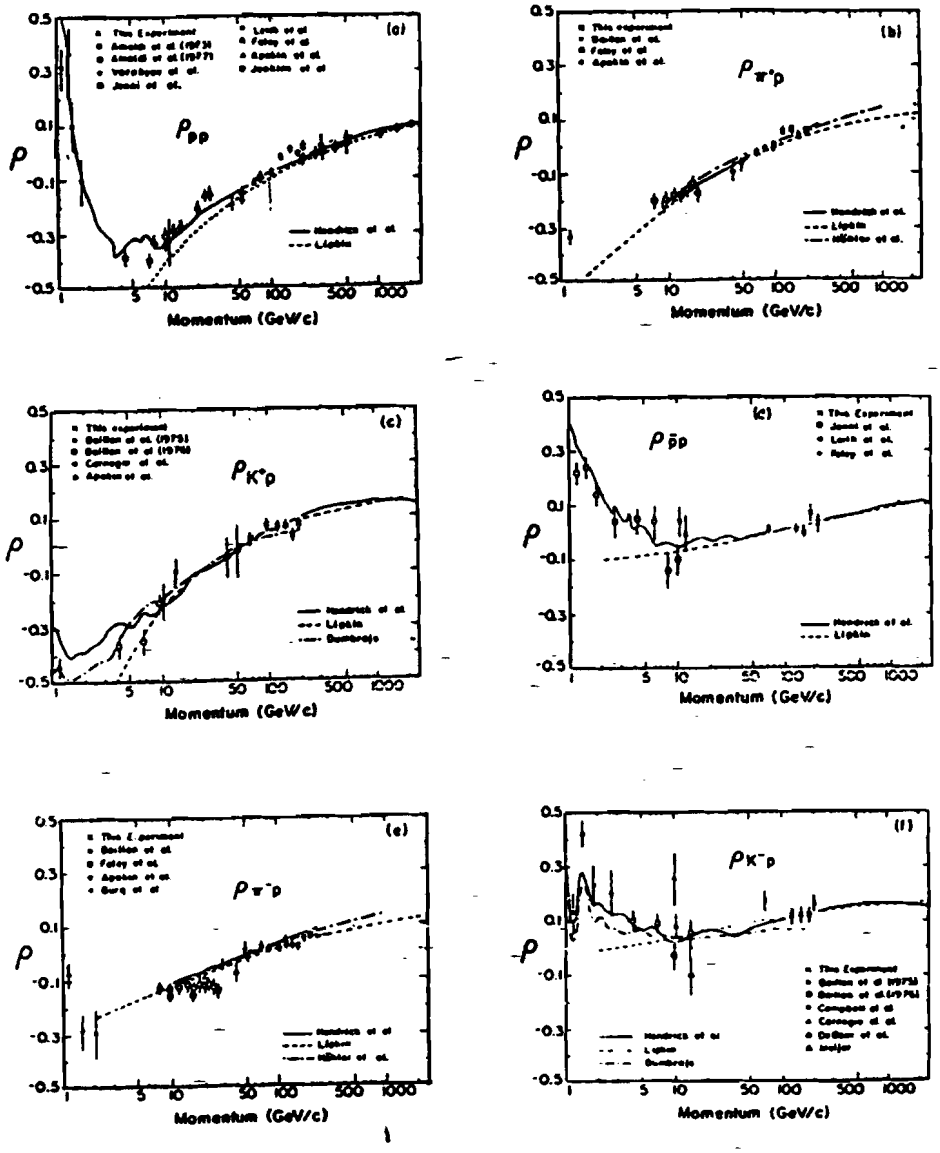

Figure I-9. ρ for various elastic scattering reactions. Data points are from various sources; dotted and solid lines are various theoretical predictions. (Figure adapted from ref. 28.)

GeV/c. This could be why the $-t = 1.4$ (GeV/c)^2 dip is gradually disappearing with energy in the ISR range. At 200 GeV/c, ρ_{pp} is very close to zero, so we expect a relatively deep dip at that energy.

We have measured pp elastic scattering at 100 GeV/c. Would one expect the dip to be apparent at that energy? At 100 GeV/c, $|\rho_{pp}| \approx 0.1$. pp elastic scattering has been measured before at this value of $|\rho|$--at $\sqrt{s} = 62$ GeV. There a shallow dip is observed. Therefore, on the basis of these simple considerations (ignoring, e.g., spin effects) we should see one, too (even though Rusack et al. do not) (and we claim we do possibly see some evidence for one--see Chapter VII).

At this point the reader may recall that for pp elastic scattering the value of $\frac{d\sigma}{dt}$ at the "bottom" of the dip appears to be proportional to $\rho^2\sigma_{tot}^2$ (not just $|\rho|$) in the ISR range, and therefore object. However, we can answer this objection simply by noting that $\sigma_{tot}(\bar{p}p)$ for 100 GeV/c $\approx \sigma_{tot}(pp)$ for $\sqrt{s} = 62$ GeV. (Actually $\sigma_{tot}(\bar{p}p)$ at 100 GeV/c is just slightly lower than $\sigma_{tot}(pp)$ at $\sqrt{s} = 62$ GeV--which makes our argument that there "should be" a shallow dip at 100 GeV/c for pp-scattering stronger.)

Also, we note that $\sigma_{\bar{p}p}$, which goes through zero at $p_{lab} \approx 70$ GeV/c is still very close to zero at both 100 and 200 GeV/c; hence we expect to see a prominent dip at these energies (and, of course, at 50 GeV/c, where such a dip was seen at CERN). Keeping in mind the prediction for a rise in $\sigma_{\bar{p}p}$, we expect that the dip would begin to fill in at higher energies.

However, the situation is not exactly the same as for pp. Results of recent measurements of ρ at CERN for $\sqrt{s} = 52.8$ GeV show that ρ_{pp} is

about 0.065±0.005 while $\sigma_{\bar{p}p}$ seems to be about 0.11. Also, $\sigma_{tot}(\bar{p}p) \approx \sigma_{tot}(pp)$ at this energy. Thus at $\sqrt{s}$ = 53 GeV, we might expect the $\bar{p}p$ dip to be shallower than the (already shallow) pp dip. This should be checked experimentally. It has been proposed to measure both elastic scattering and the total cross section for $\bar{p}p$ at $\sqrt{s}$ = 2000 GeV with the Fermilab collider. Would a dip be seen at this energy? From our point of view this will depend on the value of ρ at that energy. Here we wish merely to mention the remarkable result that, if the total cross section rises asymptotically as some power of log s, crossing and analyticity require that ρ must approach zero from above.[29] Thus, it was expected that the "rising total cross section" would cause ρ, which is negative at AGS energies, to pass through zero and become positive [and this is indeed observed], and then return to zero.

So we see something interesting: as the energy continues to increase, after wishing out the dip should start to deepen again. This should also be checked experimentally. The question is: At what energy does all asymptopia begin to come into view? That is a good question. But the fact that ρ is still rising means we haven't gotten there yet.

π^-p

The application of the Chou-Yang model to π^-p elastic scattering is notoriously difficult, as the pion form factor is not known beyond $-t \approx 1.2$ (GeV/c)^2. However, let us "speculate": for π^-p ρ is seen to be close to zero at 50, 100, and 200 GeV/c, and so we could be led to expect a dip at all these energies. In this experiment we have observed one at 200 GeV/c[30] but at a higher -t value than for pp scattering. We can even guess that the dip "should" be at a higher -t value for πp than

for pp within the framework of the Chou-Yang model--$\sigma_{tot}(\pi p) < \sigma_{tot}(pp)$ at 200 GeV/c. The reader may draw his/her own conclusions about kaons.

(β) More on Predicting Energy Thresholds and Depth of Dips

In analogy with the Kramers-Kronig relations[31] of classical optics, one can relate the real part of the scattering amplitude to the integral of the absorptive part (i.e., total cross section of t = 0) through a dispersion relation. (Dispersion relations of this type are based on the assumptions of analyticity, unitarity and crossing symmetry, since the exact connection between causality and analyticity has been difficult to establish rigorously.) Thus, if $\sigma_{tot}(pp)$ and $\sigma_{tot}(\bar{p}p)$ were known at all energies it would be possible to predict $\rho \equiv$ Re $f(t=0)$/Im $f(t=0)$. Then, assuming that the dip depth depends only on σ_{tot} and ρ, a knowledge of σ_{tot} at all energies would allow the prediction of $\frac{d\sigma}{dt}$ at the dip. Conversely, the high energy behavior of σ_{tot} could be predicted by integrating the real part of the scattering amplitude. An example of this is shown in Figure I-10. However, the cumbersome non-local integral connection creates potential problems for the prediction of ρ because σ_{tot} has not been measured at all energies yet.*

---

*As far as the high energy end is concerned, current data[32] cannot distinguish between

(i) $\sigma_{tot}(s) = \sigma_0(0) + \sigma_1 \log(s/s_0) \approx 28.2 + 1.92 \log s$

(ii) $\sigma_{tot}(s) = \sigma_0 + \sigma_1 \log^2(s/s_0) \approx 38.4 + .49 \log^2(s/122)$

(iii) $\sigma_{tot}(s) = \sigma(\infty) - \sigma'(\infty)/\log(s/s_0)$

It should be mentioned that a growth of the $\log^2(s)$ type is the quickest allow by unitarity ("Froissart bound").

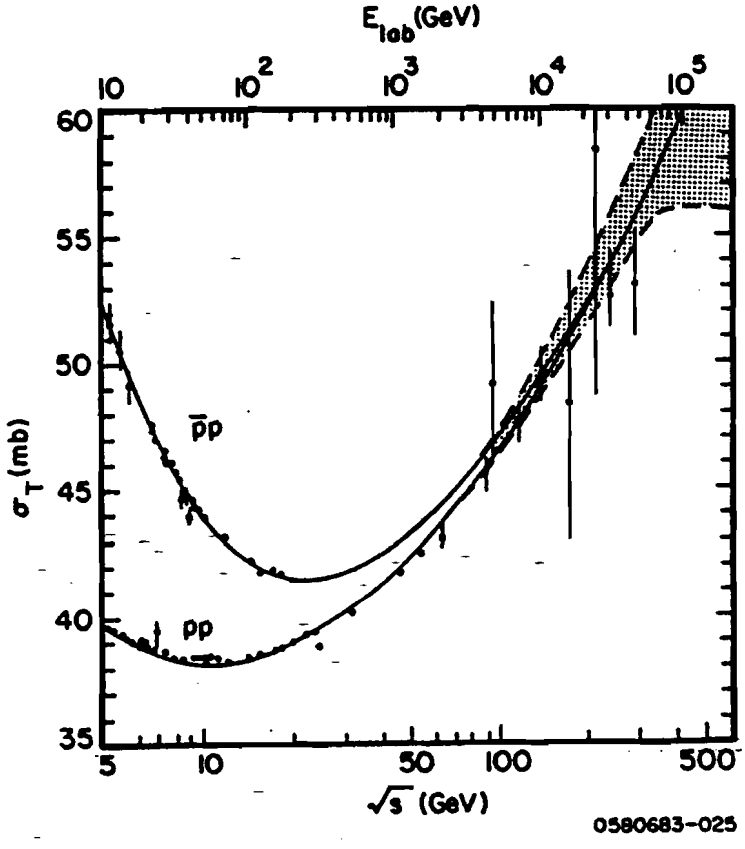

Figure I-10. Data and predictions for σ_{tot} (see text). (Adapted from ref. 114.)

In any case, though, the readers may be wondering why we have been relating the dip depth at all to ρ (which from now on will also be called "$\rho_{t=0}$"), when, if anything, it should be related to [Re f/Im f] at t_{dip} ($\equiv$ "ρ_t" from now on). For the approximate analysis of part (α) of this subsection we have been tacitly assuming for simplicity that ρ_t is not too different from $\rho_{t=0}$. (The ISR data on the dip depth seems to bear this out.)

There is, however, reason to believe that for $p_L \gtrsim 100$ GeV/c our "approximation" is, in fact, almost exact. Within the context of "geometrical scaling" (which seems to work at these energies--see Section C.4). Dias de Dues and Kroll[51] have derived

$$\frac{d\sigma}{dt}(s,t_{dip}) \Big/ \frac{d\sigma}{dt}(s,0) = K^2 \frac{\rho^2(s,t=0)}{1+\rho^2(s,t=0)}$$

in obvious notation, where K^2 is independent of energy. Indeed, they also find a differential equation (see (I.13)) relating $\rho(s,t=0)$, $\frac{d\sigma}{dt}(s,t)$ and $\frac{d\sigma}{dt}(s,\phi)$. With this equation, using the ISR data they can predict $\rho(s,0)$ in good agreement with experiment (see page 62). Conversely, inputting ρ and $\frac{d\sigma}{dt}(s,0)$ the equation can be solved for $\frac{d\sigma}{dt}(s,t_{dip})$ (see later). This gives us a quantitative handle on the relationship between $\rho_{t=0}$ and the dip depth! It is seen[51] that at ISR energies $\rho = 0.13$ is large enough to make the dip disappear (see Figure I-11). With reference to our argument about a dip in pp scattering at 100 GeV/c, note that $\rho_{t=0}$ there is $\approx$0.10.

Strictly speaking, however, this assumption is unnecessary. It has been shown by Bronzan, Kane and Sukhatme[33] that one can, in fact, obtain the real part of the scattering amplitude by knowing the imaginary part

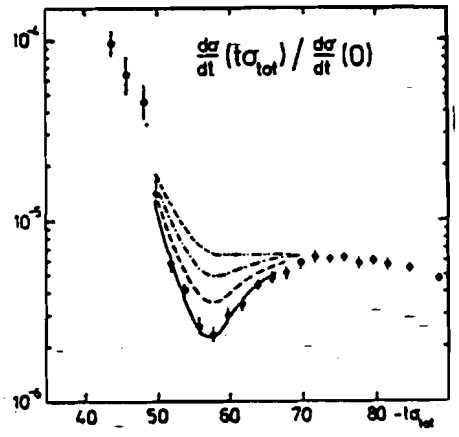

Figure I-11. Predictions for $d\sigma/dt$ near the dip at high energies as calculated from Eq. (I.14) with varying values of ρ, fit to data from ref. 51, $\rho \equiv \rho(s,0)$ (see text). Units of $-t\sigma_{tot}$ are $(GeV/c)^2 \cdot mb$.

—— $\rho = 0.078$
----- $\rho = 0.10$
-·-·- $\rho = 0.12$
---- $\rho = 0.14$

only at nearby energies. The so-called "derivative dispersion relations" are obtained by means of Taylor expansion. In Ref. 33 it is shown that at high energy the following simple relation holds:

$$\frac{1}{4}\pi \frac{d}{d \log s} \log \frac{d\sigma}{dt} \approx \frac{\text{Re } f(s,t)}{\text{Im } f(s,t)}$$

This, of course, breaks down at the dip in the Chou-Yang model since Im f(s,t) is zero there. However, Re f(s,t) can be approximated at t_{dip} by noting that it [Re f(s,t)] should be zero at the second maximum for $\sqrt{s} \sim 53$ GeV since $\frac{d\sigma}{dt}$ there does not seem to have any energy dependence there near that energy. One can then assume that Re f can be extrapolated in a reasonable way from $-t \approx 1.0$ GeV/c to the second maximum. In Figure I-12 we show the results of a calculation of Re f(t) by Miettenen[34] at $\sqrt{s} = 53$ GeV. From the resulting Re f(t_{dip}) one can get the dip depth.

(iv) Dip Movement in Basic Chou-Yang Model

In the basic Chou-Yang model dips move to lower -t with increasing σ_{tot} and to higher -t with decreasing σ_{tot}. Recall that 5 GeV/c $\bar{p}p$ scattering shows a dip near $-t = 0.8$ GeV/c. According to the Chou-Yang model the position of this dip at 50 GeV/c ($\sigma_{tot} = 44$ mb) is near $-t = 1.4$ GeV/c--as is observed! This has also been noted by Chou and Yang.[27] [The structure near $-t = 2$ (GeV/c) in 5 GeV/c $\bar{p}p$ scattering may also turn up again at a different -t value at higher energy--Yang's "double dip"?!]

Continuing this train of thought we could speculate about $\pi^- p$ elastic scattering. In low energy $\pi^- p$ scattering there is a dip which near $-t = 2.8$ (GeV/c)^2 which washes out by 25 GeV/c. At 200 GeV/c $\sigma_{tot}(\pi^- p)$ is less than it is at 10 GeV/c. So if the same dip survives

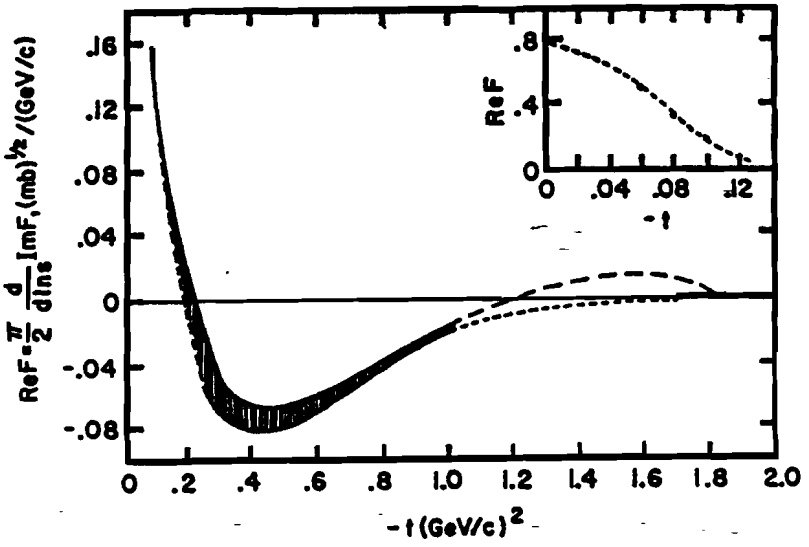

(a)

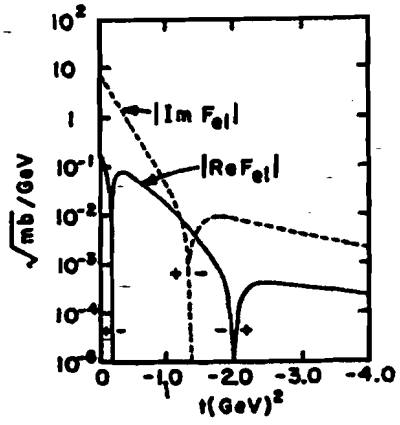

(b)

Figure I-12. (a) Extrapolation of Re F (see text). Black "bar" indicates region of second max where Re F is apparently zero (with error).
(b) As compared to Im F.

it should be at higher -t at 200 GeV/c than at 10 GeV/c. Perhaps the dip observed near $-t = 3.8$ (GeV/c)^2 at 200 GeV/c is this "same" low energy dip moved out!

(v) Connection of the Basic Chou-Yang Model with the Parton Model and with the Glauber Expansion

In a later part of this subsection we will discuss the effects of constituent substructure (i.e., quarks) of hadrons on the optical model (Glauber expansion). However, it seems well to mention the relationship of the basic Chou-Yang model to these constituent optical models and to the parton model here. Following Nina Byers[23] we mention that the Chou-Yang model is the limit of a Glauber series expansion for which:

a) the number N of constituents (of the e-p proton) approaches infinity. This is reminiscent of a famous theoretical result of inelastic e-p scattering. In this context, call the constituents partons,

b) the parton-parton interaction is "contact" in impact parameter and absorptive (partons in colliding hadrons interact like colliding "black dots" in an optical model). Thus, the amplitude for constituent-constituent scattering is

$$t_{qq}(q^2) = i\int \frac{d^2b}{2\pi}\,\alpha(b)e^{i\bar{q}\cdot b}$$

where $\alpha(b) = \frac{A}{N}\delta^2(b)$, with A a constant. Thus it is seen that the parton-parton scattering amplitude is flat in q^2.

The Glauber expansion to be discussed later is the same optical model except that

a) the number of constituents is equal to the number of valence

quarks in the hadron, and

b) the constituents are not necessarily pointlike--their size is determined from the data. Thus $t_{qq}(q^2)$ is not necessarily flat. This involves introducing about two parameters.

The Glauber expansion model should use the same form factor as Chou-Yang. Thus, if the form factor were known well, elastic scattering data could very plausibly determine

i) the number of hadronic constituents in the proton, and

ii) their size.

b. The "Current-Current" Modification of the Chou-Yang Model

In addition to using an inaccurate formula for a given form factor, there is also the danger of using the "wrong" form factor. That is, in the original Chou-Yang model both the spin and isospin of the participants were neglected. This leads to an ambiguity[23]--which form factor does one use (e.g., G_E^P or G_M^P)?

For $|t| \leq 2$ (GeV/c)^2 this is not much of a problem as measurements show that to within experimental accuracy $G_E^P(q^2) \propto G_M^P(q^2) \propto G_M^N(q^2)$ in this range.[26] (Thus to the extent that $G_E^N(q^2) = 0$ we have $G_E^{(S)} \propto G_E^{(V)} \propto G_M^{(S)} \propto G_M^{(V)} \propto G(q^2)$ for $q^2 \leq 2$ (GeV/c)^2). However, for $-t \geq 2$ (GeV/c)^2 this is not true--e.g., $G_E^P(q^2)$ appears to fall faster than $G_M^P(q^2)$ and $G_E^N \approx -G_M^N$. Hence for $-t \geq 2$ (GeV/c)^2 the predictions of the "naive" Chou-Yang model[1] for pp elastic scattering would depend on the form factor used, and those for pp, $\bar{p}p$, np, nn, $\bar{n}p$, $\bar{n}n$ would differ.

Lo[35] has proposed a model in which both isospin zero and isospin one exchanges are allowed in p-p elastic scattering (and which hence involves

both the isoscalar and isovector form factors of the nucleon). In this model

$$\Omega(s,b) = \sum_j \iint \rho_N^j(x)\rho_N^j(x')I^j(\vec{b}-\vec{x}'+\vec{x})d^3x'd^3x$$

where ρ_N^j is the nucleon density function corresponding to SU(3) quantum number j. (Recall there are 8 "λ matrices", but only λ_3 and λ_8 are non-strangeness changing and hence allowed.) $j = \phi$ corresponds to "vacuum exchange" and is assumed to be given by an energy independent contact interaction with ρ^o the Fourier transform of the nucleon isoscalar form factor. On the other hand, the interactions where a quantum number is exchanged are assumed to be given by energy dependent contact interactions. The $j = 3$ interaction is assumed to decrease with energy, with ρ^3 corresponding to the "fourth" (i.e., zeroth in our metric, but we use the "4" here) component of an isovector current. Thus

$$\Omega(s,b) = 2\pi\mu_o(s)\iint d^3\kappa\, d^3\kappa'\, j_4^{sc}(\vec{\kappa},0)j_4^{sc}(\kappa',0)\delta^2(\vec{b}-\vec{\kappa}'+\vec{\kappa})$$

$$-2\pi\mu_1(s)\iint d^3\kappa\, d^3\kappa'\, j_4^{(3)}(\vec{\kappa},0)j_4^{(3)}(\kappa',0)\delta^2(\vec{b}-\vec{\kappa}'-\vec{\kappa})$$

("sc" means isoscalar). The currents are then quantized and matrix elements (between proton states) of their appropriate components are then calculated in a manner reminiscent of the derivation of the Rosenbluth formula leading to spin-flip and spin non-flip amplitudes. σ_{tot} is used to fix $\mu_o(s)$ which is assumed to have the form

$$\mu_o(s) = \mu + \mu' \log^2(s/s_o), \qquad \mu = 9.76\ \text{GeV}^{-2},$$
$$\mu' = 0.23\ \text{GeV}^{-2}, \qquad s_o = 200\ \text{GeV}^2$$

Originally it was found possible to reproduce the ISR data at

p_L = 1480 GeV/c very well out to at least $-t \approx 2.8$ $(GeV/c)^2$ with $\mu_1(s) = \mu(s_0/s)e^{i\phi}$ where ϕ depends linearly on t and where μ, s_0 and $\phi(t=0)$ were set by the lower energy $p_L \lesssim 30$ GeV/c data. This was interesting in that it implied that the s-dependence of p-p elastic scattering at high energy is completely specified by the low energy behavior.

Unfortunately, closer examination revealed[36] that the s-dependence is not quite so steep or simple--$\mu_1(s)$ seems to decrease like $s^{-2/3}$ from 50-175 GeV/c (at least at low $|t|$) and more gradually at higher energies and high $|t|$ (still at least $\sim s^{-1/2}$ at ISR energies).

However, the most interesting feature of the model lies in the t dependence it predicts once $\mu_1(s)$ is set. The main characteristics (dip and peaks) are due to the isoscalar exchange amplitude. The effect of the $\Delta I = 1$ piece is to fill in the $-t \approx 1.4$ $(GeV/c)^2$ dip to about the right extent and to completely eliminate the notorious second dip. As the isovector piece becomes more important at low energies the first dip is completely filled in below $p_L \approx 200$ GeV/c and the model is capable of providing good fits down to $p_L \approx 3$ GeV/c. Some fits obtained are shown in Figure I-13.

Unfortunately at the higher energies and larger $|t|$'s ϕ is no longer a linear function of t. The reader may think that this introduces complete freedom in fixing the t-dependence of the model. This is not so. The "range of freedom" in the prediction obtained by varying the phase ϕ is shown in reference 36 for $p_{lab} = 6000$ GeV/c ("error bars" around the solid line). Presumably the ranges of freedom at lower energies, not shown by the authors, are comparable. In that case it would

Figure I-13 (adapted from ref. 36)

(a) (page 44) Theoretical fits to pp elastic scattering data corresponding to total cross sections of 38.97±0.04 mb (p_{lab} = 200 GeV/c), 38.46±0.04 mb (p_{lab} = 100 GeV/c) and 38.20±0.05 mb (p_{lab} = 50 GeV/c) for $0 \leq -t < 3.4$ GeV^2. (Total cross sections used are from Carrol et al., Phys. Lett. 61B, 303 (1976)). The broken line is the curve for p_{lab} = 100 GeV/c, and the values of μ_1 used are 0.80, 0.22 and 0.11 for p_{lab} = 50, 100 and 200 GeV/c, respectively.

(b) (page 45) Theoretical fits to ISR data and large $-|t|$ for σ_{tot} = 39 mb (p_{lab} = 200 GeV/c). Total cross sections corresponding to ISR data are 42.5±0.27 mb (Rubbia and DeKerret, p_{lab} = 1480 GeV/c and 1500 GeV/c respectively) and 43.04±0.31 mb (Kwak, p_{lab} = 2052 GeV/c). The theoretical curve used to fit the ISR data has an input total cross section of 42.8 mb and μ_1 = 0.100. The broken line is the curve for p_{lab} = 200 GeV/c, with μ_1 = 0.110.

(c) (page 46) Theoretical curve for σ_{tot} = 49.1 mb (p_{lab} = 6000 GeV/c) using μ_1 = 0.050. The "error" bars superimposed on the curve indicate the range of $d\sigma/dt$ values accessible at given $|t|$ through variation. The spin-flip contribution has been suppressed. (Data are from ISR.)

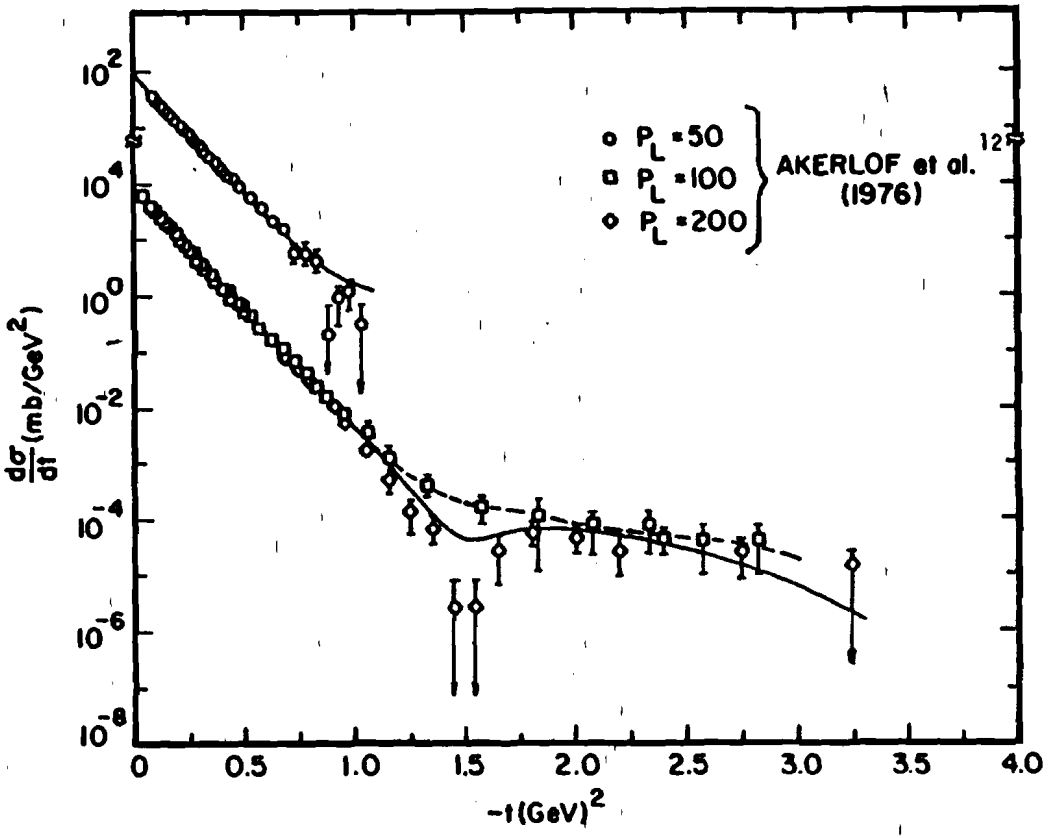
10^2
10^0
10^{-2}
10^{-4}
10^{-6}
10^{-8}
$\frac{d\sigma}{dt}$(mb/GeV^2)
0
0.5
1.0
1.5
2.0
2.5
3.0
3.5
4.0
$-t$(GeV)^2
o P_L=50
□ P_L=100
◇ P_L=200
AKERLOF et al. (1976)

Figure I-13(a)

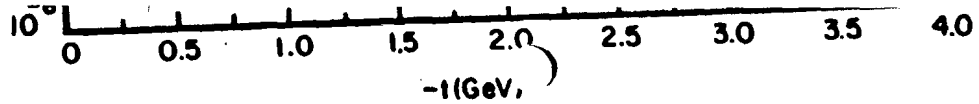

Figure I-13(a)

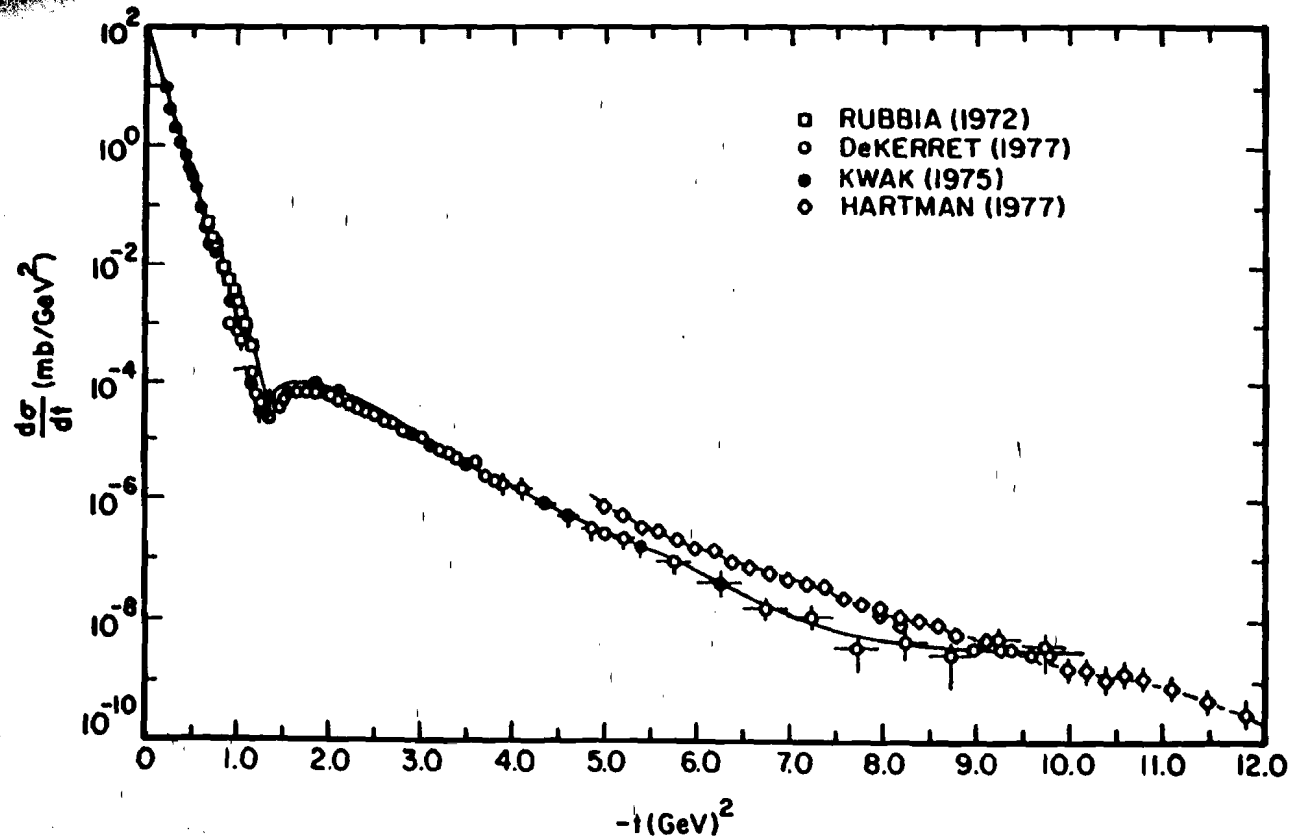

Figure I-13(b)

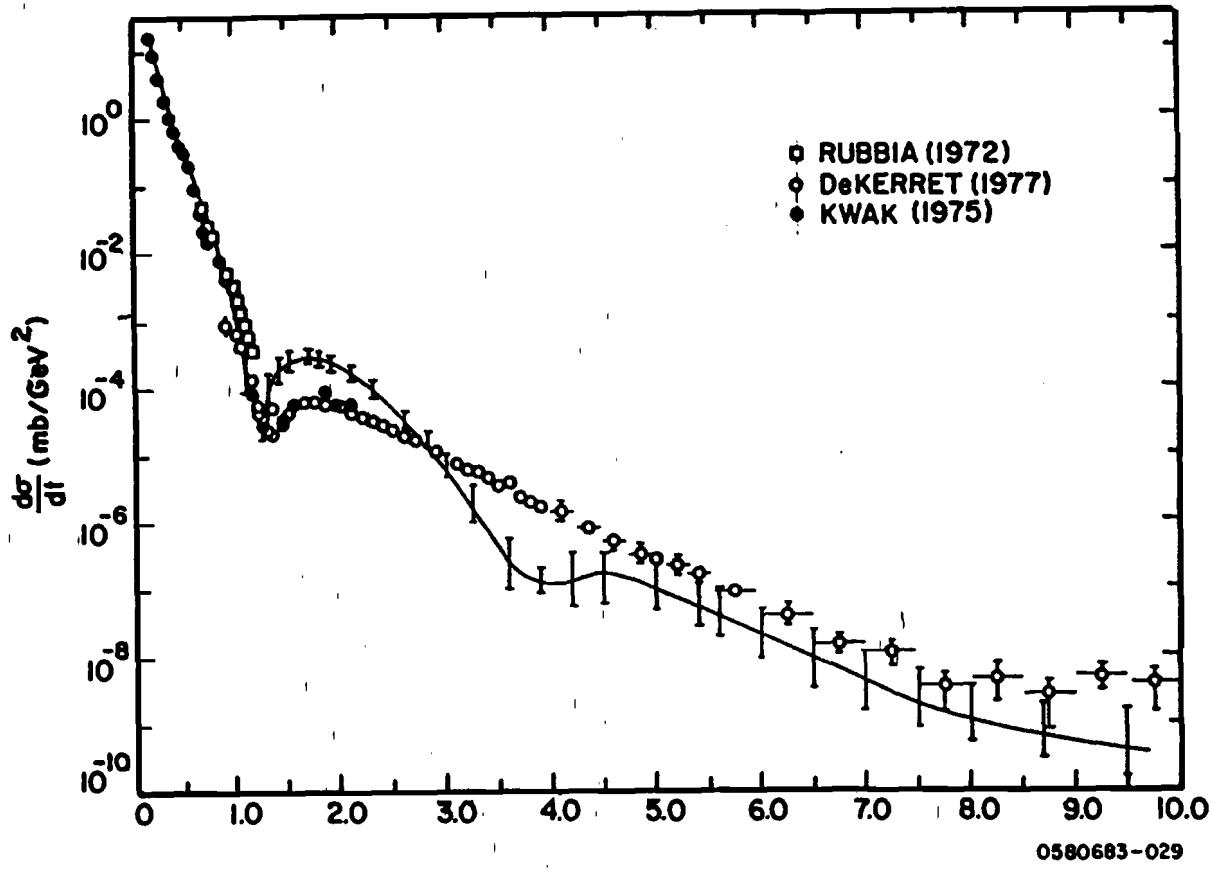
RUBBIA (1972)
DeKERRET (1977)
KWAK (1975)
$\frac{d\sigma}{dt}$ (mb/GeV^2)
10^{0}
10^{-2}
10^{-4}
10^{-6}
10^{-8}
10^{-10}
0
1.0
2.0
3.0
4.0
5.0
6.0
7.0
8.0
9.0
10.0
0580683-029

Figure I-13(c)

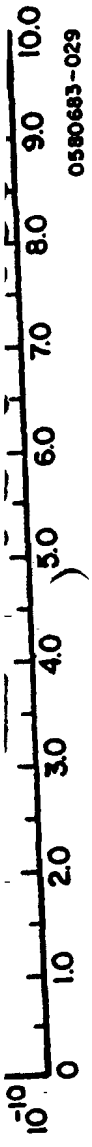

Figure 1-13(c)

still probably be ambiguous whether the model predicts a shallow dip or not at p_L = 100 GeV/c for pp.

In view of the partial success of the model I have questions, some of which could be answered by direct numerical integration. For example, since the isovector contribution is diminishing with energy it is difficult for me to see how the gradual disappearance (with energy) of the ISR dip could come out of the model in a natural way. This might be the results of including the spin flip terms (which fill in dips and which have largely been suppressed in the figures); however, Clarke and Lo claim that the isovector contribution overwhelms the spin flip contributions.

Another question is, at a given energy, with the isovector parameters fixed by pp scattering, could one reproduce $\bar{p}p$ elastic scattering with $\sigma_{tot}(pp)$ fixing the isoscalar contribution)? Or, consider energies around $p_L \approx 10$ GeV/c. The model seems to work for pp elastic scattering there and gives no dips. With the same (pp) isovector strength with the much higher $\sigma_{tot}(\bar{p}p)$ giving a greater ratio of isoscalar/isovector strength, would one get the observed $\bar{p}p$ dip at $|t| \approx 0.7$ GeV/c? This would be a stunning success. Would the dip movement be similar to that of the original Chou-Yang model over a wide range of energies? Probably yes. Possibly one could then "track" the 10 GeV/c $\bar{p}p$ at $|t| = 0.7$ $(\text{GeV/c})^2$ out to the 50 (GeV/c) dip at $|t| \approx 1.4$ $(\text{GeV/c})^2$.

Also, non-negligible polarization has been observed near the pp dip; in this model this is described well. Would that be true of $\bar{p}p$ also? As another point, within the framework of this model there is the

possibility of isolating the isovector contribution (e.g., ρ-A_2)* to n-p elastic scattering and thus predicting the difference between n-p and p-p elastic scattering. If the model were successful in predicting the phenomena mentioned above its credibility would be greatly strengthened. If it were a failure in all of them it could possibly be eliminated from consideration.

3. Impact Parameter Analysis in the Optical Model

The basic Chou-Yang model ignores the inelastic channels of which elastic scattering is the shadow. A number of modifications of the Chou-Yang model that "correct" for this have been proposed; we do not wish to discuss them here. However, a general sort of optical model analysis, called "impact parameter" analysis, demonstrates that the indirect inclusion of "virtual" inelastic channels via the unitarity condition allows elastic scattering to provide much additional information about the structure of hadrons. The approach we will describe is originally due to Van Hove[34] and has been developed by Miettenen[38] and others in the mid-1970s.

---

*Recall that, e.g., in Regge language, if A is the amplitude for elastic scattering,

$A_{pp} \sim P + f_0 + A_2 - \omega - \rho$
$A_{\bar{p}p} \sim P + f_0 + A_2 + \omega + \rho$ } charge conjugation

$A_{np} \sim P + f_0 - A_2 - \omega + \rho$] rotation in isospin space from pp case

since P, f_0, ω are isoscalars, A_2, ρ are isovectors,

where P is the Pomeron trajectory.

i) The Technique

Conservation of probability implies that the s matrix is unitary

$$ss^+ = s^+s = 1$$

As usual, we separate out the scattering wave:

$$s_{if} = \delta_{if} + i(2\pi)^4\delta^{(4)}(p_1 + p_2 - p_3 - p_4)\frac{T_{if}}{\prod_{k=1}^{4} n_k}$$

where the normalization factor n_k is given by

$$n_k = \begin{cases} (2\pi)^{3/2}\sqrt{2E} & \text{(for bosons)} \\ (2\pi)^{3/2}\frac{E}{m} & \text{(for fermions)} \end{cases}$$

To avoid clutter, we will write this symbolically as

$$s = 1 + iT$$

Then, the unitarity condition gives

$$i(T - T^+) = T^+T$$

Let $|i>$ be $|i>$ initial state, and let $|f>$ be a final state. Then, using completeness ($\sum_n |n><n| = 1$) and time reversal invariance ($T_{if} = T_{fi}$) we get (with suitable normalization)

$$4\sqrt{\pi}\ \mathrm{Im}\ T_{if}(t) = \sum_k T_{kf}T^*_{ki}$$

This can be "decomposed" as

$$4\sqrt{\pi}\ \mathrm{Im}\ T_{if}(t) = \sum_{i''=(\text{elastic states})} <f|T^+|i''><i''|T|i> + \sum_{n=(\text{inelastic})} <f|T^+|n><n|T|i> \qquad (I.1)$$

This equation is called the "s channel unitarity relation". It is a set of non-linear coupled (integral) equations. When s becomes very large, the number of intermediate states $|n\rangle$ approaches ∞.

Now we consider the case of forward elastic scattering.[39] Here we take $|i\rangle = |f\rangle$. Then Im $T_{ii}(t)$ becomes a sum of a very large number of positive definite terms. Moving slightly away from the forward direction, $|i\rangle \approx |f\rangle$, the phases of each of the terms $T_{\ell f}T^{*}_{\ell i}$ change slightly, but the complete sum must remain real. The more we increase θ the more random cancellations must occur. Hence, the coherent sum at t=0 gets rapidly suppressed. Thus, already the imaginary part of the scattering amplitude must be very peaked at low t. The real part of the scattering amplitude, however, has no such constraining equations. Hence we are not surprised if it is small for all t. So we expect a "forward diffractive peak" in $d\sigma/dt$ that falls off quickly angle. The pieces of (1) have been named, a long time ago, by Van Hove,

$$\tau_{tot}(t) = 4\sqrt{\pi}\ \text{Im}\ T_{el}(t) = \text{"total overlap function"}$$

$$\tau_{el}(t) = \sum_{f_n} (\text{elastic states}) = \text{"elastic overlap function"}$$

$$\tau_{inel}(t) = \sum (\text{inelastic states}) = \text{"inelastic overlap function"}$$

We see that (with our normalization)

$$\tau_{tot}(0) = \sigma_{tot}$$

$$\tau_{el}(0) = \sigma_{el}$$

$$\tau_{inel}(0) = \sigma_{inel}$$

The second term on the RHS of the "decomposition" equation (I.1) is the shadow of the inelastic channels, the first, the "direct" elastic scattering.

Following common practice, now make a Fourier transformation to impact parameter space:

$$\tilde{\tau}(\vec{b}) = \frac{1}{2\pi}\int d^2p_\perp e^{-ip_\perp\cdot b}\tau(p_\perp), \qquad |p_\perp| \equiv \sqrt{-t} \tag{I.2}$$

$$h_{el}(s,t) = \frac{1}{4\pi}\int db\, e^{iq\cdot b}h_{el}(s,b)\ ,$$

one then gets

$$\text{Im}\, h_{el}(s,b) = \frac{1}{4}|h_{el}(s,b)|^2 + \tau_{in}(s,b)\ , \qquad h_{el} \equiv T_{fi} \tag{I.3}$$

From this we immediately see that the elastic amplitude at impact parameter b is made from absorption into inelastic channels at the same b only ("unitarity is diagonal in b-space").

We note that $h_{el}(s,b)$ is nothing but $2ik\,\Gamma(s,b)$, where $\Gamma(s,b)$ is the absorption "profile" function mentioned earlier. Thus

$$\sigma_{tot}(s) = \frac{1}{k}\int d^2b\,\text{Im}\, h_{el}(s,b) = 2\int d^2b\,\text{Re}\,\Gamma(b) \tag{I.4}$$

$$\sigma_{in}(s) = \sigma_{tot} - \sigma_{el}(s) = \int d^2b\, G_{in}(s,b)$$

$$= \int d^2b[2\,\text{Re}\,\Gamma(b) - |\Gamma(b)|^2] \tag{I.5}$$

$$\sigma_{el}(s) = \int d^2b|\Gamma(b)|^2 \tag{I.6}$$

(The third part of (I.5) is seen from equation (I.3). The fourth part of (I.5) follows from this also, or from "noting" that the ratio of outgoing to incoming flux is $[1 - |s|^2] = 2\,\text{Re}\,\Gamma - |\Gamma|^2$. The integral of this must be σ_{in}.)

Since $0 \le \Gamma(s,b) \le 1$,

$0 \le \text{Im}\, h_{el}(s,b) \le 2$ (dropping a k factor)

Unitarity then requires

$$0 \le G_{in}(s,b) \le 1$$

By ignoring spin and using the derivative analyticity condition, one can obtain Im $h_{el}(s,b)$ and $G_{in}(s,b)$:

$$\text{Im } h_{el}(s,b) = \int_{-\infty}^{\infty} J_o(b\sqrt{-t}\ \frac{d\sigma}{dt} - \frac{d\sigma}{dt}\Big|_{real}^{1/2} dt \qquad (I.7)$$

ii) Results[40-46]

This sort of program has been carried out for the ISR data in approximation by Pirila and Miettenen[40], somewhat more carefully by Grein, Guigas and Kroll[41], and definitively by Amaldi and Schubert.[42] Some very interesting results obtain.

First of all, one expects Im $h_{el}(2\Gamma)$ to be almost a Gaussian because the cross sections are almost exponential in t. This guess is correct. One also observes a long non-Gaussian tail that extends out past b = 2 fermi. This is due to the continuous curvature of the cross section in what used to be called the "Carrigan break" region. The inelastic overlap function is observed to flatten out (as compared to a Gaussian) at low impact parameters which indicates that $G_{in}(s,t)$ apparently has a zero near $-t = 0.6$ (GeV/c)^2. Also, throughout the ISR region, the value of $G_{in}(s,b=0)$ stays at $(0.94\pm\sim0.01)$. That is, the black disc limit is only 94% saturated (see Figure I-14a).

This last point is intriguing. Why 94%? No one knows. Also, for Kp and πp scattering $G_{in}(s,b)$ is much more below the unitarity limit. Thus, apparently the reason why σ_{tot}'s for Kp and πp are so much smaller than σ_{tot}(pp) is that mesons are more transparent than baryons, <u>not that their radii are smaller!</u>[40] Assuming that most of the scattering comes from quarks rather than glue-glue interactions, maybe the decreased opacity is due to the absence of the third quark. (On the other hand,

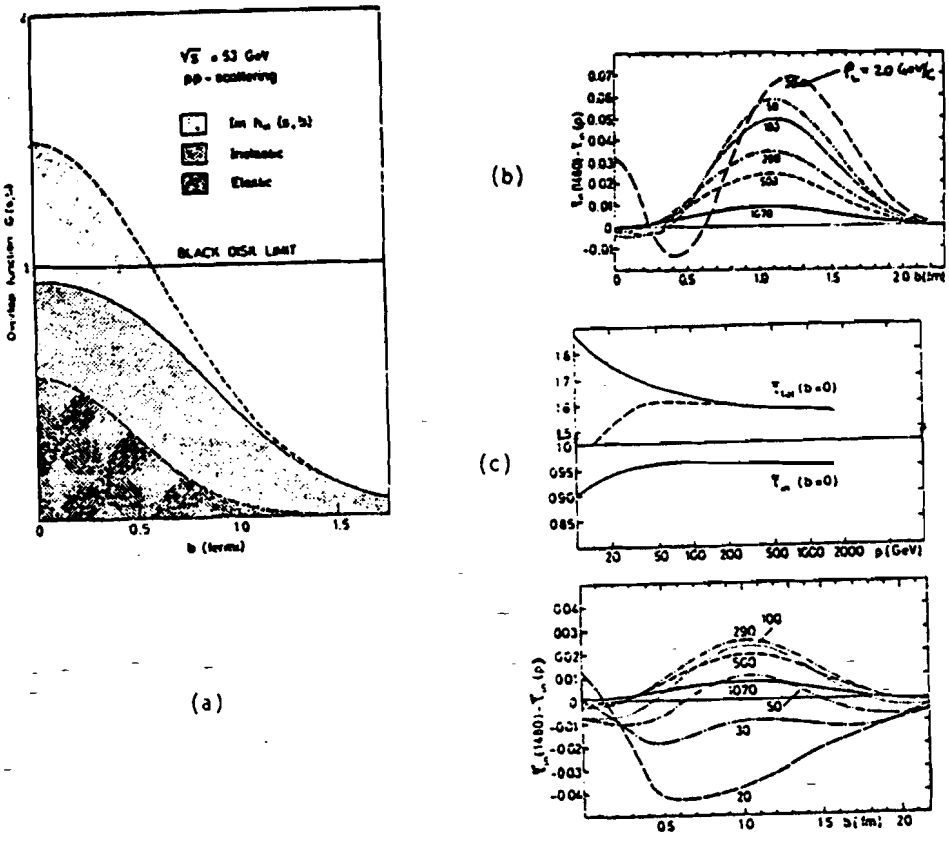

Figure I-14. (a) and (b). Impact parameter analysis of pp-elastic scattering from references 40 and 41, respectively. (c) Same for $\bar{p}p$ scattering, from reference 4.

Van Hove has proposed a model with a flattened Gaussian distribution of glue.*)

Over a broader range, the energy dependence of $G_{in}(s,b)$ is shown in Figure I-14b. From this and from Figure I-14a (showing that Im h_{el} is almost completely saturated by G_{in} for $b \geq 0.7$ f), we see that most of the increase in σ_{tot} for pp over a broad energy range comes from the peripheral region.[40] It has already also been seen that most of the increase in σ_{el} comes from low t. Also, from Figure I-14a, we see that the "two-body" part of σ_{el} is essentially central. At large b, elastic scattering is all shadow scattering.

This last point may be an indication of the existence of a proton core. From Figure I-14a, one sees that the radius in b of the elastic overlap region is $\sim$0.5 f. Since b corresponds to the distance between the centers of the (two) interacting particles the RMS radius of the core region for each would be about 0.25 fm. This estimate agrees with the 0.22 fm radius of the core found by Orear several years ago. We shall return to this point later.

A similar analysis has been done for $\bar{p}p$ scattering (see Figure I-14c). For ISR energies the results are practically the same as those for pp; however, at 100 and 200 GeV/c they are <u>not</u>--we remind the reader that $b(\bar{p}p)$ is significantly larger than b(pp) at these energies. The overlap functions are shown in the figure.

---

*At this state of our knowledge, I do not see any functional difference between having the gluons do the scattering or the quarks, except that the meson baryon difference is more naturally "explained" with quarks. Also, the distribution of glue in Van Hove's model is completely ad hoc and simply corresponds to knowing the result above after seeing the data!

One sees that at energies below ISR range the antiproton is somewhat "bigger" than the proton*; however, the central opacities are very similar except for $p_{lab} \leq 50$ GeV/c, for which the antiproton core is somewhat blacker. The main energy dependence is again centered near 1 fermi, but decreases before rising.

One might also ask how the dip near $-t = 1.4$ $(GeV/c)^2$ shows up in Im $h_{el}(s,b)$. The effect is to produce a flattening[40] near $b = 0$; however, this flattening is too small to be noticed in the figures shown because the dip occurs so far out in t (where $d\sigma/dt$ is so far down. This effect dominates the adage that "most of high t is low b"). (Similarly, in b-space our experimental data would look essentially similar to that obtained by Ayres et al.[43] (whose work cuts off at $t \approx 0.75$) at the same energy.)

However, <u>with the application of another Fourier transformation the effect of our data would probably be important to $G_{in}(s,t)$ for $t \geq 0.6$.</u> For example, if h_{el} were purely imaginary, from (I.3)

$$G_{in}(s,t) = h_{el}(s,t) - \frac{1}{4}\int dt' \, h_{el}(s,t'-t)h_{el}(s,t')$$

Thus one can obtain information about the t-dependence of the decomposition of the elastic scattering amplitude into its two and many body intermediate state contributions without having to perform explicitly the sum over states. One should also be able to learn something interesting about inelastic scattering in the process.

---

*For example, below ISR energy, the inelastic overlap function is slightly larger for $\bar{p}p$ than for pp.

Knowledge of the form of the high t overlap function would also be useful in making predictions about elastic scattering at other energies. For example, the decomposition over states, equation (I.1), can be written[44]

$$\mathrm{Im}\, h_{el}(s,t) \propto \frac{1}{32\pi^2}\iint d\theta_1\, d\theta_2\, \frac{\sin\theta_1 \sin\theta_2\, h_{el}(s,\theta_1)\, h^*_{el}(s,\theta_2)}{\sqrt{\{\cos\theta-\cos(\theta_1+\theta_2)\}\{\cos(\theta_1-\theta_2)-\cos\theta\}}} + G_{in}(s,t) \qquad \text{(I.8)}$$

where $|\theta_1 - \theta_2| \leq \theta$, $\theta \leq \theta_1 + \theta_2 < 2\pi - \theta$, θ = c.m. scattering angle. Most of the integral comes from the region around $\theta = \theta_1 + \theta_2$ (since h_{el} falls so quickly). Thus, for example, inserting a low t from $h_{el} \sim e^{-bp^2\theta^2}$, one sees[45] that at low t the main contribution to h_{el} comes from $G_{in}(s,t)$.

Now, at high energies, the low-t $\frac{d\sigma}{dt}$ can be parametrized[45] reasonably well by

$$\frac{d\sigma}{dt} = \left.\frac{d\sigma}{dt}\right|_{t=0} \begin{cases} e^{b_1 t}, & -t < t_o \\ e^{b_2 t}, & -t > t_o \end{cases} \qquad b_1 > b_2,\ t_o \sim 0.15\ \mathrm{GeV}^2$$

Plugging this into equation (I.8), one can obtain the high t differential cross section in terms of the low t cross section with a simple assumption about $G_{in}(s,t)$ at high t. For example, neglecting $G_{in}(s,t)$ beyond the diffraction peak, Nazerov and Chernov obtain a solution of the form

$$\mathrm{Im}\, h_{el}(s,\theta) = h_o(s) e^{-ap\theta/2} \ , \quad \theta \gg \theta_c$$

with high energy energy values of a about 5 GeV^{-1}. We recall that experimentally $a \approx 6$ for $p_L > 50$ GeV/c. Agreement with the data can be

improved by taking

$$G_{in}(s,t) = G_o e^{-\frac{1}{2}bp\theta}$$

It is then found that $G_o/h_o \approx 0.15$, for $p\theta \geq 2.2$ GeV. This already shows us that it is probably not necessary (although it may be nice) to invoke quarks or cores to "explain" the available high $p_\perp$ data--unitarity shows that the high $p_\perp$ data "follows" from the form of the diffraction peak. However, we believe that yet higher -t data will probably tell us something about quarks.

Assuming a completely imaginary amplitude, the $G_{in}(s,t)$ has in fact been calculated[40] and looks as shown in Figure I-15 for ISR data. The zero at $-t = 0.6$ is also present at low energy ($\sim$20 GeV) and was apparently first noticed by Zachariasen.[46]

One would, of course, like to be able to extract $G_{in}(s,t)$ from inelastic data and then predict $\frac{d\sigma_{el}}{dt}$ using the unitarity equation. Because of the zero of G_{in}, life is not so simple, however. Information on the moduli of multiparticle production matrix elements is not enough--around the zero G_{in} is sensitive to the phases, and hence a model which supplies them is needed. It can be seen[40] that the phase of a multiparticle production matrix element is directly related to the impact parameter at which the particles produced. Since one already knows that the opacity of the proton depends strongly on impact parameter, and since the elastic shadow depends on opacity, this is certainty not unreasonable.

Data on multiparticle production suggest[40] the existence of both a nondiffractive ("pionization") and a diffractive component in production. In a geometrical picture it would be logical that high multiplicity collisions are head on (high opacity) and low multiplicity collisions are

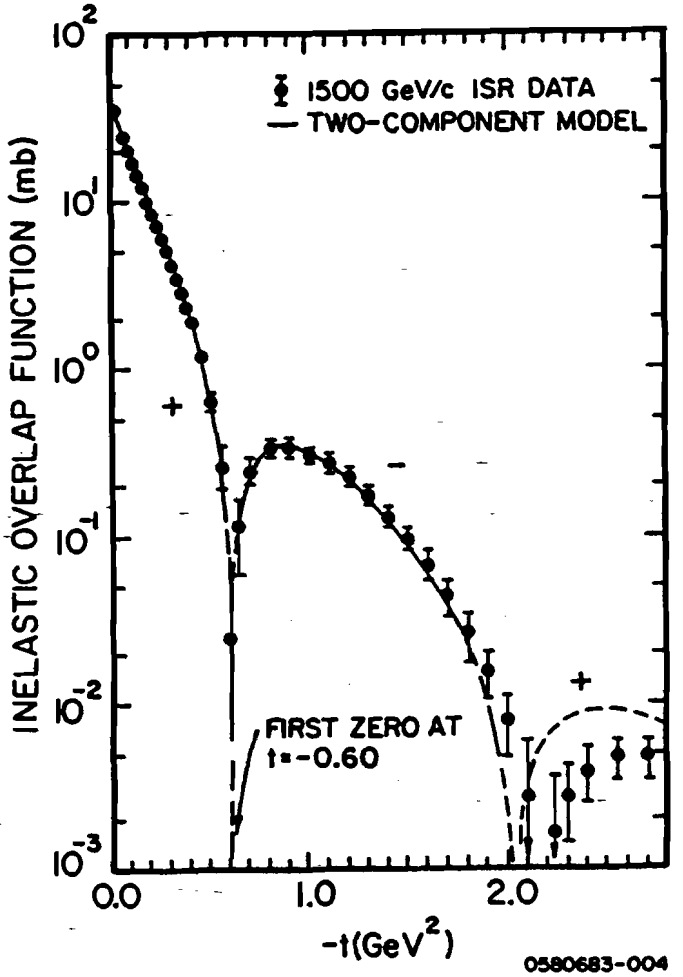

Figure I-15. Inelastic overlap function as calculated by Groot and Miettenen (see text). (Figure from ref. 40.)

peripheral (in contrast to the multiperipheral model). Analysis of data seems to indicate that the diffractive component involves how multiplicities --hence it might be peripheral.* In a simple two component play-model Miettinen and DeGroot[40] have used a zeroth order Bessel function (scattering from a ring) for the diffractice part and a black disc assumption for nondiffractive:

$$G_{in}(-t) = \sigma_D f_D(-t) J_0(R\sqrt{-t}) + \sigma_\pi f_\pi(t)\, 2J_1(\sqrt{-t})/R\sqrt{-t}$$

σ_D and σ_π come from data. The results of this parametrization are shown in Figure I-15. Beyond this however, the results of trying to predict $d\sigma_{el}/dt$ solely from production models are cloudy and we refrain from further discussion.

4. Geometrical Scaling

As we have mentioned, the basic optical model does a better job of predicting the t dependence of elastic scattering than the s-dependence. Geometrical scaling is very useful in trying to understand the s-dependence.

Geometrical scaling (G.S.) was first proposed[47] to explain multiplicity scaling in inelastic collisions. In this original formulation, G.S. states that

$$D_A(r^2, R_A^2) \underset{s\to\infty}{} D_A(r^2/R_A^2)\ ,$$

where D_A is the density function** and R_A is the (s-dependent) "radius" of hadron A. If two colliding hadrons A and B have an interaction radius $R_{AB}(s)$ and (inelastic) collision density*** $D_{AB}(b^2, R_{AB}^2)$, then

---

*This would account for the forward peak in production.

**In the original paper, $D_A(r^2/R_A^2)$ was assumed to be universal for all hadrons.

***This could be determined by convolution, for example.

$$-\frac{d\sigma_{AB}^{in}}{db^2} = \pi D_{AB}(b^2, R_{AB}^2) \xrightarrow[s\to\infty]{} \pi D(b^2/R_{AB}^2) \ , \qquad \text{(I.9)}$$

i.e., the inelastic overlap function $G_{in}(s,b)$ depends only on b^2/R^2 ("scales"). The application of this idea to elastic scattering was historically touchier because of stronger s dependence at lower energy. However, the connection is conceptually simple and was first made by Buras.[48] At energies where the real part of $h_{el}(s,b)$ is very small, (I.9) implies that $h_{el}(s,b)$ is also only a function of b^2/R^2. Then a simple change of variables in the Fourier transformation gives $f_{el}(s,t) = R^2 f[tR^2(s)]$. From this follows immediately:

$$\frac{d\sigma_{el}}{dt} \sim R^4 f(R^2 t) \qquad \sigma_{el} \sim R^2 \qquad \frac{\sigma_{el}}{\sigma_{in}} \sim \text{const.} \qquad b_{t=0} \sim R^2$$
$$\sigma_{tot} \sim R^2 \qquad \sigma_{in} \sim R^2 \qquad t_{dip} \sim \frac{1}{R^2} \sim \frac{1}{\sigma_{tot}} \qquad \text{(I.10)}$$

(Again neglecting the real part of f) we get the result that curves of

$$\frac{1}{\sigma_{tot}^2(s')} \frac{d\sigma^{el}}{dt}(s', \xi) \ , \qquad \xi \equiv R^2(s) \cdot t$$

at different energies should fall on top of each other. This program has been tried for the $\sqrt{s}$ = 23 GeV, $\sqrt{s}$ = 62 GeV and $\sqrt{s}$ = 45 GeV, $\sqrt{s}$ = 62 GeV pairs of ISR cross sections. Except for $t \approx t_{dip}$ (where the real part cannot be neglected), G.S. worked well for the second pair even out to $-t \approx 6$, but failed* for the first beyond the dip (probably indicating a still significant non-diffractive component at $\sqrt{s}$ = 23 GeV). In n-p scattering, a scaled comparison of 200 and 360 GeV/c data shows

*Or perhaps was only moderately successful.

significant differences even before the dip, but such a comparison of n-p at 280 GeV/c with pp at 2050 GeV/c seems to work very well to well beyond the dip (the unscaled data sets differ substantially).[49] Thus we do not expect this naive form of G.S. to work very well for pp elastic scattering at 100 or 200 GeV/c. For $\bar{p}p$, however, the situation could be entirely different (especially in view of the larger amount of absorption) at these energies. A careful comparison of elastic $\bar{p}p$ data at 100 and 200 GeV/c with CERN data would indicate how low in energy G.S. holds in this interaction.

By combining G.S. of Im f(s,t),

$$\text{Im } f(s,t) = \text{Im } f(s,0)\phi(\tau) \qquad \tau \equiv R^2(s)t, \qquad \text{(I.11)}$$

$$\phi(\tau) = \text{"scaling function"}$$

with the requirement of crossing symmetry, de Deus has derived*[50], the so-called "t-derivative relation"

$$\text{Re } f(s,t) = \text{Re } f(s,0)\frac{d}{d\tau}[\tau\phi(\tau)] , \qquad \text{(I.12)}$$

the results of which agree** with those of the derivative dispersion relations of Bronzan et al.[33] but which have the advantage that Re f can be obtained from Im f with no knowledge of the s-dependence. Combining (I.11) and (I.12) one gets[49] the differential equation

$$\frac{d\sigma}{dt}(s,t) = \frac{d\sigma}{dt}(s,\phi)\left\{\phi^2(\tau) + \rho^2(s,0)\left[\frac{d\sigma}{d\tau}(\tau\phi(\tau))\right]^2\right\} \times \frac{1}{1+\rho^2(s,0)} \qquad \text{(I.13)}$$

*This derivation assumes Pomeron exchange.

**In fact, assuming G.S., this can be transformed[50] into Bronzan et al.'s[33] expression at fixed s.

At the dip $\phi(\tau=\tau_D) = 0^*$ and hence

$$\frac{d\sigma}{dt}(s,t_o)\,\frac{d\sigma}{dt}(s,0) = K^2\,\frac{\rho^2(s,0)}{1+\rho^2(s,0)} \quad , \quad K = \tau\frac{d\phi}{d\tau}\Big|_{\tau=\tau_o} = \text{energy independent} \tag{I.14}$$

This is part of the theoretical justification for our earlier remarks about the correlation between the dip-depth and $\rho(s,0)$; see page 35. Equation (I.14) is found to agree very well with the ISR elastic scattering pp data[51], as mentioned on page 35. Using the data around the dip to compute κ, the full equation (I.13) can then be used for a prediction of $\rho(s,0)$. For the ISR data, the value of ρ so obtained is in agreement with experiment. Indeed, we can see why--using the optical theorem (I.14) simply says that

$$\frac{d\sigma(s,t_o)}{dt} \propto \sigma_{tot}^2\rho^2(s,0) \ ,$$

a relationship that we have already remarked (see page 17) holds empirically for the data!

Conversely, inputting $d\sigma/dt$ and ρ, (I.13) can be solved numerically. It is then seen, e.g., that for ISR energies, $\rho = 0.13$ is enough to make the dip disappear (see Figure I-11). As we've already remarked, these conclusions should be at least qualitatively valid at 100 GeV/c for pp elastic scattering; hence observation of a shallow dip there at $|\rho| = 0.10$ would lend some support to this.

Working with (I.13) and the π^-p elastic scattering data obtained in this experiment at 200 GeV/c, Kroll[52] claims that generalized G.S. works in this interaction at this energy. (Again, $d\sigma/dt$ at only this "s"

---

*$\phi(\tau_D) = 0$ is, in fact, shown by a comparison of experiment with G.S. in ref. 50.

needed.) Transforming to b-space he has extracted the πp eikonal at 200 GeV/c and compared it with the pp eikonal at p_{lab} = 1480 GeV/c. The results of this indicate universality in that

$$\text{Im } \chi_{\pi N}(b/R_{\pi N}) = \lambda \text{ Im } \chi_{pp}(b/R_{pp}), \quad \chi = \text{eikonal} \qquad (I.15)$$

with $\lambda = 0.643$ and $R_{\pi N}/R_{pp}(1480 \text{ GeV}) \approx 0.89$. Note how close λ is to 2/3 (naive quark model).

After subtracting the nondiffractive component* (since the energy is so low) Kroll has attempted to predict the cross section for $\bar{p}p$ elastic scattering at 50 GeV/c from the pp cross section at 1480 GeV/c by this method. He finds[52] $\lambda = 0.95$, $R_{\bar{p}p}/R_{pp}(1480) = 1.08$, $\rho = -0.02$. The value of ρ found is in very agreement with experiment and the predicted $d\sigma/dt(\bar{p}p)$ agrees very well with the CERN data[18] out to $-t = 5$ (limit of measurement); see Figure I-16). The uncertainty in the non-diffractive component would make such a test more telling, however, in the comparison of a prediction for elastic $\bar{p}p$ at 100 or 200 GeV/c with solid data.

As predicted by naive G.S., σ_{el}/σ_{tot} is independent of energy (for s large enough); however, it is different for pp, πp, and Kp. Barger, Luthe and Phillips[53] have investigated generalized G.S. prescriptions that unify all of these processes. For example, one could try $h_{el}(s,b) = \eta\, h_{el}(b/R)$ where η might depend on s. Then equations (I.10) would have to be modified (e.g., in this case $\sigma_{el}/\sigma_{tot} \sim \bar{\eta}$). However, as reference 53 points out, there is no reason why this kind of scaling is more sacred for $h_{el}(s,b)$ than for $\chi(s,b)$, $G_{in}(s,b)$, or the unabsorbed overlap function function. [With the presence of η these are not all equivalent as they are for "naive" G.S."--beyond $-t = 1$ there are very

*By assuming it is Regge-like with a straight line trajectory.

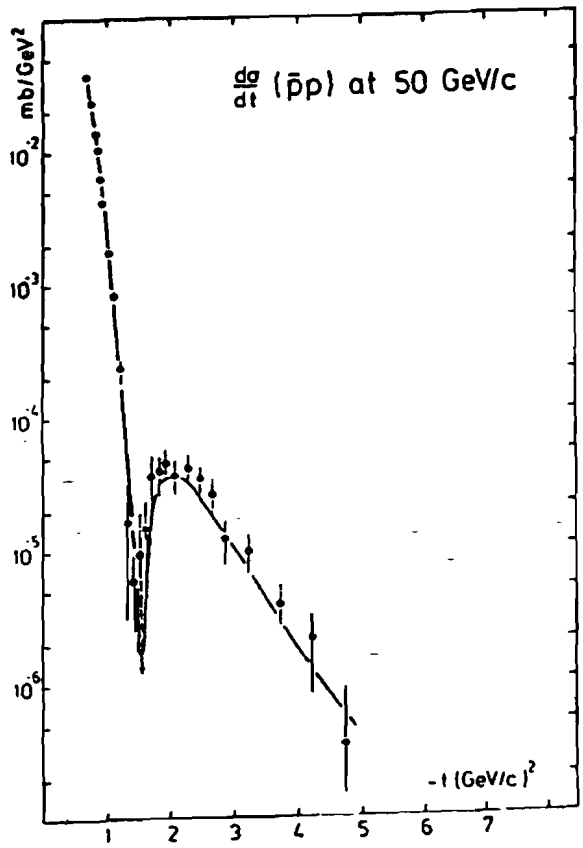

Figure I-16. Kroll's G.S. prediction/fit for $\bar{p}p$ at 50 GeV/c compared with data (figure from ref. 52).

significant differences.] In fact, scaling χ on the unabsorbed overlap function (UOF) has theoretical advantages in preserving unitary and including absorption corrections.[53] Indeed, scaling the UOF predicts a dip in both πp and Kp elastic scattering at $-t \approx 3.8$ (GeV/c)^2 for 200 GeV/c, in agreement with our 200 GeV/c $\pi^- p$ data. A comparison with this data has not previously made yet, though.

In the future people will be able to make searching tests of the geometrical scaling hypothesis over a very broad energy range. For example, naive G.S. predicts that $G_{in}(b)$ will broaden without growing at small b for very high energies, in marked contrast to some other models.[54] Also, G.S. predicts[54] that at values of σ_{tot} approaching 60 mb, the famous $-t = 1.4$ GeV/c dip in pp elastic scattering will have practically disappeared. This is the situation envisioned for CERN collider energies $\sqrt{s} = 540$ and is due to the fact that dispersion relations predict[55] that ρ_{pp} must reach a maximum at $\sqrt{s} \sim 800$ GeV. However, for Fermilab collider energies ($\sqrt{s} \sim 2000$ GeV) the situation may be very different since as we've already remarked by that energy ρ might approach zero. The differential equation (I.13) must be solved for that energy.

5. Optical Model with Constituents

a. Introduction

We shall initially discuss the scattering problem with an optical model expansion that "explains" elastic hadron-hadron collision in terms of absorptive collisions of constituents. It is seen that one can get good results with this over a broad range of -t with a minimum of free parameters. The basic idea is to fix these parameters by comparison with

the low -t data ($t \leq 0.9$ GeV/c) and then predict the mid- and high -t ($t \geq 0.9$ GeV/c) data solely from these already fixed parameters. The question of exactly how many parameters are needed for what quality of fit is discussed. It will be seen that the results are probably not "trivial".

Perhaps somewhat surprisingly the best (assuming the proton form factors used are "correct") results for pp elastic scattering obtain when one assumes that the proton is made of <u>three</u> constituents. (This naturally raises the question of what happened to the gluons, etc.). One can also, as will be seen, use the expansion to make estimates of the sizes of constituents.

The next step would probably be a comprehensive field theory approach. QCD seems to be successful in explaining some general features of pp elastic scattering for $q^2 \geq 7$ $(\text{GeV/c})^2$. However, attempts to extend "pure" QCD back to the dip region have not yet met with much success (due to the preturbative nature of the approach). Attempts have been made (e.g., by Alan White and collaborators) to combine QCD with RFT and predict the mid -t behavior from that. These attempts seem to look promising.

In any case, however, it seems to the author that to date the best non-trivial fits in the mid -t region (the region of our experiment) have been obtained with optical models of the sort discussed here. As we mentioned, perhaps they will serve as a guide in the application of QCD to mid and low -t elastic scattering.

b. <u>Motivation for and Derivation of Glauber Expansion</u>

A method for handling the scattering of composite hadrons from each other is based on the so-called "Glauber expansion", the essence of which

was first proposed a generation ago[56] to explain the fact that (the then high energy) total cross sections of protons on deuterons are noticeably smaller than the sum of $\sigma_{tot}(pp)$ and $\sigma_{tot}(pN)$. (The explanation was that this is due to the quantum mechanical analogue of "eclipses" of one constituent of d by the other.) These expansions are usually derived with a fair amount of formalism[57]; however, by bearing in mind the physical meaning of the form factor of a hadron, we would like to present here a much simpler heuristic derivation. (In addition to the simplicity, this derivation allows one to largely bypass arguments depending on wavefunctions, and thus perhaps has some relativistic validity.)

Let us first suppose that the scattering of, e.g., hadron A with hadron B occurs only via the interaction of one constituent (constituent "i") in A with one constituent in B (constituent "j'"). Let $t_{q_i,q_{j'}}(\vec{q})$ be the amplitude for this scattering to occur with the exchange of transverse momentum $\vec{q}$. Let $f_{A,(B)}(\vec{q})$ be the form factor of hadron A,(B). Then $f_{A,(B)}(\vec{q})$ is the amplitude for the composite hadron to absorb $\vec{q}$ and remain intact. Thus, the amplitude for the two hadrons to scatter elastically must be

$$T_{fi}^{(1)}(q) = \sum_{i=1}^{N_A} \sum_{j'=1}^{N_B} \left\{ \begin{array}{c} \text{amplitude for} \\ \text{scattering between} \\ \text{constituents i and j'} \end{array} \right\} \times$$

$$\times \left\{ \begin{array}{c} \text{amplitude for} \\ \text{hadron A to} \\ \text{hang together} \\ \text{after releasing q} \end{array} \right\} \times \left\{ \begin{array}{c} \text{amplitude for} \\ \text{hadron B to} \\ \text{hang together} \\ \text{after absorbing q} \end{array} \right\},$$

where $N_A(N_B)$ is the number of constituents in hadron A(B), i.e.,

$$T_{fi}^{(1)}(q) = \sum_{i,j'} t_{q_i q_{j'}}(q) f_A(q) f_B(b) \qquad \text{(I.16)}$$

Consider, now, second order scattering. This involves exchanges $\vec{q}_1$ and $\vec{q}_2$ (see Figure I-17) where we must integrate over all $\vec{q}_1,\vec{q}_2$ subject to $\vec{q}_1 + \vec{q}_2 = \vec{q}$. Let $S_{A,ik}(q_1,q_2)$ be the amplitude for hadron A to hang together after absorbing (separately) $\vec{q}_1$ and $\vec{q}_2$ ("generalized form factor"[58]). There are two "types" of second order terms and 18 ways (clear from Figure I-17c) (for pp scattering) that each type of second order term can be achieved. Therefore, applying logic exactly analogous to that used above, it is clear what the form of the second order contributions is. In fact, it is then clear (except for constant factors like $\sqrt{\pi}$'s, etc.) that for p-p elastic scattering the entire series is (modulo a factor of k or so):

$$
\begin{aligned}
T_{fi}(q^2) = {} & 9t_{qq}(q^2)S_N^2(q,0,0) \\
& + \frac{2i}{4\pi}\int dq_1 d^2q_2 \delta^2(\vec{q}-\vec{q}_1-\vec{q}_2)t(q_1)t(q_2)\ \ 18S_N^2(q_1,q_2,0) \\
& \qquad + 18S_N(q,0,0)S_N(q_1,q_2,0) \\
& + \frac{(2i)^2}{4\pi}\int dq_1 d^2q_2 d^2q_3 \delta^2(\vec{q}-\vec{q}_1-\vec{q}_2-\vec{q}_3)t(q_1)t(q_2)t(q_3) \\
& \quad 6S_N^2(q_1,q_2,q_3) + 36S_N(q_1,q_2,q_3)S_N(q_1+q_2,q_3,0) \\
& \qquad + 36S_N(q_1+q_2,q_3,0)S_N(q_1,q_2+q_3,0) \\
& \qquad + 6S_N(q,0,0)S_N(q_1,q_2,q_3) \\
& \qquad + \text{4th and higher orders} \qquad\qquad (I.17)
\end{aligned}
$$

(where $S_N(q,0,0) \equiv f_N(\vec{q})$, N ≡ nucleon).

This is the basic modern form of the Glauber expansion. Part of the connection between this and the diffraction models can be made by noting that the multiplicative property of the transmission factor S implies (since $\Gamma(b) = 1 - S(b)$)

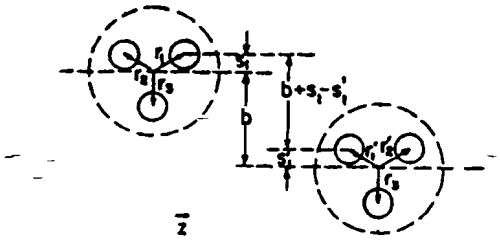

(a)

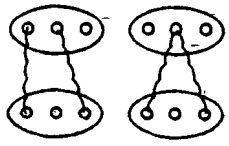

(b)

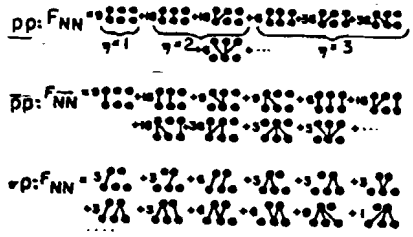

(c)

Figure I-17. (a) Collision of two composite protons. $\{s_i, s_i'\}$ are projections of $\{r_i, r_{j'}\}$ into plane perpendicular to z-axis.

(b) Two types of second order scattering terms. Wavy lines are not necessarily single gluons. There are 18 terms of the first type and 18 of the second.

(c) Diagrams representing the multiple-scattering expansions for the NN, $\bar{N}\bar{N}$, and πN scattering amplitudes. The integers indicate the number of equivalent terms of a given type.

$$\Gamma_{tot}(b,r_1,r_2,r_3,r_1',r_2',r_3') = 1 - \prod_i \prod_{j'} [1 - \Gamma_{ij'}(b + s_i - s_{j'})] \quad (I.18)$$

(refer to Figure I.17) where $\Gamma_{ij'}(b + s_i - s_{j'})$ is the profile function for (a partially absorptive) "collision" between constituents i and j'. Then we must have

$$t_{q_i,q_{j'}}(q) = \frac{i}{2\pi}\int d^2b\, e^{iq\cdot b}\, \Gamma_{ij}(b) \quad (I.19)$$

By expanding out Equation (I.18), the reader may easily convince him/herself that there are a total of nine "orders" for baryon-baryon scattering (and six for meson-baryon scattering)*. Thus, an alternative form for the series is

$$T_{fi}(q^2) \equiv \frac{i}{2\pi}\int e^{iq\cdot b}\left[\sum_{(ij)} \Gamma_{ij}(b + s_i - s_{j'}) - \sum \Gamma\Gamma + \sum \Gamma\Gamma\Gamma - \ldots\right] \quad (I.20)$$

c. Some First Order Results and Comparison to Data. First Order Estimates of Sizes of Constituents.

Let us now look at just the single scattering term (Equation (I.16). The hope is that this is all that is necessary to explain the forward peaks. The connection with the conjecture of Wu and Yang (see Figure I-3) that elastic p-p cross sections should go like $f_p^4(q^2)$ can be easily seen.

Let us see how good the first order approximation is. At $-t \approx 0.5$ $(GeV/c)^2$, for example, the dipole formula is locally falling like $e^{1.65t}$, which implies that $f_p^4(q^2) \sim e^{6.6t}$. At 200 GeV/c, the local exponential slope b(t=0.5) is observed to be about 9.5 $(GeV/c)^{-2}$. At $-t = 0.03$ $(GeV/c)^2$, the local dipole behavior is like $e^{2.8t}$. This is easy to see because at $t = 0$ the dipole must be locally approximable

*If one assumes three constituents in a baryon and two in a meson.

by $f_p(t) = e^{1/6\langle r^2\rangle t}$. $\langle r^2\rangle = (0.8f)^2$ gives $\frac{1}{6}\langle r^2\rangle = 2.8$ GeV^{-2}. Then $f_p^4(z \ 0.03) \sim e^{11.2t}$. Experimentally, at 200 GeV/c, $b(t \approx 0.03) \approx 12$ GeV^{-2}. Thus, suppose we take $t_{qq}(q^2) = Ae^{-\frac{1}{8}aq^2}$. Then

$$T_{fi}^{(1)}(t) \sim e^{1/2(a + 2/3\langle r^2\rangle)t}$$

or

$$a \approx 1.6 \text{ (GeV/c}^{-2} << \langle r^2\rangle \approx 16.5 \text{ (GeV/c)}^{-2}$$

Hence, in the framework of "single order scattering only" almost all of $d\sigma/dt$ is "form factor scattering"--the constituent-constituent amplitude is relatively flat. This corresponds loosely to the adage that at low q^2 one tends to scatter from the hadron as a whole. That $a << \langle r^2\rangle$ tells us that the constituent (dressed quark) is probably relatively small in size compared to a hadron* (since the q-q central maximum is so broad). Thus already hadron-hadron elastic scattering provides a result not inconsistent with a famous result of inelastic electron-proton scattering. This result is also, of course, qualitatively consistent with the Chou-Yang model, which is just a Glauber expansion with an infinite number of pointlike constituents (partons) for which $a = 0$ (as we have already mentioned). (As $a \to 0$, the "grey disk" approach becomes more and more valid.) (In particular, f_p^4 corresponds to the first order Chou-Yang terms.

We would then like to be able to say that the nonzero value of "a" found above indicates that the Glauber expansion with a non-flat t_{qq} is a better fit to the low $|t|$ data than the Chou-Yang model. Calculation shows (or see Byers[23]) that the ratio of the full Chou-Yang amplitude to

*A similar conclusion with a similar argument at low energy has been reached by Wakaizumi.[59]

the first order Chou-Yang amplitude is about 23% at t = 0, about 27% at $-t = 0.1$ (GeV/c)^2, and over 60% at $-t = 0.5$ (GeV/c)^2. Also, the multiple scaetering corrections in the Glauber expansion seem to be ~10-15% at $-t \to 0$. Therefore, without doing a more careful analysis we cannot favor one model over the other on the basis of low |t| data alone. However, if we take the value of "a" that we found (probably over-seriously, we note that it would correspond to a (dressed) quark radius of about 0.35 fermi.*

To some extent a more careful analysis than ours above has been done in conjunction with a series of two experiments carried out at Fermilab with the "single arm spectrometer" using a previous version of our "M6" (see Chapter II) beam line. However, this analysis also suffers from excluding the higher order terms.

In the first experiment[28], two fits, $\frac{d\sigma}{dt}^{\text{"exp"}} \sim e^{Bt+Ct^2}$ and $\frac{d\sigma}{dt}^{\text{"ff"}} \sim G_a^2 G_p^2 e^{ut}$ were applied to elastic scattering data at 200 GeV/c in the range $0.01 < -t < 0.36$ (GeV/c)^2. (Here G_p is the dipole form factor of the proton and G_a is the (electromagnetic) form factor of the projectile.) The "exp" fit was good (χ^2/d.o.f. = 1.09 for 97 d.o.f. for pp scattering); however, B and C were found to depend on the subrange of t used (i.e., the curvature in the exponential slope is <u>not</u> constant).

However, with a comparable χ^2/d.o.f. (1.02 for 112 d.o.f.), the "ff" fit fit well all six ($\pi^{\pm}p$, $K^{\pm}p$, $p^{\pm}p$) hadronic reactions at once with a single value of u which was insensitive to the subrange of t. (u was

---

*I have simply used the "grey disc formula" $R = \sqrt{2a}$, which is applicable to a Gaussian (in q^2) "t_{qq}".

found to be 1.839±0.049 GeV^{-2} (compared to our estimate of 1.6 GeV^{-2}). This provides a powerful indication that the first order Glauber term follows the observed curvature of the low -t exponential slope very well. It is also a good indication that at low q^2 the matter and charge form factors of the proton are identical.

In the second experiment[60], $\frac{d\sigma}{dt} = G_a^2 G_p^2 |t_{qq}|^2$ was used as a fit, but with two different t_{qq}'s: $|t_{qq}^{\text{"exp"}}|^2 \propto e^{ut}$ and $|t_{qq}^{\text{"quad"}}|^2 \propto (1+ut/2)^2$. The range of this experiment was $0.025 < -t < 0.620$ (GeV/c)^2 for p-p elastic scattering at 200 GeV/c. It was found that over this entire "curvature range" the quadratic form worked very well. In this fit, $\langle r_p \rangle$ in the dipole formula was allowed to vary; the resulting fit $\langle r_p \rangle$ was found to be almost exactly the electromagnetic one ($\langle r_p \rangle_{\text{fit}} = (0.79 \pm 0.01)$ fm, χ^2/d.o.f. was 125/122).

Over a restricted range $0.025 < -t < 0.320$ (GeV/c)^2 the "exp" version gave good fits (78/78); however, the full range fits with the "exp" form were not as good (154/122) and $\langle r_p \rangle$ had to be about 10% lower than the electromagnetic value. Because of the great sensitivity to $\langle r_p \rangle$, constraining $\langle r_p \rangle$ to be 0.81 fm with the "exp" version gave a "quite poor" fit. These results seem to favor the quadratic fit; however, again one must tread carefully without a higher order calculation. (The uncertainty in $\langle r_p \rangle$ from electromagnetic scattering is also a potential problem in assessing these results.) To the best of my knowledge a multiple-order calculation with a quadratic t_{qq} has never been done; it should be.

Now we come back to another question--does one use the Sachs or Dirac form factor for the proton? [We remind the reader that the Sachs form factor is the familiar $G_M(t)/\mu$), usually parameterized by the dipole

formula. The Dirac form factor is $F_1(t) = (G_m(t)/\mu)(\frac{1 - \mu t/4M^2}{1 - t/4M^2})$. There is both some theoretical and some experimental evidence[61] supporting the use of $F_1(t)$. Also, the Chou-Yang model was originally proposed with $F_1(t)$.]

Using a preliminary version of the S.A.S. data referred to above, together with earlier S.A.S. data, Levin and Shekter[61] have obtained satisfactory fits to the total change of the exponential slope "b" between $-t = 0$ and $-t \approx 0.4$ $(GeV/c)^2$ for p-p elastic scattering at 100 GeV/c for both cases of proton form factor using an exponential type "t_{qq}" with an estimate of double scattering effects included. (They have also indicated that there may be a preference for using $F_1(t)$ to describe the difference between π-p and p-p elastic scattering; however, this conclusion is somewhat shaky.) Unfortunately they have not tried a "quadratic t_{qq}" fit. (At low $|t|$ there is not much difference between the Dirac and Sachs forms, but at high $|t|$ there is (recall $\mu_p = 2.74$).) It should also be noted that the value of "a" used in $|t_{qq}| \sim e^{-\frac{1}{2}aq^2}$ by Levin and Shekter has to be quite different depending on which form factor is used. This would also be quite noticeable at high $|t|$, then.

It has been proposed[9] that dressed constituents are small ($R < 0.3f$) and almost completely black. Let us investigate this possibility within the framework of hadron-hadron elastic scattering. If quarks were black, t_{qq} would be given by $A[J_1(\xi/2)/\xi/4]$ where $\xi = 2qR$, R = dressed quark radius. In that case, at low q^2, t_{qq} would behave like $e^{-q^2R^2/8}$. However, we have seen evidence that at low q^2, t_{qq} behaves like $e^{-\frac{1}{3}(1.6)q^2}$, using our estimate for "a". Equating these two expressions and solving for R, we find $R \approx 0.7$ fm. Therefore, from elastic scattering we can say

that if constituents are small (0.3 fm) they are not very black, and if they are completely black they are not so small. (Therefore we disagree with some of the conclusions of reference 9.)

d. An Interesting Comparison of a Higher Order Calculation with Low Energy Data Yields Improved Estimates of Sizes and Numbers of Constituents in a Proton

For $-t \geq 1$ (GeV/c)^2 it is essential to include the higher order terms in the Glauber expansion (see Equation (I.17)). For orders greater than first there are many such terms; fortunately, many of them are equal (see Figure I-17).

We now consider the results of some calculations through third order made by Schrauner, Benofy and Cho[57] (see Figure I-18).

(i) Quality of General Fit. Number of Constituents in Proton. Support for "Dressed Quark Model" of Hadrons

For the first calculation Schrauner, Benofy and Cho used the dipole form factor for the proton. For the quark-quark scattering amplitude they essentially took $t_{qq}(t) = Ae^{-\frac{1}{2}\xi q^2}$, where A is given by $\frac{\sigma_{tot}^{(pp)}}{4\pi} \cdot \frac{1}{q} \cdot (i-\rho)$ where $\rho = \frac{\text{Re } f(s,0)}{\text{Im } f(s,0)}$. Thus, in this model the absolute normalization is fixed and is not a parameter. The number of constituents in the proton was taken as three. ξ was allowed to have an imaginary part as well as a real part. The imaginary part of ξ has the effect of adding a t-dependence to the real part of the amplitude, and thus serves to adjust the depth of dips without changing their position. This was the only parameter in this calculation. Figure I-18a shows this one-parameter fit and is very impressive. It should be noted that at $p_{lab} \lesssim 100$ GeV/c, Im ξ must be relatively large to avoid dips at the points where the different orders interfere with each other.

Figure I-18 (from ref. 57)

(a) (page 77) Fit of Schrauner et al. to low energy pp data (third order calculation).

(b) (page 77) Dependence on Im ξ in the Schrauner et al. fit. The curves labeled -4, -7, and -13.0 $(GeV/c)^{-2}$ refer to values of Im ξ in the quark-quark amplitude.

(c) (page 78) Dependence of the Schrauner et al. fit on the number of constituents used for the proton in the calculation.

(d) (page 78) Dependence of the Schrauner et al. fit on the parameter "μ^2" in the dipole form factor. $\mu^2 = 0.71$ implies pointlike constituents, $\mu^2 > 0.71$ implies larger constituents (see text).

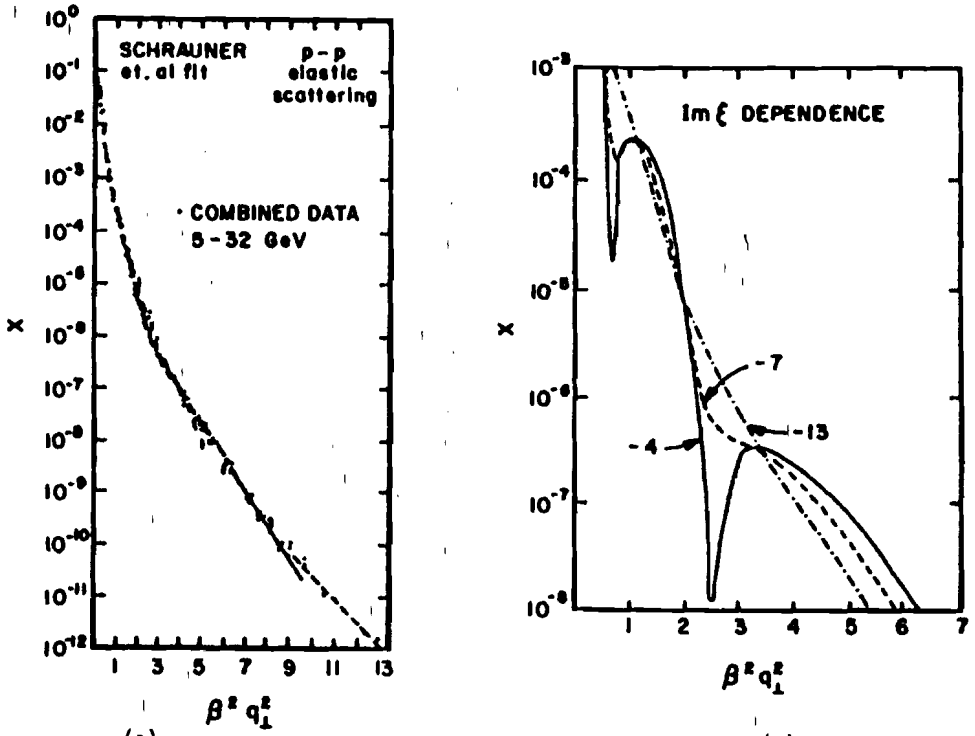
SCHRAUNER
et. al fit
p - p
elastic
scattering
· COMBINED DATA
5 - 32 GeV
X
$\beta^2 q_\perp^2$
(a)
Im ξ DEPENDENCE
-7
-13
-4
X
$\beta^2 q_\perp^2$
(b)

Figure I-18

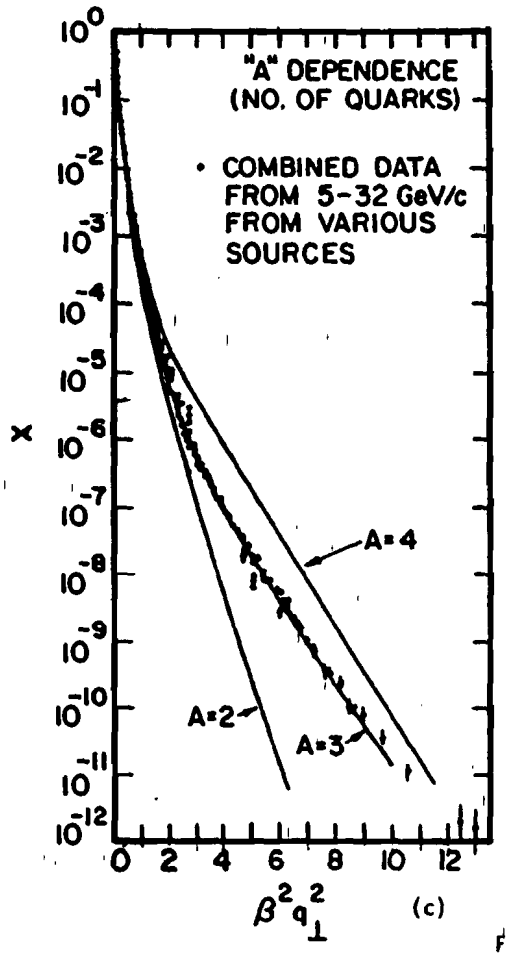

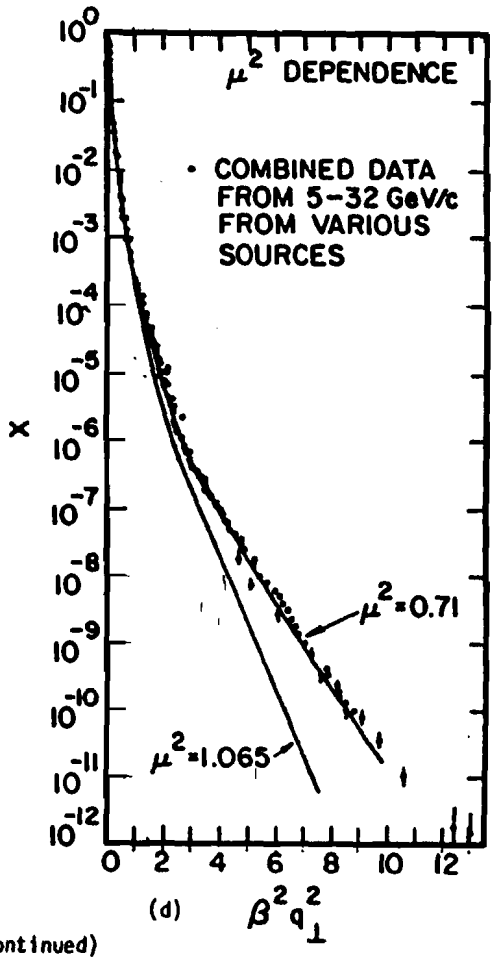

Figure 1-18 (continued)

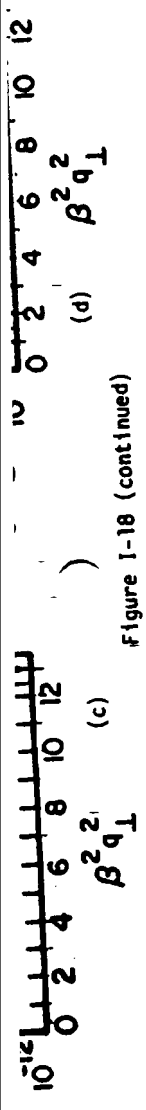

Figure I-18 (continued)

In Figure I-18c we see the results of a calculation where everything was the same but where the number of constituents in the proton was allowed to vary. We see that the model favors the proton to have three constituents. This, of course, seems to provide support for the static quark model. However, from several points of view it is somewhat surprising that these simple results obtain*:

Firstly, one wonders how to interpret these results in light of the inelastic e^-p results alluded to earlier. Here we do not see an infinite number of "partons" even at high q^2. This is probably related to the old problem of "constituent quarks" versus "current quarks". At one time, the Melosh transformations were proposed to make the connection. However, to some extent, modern QCD has "reversed" this problem and we discuss it no further here.

One also wonders what has happened to the gluons, which can also participate in the strong interaction. In the framework of this model, these elastic scattering results would seem to suggest that the gluon population in a hadron is somehow proportional to the number of valence quarks. This is by no means obvious in QCD for $q^2 \leq 10\ (\text{GeV}/c)^2$. One way out of this is to interpret these results as providing support for a model of a finite number of dressed valence quarks in a hadron. (The dressing can be glue or sea quarks.) We have thus far been using this point of view; we shall continue to use it for the time being.

(ii) The Radius of a Dressed Quark

α). Introduction

Can we use, then, the elastic scattering of hadrons to get a

---

*As is the case for many quark model predictions. However, this is at high q^2.

quantitative measure of the radius of a dressed quark? We have already remarked that our earlier "result" ($r \approx 0.35f$) should not be taken too seriously. This is because of the ambiguity (e.g., quadratic or exponential t_{qq}) at low $|t|$ and high energy. In fact, later it will be seen that there is doubt whether the Glauber series can be applied at all to elastic scattering at high energy for $t \lesssim 0.2$ $(GeV/c)^2$. Therefore it would be nice to have a higher q^2 measure of the dressed quark radius. Actually Schrauner had done something interesting along these lines long ago. However, in order to understand this we need to make another remark about "what form factor" belongs in the Glauber expansion. But this time we mean something different by the phrase "what form factor" than we did before.

β) The "Form Factor of a Dressed Quark"

Let $F(q)$ be the form factor of a hadron as measured, e.g., by electromagnetic scattering. Suppose a dressed quark has a finite radius. Let $F_Q(q)$ be the form factor that a hadron would display if it were composed of point quarks. Then it is not difficult to see that $F(q) = F_Q(q)f_H(q)$. Which form factor belongs in the expansion--$F(q)$ or $f_H(q)$?

A moment's reflection (or alternately, the realization that to first order T_{fi} must involve a relativistic generalization of $\int d^3r_i\, d^3r_j\, |\psi_A|^2 |\psi_B|^2 e^{-is_i\cdot q} e^{is_j\cdot q}$ where $\psi_{A,B}(\vec{r}_1,\vec{r}_2,\vec{r}_3)$ is the internal wave function of the quarks in hadron A,B) convinces one that the answer is $f_H(q)$. This is very interesting, for it means that if $F_Q(q)$ does not equal one, in order for the expansion to work it requires an input that is: a) unknown, and b) not given by the dipole formula. Yet the expansion works well with $f_H(q)$ given by the dipole formula. This is already another indication that the radius of a dressed quark must be very small

compared to the size of a hadron (since it implies $F_Q(q) \approx 1$).

Schrauner has parameterized $f_H(q^2)$ by $(1 + q^2/\mu^2)^{-2}$ with variable μ^2 and input this into the expansion. The results of this are shown in Figure I-18d. $\mu \approx 1$ corresponding to a quark radius $\sim 1/2$ proton radius is clearly eliminated. The results are consistent even with point-like quarks. This also, of course, provides support for the conjecture that the distributions of electricity and hadronic matter are similar in the hadron.

The reader may wonder why we are discussing the expansion at energies somewhat lower than those of our experiment. For one thing, the "variable μ^2" method of measuring the dressed quark radius has never been tried at high energy and high $|t|$. This should be done.

However, from the measurements at low $|t|$ and high energy, Schiz et al. state (from the "exponential" t_{qq} fit to pp elastic scattering) a dressed quark radius of about 0.48f. (We feel that this is subject to the same ambiguities we've already discussed.) However, they have also (probably unwittingly) provided evidence for smaller dressed quarks. This is because, as we recall, in their "quadratic fit" they found a great sensitivity to the value of $\langle r_p \rangle$ in the dipole formula and that the fit value of $\langle r_p \rangle$ was very close to the electromagnetic one. This is a low $|t|$ measurement, though.

e. A "Problem" in the Application of the Glauber Series at High Energy

There is another reason why we have shown relatively low energy Glauber series results. There is a problem at high energy. Its resolution is not completely clear, but is probably related to "confinement" in QCD.

The "problem" is that dips like to appear at the points where

successive orders become equal in magnitude and interfere. With the expansion of Eq. (I.17) the place where second order becomes equal to first is near $-t = 0.7$ (GeV/c)^2. (This is easy to see roughly by trying to fit $d\sigma/dt$ for $|t| \leq 0.2$ (GeV/c)^2 crudely with $\frac{d\sigma}{dt} = A_1 e^{b_1 t} + A_2 e^{b_2 t}$.) One can adjust the depth of this dip with Im ξ, even make it disappear, but one cannot move it out to, say, $-t = 1.4$. One way of phrasing this is to say that the multiple scattering terms are too strong to allow both σ_{tot} and the dip position to come out right.

Now let us backtrack briefly to the low $|t|$ results of Schiz et al. and note an "unclarity" that probably turns out to be related to this. We recall that no multiple scattering corrections were made there. Yet, based on other work[61-63] it is certainly plausible that multiple scattering effects should be observable (even in the slope) for $q^2 \leq 0.5$ (GeV/c)^2. But the single order Schiz et al. "quadratic t_{qq}" fit was very good voer the whole $q^2 \leq 0.6$ (GeV/c)^2 range. (This could be due to the accident that the quadratic t_{qq} is somehow simulating the multiple scattering effects to the "real" exponential t_{qq}; however, this is unlikely and later we shall mention more evidence that t_{qq} may really be quadratic)--and their statistics were very high (statistical errors in the local slope determinations were about 1%.) This could be for one of at least two possibilities:

(i) that the multiple scattering terms are somewhat suppressed at high energy, or

(ii) that at high energy the Glauber series does not apply for very low q^2. This could, e.g., be due to a low q^2 "threshold" for "confinement" effects to appear--i.e., that the "dressed"

quark model that we have been using breaks down at (high s and) low t due tothe presence of many gluons causing glue-glue scattering, etc. (which, recall, has not been included in the Glauber series so far.

Let us investigate possibility (i) first:

It has been shown that (within certain bounds) the form of the quark-quark scattering amplitude is not at fault. This means one perhaps should look to the form factor contributions for the source of trouble. The form factors come into the expansion formally by

$$f(q^2) = \frac{i}{2\pi}\int e^{iq\cdot b}\,\langle f|\Gamma_{tot}(b,\{s_i\},\{s_j,\})|i\rangle\, d^2b\,, \qquad (I.21)$$

where

$$\langle f|\Gamma_{tot}|i\rangle = \int d^2s_1^A\, d^2s_2^A \ldots d^2s_3^B D_A(\{s_i^A\})D_B(\{s_j^B\})\Gamma_{tot},$$

where Γ_{tot} is expanded as in (I.20); t_{qq} is pulled out using (I.19) and where $D_{A,B}$ is the quark density function in the impact parameter plane for hadron A,B. For $|t| \gtrsim 2$ (GeV/c)^2 it is crucial to include recoil corrections in D--this can change $\frac{d\sigma}{dt}$ by several orders of magnitude*.[62] But this correction does not solve the problem.

It turns out that a variety of distribution functions D will reproduce the dipole form factor for first order when plugged into (I.21).** So far, we have only discussed using a D with a weak correlation (a $\delta^2(\vec{s}_1+\vec{s}_2+\vec{s}_3)$ factor, e.g., for recoil correction) between the quarks. Yet, is is natural that repulsive short-range forces between them would reduce the

*This can be a simple factor $\delta^2(\vec{s}_1+\vec{s}_2+\vec{s}_3)$ in D. Interestingly, no recoil correction is necessary when the number of constituents goes to ∞ (as in Chou-Yang model).

**However, they affect the higher order terms differently.

multiple scattering contributions.[63] These could be either dynamical forces, or could be "fictitious forces" that occur due to something that we have left completely out of the problem.

One such something is the third dimension. Quarks in a hadron have longitudinal degrees of freedom. Van Hove and Fialkowski[64] have shown that these are important in inelastic diffraction. Work has been done[63] with a variety of density functions $D(\{s_i\})$ that introduce correlation between the transverse positions of quarks after integration over longitudinal degress of freedom, but which maintain the single quark distributions in transverse position (and thus give a dipole form factor). The results are that the dip can be moved out to about the right place but that beyond the dip the model still overestimates the cross section.

f. Phenomenological "Resolution" of the "Problem"

The preceding was the situation in early 1978. Now let us investigate possibility (ii) (page 82).

In 1978 Wakaizumi[65] apparently* noticed something interesting. This was that the dip moves out to about the right place and the multiple scattering terms are of about the right strength to fit the data beyond the dip if the Glauber expansion as given previously is fit only to the data beyond the region of the extremely steep first slopes (the "Carrigan region"). (Longitudinal correlations are ignored (this does not mean they are not important) at least explicitly.)

Let us investigate this result: That it is plausible is easy to see.

*Wakaizumi has indicated[66] that the inclusion of geometric scaling is responsible for this success. This is not so. Unfortunately, the true reason for the success and its implications seem buried in his paper.

The problem was that the experimental value of $\frac{d\sigma}{dt}$ at $t \to 0$ is too large for the expansion to extrapolate back to if the dip region and beyond is fit. However, the somewhat shallower exponential slope beyond the "Carrigan region" would extrapolate back to give a lesser $\frac{d\sigma}{dt}$ (t=0) than the experimental $\frac{d\sigma}{dt}$ (t=0). In that case the amplitude of t_{qq} [here $t_{qq}(q^2) = (i+\rho)\frac{1}{9}\frac{B_1}{4}e^{-\frac{1}{2}aq^2}$, where $\rho = \rho(s,0)$, "9" = 3^2 (no. constituents), $a \equiv a_R + ia_I$] does not have to be so strong to fit the data. Since higher orders involve more powers of t_{qq}, they are thus cut down relative to first order.

At this point one might object that the predicted dip could be moved out arbitrarily simply by "starting the series fit" at an arbitrary $|t| \leq 1.4$ $(GeV/c)^2$. This is not true because the exponential slope is observed to decrease only very slightly between $-t \approx 0.3$ and $-t \approx 0.8$ $(GeV/c)^2$--therefore the ratio of second to first order term strength would change only slightly by moving the "starting point" in this region (hence the position of the dip would only move slightly). For $-t \geq 0.8$ GeV/c, an increase in the exponential slope is observed until the dip is encountered. Thus it does not make much difference where in the range $0.3 \leq -t \leq 1.4$ $(GeV/c)^2$ the fit is started.

In fact, there are at least five features of the cross section that must be matched--the exponential slope at the "starting point" (SP) $\left.\frac{d\sigma}{dt}\right|_{SP}$, t_{dip}, $\left.\frac{d\sigma}{dt}\right|_{2nd\ max}$, exponential slope after second maximum--and only two parameters--B_1 and a (recall $t_{qq} \propto B_1 e^{-a/2\,q^2}$).

Actually, the freedom of choice of the starting point could theoretically be removed completely in two ways:

i) since the exponential slope decreases steadily for $0 \leq -t \leq 0.8$

$(GeV/c)^2$ (the increase being interpreted as due to sizeable interference with multiple scattering terms), $-t \approx 0.8\ (GeV/c)^2$ suggests itself as a natural starting point; or, more precisely by

ii) the addition of a term $T_0 = iB_0 e^{\frac{1}{2}b_0|t|}$ to the series to describe the steep slope at extremely low $|t|$ (and thus approximate σ_{tot}). (Then the starting point is $-t = 0$). With this method, if B_0 and b_0 are to be determined completely from data with $-t \leq 0.2\ (GeV/c)^2$ and if A_1 and a are determined completely from data with $-t \leq 0.9\ (GeV/c)^2$, the data with $-t \geq 0.9\ (GeV/c)^2$ would be completely (except, of course, for the real part of the amplitude) predicted in this model from the data below $|t| \approx 0.9\ (GeV/c)^2$. This would be very impressive regardless of how many parameters were needed to set the low $|t|$ data (in this case four). However, by sacrificing some quality on the low $|t|$ fit one could finagle slightly, e.g., the dip position. Wakaizumi has apparently done this to a certain extent but the results still seem impressive. The additional term could correspond to scattering off of the pion cloud of the nucleon[66], or could correspond to the physical explanation we have already offered for it in terms of glue-glue scattering at low q^2.

[Wakazumi's results for pp scattering are shown in Figure I-20.] [However, perhaps we should mention that it has been pointed out[62] that in order to have a sufficient amount of inelastic diffractive cross section, quarks should be essentially black at zero impact parameter. That is, if $\Gamma_{qq}(b) = \gamma(0)e^{-b^2/R^2}$ (where R is the diffractive radius of a quark) which corresponds to the choice of $t_{qq}(q^2)$ above, we should have $\gamma(0) \approx 1$. Thus there are really not two free parameters in t_{qq} as we said above--B_1 and a should be related. In fact, by combining the

Fourier transform definition of t_{qq} (eq.(I-19)) with the form used for t_{qq} (see page 85) we get $1/9\ B_1/4\pi = a$. Wakaizumi's values of B_1 and a seem to violate this.]

g. Results at High Energy

(i) Number of Constituents

In the approximation to the theory with Gaussian distribution functions D (this approximation is good enough out to about $-t = 3.5\ (\text{GeV/c})^2$ or so, at which place the Gaussian begins to underestimate the true form factor too severely) all orders of the expansion are exponential in -t. One obtains[65]

$$b_1 = a + \frac{N-1}{N}\langle r^2\rangle$$
$$b_2 = \frac{1}{2}\left(a + \frac{N-2}{N}\langle r^2\rangle\right), \quad a \equiv R_o^2 a^o, \tag{I.22}$$

for the slopes of the first two orders. ($\sqrt{\langle r^2\rangle}$ = r.m.s. distance of a constituent from center of hadron.)

Now, if the size of a constituent were comparable to the size of a hadron we would have $b_2 \sim \frac{1}{2} b_1$, which is <u>similar</u> to the Chou-Yang value.* Experimentally, at $\sqrt{s} = 53$ GeV, $b_2 \approx 0.2\ b_1$.** If constituents are small and widely distributed in a hadron $a << \langle r^2\rangle$, then $\frac{b_2}{b_1} = \frac{N-2}{2(N-1)}$. For $N = 3$ one gets $b_2/b_1 = \frac{1}{4}$, which is close enough to the data (see Figure I-19). Thus in a rough way one has corroborating independent evidence for earlier conclusions about the number of constituents in a hadron and the relative size of a constituent. We use the word independent

---

*Some authors have claimed that this is exact in the Chou-Yang model. That is wrong.

**At 200 GeV/c this seems to be somewhat less than $0.2\ b_1$.[67]

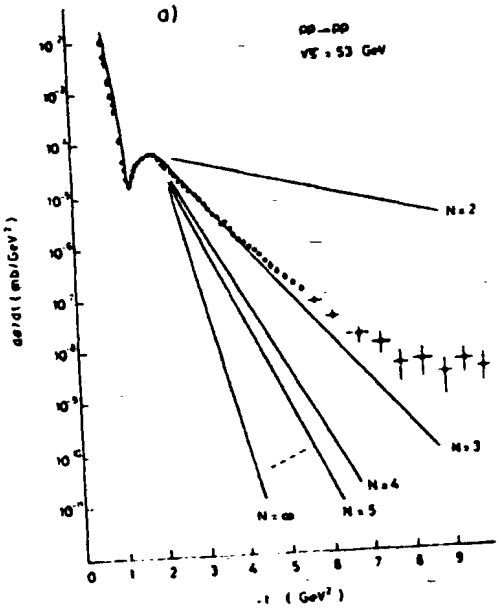

Figure I-19. Wakaizumi's results with the approximation of a Gaussian form factor and in the variable number of constituents for $\sqrt{s}$ = 53 GeV as compared to the early CERN data. N is the num-er of constituents. (See text.) (from ref. 65).

because, e.g., the earlier argument about the size of the constituents came only from the first exponential slope, whereas Wakaizumi's concerns the relationship of the slope after the dip to that before.

(ii) Results of Glauber Expansion pp Fits

Results of the model with more realistic form factors are shown in Figure 1.20. We see that p-p elastic scattering at $\sqrt{s}$ = 53 GeV is predicted remarkably well out to about $-t = 4.5$ $(GeV/c)^2$. The first dip occurs at $-t = 1.37$ $(GeV/c)^2$, which compares well with the experimental value[68] $t_{min} = -(1.34 \pm 0.02)$ $(GeV/c)^2$. The exponential slope of the second peak after the dip is predicted to be 2.13 $(GeV/c)^{-2}$ for $2.55 \leq |t| \leq 4.6$ $(GeV/c)^2$, which is reasonable compared with the experimental value of $b_2 = (1.81 \pm 0.02)$ $(GeV/c)^{-2}$. A shoulder is predicted near $-t = 7$ $(GeV/c)^2$, this agrees qualitatively (but not quantitatively) with the data.

The relatively gentle second slope b_2 is a big improvement over the Chou-Yang model. As a function of energy both the shrinkage of the forward peak and the use in $d\sigma/dt$ at the second maximum are well predicted, through this is probably mostly forced by the geometrical scaling incorporated into the model. Wakaizumi has not attempted to include any of the schemes in which the energy dependence of the real part of the amplitude at the dip can be predicted; as a result "ρ" and "ξ_I" must be adjusted at each energy to fit the experimental values of ρ and the depth of the first dip. This, however, could be "fixed" in the future.

It should also be mentioned that there are several more parameters in this version of the model than are "really necessary". For example, in an effort to predict the proton form factor, a modified dipole

Gaussian
tuents
ta. N
om ref. 65).

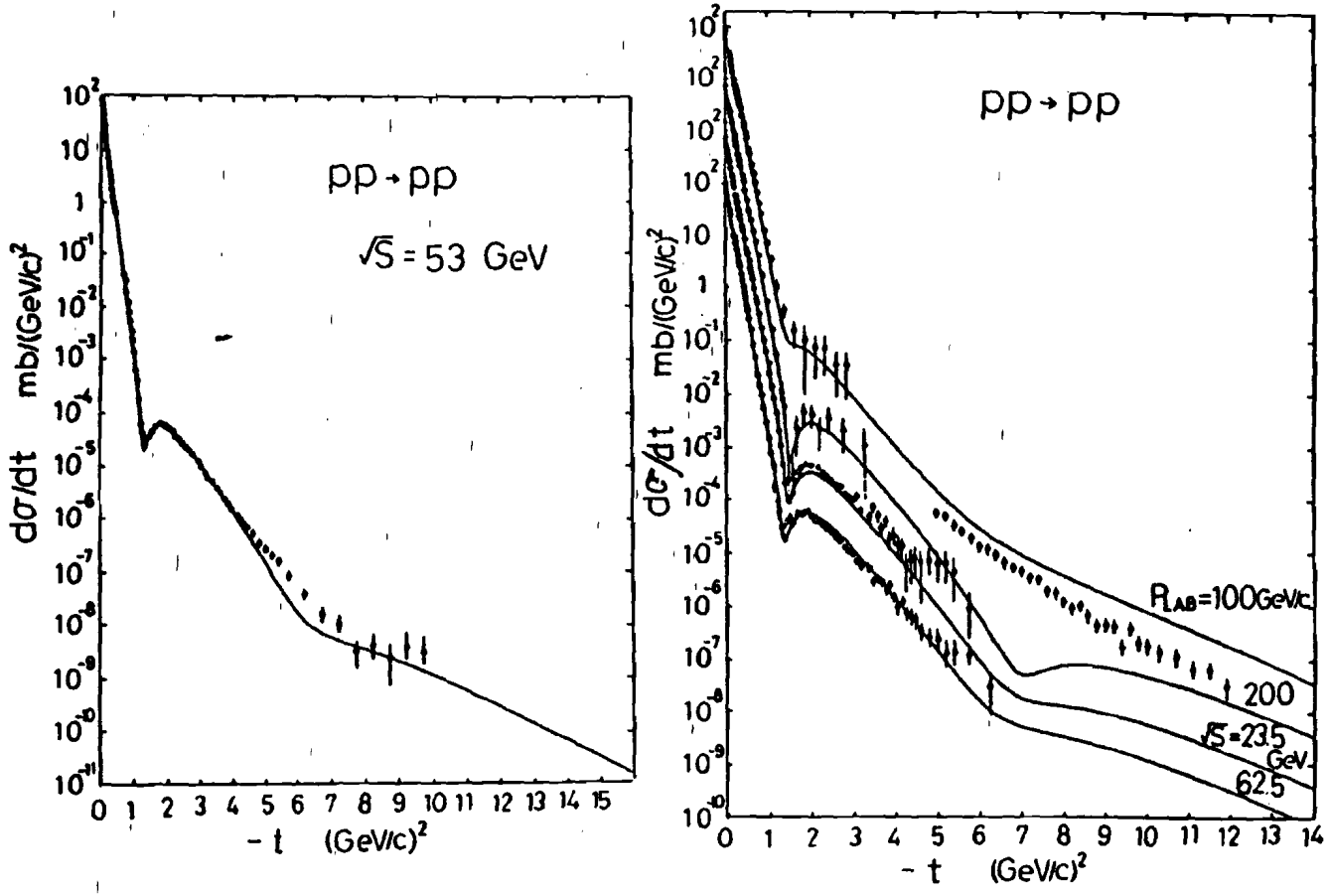

Figure I-20. Wakaizumi's pp results (from ref. 65).

parametrization $f_\pi(t) = [(1-t/\mu_1^2)(1-t/\mu_2^2)]$ is used. The values of μ_1 and μ_2 found bring this form factor close to that found by electron scattering techniques; however, it would be of interest to see how the quality of the fit is changed if one does an "honest" calculation, with, e.g., the three pole formula mentioned earlier. (Still, these comments should not be taken to negate the successes of the model at $\sqrt{s}$ = 53 GeV.

At p_{lab} = 200 GeV/c for p-p the model starts to fail beyond $-t \approx 2$ (GeV/c)^2. An unobserved dip for p_L = 200 GeV/c is predicted near $-t = 7$ (GeV/c)^2. For Isabelle energies ($\sqrt{s}$ = 800 GeV) it is predicted that the first dip almost disappears and a sharp second dip comes in again (it had been predicted to disappear at ISR energies) at about $-t = 5.5 - 6$ (GeV/c)^2. This is in contrast to the Chou-Yang and Lo-Clarke (Current Current Chou-Yang) models which put the second dip at about $-t = 4$ (GeV/c)^2 and $-t = 3.2$ (GeV/c)^2 respectively for this energy with the Shaw form factor.

Unfortunately, we cannot take any of Wakaizumi's predictions beyond $-t \approx 4$ (GeV/c)^2 seriously anyway. This is because he has only included terms through third order in his calculations. It has been stressed by several authors[74] that at least a fifth order calculation is necessary for the range up to $|t| = 8$ (GeV/c)^2. Notice how the cross section is always underestimated at high $|t|$ (especially serious at p_L = 200 GeV/c). Wakaizumi wonders if this is due to an inconsistency in the assumptions. We feel that part of the problem at p_L = 100 and 200 GeV/c may be due to a still significant non-diffractive component at high $|t|$ more important at 100 GeV/c) and part is due to an incomplete calculation. This is especially important when one realizes that the (dominant) imaginary parts

Figure I-20. Wakaizumi's pp results (from ref. 65).

of successive orders have opposite signs. Thus the "dip" at $-t \approx 7$ $(GeV/c)^2$ in the 200 GeV/c calculation must be due to a partial cancellation of second and third orders (and can be filled in by fourth). Wakaizumi has used analytic formulas for each order of the amplitude and has truncated the series due to the great length of the analytic fourth order formula. Actually, with a modern computes such as the CYBER 175 at Fermilab all nine orders of $\bar{p}p$ scattering could be done at once by numerically integrating equation (I.17).

(iii) $\bar{p}p$ Results and a πp Prediction

Using the same form factors and quark-quark scattering amplitudes as in the p-p case (except for adjusting to the larger σ_{tot} and the experimental value of ρ and tuning the dip depth slightly) Wakaizumi has used his model[69] to make a prediction for $\bar{p}p$ scattering--this is shown fit to the data for $p_L = 50$ GeV/c in Figure I.21. Also shown at the $p_L = 200$ GeV/c and $\sqrt{s} = 540$ GeV predictions. As these calculations are "third order" the remarks made above for pp apply here, too.

Wakaizumi has also made a π-p elastic scattering prediction for $p_L = 200$ GeV/c. Taking two constituents for the pion seems to give the best fit for $|t| \leq 2$ $(GeV/c)^2$. However, for $|t| \geq 2$ (GeV/c we take this calculation even less seriously than the above because the pi form factor is severely underestimated. This is unfortunate because a successful πp calculation with t_{qq} determined from p-p scattering would be a very impressive verification of the model. However, people have difficulties with the pion[70] and πp elastic scattering may prove a very tough nut to crack theoretically.

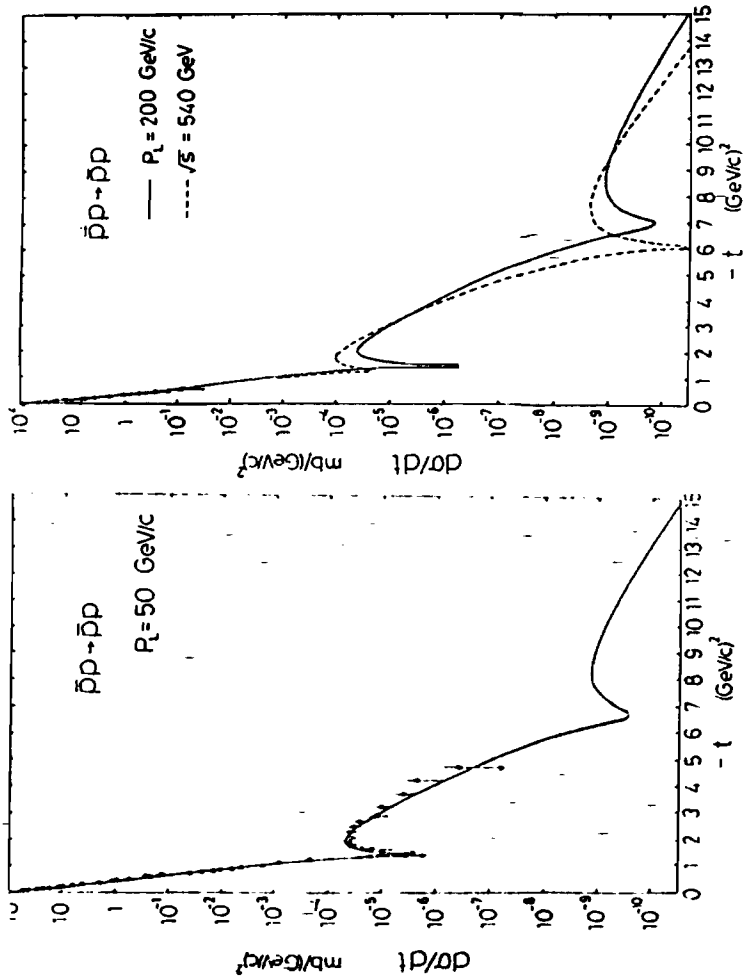

Figure I-21. Wakaizumi's $\bar{p}p \to \bar{p}p$ results (from ref. 69).

(iv) Motivation and Results for Another High Energy pp Glauber Calculation

It has been shown[71] that the Lorentz invariant four dimensional wave function*

$$\psi(r,s;p) = \left(\frac{3}{\pi\langle r_c\rangle}\right)^2 \exp\left\{\frac{3}{2\langle r_c\rangle^2}\left[r^2+s^2-\frac{2}{M^2}(p\cdot r)^2-\frac{2}{M^2}(p\cdot s)^2\right]\right\} \qquad (I.23)$$

used in conjunction with the relativistic overlap integral

$$W_R = \iint \psi^*(r,s;p_f)e^{iq\cdot(ar+bs)}\psi(r,s,p_i)d^4r\,d^4s \qquad (I.24)$$

With proper values for a, b and $\langle r_c\rangle$ gives W_R almost exactly equal to the dipole formula $G_D(q^2)$ for $q^2 \approx 7$ (GeV/c)^2 (and provides a better fit to e^-p data than $G_D(q^2)$ for $q^2 \geq 7$ (GeV/c)^2. When one plugs (I.23) into (I.24), the result is

$$W_R = \left(\frac{1}{\sqrt{\Gamma}}\right)^4 e^{-1/6\langle r^2\rangle_c \Gamma^{-1}|t|} \qquad (I.25)$$

Since Γ is a Lorentz contraction factor in $|t|$, the physical meaning is that Lorentz contraction of a nucleon core with a (4-dimensional) Gaussian relative wave function can be viewed as the "cause" of the dipole formula. $\sqrt{\langle r^2\rangle_c}$ is the "core radius". Using a value for $\sqrt{\langle r_c\rangle^2}$ determined from the slope of the experimental proton form factor at low $|t|$, and fitting three parameters, Goloskokov and collaborators[72] did a fifth order calculation in 1979 using (I.25) for the proton form factor. They claim that the use of this form provides theoretical advantages over earlier work

*Here the three quarks have position 4-vectors x_1, x_2, x_3. There are three independent coordinates $R = \frac{x_1+x_2+x_3}{3}$ (c.m.), and two relative coordinates "r" $= (x_2-x_3)/\sqrt{6}$ and "s" $= (-2x_1+x_2+x_3)/3\sqrt{2}$. p is the c.o.m. (i.e., hadron) momentum. $\Gamma \equiv 1 + |t|/2M^2$ ($M=M_p$). $\langle r_c\rangle$ is the "core radius".

(e.g., Wakaizumi) in that it allows ...orentz contraction of the constituent distribution longitudinally ... takes into account recoil. This, however, is not true--since (I.25) is ...ential equal to $G_D(q^2)$, any Lorentz contraction in this work is al... ...resent in Wakaizumi's.

In 1981 Kuleshov et al.[73] extend... ...his work by performing a full ninth order calculations leading to t... ...esults shown in Figure I- 22. (Unfortunately, they did not do calcula... ...s for p_L = 100 GeV/c and 200 GeV/c, so the previous discussion abou... ...ose energies still holds.) They use a slightly more general form (...3) which leads to the two pole form factor

$$F(t) = \gamma(t) e^{-\frac{1}{6}\langle r_c \rangle^2 \gamma_1(t)\cdot|t|}, \qquad \gamma(t) = \gamma_1(t)\cdot\gamma_2(t),$$

$$\gamma_1(t) = \left[1 - \frac{\lambda t}{2M^2}\right]^{-1}, \qquad \gamma_2(t) = \left[1 - \frac{\lambda}{2\lambda-1}\frac{t}{2m^2}\right]^{-1}$$

with λ as a "fine-tune" parameter. This ...s very similar to the form Wakaizumi used. Using $T_{qq}(s,t) = \frac{i}{4\pi}[\alpha(s) + i\beta(s)]e^{b(s)t}$, b real, they find

$$\left.\begin{aligned}
\alpha(s) &= (12.64\pm0.55)+(1.03\pm0.30)\ln\frac{\sqrt{s}}{\sqrt{s_0}}\ (\mathrm{GeV/c})^{-2} \\
\beta(s) &= (-0.751\pm0.040)+(1.54\pm0.30)\ln\frac{\sqrt{s}}{\sqrt{s'}}\ (\mathrm{GeV/c})^{-2} \\
b(s) &= (0.250\pm0.025)+(0.175\pm0.023)\ln\frac{\sqrt{s}}{\sqrt{s_0}}\ (\mathrm{GeV/c})^{-2}
\end{aligned}\right\}
\begin{aligned}
&\sqrt{s_0} = 52.8\ \mathrm{GeV/c} \\
&\sqrt{s'} = (28.49\pm1.55)\ \mathrm{GeV} \\
&a = 0.71(\mathrm{GeV/c})^{-2}\pm0.04 \\
&\lambda = 0.84\pm0.05
\end{aligned}$$

Wakaizumi, on the other hand, builds geometrical scaling into his model, with consistent results.[1]

Figure I-22. Fits of the Glauber expansion with the Lorentz contracted form factor (I.25) to pp elastic scattering by Kuleshov et al. Numbers on curves indicate c.m. energies. Data are from ISR as explained in text. Note that the fits "start" at $|t| \sim 0.8$ GeV/c; thus they are no more capable of fitting full range $|t|$ with Glauber expansion than was Wakaizumi. (Figure taken from ref. 73.)

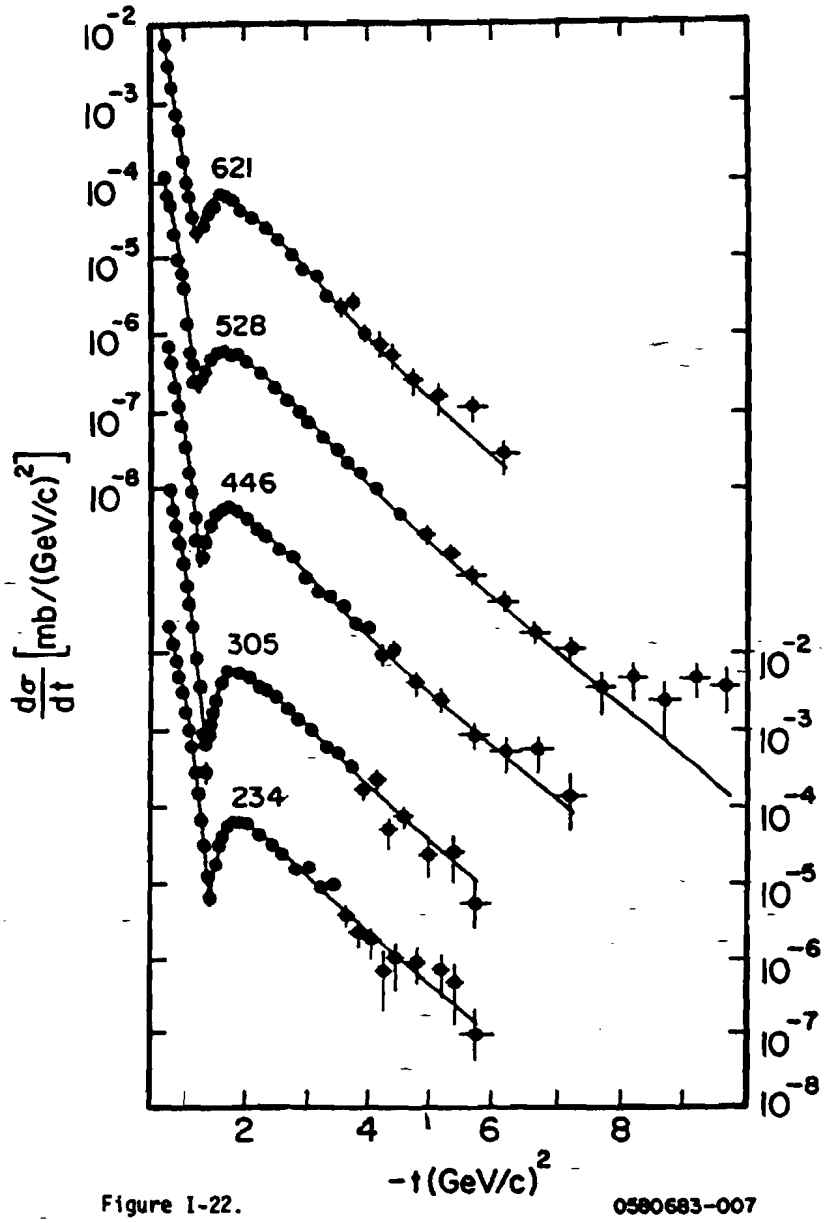

Figure I-22.

0580683-007

h. Some Thoughts About These Results

In view of possible theoretical ambiguity in Wakaizumi's "fix", we would like to mention that in the "quadratic t_{qq}" of Schiz et al., $|t_{qq}(q^2)|^2 = (1+ut/2)^2$, a value of $u \approx 1.6$ $(GeV/c)^{-2}$ was found to fit the low $|t|$ data. Schiz points out that this expression for t_{qq} goes to zero at $-t \approx 1.2$ $(GeV/c)^2$, and that this is near the experimentally observed dip. Here, then, we would like to remark that the use of this expression in a high $|t|$ expansion would provide a very natural method of moving the dip out in the right direction without the need for extra "T_o" terms or nonzero "starting points". There would still have to be slight tinkering to get the dip position right--since all Glauber terms have t_{qq}, they would all be zero at $-t \approx 1.2$ $(GeV/c)^2$. However, using $u \approx 1.49$ (which gets the dip about right) shouldn't mess up the extreme-low $|t|$ fit too much. It is a pity no one's tried this.

We now ask, "Are Wakaizumi's "fix" and the fits of Schiz et al. mutually contradictory?" The contradiction (if there is one) is the following: Wakaizumi's results imply that the Glauber series cannot be consistently applied to both low and high $|t|$ scattering; therefore, he proposes that the expansion not be applied to low $|t|$ ("T_o" term). Yet Schiz et al. got such nice fits at low $|t|$ with the first order expansion term.

Actually there is no real evidence for a contradiction yet. First of all, there is, of course, the fact that Wakaizumi uses an exponential "t_{qq}" and Schiz a quadratic one, as mentioned above. (In fact, Schiz showed that an exponential t_{qq} didn't work so well over the whole "low $|t|$ range"). But even conceptually there is no paradox. Although Schiz

et al. claim that their experimental results are a success for the "additive quark model", there is actually no real evidence that low |t| scattering has anything to do with quarks or constituents. For example, the first Glauber term is completely independent of the number of constituents in the hadron! The reader may then wonder about the effect of the factor 9 ($=3^2$) in the first order term in equation (I.17). This factor is, in fact, cancelled off by a "1/9" in the definition of t_{qq} (it is the experimental value of σ_{tot} that sets the normalization). The number of constituents is reflected only in the higher order terms. (To see this graphically, the reader need only look at Figures I-18 and I-19.) The results of the Schiz et al. experiments show that the curvature at low |t| can be explained using the dipole form factor, not that the GTauber series or constituents are necessary.

Then there is another question. This involves the ambiguity in the choice of form factor. (Recall $G_E^p(q^2) = \frac{1}{\mu} G_M^p(q^2) = G_M^N(q^2)$ only for $q^2 \leq 1.5\ (\text{GeV})^2$.) Should one G_E or G_M? What about the difference between the isoscalar and isovector form factors? From our experience with Current-Current Chou-Yang we know that at low energies the isovector contribution becomes important and can certainly fill in dips. So this might be important at 200 GeV/c. However, it is hard to precict what would happen until someone tries it.

Also, to the best of my knowledge no one has ever introduced spin into the Glauber expansion at high energy. However, it has been done[75] for $p_L \leq 30$ GeV/c. The results are the qualitative features (e.g., dips) remain. Maybe at high energy this would remove the need for the "Im a" parameter. Someone should try this.

6. Playful Thoughts on Some Simple "Hybrid Models"

We have remarked that $(G_D)^4$ provides a good fit to $p^{\pm}p$ elastic scattering for $-t \lesssim 1.0$ $(GeV/c)^2$. It is interesting to note that, properly normalized, it agrees well with $\frac{d\sigma}{dt}$ after the second maximum! (This is because, at high -t, $(G_D)^4 \sim t^{-8}$.) One could thus imagine a model in which the dip near $-t = 1.4$ $(GeV/c)^2$ is caused by the interference of this with, say, a simple exponential Pomeron amplitude.

Or, noting that the normalization could include a relatively flat quark-quark amplitude (implying very small quarks if form factors are to dominate the slope at such high $|t|$) one could picture a model in which low $|t|$ scattering is Chou-Yang like and high $|t|$ scattering involves constituent interactions à la Glauber. (Orear[76] has already attempted to apply the first order Glauber term to high $|t|$ region well beyond the second maximum. However, he has not attempted to extend, e.g., "t^{-8}" back far enough to see if, in interference with Chou-Yang the dip would be filled in to the right extent. Here we note that, extrapolating the high -t behavior back it would seem to fill in the dip to roughly the right extent at 200 and 400 GeV/c (recall that the naive Chou-Yang amplitude is zero at the dip and seems to generally underestimate $\frac{d\sigma}{dt}$ beyond it). At higher energy the back extrapolation may be too large, though.)

7. A Three Layer Proton?

a. Simple Grey Disc Argument

It has been well pointed out by Orear[76] that the relatively gentle "second" exponential slope ("b_3") after the dip is reminiscent of classical diffraction from an object of radius much smaller than 0.8 f.

This is true for a grey disc with a Gaussian profile. Then $R^2 = 2b$ and $b \approx 1.2$ (GeV/c)$^{-2}$ implies $R \approx 0.31$ f. (Actually, at, e.g., 200 GeV/c, b varies from 1.5 to 0.9 (GeV/c)$^{-2}$ as t varies from 4.9 to 12.1 (GeV/c)^2.[67] Orear (and others) have thought of this central region of the proton as a "core" of valence quarks (although he uses a slightly different argument than we do to get its size.) (At $\sqrt{s} = 53$ GeV, "b_3" seems to be bigger than at lower energy and hence the core radius would be about 0.4 f by our simple argument. We could extend this a bit by noting, e.g., that at 200 GeV/c the first exponential slope (extreme low -t) is about 12 (GeV/c)$^{-2}$. In the picture we are discussing this would correspond, e.g., to scattering off the whole proton plus, say, pion cloud (recall Wakaizumi)--$R^2 = 2b$ (grey disc formula) implies $R = 0.97$ fm for exponential slope of 12 (GeV/c)$^{-2}$.

Following this simple game one is led to an amusing three layer picture of the proton-core of radius ≈ 0.4 fm, mantle out to 0.84 fm, and crust (e.g., pion cloud) out to about 1.0 fm, corresponding to the (crude) three characteristic slopes--b_1 (for $t \approx 0$), b_2 (for $-t \approx 0.8$ (GeV/c)^2) and b_3 (for -t after the second maximum). In the simple grey disc picture of this the scattering amplitude would be $A_1 e^{b_1 t} + A_2 e^{b_2 t} + A_3 e^{b_3 t}$, the form of which we have met, via different logic, in Wakaizumi's version of the Glauber expansion. Amusingly, this pictorial representation of a "triune" proton may actually be reality.

b. Alternative Explanation of the "Crust"

Let us now consider the collision of two hadrons from a slightly different point of view--that of a "play" QCD model. Suppose confinement

occurs suddenly when quarks are a distance x_0 apart. Consider a "single order scattering" between quark i in hadron I and quark j' in hadron II. Then when i and j' are separated by a distance x_0 the force between them is much enhanced (compared to when they are closer together) due to the presence of many gluons. Roughly speaking, this situation occurs when the impact parameter I between the hadrons is x_0. This means that at sufficiently low $q^2 \approx "q_0^2"$ one expects the interhadron force to increase sharply with decreasing q^2.*[61] This could be accomplished, for example, by the exponential slope in elastic scattering "b" increasing sharply for $q^2 \approx q_0^2$.

Let us try to calculate this semiquantitatively. A Fourier transform relation exists between $\Gamma(b)$ and $f_{el}(q^2)$. Let us assume here** that one exists between impact parameter and q, i.e.,

$$\Delta I \, \Delta q \gtrsim h$$

(This implies that in a quantum field theory $[\Delta I_{op}, q_{op}] = ih$.)

Now let us look for evidence of structure in $\frac{d\sigma}{dt}$ at sufficiently low q^2. In, e.g., pp elastic scattering at 200 GeV/c, there is a sudden big increase in exponential slope with decreasing q^2 for $q^2 \sim 0.1$ $(GeV/c)^2$, where $-\frac{db}{dq^2}$ is apparently about 20 $(GeV/c)^{-4}$ (see Figure I-23, adapted from Schiz et al.[60]). This value of q^2 plugged into the uncertainty relation gives*** $\Delta I > 0.6$ fm ≈ 0.8 fm. Then, roughly speaking, from this point of

---

*A qualitative remark to this effect is made in reference 61. I thank Dr. Alan White for making me aware of this reference.

**We have not seen this uncertainty relation in the literature before, so we propose it here.

***One must, of course, bear in mind that this is only an order of magnitude argument, and 0.4f and 0.8f are same order.

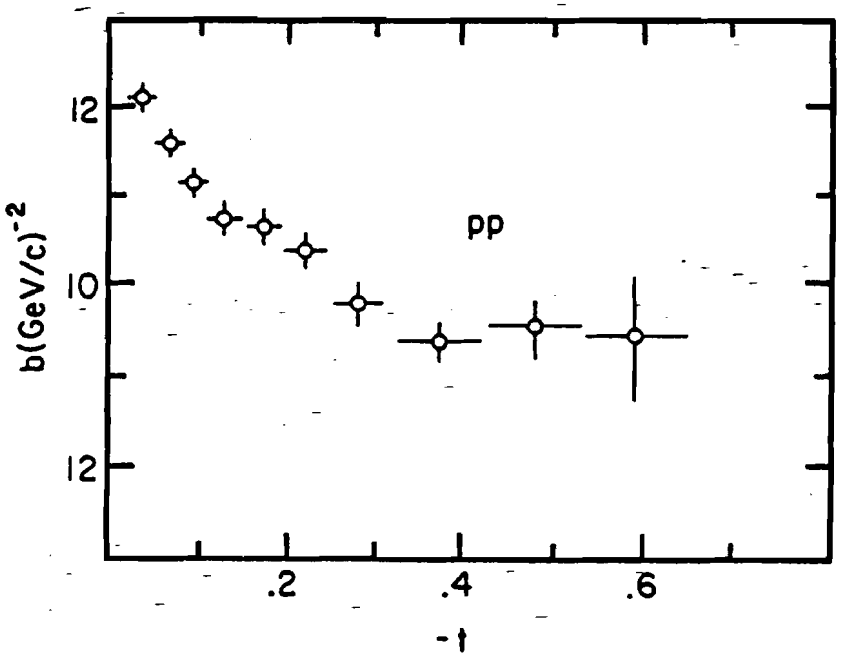

Figure I-23. Low -t pp data (adapted from ref. 60).

view the observation of the extremely steep "first" $-dt/dq^2$ is consistent with sampling confinement. Thus, both the magnitude of the first exponential slope and the corresponding q^2 values correspond to probing confinement.

Let us ask what this picture implies for the Glauber expansion. We see that "there are many gluons around" in very low q^2 scatters. These gluons are of the type that do not correspond to quark dressing; rather they are exchanged between quarks. There is no allowance for this type of gluon in the original Glauber expansion. Thus we do not expect it to work at low q^2. Thus we have arrived at one "alternative" to Wakaizumi's ("pion-cloud") explanation of the "T_o term" (see page 86).

c. Evidence for the Core and Discussion of Its Effects on the Glauber Expansion

We have seen the 0.4 fermi (core radius) number before. We have already noted that an impact parameter analysis of the proton indicates that the r.m.s. radius of the two body ("elastic") overlap function is about this size. It has also been pointed out[77] that a core of this size gives a value of about 0.6 GeV/c for the average transverse momentum of a quark inside a proton, which agrees with the Feynman, Field and Fox[78] estimate.

[Although Orear obtains a core radius of only 0.22 fm, this might be due to his use of $e^{\langle r_c \rangle^2 t/6}$ for the form factor of the core. In fact, we should point out here that a more accurate calculation allowing for the Lorentz contraction of the core at high $|t|$ would use something like equation (I.25) for the core form factor. Since r^{-1} there goes like $2M^3/|t|$, this form factor would go like t^{-2} (like a dipole) at high t

(actually like $t^{-2} \exp(-\frac{M^2}{3} \langle r^2 \rangle_c)$), thus ruining the simplicity of Orear's arguments. Another prescription has proposed a form factor that goes exponentially with $p_\perp$ when the Lorentz contraction is put in (thus generating Orear falloff directly). (For these reasons we feel that any increase in accuracy of Orear's argument over our grey disc approach is illusory.]

A semi-popular interpretation of the Glauber series results is that the additive quark model (AQM) works only for $Q^2 \lesssim 1$ (GeV/c)^2. With this in mind one might wonder how we could envision a model with the valence quarks in the core, since this would imply that the AQM works only for $Q^2 \gtrsim 1$ (GeV/c)^2. ($Q^2 \approx 1$ (GeV/c)^2 corresponds to a radius of about 0.2f by the uncertainty principle.) Actually the only conclusions that can be drawn from the Glauber expansion about the AQM are almost the opposite --by construction the model is independent of the number of constituents at $Q^2 \to 0$, and the AQM seems to work beyond the second maximum where the multiple scattering terms dominate (see Figures I-18c and I-19).

One might think that such a valence core picture is further inconsistent with the Glauber expansion results, since the "success" there was obtained with the quarks distributed throughout a radius of 0.6-0.7 fermi. However, we remind the reader that this "success" was attained at the cost of postulating that the series does not apply at extremely low q^2. [Recall that this had to be done to partially suppress the multiple scattering terms.]

We would like to point out here that another method of suppressing the multiple scattering terms <u>without affecting the quality of the fit below the dip</u> would be to use a smaller constituent distribution radius

(see also ref. 86). An example of this would be a dipole $G(q^2) = (1 + q^2/\mu^2)^{-2}$ with $\mu^2 > 0.71$ (assuming small quarks). To see the effects of this the reader need only look at Figure I.18d where this form was used at low energy, but with another purpose in mind. Unfortunately, it seems no one has thought about this at high energy.

d. Some Theoretical Justification

Although in the past some[79] have thought about having the valence quarks localized in a core within the framework of the parton-mode, the general theoretical drift in the middle 1970s had been away from this. The typical quark-parton picture has had the valence quarks in the periphery of the hadron, with, e.g., Kogut-Susskind flux tubes joining them. Also, the popular M.I.T. bag model[80] had the valence quarks distributed throughout a radius of about 1 fermi. Remarkably, though, in recent years this picture has been turned around to some extent.

Brown and Rho[81], for example, have proposed a model in which the valence quarks sit in a core whose size is only about 1.5 nucleon Compton wavelengths. To ensure continuity of the axial-vector current pions are then allowed to exist only outside the bag. This gives a picture strikingly like the old Yukawa one (even in theoretical details) in which hadrons interact with each otehr via $q\bar{q}$ exchange rather than "bag fissioning" ($qq\bar{q}$ exchange would be difficult to imagine with a big bag. For example, in close-packed nuclei, there would be no room for the pions). And, Callan, Dashen and Gross[82] have recently done a full-blown QCD calculation which also leads to a picture of a hadron with a valence quark core ("abnormal vacuum phase") surrounded by a more dense vacuum phase which is analogous to perfect paramagnetism and which consists of close packed

instantons and mesons.

e. A Question

However, with all this the problem of reconciling the charge radius of the proton gotten from e^-p scattering with the core size (if core is valence quarks) remains. Both Orear[76] and Islam[83] have tackled this question, but the author is satisfied with neither of their answers.

f. A Possible Answer

It is, of course, possible that there is a core, that it is "hadronic" but that it is not composed of valence quarks. For example, Gerrity and Pagnamenta[84] have proposed a core model with a core full of glue and by an argument somewhat different than those cited above, find a core radius of 0.34f. And, Miettinen and Thomas[85], in a very interesting generalization of the Chou-Yang model find (by inversion of elastic scattering data) that the distribution of matter in nucleons is denser than that of charge. The results seem to imply that there is a core of glue or sea quarks with an r.m.s. radius of about 0.3f.

g. Another Possible Answer

Yet, there is a method for reconciling the charge radius of the proton from e^-p with a small core of valence quarks. It has been pointed out[86] within the framework of the Glauber expansion that the assumption of a quark-diquark structure of the proton may make it possible to fit elastic scattering at all observed -t without resorting to additional "T_0 terms". (With only two bodies in the expansion the multiple scattering terms are automatically suppressed and also one can only get <u>one</u> dip.) Here we would like to identify the core "seen" in elastic scattering with a

spin-zero, isospin zero dynamically bound two quark (diquark) state. The third quark occupies the region outside the core; hence the large charge radius.

Justification

The reader may think that this quark-diquark idea is ad hoc and whimsical. In fact, one is led to it on other grounds. For one, it has been used to explain SU(6) violations in many cross section sum rules for strangeness and charge exchange reactions.[87]

The quark-diquark concept apparently first appeared in the work of Ida and Kobayashi[88] and that of Lichtenberg.[89] Feynman[90] has referred to diquarks as "squeezed wee quarks" and more recently Gunion and Soper have used the "quark pair" idea.[91] Spectroscopic indications of specifically "q-dq" type SU(6) breaking include observation of the so-called "minimal" baryon spectrum[92] and the natural absence of a {20}-plet in this picture. Indeed, just very recently, Lichtenberg and co-workers[93] have obtained remarkable agreement with experiment by using a q-dq model with a QCD motivated potential to calculate the masses of the ground-state spin 3/2 baryons (both of the parameters in the model are set by the vector meson masses, so this is a no-parameter calculation). (This can be viewed as a relativistic generalization of the Schrödinger equation approach to treating the ψ and Υ levels.) Other evidence includes[92]: the G_A/G_V ratio in nucleon β-decay, hadronic weak decays, counting rules, the "σ_L/σ_T" ratio in deep inelastic electroproduction of hadrons, polarized inclusive Λ production, and the F_2^{e-n}/F_2^{e-p} structure function ratio. Theoretically, within lattice gauge theory[94] and also within the instanton framework[95] arguments for a q-dq structure of baryons have been made.

Interestingly, the apparently negative neutron charge radius finds a natural explanation[96] within the q-dq model. (This was a long-standing problem in theoretical physics. Simple SU(6) models give a zero $\langle r^2 \rangle_n$.) Qualitatively this is not hard to see--if both the proton and the neutron have a u-d core (charge +1/3) and the proton (neutron) has a positive u (negative d) quark outside the core, the charge radius will be positive (negative). Carlitz has shown that this difference holds up in a one-gluon exchange model that relates this and the n-p mass difference. Further quantitative work has been done by Dziembowski et al.[92] who show that the q-dq structure needed to explain the neutron charge radius is quantitatively the same as that needed to explain SU(6) violations in meson-baryon scattering. More thought in this framework might allow one to solve for the diquark (core) radius.

Another indication of a q-dq core structure of the proton comes from the apparent absence of a $P \times P \times P$ cut in the model of Collins and Gault.[19] Other indications of a core come from the work of Shanker and Warke[97] (radius about 0.31 fm) and that of Ribeiro.[98] If we accept the q-dq concept, returning to our three layer picture of the baryon, we can then identify the three layers: core $\leftrightarrow$ diquark, "mantle" $\leftrightarrow$ third valence quark, "crust" $\leftrightarrow$ pion cloud (on confinement gluons). In any case, though, our experiment has enough acceptance to probe the core region of the antiparton and proton. More thought is probably still required, though, to really pin down what this core is made of, if it exists.

II. OVERVIEW OF EXPERIMENTAL METHOD

A. Introduction. What We Hoped to Measure

In light of some of the questions raised by the previously existing data described in Section I.A of this thesis, certain experiments were undertaken at Fermilab in Batavia, Illinois, to measure elastic scattering cross sections. These experiments, all done using the "M6 beam line"[99] of the Meson Laboratory at Fermilab, shall be jointly referred to in this thesis as "E577".

One of the purposes of E577 was to measure $\pi^- p$ elastic scattering cross sections at an incident beam momentum of 200 GeV/c out to $-t \approx 11$ $(GeV/c)^2$, to compare with pp large -t elastic scattering. The results of this are reported in an earlier thesis by Paul Karchin.[24]

Another purpose was to measure $\bar{p}p$ elastic scattering cross sections at incident beam momenta of 100 and 200 GeV/c in the large momentum transfer region. The motivation for this was heightened about midway through E577 by the previously referred to announcement of the discovery at CERN of a dip near $-t = 1.4$ $(GeV/c)^2$ in the 50 GeV/c $\bar{p}p$ elastic scattering cross section. We were particularly interested in seeing if this dip would persist to 100 (GeV/c) and 200 (GeV/c) incident momenta. The results of these measurements are reported in this thesis along with those of similar measurements made of pp elastic scattering at the same incident momenta and with the same equipment.* Other results on $K^{\pm}p$ and $\pi^+ p$ elastic scattering obtained at the same time will be reported elsewhere.[24,100]

*Some of these results have already been published in preliminary form. See reference 101.

B. Overview of How the Measurements Were Made

1. Two General Problems

In order to determine specific elastic cross sections it is generally necessary to (a) distinguish, as well as possible, general elastic events from inelastic bakcground, and (b) count the number of elastic events meeting specific criteria. The counting problem is described in general overview in part b of this subsection and in more detail throughout the later parts of this thesis. In part a of this subsection we make some general statements about the separation of the general elastic signal from the background. A slightly more detailed overview of the solution of this problem is given in Subsections B.2-B.5. Detail on this is given later in the thesis.

a. Two General Stages in the Separation of Elastics from Inelastics

The separation problem was complicated by the fact that the elastic cross sections that we wished to measure were in general much, much smaller than the corresponding inelastic background. (For more detail on the magnitude of the comparison, see later.) Thus, the problem was rather like picking proverbial needles from a haystack.

A hardware "trigger" was designed to strongly favor elastic events of the type that we were looking for. Events that passed the trigger requirements will be referred to as "candidate events" or "triggers".

Data pertaining to candidate events were ultimately recorded "on-line" on magnetic tape by a DEC PDP11/45 computer. However, in general, most triggers were not elastic events (e.g., at -200 GeV/c only 4% of triggers were elastic; at -100 GeV/c almost 50% were); therefore, additional event selection was done "off-line" using CDC Cyber 175

computing system at Fermilab.

Due to the relative infrequency of occurrence of desired elastic events, for efficient use of the "on-line" and "off-line" computers it was necessary that the experimental trigger requirements be fairly "tight" so as to severely limit the total amount of data that was written on tape. The triggering system will be described in overview shortly, and in detail in Section III.

b. General Statement of the "Counting Problem"

Since we wished to measure elastic $\frac{d\sigma}{dt}$'s, after determining to our satisfaction that an event was indeed elastic we had to measure -t for the event. Finally, the range of -t for all the events had to be broken into "bins" and the number of desired events in each bin had to be counted. How -t was measured will be described shortly. However, not all elastics gathered over a certain period of time that fell into a given -t bin could be counted together--the beams were far from being pure $\bar{p}$ or p!

For each incident energy (100 GeV/c, 200 GeV/c) the experiment was run at two "polarities"--with a beam of negatively charged incident particles and with a beam of positively charged incident particles. Each of these beams was composed of at least three species--the "negative" beams at each energy were predominantly pi minus with some ka-minus and $\lesssim$1% antiproton composition, while the positive beams at each energy were predominantly protons, with a substantial admixture of π^+ and a lesser component of K^+. [The existence of a small $\bar{p}$ component in the negative beams was fortunate in that it allowed us to measure the $\bar{p}p$ cross sections reported in this thesis!]

Thus, after an event was determined to be elastic, there still remained the problem of determining if the event was π-p, K-p, or $\bar{p}p$ scattering. This species identification problem was solved by using Cerenkov counters. In Sections III and V of this thesis we will describe in some detail how this was done. For now, however, we return to continue our overview of how general elastics were separated from inelastics.

2. Overview of Separation of Elastics from Inelastics

a. Definition of Kinematic Variables and Necessary Range of Equipment Sensitivity

Any "two-to-two" scattering process can be written symbolically as

$$a + b \rightarrow c + d.$$

In the laboratory frame b is at rest (in the target). We then define:

p_{lab} = magnitude of three-momentum of incident particle "a",

θ_f = scattering angle of outgoing particle "c" with respect to incident direction of "a",

p_f = magnitude of three-momentum of outgoing particle "c",

θ_r = scattering angle of outgoing particle "d" with respect to incident direction of "a",

p_r = magnitude of three-momentum of outgoing particle "d".

The above five variables are defined as measured in the laboratory frame of reference. For elastic scattering a = c, b = d.

For elastic scattering at high energy, $-t = q^2$ can be related to the scattering angles as follows[1]:

$$\frac{1}{\sin^2\theta_r} \approx 1 - \frac{t}{4M^2} ,$$

$$\theta_f^2 \approx \frac{-t}{p_1(p_1/t + 1/2M)} ,$$

the approximations being good to $\frac{\Delta\theta}{\theta} \geq 2\times10^{-3}$ in each case for $p_{lab} \geq 100$ GeV/c.

From these equations it is then seen that a $-t = 1$ $(GeV/c)^2$ elastic scattering event has $\theta_f \approx 0.3°$ and $\theta_r \approx 80°$, that a $-t = 5$ $(GeV/c)^2$ elastic scattering event has $\theta_f \approx 0.7°$ and $\theta_r \approx 38°$, and that a $-t = 10$ $(GeV/c)^2$ elastic scattering event has $\theta_f \approx 0.9°$ and $\theta_r \approx 29°$.

b. Information Recorded on Tape and Most General Designs Considerations

As is well known, for elastic scattering all kinematic variables depend on only two parameters--e.g., s and t. s is simply related to the laboratory incident momentum p_{lab}, which was easy to measure (see below). Thus, theoretically, elastic differential cross sections could be measured by measuring only one additional (to s) kinematic variable --e.g., θ_f, the forward scattering angle.

However, in order to get a maximally good separation of elastics from background it was decided to record on tape information from which (to "sufficient" accuracy) all four laboratory kinematic variables, θ_f, p_f, θ_r and p_r, could be reconstructed.

In order to measure the forward and recoil scattering angles arrays of multiwire proportional chambers (hereafter referred to as "wire chambers") were used. Measurement of forward and recoil momenta required forward and recoil magnetic spectrometers. Since we wished to measure elastic scattering from $-t \approx 1$ $(GeV/c)^2$ to $-t \approx 11$ $(GeV/c)^2$ at

P_{lab} = 200 GeV/c, it is apparent from preceding discussion that the spectrometers had to be sensitive in the ranges $20° \leq \theta_r \leq 85°$ and $0.1° \leq \theta_f \leq 1°$.

c. Layout Overview I--Equipment Used to Record Kinematic Information

An overview of the most relevant parts of the layout is shown in Figure II.1. Not shown is the beam line, which is described in some detail in Paul Karchin's thesis.[24] Partial species identification in the incident beam was made with a differential Cerenkov counter that is not shown; this will be discussed in detail in Section III. Also not shown are several scintillator hodoscopes in the beam; these will also be discussed later.

The target was liquid hydrogen that filled a flask that was cylindrical in shape whose inner length was about one meter (about 15% of an interaction length for LH_2) and whose inner diameter was about three inches. Surrounding the target on three of its four long faces were 1.5" thick aluminum plates to absorb delta rays. Outside of the plates were scintillation counters called A_2, A_3 and A_4; a signal from these counters vetoed the event. The "fourth face" and the two edges of the target were not inside of aluminum plate or scintillator so that desired particles could enter and leave the target without being absorbed.

Referring to Figure II.1, P_5 and P_6 were arrays of "x" and "y" wire chambers used to determine the forward scattering angle; P_1 was a corresponding array of "x'" and "y" wire chambers used to determine the recoil scattering angle (directions x,y,z and x',y,z' are defined on the figure). The magnets labelled "BM109" and "72D18" were used to bend

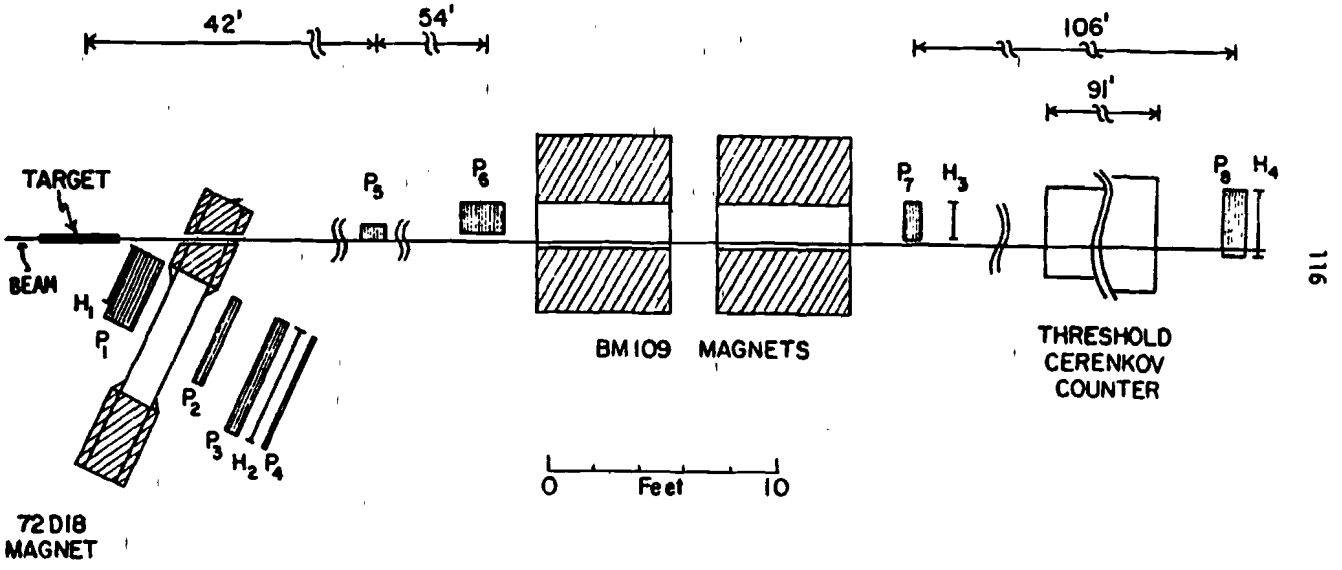

Figure II-1. Layout of the experiment (from ref. 30).

Figure II-1. Layout of the experiment (from ref. 30).

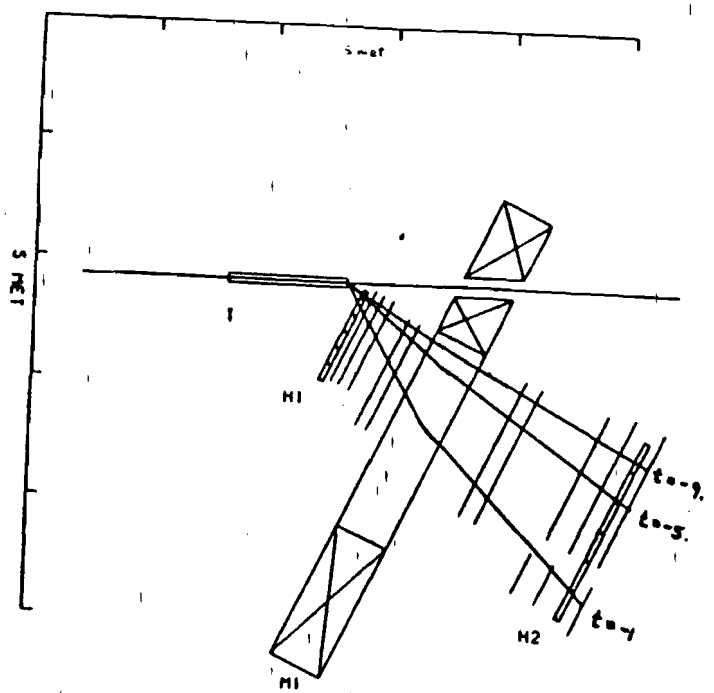

Figure II-2. Detail of recoil arm. M1 is "72D18" magnet. (Figure made by Sean McHugh and used with his permission.)

forward and recoil scattered particles respectively so that momenta could be measured.

P_7 and P_8 were arrays of wire chambers used to determine the forward trajectory exit angle from the BM109 magnets; the arrays P_2, P_3 and P_4 performed the analogous duty in the recoil arm. By measuring entrance and exit angles to and from the magnets and by knowing field integrals (66.2 Kg-m for the BM109's and 9.0 Kg-m for the 72018) moment were easily determined.

Thus, for candidate events "addresses" of hit wires were recorded on tape. From this kinematic information could be determined off line and further event selection and analysis could be performed. Fruther information about the proportional wire chambers themselves and the electronic "read-out" systems used to provide addresses of "hit wires" to the computer will be found in Section IV.D of this thesis. Further information about the analysis of wire chamber information (track finding, tests for elasticity, etc.) will be found in Section III of this thesis and in Paul Karchin's thesis.

d. Layout Overview II--Selecting Candidate Events

We have mentioned that a tight experimental trigger was needed. This was carried out through the use of several individual scintillation counters and a number of scintillation counter hodoscopes.

Referring again to Figure II.1, H_3 was a seven-element scintillation hodoscope (also referred to as the "F^{α} hodoscope", with elements F_i^{α}, i=1,2,...,7) designed to provide a loose measure of the scattering angle of the forward going particle. H_4, another seven element scintillation

counter hodoscope (also referred to as the "F^{β} hodoscope", with elements F_i^{β}, i=1,2,...,7), was used in conjunction with H_3 to cut on the forward momentum (i.e., it was required to be close to the elastic value).

In the recoil arm, H_1 and H_2, often called the "R" and "S" hodoscopes respectively, were installed to perform similar functions as H_3 and H_4 in the forward arm (although they did this less successfully).

Ultimately, for an event to pass the trigger requirements, a matrix was required between elements of H_1 and H_2 in the recoil arm and H_3 and H_4 in the forward arm. [By this we mean that if given elements of the recoil arm hodoscopes "fired" only certain elements of the forward arm hodoscopes were required to fire. If the "wrong" elements fired, or if more than one element of any H_1,H_2,H_3,H_4 gave a signal the trigger was not set and the event was rejected.] This scheme, borrowed and modified from an earlier successful Brookhaven experiment[102] allowed one to cut loosely on opening angle and thus further bias the trigger toward elastic events. This forward recoil matrix was referred to as the RSF matrix.

We have mentioned that there were also scintillation counters in the beam. A coincidence of signals from B_1 and B_2, two single element scintillation counters directly in the beam path, was required as part of the trigger. "A_1", a single element scintillation counter with a hole in it for the beam to pass through, was used in anticoincidence with $B_1 \cdot B_2$ in the trigger as a veto counter.

We have also mentioned the existence of anticounters around the target; these were called "A_2", "A_3" and "A_4". The full trigger, then, was a proper coincidence labelled $B_1 \cdot B_2 \cdot \bar{A}_1 \cdot \bar{A}_2 \cdot \bar{A}_3 \cdot \bar{A}_4 \cdot RSF$ where a bar

above a counter name indicates the requirement of the absence of a signal from that counter, where "·" means "and", and where RSF refers to any of the correct combinations of signals from the forward and recoil arm hodoscopes that satisfy the RSF matrix conditions.

The singles rates in the above-mentioned scintillation counters and the implementation and design of the experimental trigger including temporal considerations are discussed in some detail in Section IV.C of this thesis.

III. SPECIES IDENTIFICATION

A. Identification in the Incident Beam

At high energy it is difficult to effect a three way separation with a single Cerenkov counter. Thus, as there were three species in each of the high energy incident beams, it was decided to use two Cerenkov counters to get a particle identification--one in the beam to tag the incident particle and one toward the downstream end of the forward arm.* We could have used another Cerenkov ocunter or ionization detector in the (relatively low energy) recoil arm; however, realistically speaking this was unnecessary. Let us consider the beam Cerenkov counter first.

It was desired to distinguish pions and kaons from each other at 200 GeV/c. Let $d\beta_{\pi-K}$ be the difference in velocity (as a fraction of the speed of light) between pions and kaons in a given energy beam for our experiment. At 200 GeV/c, $d\beta_{\pi-K} \approx 2.8\times10^{-6}$. Therefore for a Cerenkov counter to make a practical separation of π and K in our beam, it would be desirable to have a resolution $\frac{d\beta}{\beta}$ at least as good as 1×10^{-6}. To accomplish this task a threshold counter would have to be prohibitively long, so we thought about the possibility of using a differential counter.

Using the fundamental relation $\cos\theta = \frac{1}{n\beta}$, where θ = Cerenkov angle and n = index of refraction of the radiator, we find $d\beta = \tan\theta d\theta$, which tells us that to obtain good resolution in β it is helpful to use a very

*We could have used a pair of threshold counters in the forward arm, but due to practical considerations we decided against this. Also, as we shall see, a pair of counters in the beam would have been very expensive.

small Cerenkov angle. However, the light yield in Cerenkov radiation is relatively meager and goes as $\sin^2\theta$; therefore, a compromise must be struck.

In order to maximize the usable photon signal it is desirable to position a number of photomultiplier tubes around the annular opening (which will often be referred to as the "diaphragm") of the counter. If, for example, eight photomultiplier tubes are placed around the diaphragm and a coincidence of all of them is required, it is possible to reject very well unwanted light which does not form a good circle of the right radius; however, in that case care must be taken not to reject wanted light. We used eight photomultipliers around the diaphragm.

What would be a sufficient number of electrons for the counter to provide? For a single photomultiplier the inefficiency is $e^{-\bar{n}}$, where $\bar{n}$ is the mean number of photoelectrons. So, for 99% efficiency, $\bar{n} \approx 4.5$. Suppose a coincidence is required in all eight photomultipliers. Let ϵ be the efficiency. Then $\epsilon = (1 - e^{-\bar{n}})^8 \approx 91.45\%$ for $\bar{n} = 4.5$. With $\bar{n} \approx 6$, $\epsilon \approx 98\%$. So $N = 40$ total photoelectrons would seem a reasonable requirement.

The length of the counter would then be given by $N = AL\sin^2\theta$, where L is the length of the counter and A is a number that depends on the performance of the photomultiplier tube when used with the Cerenkov tank. Because Cerenkov light tends to be at short wavelength (it extends down to $\lambda \approx 250$ nm) and meager, a photomultiplier with extended ultraviolet response (implies need for quartz entrance window) and a high quantum efficiency (implies need for bi-alkalai cathode) was desired. The RCA 31000M seemed to have the highest quantum efficiency available;

therefore, we used eight of them around the diaphragm. Experiments done at Cornell University's Wilson Synchrotron by D. D. Yovanovitch et al.[103] using an extracted electron beam to evaluate the performance of this phototube in a Cerenkov counter have indicated that $A \approx 150\ cm^{-1}$. If we then desired a one meter long counter (much longer gets very expensive) and 40 photoelectrons, $\theta \approx 52$ mr. Then the annulus diameter would be $r = L\theta = 5.2$ cm and the diaphragm slit width would be $\Delta r = L\Delta\theta = L\,d\beta/\tan\theta \approx 2\times10^{-5}$ m, which is small but within the limits of modern technology.

However, such a counter would never have worked for our purposes. Consider the optical dispersion in the counter. A Cerenkov photon of wavelength λ is emitted at Cerenkov angle $\theta(\lambda)$, where $\theta(\lambda)$ is given by the fundamental relation

$$\cos\theta(\lambda) = \frac{1}{\beta n(\lambda)}$$

From this it is easy to see the well-known result

$$d\theta_{disp} = \frac{1}{\tan\theta(\bar{\lambda})}\,\frac{dn(\bar{\lambda})}{d\lambda}$$

where $d\theta_{disp}$ is the mean angular width due to chromatic dispersion and where $\bar{\lambda}$ is the most probable wavelength for a Cerenkov photon. Putting this into the standard form that appears in the literature[104], one has

$$d\theta_{disp} \approx \frac{n(\bar{\lambda}) - 1}{\nu n(\bar{\lambda})\tan\theta(\bar{\lambda})}\ ,$$

where ν, the "dispersion", is given by

$$\nu \equiv \frac{n(\bar{\lambda}) - 1}{n(\lambda_1) - n(\lambda_3)}\ ,$$

where $n(\lambda_1)$ and $n(\lambda_3)$ are the values of the index of refraction of the medium at the (suitably defined) "extremes" of the Cerenkov spectrum.

The least dispersive, safe, commonly available gas is helium (for which $\nu \approx 55$), so we used it. Then, using the relation

$$\theta^2 = 2(n-1) - 1/\gamma^2$$

where $\gamma \equiv (\sqrt{1-\beta^2})^{-1}$, we get, following reference 104,

$$d\theta_{disp} \approx \frac{\theta}{2\nu}\left[1 + \frac{1}{\gamma^2\theta^2}\right] \approx \frac{\theta}{110} \text{ for He} .$$

This implies that for $\theta = 52$ mr with Helium,

$$d\theta_{disp} \approx 4.7\times10^{-5}$$

However, we recall that at 200 GeV/c we desired that the resolution in β, $\frac{d\beta}{\beta}$, be equal to or better than 1×10^{-6} which implies that the desired resolution in θ, given by

$$d\theta_{res} = d\beta/\tan\theta$$

would be equal to or better than $2\times10^{-5} < d\theta_{disp}$! Therefore, we see that a differential counter filled with Helium and using $\theta = 52$ mr cannot be used to separate pions from kaons at 200 GeV/c.

In order that the divergence in Cerenkov angle due to chromatic dispersion be less than the desired resolution one must, then, use a smaller Cerenkov angle, and hence, unfortunately, a longer Cerenkov counter. Indeed, from the above one must have[104]

$$\frac{\theta}{2\nu}\left[1 + \frac{1}{\gamma^2\theta^2}\right] < \frac{d\beta}{\theta}$$

where $d\beta$ is the desired resolution in β. Using $\frac{1}{\gamma^2} = \left(\frac{m_K}{E}\right)^2 \approx 6.1\times10^{-6}$ (where m_K is the kaon mass) for kaons at 200 GeV/c, one finds that θ must be $\lesssim 10$ mr. Choosing, say, $\theta = 7$ mr and requiring a total of 40 photoelectrons would imply a counter length $L \approx N/A\theta^2 \approx 53$ meters, which would be prohibitively long. Therefore, a conventional differential

Cerenkov counter would not have suited our purposes.

This problem was attacked at CERN, where "chromatic correctors" were developed which cut dispersion by a factor of about 15. So then one could have $\theta_c^2 \leq 15\times10^{-4}$ rad or $\theta_c \leq 38$ mr. Then $L \approx 53/15 \approx 4$ meters, a manageable length. For $\theta_c \approx 30$ mr, the annular slit width $\Delta r = L\Delta\theta = L\times10^{-6}/0.030 = 1.2\times10^{-4}$ meter. Interestingly, it is found experimentally[105] that $\Delta r \approx 10^{-4}$m $\pm$ 50% also minimizes other residual aberrations after correcting for coma (which goes like θ^3). The aperture diameter would then be given by $r \approx L\theta \approx 110$ mm, and the mirror diameter would be about $2L\theta$ + beam spot size $\approx$ 200 mm + b.s.s.

However, at such small Cerenkov angles there are other line broadening effects that had to be considered by the designers at CERN before it was clear that a counter with the parameters given above would be practical. For example, there is a contribution to $\Delta\theta$ (width in θ of Cerenkov cone) due to diffraction. This, of course, would be of order $\bar{\lambda}/L\theta$, where $L\theta$ is the mirror radius. For $\theta \approx 30$ mr, $\bar{\lambda} \approx 350$ nm, and $L\theta \approx 4$m one sees that $\Delta\theta$ due to diffraction alone is $\sim3\times10^{-6}$. This value corresponds to $\Delta\beta \sim 8\times10^{8}$. Thus we see the interesting result that our needed resolution of $\leq1\times10^{-6}$ in β is only about a factor of ten from the diffraction limit for a counter of this size!

Another contribution to line broadening that had to be thought about is multiple scattering. Cerenkov counters used at high energy typically have aluminum entrance and exit windows (for the beam) in order to hold pressures that may differ considerably from that of the atmosphere. Thus there is then multiple scattering in these windows.

There is also another contribution to multiple scattering due to

the Helium itself. However, there is a distinction between multiple scattering in the gas and that in the Al windows that has been pointed out.[105] The multiple scattering in the gas corresponds to a particle changing direction randomly and frequently while it is radiating. Since the total photon yield in a Cerenkov counter is small, one can think of the beam particle as shaking off one photon at a time. Then it can be seen that multiple scattering in the gas has the effect of broadening the angular width of the Cerenkov cone. (However, as the phase space changes are random, this cannot be corrected for with an optical device such as a lens.)

On the other hand, the multiple scattering in the entrance window does not occur while the particle is radiating. Therefore, this does not cause a broadening of the Cerenkov cone; rather, it translates the "circle of photons" at the annulus so that it may miss the aperture. This lowers the efficiency of the counter but does not (in normal operation) contribute to the confusion of kaons with pions. It has the same effect as beam divergence. We shall discuss this later.

For now, then, let us consider only the multiple scattering in the gas. This is given by the well-known formula

$$\Delta\theta_{m.s.} = \frac{E'}{\beta p}\sqrt{t}\ ,$$

where $\Delta\theta_{m.s.}$ is the line width of θ caused by the multiple scattering, where t is the path length in the gas in units of a radiation length, and where E' is about 20 MeV. Thus, one finds $\Delta\theta_{m.s.} \sim 10^{-5}$ radian, which corresponds to a $\Delta\beta$ of about 2.5×10^{-7}. Thus we are okay again, but this time only by a factor of five or so. One can see what this says

about the possibility of building longer optically corrected differential counters in the future for use at high pressure and high energy!

An optically corrected differential counter (called a "DISC") was built at CERN with $\theta = 24.5$ mr. The focal length of the counter was 4.51 m, and the other dimensions were very close to those calculated above. We used this counter for our experiment. The relevant dimensions and construction are indicated in Figure III-1.

It is not difficult to see what pressure we needed to keep the Helium at in the counter. Suppose one wished to "see" antiprotons at Cerenkov angle $\theta = 24.5$ mr. Using $\theta_c^2 = 2(n=1) - 1/\gamma^2$ and $(n=1) = (n_o - 1)P$, where P is the pressure of He and where n_o is the index of He at 20°C, 1 atm. for $\lambda = 350$ nm, implies $(n-1) \approx 3.3\times10^{-5}$, i.e., one needs $P \approx 10$ atm., an unfortunately high pressure.

Since the angular broadening in the Cerenkov cone due to change in n is given by $d\theta_n = \frac{1}{\tan\theta_c}\frac{dn}{n}$, one needs $\frac{dn}{n} < \frac{d\beta}{\beta}$ to separate π and K--i.e., it was necessary to monitor n to $\sim$1 part in 10^7, and further n had to be uniform over the entire length of the counter to this accuracy! This was accomplished by the use of a He-Ne laser interferometer. Since λ for a He-Ne laser is 63 nm, if the half path length is 4.5 m, a change of one fringe corresponds to $\Delta n = \frac{\lambda}{2(4.5\,m)} \approx 7\times10^{-8}$. Thus, this was feasible.

Also, since $\frac{d\rho}{\rho} \approx \frac{dn}{(n-1)}$, where ρ is the density of the gas, and since $\frac{d\rho}{\rho} = \frac{dP}{P} = \frac{dT}{T}$, where T is the temperature, one sees that a temperature variation of more than $\sim$0.1°K over the entire length of counter could not be tolerated! Thus the counter had internal passive

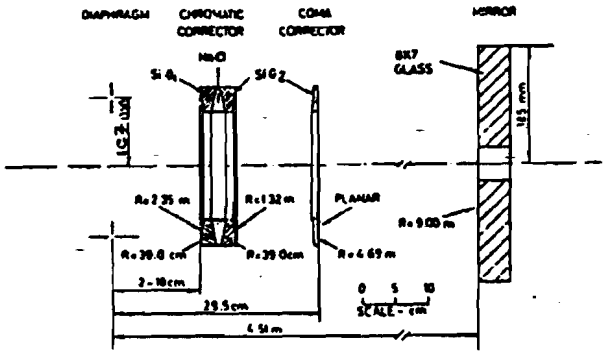

Figure III-1. Construction of DISC (from ref. 105).

elements to increase longitudinal convection and 100 mm thick polyurethane insulation around the entire gas volume.

Let us return now to discuss beam divergence effects on species identification. If a differential Cerenkov counter is to be used in a beam, then the beam must be matched to it. The reader will shortly see that this was crucially important for us.

Now, as we have already remarked, the angular divergence of the beam does not broaden the Cerenkov cone. Rather, to reasonable approximation, a beam particle travelling at an angle $\Delta\theta_b$ to the counter axis would have its "circle of photons" at the diaphragm slit translated. If there were too much translation the efficiency would start to suffer drastically. Let us estimate how much beam divergence we should have been able to tolerate.

Roughly speaking, if Δr is the (annular) diaphragm slit width, one could expect no real deprecation of efficiency if the circle of light were translated by an amount $\Delta x \leq \Delta r$. Now, if $\Delta\theta_b$ is the full width beam divergence, the translation Δx at the diaphragm due to $\Delta\theta_b$ is given by $\Delta x \sim L\theta_b$, where L is the counter length. For an annular slit of "width" about 0.4 mm, this then corresponds to "allowable" beam divergence on the order of 0.08 mr <u>full</u> width. The situation would be made somewhat more critical than this by the angular broadening of the Cerenkov cone (due to, e.g., chromatic dispersion) (which determines how quickly the efficiency falls off), and somewhat less critical by requiring less than an "eight out of eight" coincidence among the photomultipliers.

It is, of course, possible to cause the beam incident upon the counter to be less divergent than 0.08 mr full width by using appropriate

quadrupole magnets immediately upstream of the differential counter. However, the reader may be wondering if it was actually possible to make such a narrowly divergent beam inside the counter, in light of the fact that we have mentioned that the counter had an Aluminum entrance window whose minimal thickness was dictated by the requirement that the internal pressure be about 10 atmospheres.

In fact, it was possible. The entrance window to the counter was 0.6 mm Aluminum. Since a radiation length in Al is about 9 cm, this corresponds to about .01 mr divergence. So we "win", but by less than a factor of ten. Again, this is a limitation for the use differential Cerenkov counters at higher energy!

The momentum bite of the beam must obviously be limited, too. This contributes directly to angular broadening of the Cerenkov cone. It is easy to derive $d\beta = \frac{1}{F}(1-\beta^2)dp$ where F is the focal length of the counter and p the beam momentum; using this we find $d\beta \approx 3\times10^{-7}$ corresponds to about ±2.5% momentum bite at 200 GeV/c. We have already remarked that to separate π and K at 200 GeV/c one would desire a resolution in β of $d\beta \approx 1\times10^{-6}$. By similar logic, one would be barely safe in the separation of $\bar{P}$ and K^- at 200 GeV/c with a momentum bite of ±2.5%.

Now, our beam line was designed to deliver a beam of momentum bite ±1/2% and angular divergence ±.03 mr to the DISC. Theoretically this would have been fine. Unfortunately, real life was more complicated than that.

By varying the angle of the mirror relative to the counter axis, it was learned that the beam actually had a divergence of about 0.2 mr at the position of the counter. According to our little calculation

above, this would have been a very touch-and-go situation. It was found that the horizontal beam divergence could essentially not be made smaller than this by using beam collimation slits. By feeding this value of divergence into a computer program and "tracing backwards" it was found that a collimator immediately downstream of the Beryllium target that was used to produce our beam was acting as a "second source", thus making the beam more divergent than planned. The question then was "would the differential counter work efficiently enough to be at all useful to us"?

In Figures III-2 and III-3 we show experimental results. In Figure III-2 we see the π-K separation achieved at -200 GeV/c with a relatively low beam intensity and with the diaphragm slit set to about 0.36 mm (note that with θ = 24.5 mr, the theoretical maximal slit width to "just separate" π and K is $(4.55m)(2.8\times10^{-6}/.0245)$ = 0.52 mm. Thus we see that the width of the pi peak agrees with our earlier calculations and is due primarily to chromatic dispersion). It is seen that the contamination of pions under the K peak is $\sim$1%. Opening the slit wider of course worsens the contamination. A "six out of eight" coincidence of photo-multipliers was required.

Typically, however, at -200 GeV/c we ran with a much more intense ($\geq 6\times10^6$ paricles/spill) and more divergent beam. In this case a compromise had to be struck between contamination and efficiency. It was found that contamination of kaons with pions under these running conditions (with a "6/8 coincidence") approached 10% when the efficiency for tagging kaons was about 25%. Since we could not afford more

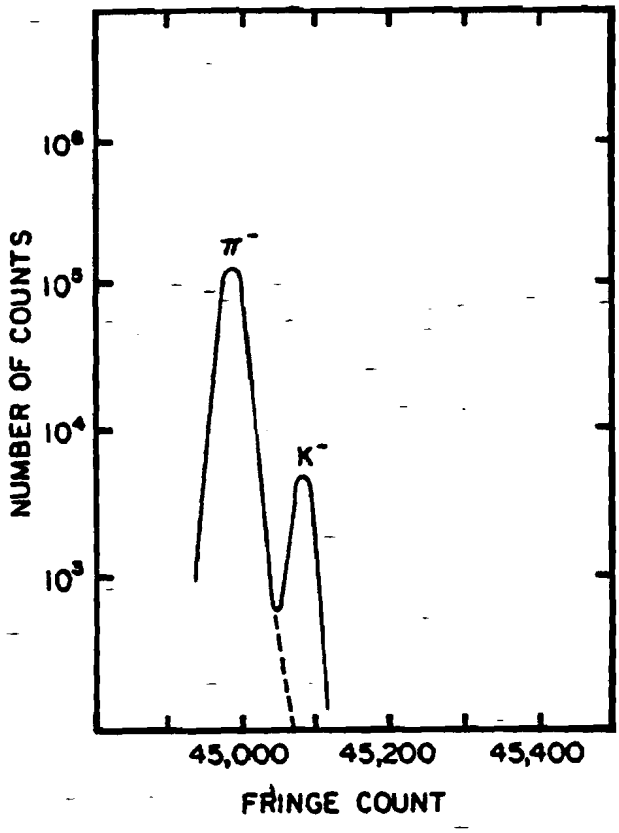

Figure III-2. Differential Cerenkov counter pressure curve at -200 GeV/c beam momentum curve is smoothed. Diaphragm slit width ≈ 0.36 mm. Beam intensity ≈ 1.7×10^6 particles per spill.

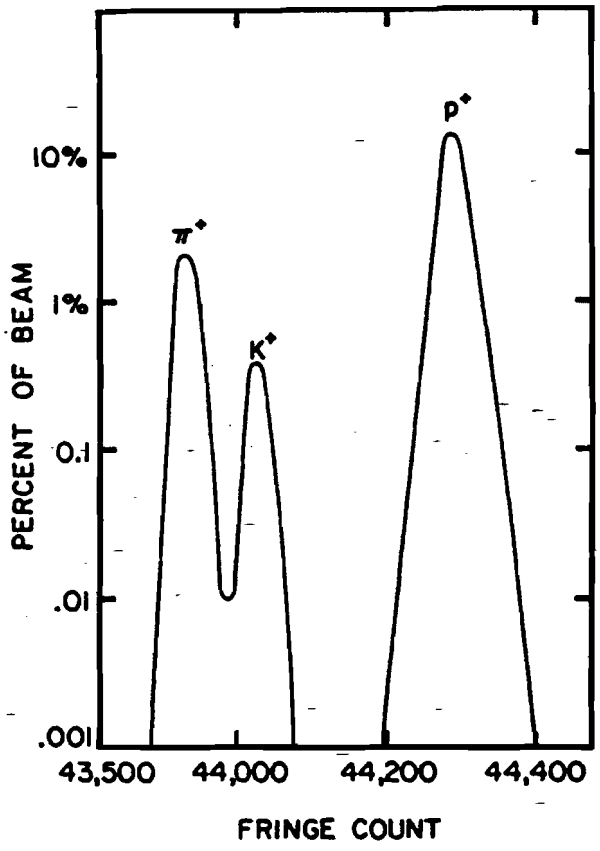

Figure III-3. Differential Cerenkov counter pressure curve at +200 GeV/c beam momentum. Curve is smoothed. Diaphragm slit width ≈ 0.36 mm. Beam intensity ≈ 8×10^6 per spill.

contamination than this we had to settle for this efficiency. As kaons comprised only about 4% of the -200 GeV/c beam, this hurt our chances of having good statistics in the K-p cross section at -200 GeV/c. For "8/8 coincidence" the efficiency was even lower, hence we did not run like that. Since the falloff of efficiency with divergence is rapid, had the beam been any more divergent the DISC would have been about useless in tagging enough kaons.

However, if the DISC was set to tag $\bar{p}$'s, the diaphragm could be opened much wider, since the ability to do a π-K separation was no longer of concern. Thus we found we could run "on $\bar{p}$'s" with the diaphragm open wider than a millimeter. The efficiency of the DISC for tagging $\bar{p}$'s, therefore, was much higher than that for tagging K's (somewhat fortunately for this author)--it often approached 90%.

Using the DISC it is clearly possible to measure both particle fractions and the beam momentum. The momentum determinations compared favorably with those obtained using elastic kinematics. An example of the attempt to determine beam composition is shown in Figure III-4. Average results for each beam are given in Table III.1.

Table III.1

Beam Composition Determined from Differential Cerenkov Counter

Beam momentum (GeV/c)	$\%\pi$	%K	%P
-200	95	4	0.6
-100	92	5	3
+200	16	3	81
+100	56	5	39

B. Species Identification of Scattered Particles--Hardware

We remarked earlier that a threshold Cerenkov counter to be used to distinguish pions and kaons from each other at 200 GeV/c would have been prohibitively long. Therefore, in the original design conception of the experiment the DISC was to be used to tag kaons. We were then left with the problem of distinguishing (anti) protons from pions. Since this is easier than "separating π's and K's" ($\Delta\beta$ is greater), it was hoped that for this purpose a threshold counter could be used. In this section we make some remarks about the implementation and success (and/or lack of success) of this plan.

In order to best separate π and P, one should fill a threshold counter to a pressure just below that where antiprotons would begin to radiate. If that is done it is well known that the number of photoelectrons produced by pions is given by

$$n_{\pi \text{ photoelectrons}} = A \frac{m_p^2 - m_\pi^2}{p^2} L ,$$

where L is the length of the radiator and p is the beam momentum. The parameter "A" has already been defined in the discussion of the differential counter.

Suppose that one wishes a threshold counter to be 99% efficient in detecting pions if only one photomultiplier tube is to be used. Then one would need about 4.5, say 5, photoelectrons. (The use of one photomultiplier is generally sufficient for a threshold counter since one does not have to detect most of a "circle of photons" (as with the differential counter) to distinguish between particle types.

But for an experiment such as ours, a mere 99% efficiency in tagging

pions would not necessarily be good enough. If the ratio of pions scattered into the counter to protons scattered into the counter were sufficiently great, those pions for which no photoelectrons were produced would have severely contaminated the protons. What we had to aim for, then, was something like 1% "contamination of protons with pions" (i.e., 1% of the scattered particles determined to be protons by using the threshold counter are actually pions). What efficiency in tagging pions (and hence how long a counter) did we need for this?

At -200 GeV/c we expected the ratio of pions to antiprotons in the beam to be of order 100 (based on previous experience with production off Beryllium targets). Indeed, as we have seen, during the experiment the DISC was used to measure this ratio and it was found to be about 160. Also, according to the results of Schiz et al.[60], at $-t \approx 0.65$ (GeV/c)^2, $\frac{d\sigma}{dt}(\pi^- p) \Big/ \frac{d\sigma}{dt}(pp) \sim 2$.

A threshold counter was made for our experiment by lengthening an existing counter to 91 feet. Then, using the Yovanovich et al. value of 150 cm^{-1} for "A", we would expect an average of nine photoelectrons from pions. Experimentally we got about eight (indicating "$\bar{A}$" $\approx$ 133 cm^{-1} for our counter-phototube (RCA 31000M) combination.

Using $\bar{n} = 8$ photoelectrons, and assuming that pions whose Cerenkov photons produce only one photoelectron can be distinguished from antiprotons, we would have expected the contamination of antiprotons with pions to be $\sim(500)(e^{-8}) \sim 17\%$ (better if the average cross section ratio $\frac{d\sigma}{dt}(\pi p)$ $\frac{d\sigma}{dt}(pp)$ would turn out to be less than our guess of two). This would have been barely tolerable, but certainly not optimal.

Now it was planned that the acceptance of our experimental apparatus

would begin to become "substantial" at a value of -t not too different than this* (so that we could compare our experimental "normalization" to those of previous experiments). It was also known that the pp elastic cross section plunges sharply to its famous dip near $-t \approx 1.4$ $(GeV/c)^2$; therefore, it would have been reasonable to expect the ratio of pions to antiprotons entering the threshold counter to be up to ~500. Thus for 1% contamination of the antiproton signal with pions we needed an inefficiency in pion detection equal to or better than $\sim\frac{.01}{500} = 2\times10^{-5}$--that is, an average of at least eleven photoelectrons from pions.

As mentioned previously, the RCA 31000M phototube has been measured to have an "A" value of about 150 cm^{-1}. We planned to use this phototube. Thus an average of eleven photoelectrons would correspond to a counter length of about 34 meters = 112 feet.

It would not have been unreasonable for us to guess roughly equal K^-p and $\pi^-\bar{p}$ integrated (over our range of -t) elastic scattering cross sections. This, combined with our previous guess of two for the expected ratio of the π^-p integrated cross section to the $\bar{p}p$ integrated cross sections, gives a "$K^-p/\bar{p}p$ cross section factor" of two. Then, using a factor of seven for the ratio of K^- to $\bar{p}$ in the beam gives a net factor of $7\times2 = 14$ for the expected ratio of K^- scattered into the threshold counter to $\bar{p}$ scattered into the threshold counter.

Now the ratio of $\bar{n}_K$ (the mean number of photoelectrons from kaons) to $\bar{n}_\pi$ (mean number of photoelectrons for pions) is given by

---

*In fact, it turned out that the acceptance began to become substantial at $-t \sim 0.8$ GeV/c for this energy and polarity--see later.

$$\frac{\bar{n}_K}{\bar{n}_\pi} = \frac{m_p^2 - m_K^2}{m_p^2 - m_\pi^2} \approx 0.74 \ .$$

Since we have $\bar{n} \approx 8$ at -200 GeV/c, we thus expect $\bar{n}_k \approx (0.74)(8) \approx 6$, and indeed this is what we observed experimentally.

Recalling, then, that the differential Cerenkov counter was only ~25% efficient in tagging kaons, one would expect the contamination of $\bar{p}$'s with K^- to be

$$(0.75)(14)(e^{-6}) \approx 2.5\% \ .$$

Thus the total expected contamination of antiprotons with mesons would be ~17% + 2.5% ~ 20%, assuming that pions whose Cerenkov photons produce only one photoelectron can be distinguished from antiprotons.

But the author is convinced that with our threshold counter and associated electronics it was impossible to distinguish between one photoelectron and no photoelectrons. (In colloquial terms "the pedestals were too wide". The reader will see ample evidence for this later.) This, of course, makes the situation worse. Thus one would expect the proposition of selecting elastically scattered antiprotons from meson background at 200 GeV/c with our beam to have been extremely dubious. In fact, it proved to be experimentally impossible! (The reader will see the experimental evidence for this later.)

In the summer of 1980 we received news of the previously mentioned dip in $\bar{p}p$ elastic scattering at 50 GeV/c at CERN. (Fortunately for the author), at this point (toward the end of our first (of two) data runs) we decided to use the DISC to tag antiprotons at -200 GeV/c. This corresponds to about half our running at -200 GeV/c, and is the basis

for the -200 GeV/c $\bar{p}p$ cross section reported later in this thesis. Unfortunately this meant that we had to sacrifice kaons. The threshold counter was too short to separate π^- from $\bar{p}$ at this energy, let alone K^- from π^-! This does not mean that the threshold counter was useless for all of the results reported in this thesis. At +200 GeV/c and ±100 GeV/c it turned out to be helpful.

IV. SELECTING THE ELASTIC SIGNAL FROM THE INELASTIC BACKGROUND--HARDWARE

Having discussed the hardware considerations concerned with identifying species, we now "backtrack" slightly in the logical development and return to discuss in somewhat greater detail than previously how the experimental equipment was designed, laid out and used to separate general elastic candidate events from inelastic background. We also describe why and how the number of candidate events generated per "spill" was severely restricted. The further "off-line" selection of "true" elastics from mere candidates is described in Sections VI and VII.

A. Magnitude of the Separation Problem and Singles Rates

1. Magnitude of the Separation Problem

As we have mentioned, in addition to particles from desired elastic events, many particles were produced inelastically in the beam-target collisions. However, we hoped to measure elastic differential cross sections as low as 10^{-35} $cm^2/(GeV/c)^2$ using "bins" of width $\Delta t \approx 0.1$ $(GeV/c)^2$. Noting that the "column density" of protons in our target was about 4×10^{-2}, it is pretty easy to see that with this magnitude cross section one expects only one event per bin for some 3×10^{11} incident beam particles. So obviously we had to be pretty darned selective! To elucidate the signal to noise problem a bit further, we note that the lowest elastic cross sections were expected at the highest -t values, and that the experimental "singles rate" in scintillation counter R6 (corresponding to our highest -t events) was close to 850,000 per spill for a one second spill of about 10^7 incident particles.

2. Maximum Tolerable Rates (A Comment on Our Limitations)

Of course, most of the background could be eliminated in the "off-line" data analysis; however, if the background rate were too high and our trigger not sufficiently selective, in addition to making an inordinate number of magnetic tapes, desired data would have been lost due to saturation of the capability of our "on-line" PDP 11/45 computer, which could not handle much more than about 100 triggers in a one-second spill. Thus, our trigger would have to be "tight" enough to keep the trigger rate below this level.

Then there is another problem with excessive background. In order to gather elastic data at a reasonable rate, a beam intensity of $\geq 10^7$ particles/pulse was required. It was known that the "average multiplicity" in p-p inelastic collisions at 200 GeV/c is about 7. A scintillation counter becomes essentially useless at a repetition frequency approaching 10 megahertz, and indeed will start to "sag" well below that rate. Proportional wire chambers can also not survive rates that are too high. Thus again, without some thought there would be danger of losing much of our data. This could of course have been compensated for by running longer, but as anyone who has worked at Fermilab knows, one does not expect this.

These potential problems could, of course, have been overcome if they had arisen in practice by changing our equipment or our layout--e.g., using more finely segmented hodoscopes for the trigger, moving hodoscopes further away from the target (if real estate considerations permit), etc. In practice, problems like this are almost always solved

experimentally. However, in this thesis we take the point of view that the layout and equipment were fixed--as indeed they "are" since the experiment has already been done. Our attitude is then one of convincing the reader that the results obtained with this apparatus and layout are due to genuine elastic events. While this does not, of course, require a complete understanding of the background, it does, in the opinion of the author, require some "handle" on it. We therefore hope that the reader will indulge the author in some of his remarks about "singles rates" in Subsection 4.

3. A Preliminary Remark About Signal to Noise Ratio

From a variety of considerations, "singles rates" were expected to (and experimentally did--see later) fall quickly with scattering angle. The elastic signal was also expected to (and did) generally fall quickly with scattering angle. However, it was known[106] that at lower energy $\frac{d^2\sigma}{dp_c d\Omega}$ (p_c is the momentum of the forward scattered "leading particle") does not fall nearly as quickly with scattering angle as does the elastic $d\sigma/d\Omega$. Hence, one expects (and finds!) a worsening with increasing $|t|$ signal to noise ratio insofar as the forward arm is considered alone.

In the recoil arm it is, of course, also true that the highest singles rates occurred closest to the beam direction. But so did the relatively rare high $|t|$ elastic scattering rays that we were especially interested in. So, as far as the recoil arm is concerned, we also expect a worsening signal-to-noise ratio with increasing $-t$. This will turn out to be important later in this thesis.

4. Singles Rates We Realistically Expected

Unfortunately the theoretical estimation of singles rates is notoriously difficult. The proof of the pudding must, of course, be experimental. However, it would have been ludicrous to set up $\sim\$10^6$ worth of equipment, do a test run and then find out that we couldn't measure anything! So we at least want to mention some of our thoughts concerning expected singles rates as they affected the layout!

a. Some Semi-quantitative Considerations

What would be the expected rate, e.g., in our "R" hodoscope? One can get an upper bound on this by noting that our LH_2 target was about 10% of an interaction length long. Then, assuming an average multiplicity of 7 final state particles per interaction, isotropy in azimuth and estimating that the azimuthal acceptance of the R counters (and upstream recoil chambers) was $\leq$10% of 2π, at an incident intensity of 10^7 particles per second, one would crudely estimate an upper bound of $(7)(.10)10^7 \leq 7\times10^6$ particles entering the hodoscope per second. Allowing for the fact that our equipment did not cover the entire range of scattering angles (i.e., for example, the recoil detectors did not extend to the beam direction), the estimate is reduced still further. Similar considerations apply to the forward arm. So our layout appeared sensible.

One can do better than this by noting that $\frac{E_c d\sigma}{d^3p_c}$ had been measured for inclusive charged pion production (the bulk of the inelastic background) for $\pi^{\pm}p$ (and $p^{\pm}p$) at 100 GeV/c and 200 GeV/c in Fermilab bubble chamber experiments. Then integration over momentum and solid angle acceptance would yield the desired rates.

Along these lines an estimate was made by Orear[107] who assumed that πp and pp inelastic scattering were not terribly different and applied the assumption of Feynman scaling to Allaby's[118] 24 GeV/c p-p data, thus estimating the inelastic differential cross section for various scattering angles at 200 GeV/c.

Now the inelastic $\frac{d\sigma}{d\Omega}$ had been measured at a scattering angle of 33° in Fermilab experiment E177 (200 GeV/c pp scattering) by using a monitor telescope of known solid angle $\Delta\Omega$. The measured cross section comes out to be within a factor of two of that calculated using scaling. Armed with this confidence, Orear then estimated that rates in our experiment with our layout would be tolerably low.

5. Experimental Singles Rates

Experimentally, the singles rate in the R hodoscope (summed over all elements) was about 2.7×10^6 for 10^7 incident particles. (The close agreement with our earlier crude guess for an "upper bound" is probably coincidental.) In the forward arm (at ~200 GeV/c the hottest counter was F_2^β which had a singles rate of about two million per spill for a spill of 10^7 incident particles, although this rate undoubtedly reflects much scattering in our apparatus. The singles rates in the F^α elements were often a factor of five less than those in the corresponding F^β elements, the F^α summed (over all elements) singles rate being about 2.4×10^6 for 10^7 incident particles, in apparent rough agreement with the total singles rate in the R hodoscope.

[It was found experimentally that the singles rate in the R hodoscope did not go to zero when the target was empty--in fact, it remained at up

to 50% of the "full target" rate. This indicates that the beam may have been surrounded by a relatively wide halo which interacted, e.g., in the aluminum around the target, the recoil magnet yoke, etc. The anti-counters could theoretically have provided a measure of the halo. However, the analysis of this proved to be somewhat complicated. In any case, for the present discussion the exact amount of beam halo is unimportant--we simply note that probably only about half of the singles rate in the R counters was caused by interactions in the target.]

Thus we note rough agreement with, e.g., the estimate of Orear. [The apparent difference (about a factor of 30) should not be alarming as Orear did not take into account the exact geometry of the recoil hodoscope and rates change quickly with scattering angle.] We conclude that there is no evidence from the analysis of singles rates that our equipment was not working as planned or that our measurements were made incorrectly.

B. Trigger Fast Logic--Design Considerations

As we have remarked, at an incident intensity of 5×10^6 particles per one second spill, we typically had $\leq 10^6$ "hits" per spill in, e.g., the R hodoscope. We had to cut down to a total of 100 triggers/spill--i.e., we had to have a means of rejecting over 99.9% of these "hits" prior to the tape writing level. Similar considerations applied to the forward arm.

1. Forward Arm Fast Logic*

In the forward arm, the seven element F^{α} hodoscope provided a loose measure of the scattering angle (and hence of -t) for a forward

*The reader would do well to refer to Figure IV-1 while reading this section.

traveling particle.

Since P_f is approximately constant for $1 \lesssim -t \lesssim 10$ GeV/c)^2 at 200 GeV/c, the bend angle in the BM109 magnets for eleastically scattered particles with beam momentum 200 GeV/c was practically the same (about ten milliradians) for any value of -t within our acceptance. This was also true at 100 GeV/c (in which case the current in the BM109 magnets was set to half of the value for 200 GeV/c).

However, away from these values of momentum, the bend angle went like P_f^{-1}. Therefore, by positioning the F^α hodoscope immediately downstream of the BM109 and the F^β hodoscope far enough downstream of F^α to have a sufficiently long "lever arm", we were able to set up a "triggering matrix" between the elements of F^α and those of F^β that required the momentum of the scattered particle in the forward arm to be close to the "elastic" value. This scheme had already been used successfully on a lower energy π^-p experiment referred to previously.[102]

Now, if the beam were infinitely thin, the F^α-F^β elements could have been positioned so that there was a "one-to-one" correspondence between them--i.e., all elastic rays striking F_3^α would strike only F_3^β, etc. However, the non-zero spot size at the target and the beam divergence prevented this, as rays striking an element of F^α at a given point had left the target with a range of scattering angles.

Therefore, to have all rays from F_α^i (i^{th} element of F^α) strike F_β^i, it was necessary to have some of them also strike F_β^{i+1} and F_β^{i-1}--the segments of the F^β hodoscope had to be overlapped. The approximate positions of the elements of F^β relative to those of F^α could be calculated on a vest-pocket calculator, but were in fact determined with a

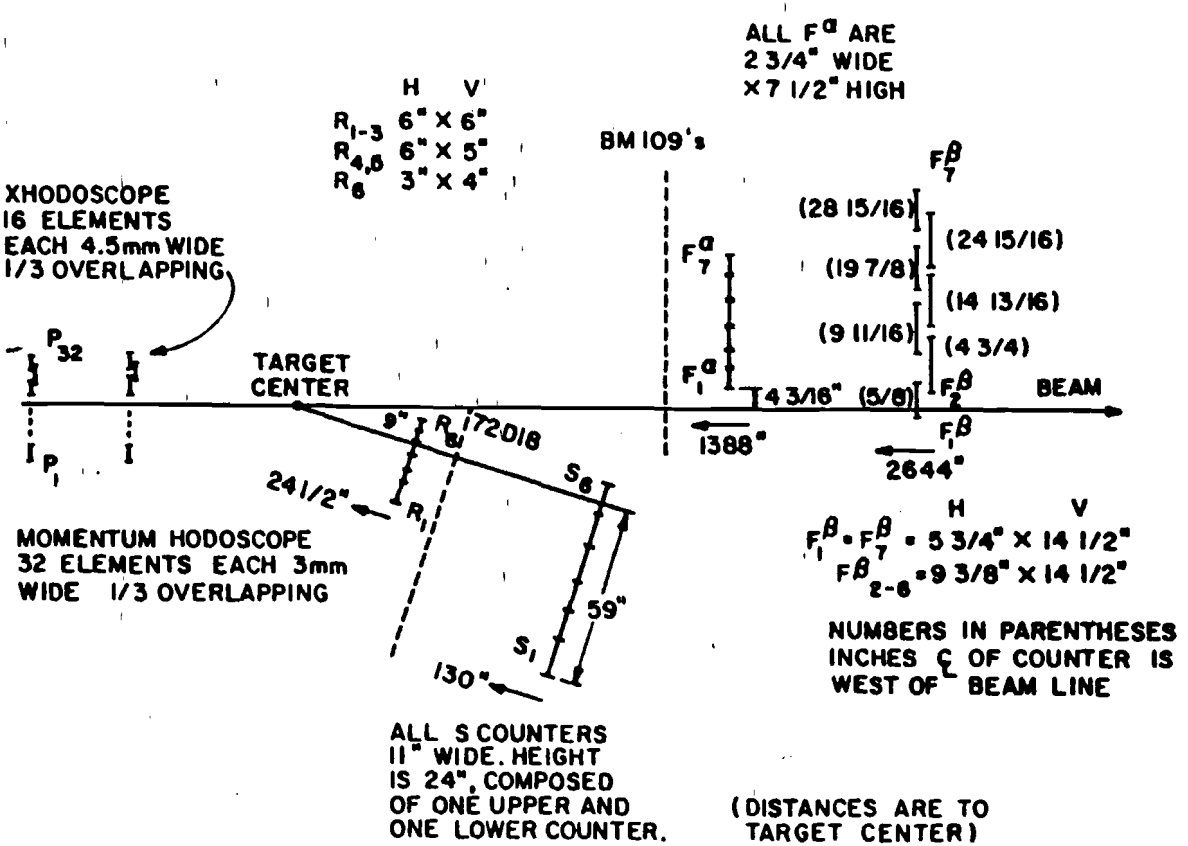

Figure IV-1. Arrangement of scintillation counter hodoscopes for the trigger. (Drawn originally by R. Rubinstein, used here with his permission.)

Monte Carlo program. In practice, the elements of F^{β} were somewhat wider than was needed; this hurt our selectivity somewhat, but not tragically.

For a typical spill of 10^7 particles at -200 GeV/c, about 20% of the F^{α} "singles" counts were removed by requiring that no more than one F^{β} element fire ("multiplicity cut"). The number of potential triggers was further reduced by requiring that no more than two elements of F^{β} go off. Experimentally, when we then required the "F^{α}-F^{β} matrix" referred to above, we were down to about 4×10^{-3} candidates per beam particle or, for a spill of 10^7 beam particles, about 40,000 candidates. This was still far too many per spill to write on tape. The forward arm matrix could have been made more selective by making both the F^{α} and the F^{β} hodoscopes more segmented; however, we decided not to do this.

2. Recoil Arm Fast Logic

The S hodoscope was set in the recoil arm so that, having roughly measured q^2 with F^{α}, the opening angle could be constrained to be near the elastic value for that q^2. However, almost as an afterthought the R hodoscope was installed. This allowed us further trigger selectivity through the requirement of further R-S coincidences ("RS matrix").

Due to the relative proximity of the R and S hodoscopes to the target, the RS matrix could obviously not be diagonal (with elements of the sizes we used). For example, 200 GeV/c elastic rays originating from the front of the target and passing through only R5 or R6 could pass through any element of the S hodoscope.

Thus, it should already be apparent that the RS matrix was not a major factor in cutting down the trigger rate. However, it did serve to eliminate combinations that correspond to rays that did not originate

within the target. The exact RS matrix was determined by Monte Carlo methods; it is given on page 150. One notices that at 100 GeV/c S4, S5 and S6 are "not allowed". This is because the acceptance at 100 GeV/c cut off at about $-t \approx 3$ $(GeV/c)^2$. At 200 GeV/c, after requiring multiplicity cuts in the R and S hodoscopes and the "RS matrix", the number of RS triggers per beam particle was about 8.9×10^{-4} or, for a spill of 10^7 beam particles, about 9000 "RS candidates" (as compared to 40,000 "F^{α}-F^{β} candidates").

3. Combining the Recoil Arm Fast Logic with the Forward Arm Fast Logic

If one inspects the diagram of the recoil arm in Figure II-2 one sees that S1, S2, and S3 could not fire on a $-t = 9$ GeV/c elastic ray originating from the target. This is an illustration of the fact that "low S - high F^{α}" combinations (e.g., $S^1 - F_7^{\alpha}$) F_7 was the high -t end of the forward hodoscopes) were forbidden.

Also by glancing at the same diagram, it is obvious that, e.g., at 200 GeV/c, an elastic $-t = 1$ $(GeV/c)^2$ ray originating from the target could only go into S1. Therefore "high S low F" combinations were also forbidden. The exact "RSF" matrices obtained by Monte Carlo methods. That for 200 GeV/c is given in Table IV.1. It is seen that the "yes" entries of this matrix lie almost completely between the two diagonal lines drawn. It is also seen that the diagonal strip is at least four elements wide except for the topmost and bottommost rows. From this one sees that the constraint of the opening angle through the use of the RSF matrix was only crudely realized.

Glancing at the rates shown on page 152, it is obvious that the entries in the lower left of the RSF matrix were much more important in

		R					
		1	2	3	4	5	6
	1	1	1	1	1	1	0
	2	0	1	1	1	1	1
	3	0	0	1	1	1	1
S	4	0	0	0	0	0	0
	5	0	0	0	0	0	0
	6	0	0	0	0	0	0

		F						
		1	2	3	4	5	6	7
	1	0	1	1	1	1	1	1
	2	0	0	0	1	1	1	1
	3	0	0	0	0	1	1	1
RS	4	0	0	0	0	0	0	0
	5	0	0	0	0	0	0	0
	6	0	0	0	0	0	0	0

(a) 100 Gev/c

		R					
		1	2	3	4	5	6
	1	1	1	1	1	1	0
	2	1	1	1	1	1	0
	3	0	1	1	1	1	1
S	4	0	1	1	1	1	1
	5	0	0	1	1	1	1
	6	0	0	0	0	1	1

		F						
		1	2	3	4	5	6	7
	1	1	1	1	0	0	0	0
	2	1	1	1	1	0	0	0
	3	0	1	1	1	1	0	0
RS	4	0	0	1	1	1	1	1
	5	0	0	0	1	1	1	1
	6	0	0	0	0	1	1	1

(b) 200 Gev/c

Table IV.1 Fast logic matrices. "1" = yes, "2" = no. (Adapted from ref. 24.)

cutting the trigger rate than those in the upper right (there were relatively few inelastics "at low -t" in the recoil arm). However, most of the reduction in trigger rate was probably due simply to the requiring of a track in each arm.

In any case, with the use of the full "RSF" matrix the trigger rates were indeed cut to acceptable levels--at 200 GeV/c, the "RSF rate" per beam particle was about 4×10^{-6}, corresponding to about 40 "RSF triggers" for a spill of 10^7 beam particles. At +100 GeV/c the RSF rate was about 2×10^{-6} per beam particle (the reason for the difference between 100 and 200 GeV/c lay in the different acceptances for these energies--see later). [In the above we have spoken about various rates per "beam" particle. By the word "beam" we mean something rather specific--a coincidence in scintillation counters B_1 and B_2 together with the absence of a signal from anticounter A_1.]

In Figure IV-2 we show some of the scintillator rates that we recorded. By looking at, e.g., how rates in the various F^i vary with i, the reader can see roughly the behavior of $d\sigma/dt$ with t!

4. Temporal Considerations

To this point we have perhaps not given the reader a proper sense of the temporal development of a trigger. The F^α and F^β hodoscopes, being in the forward arm, were much further away from the place where the coincidences were actually made (for example, in our electronics trailer) than were the R and S hodoscopes. Hence, at the instant that an RS coincidence was made the corresponding F^α-F^β coincidence had not yet occurred. Indeed, since F^α and F^β were so far away from the target, at

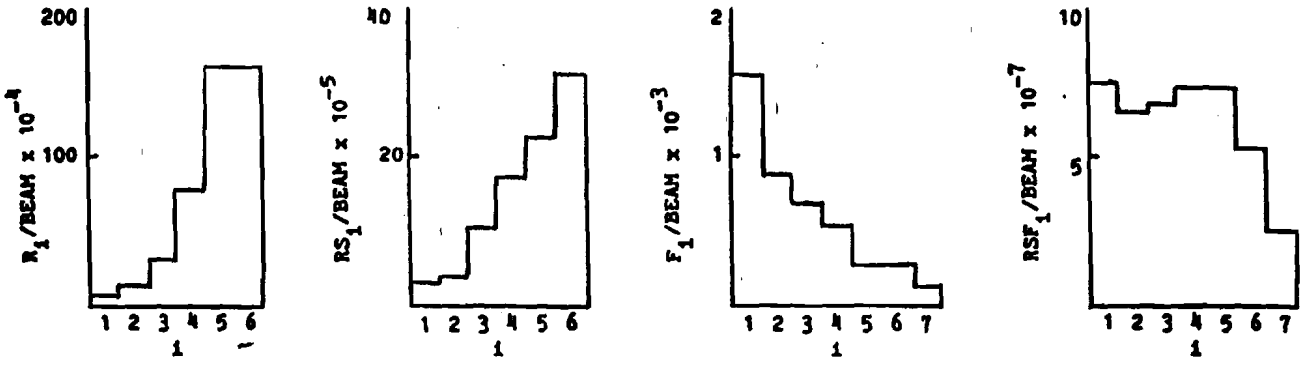

(a) Sample of spills with -200 GeV/c beam. RS/BEAM = 8.90×10^{-4} RSF/BEAM = 4.28×10^{-6}
elastics/BEAM = .048 gated-BEAM/BEAM = .858

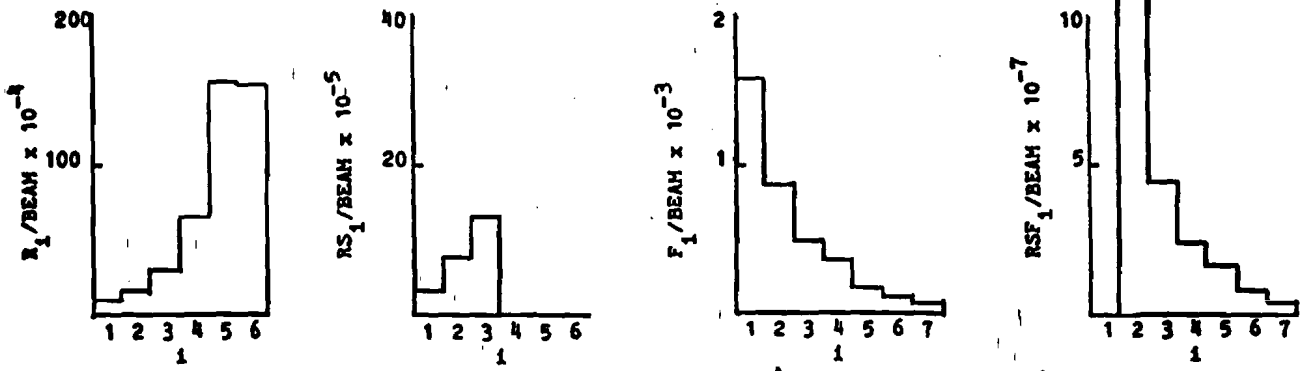

(b) Sample of spills with +100 GeV/c beam. RS/BEAM = 2.38×10^{-4} RSF/BEAM = 2.2×10^{-6}
elastics/BEAM = .53 gated-BEAM/BEAM = .915

Figure IV-2. Counting rates (from ref. 24).

the instant that an RS coincidence was generated for an elastic recoil ray, the corresponding forward traveling particle had not even reached the F^{α} hodoscope yet!

Therefore, in order to form proper "RSF" coincidences, the RS signal had to be delayed by approximately the speed of light travel time to F^{β} from our electronics portakamp and back again. To accomplish this, the RS signal was "stored" in 630 ns worth of delay cable to wait for the F^{β} signals to arrive. On the next page we show the simplified temporal development of a trigger.

Table IV.2 Typical rates (~200 GeV/c)

Beam/pulse	10^7
Beam + vetos + R	4×10^5
Beam + vetos + recoil matrix	9×10^3
Beam + vetos + recoil matrix + forward matrix	40

(a) Sample of spills with 200 GeV/c beam. RS/BEAM = 2.38×10^{-7} ~ RSF/BEAM = 2.2×10^{-9}
elastics/BEAM = .53 gated-BEAM/BEAM = .915

Figure IV-2. Count rates (from ref. 24).

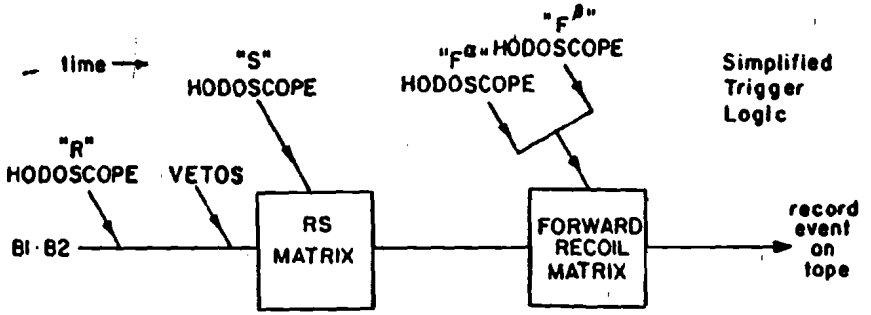

Figure IV-3. Simplified temporal development of a trigger.

5. Comment About Experimental Dead Time

In addition to keeping the trigger rate down to tolerable levels, the fast logic was also used to generate "strobes" to "read out" the information gathered by our proportional wire chambers. For example, the presence of an RS coincidence was used to strobe the recoil arm chambers. This strobe to the chambers, of course, could not be delayed by 630 ns or the relevant wire chamber information would be lost. We could have stored the wire chamber information in striplines or in a suitably large "FIFO" chip bank; however, after the generation of an RS coincidence it seemed simpler not to make (or to "veto") future RS coincidences until the information from F^{α} and F^{β} arrived.

This veto was called the "logic gating signal". It was generated by an RS coincidence and was not turned off until the formation of the next fall "RSF" trigger or 800 ns after it was turned on, whichever came first. The logic gating signal disabled the RS coincidence units (see Figures IV-4 and IV-5).

This scheme, of course, introduced dead-time into the experiment. But this dead time was not terribly consequential--there were, as mentioned, about 9,000 "RS coincidences" in a one-second spill for an intensity of 10^7. Hence the associated dead time was about $9{,}000 \times 800$ ns = 0.007 seconds $\approx$ 1% dead time. We could live with this.

Now, experimentally, the dead time at -200 GeV/c was 14.2%. We have seen that $\leq$1% was due to the "RS logic gating". The remaining $\sim$13.5% was due to the PDP 11. In a typical spill of 10^7 incident particles we had about 42 master triggers. Hence 13.5% dead time translates into about 3.2 milliseconds of dead time per trigger. In that

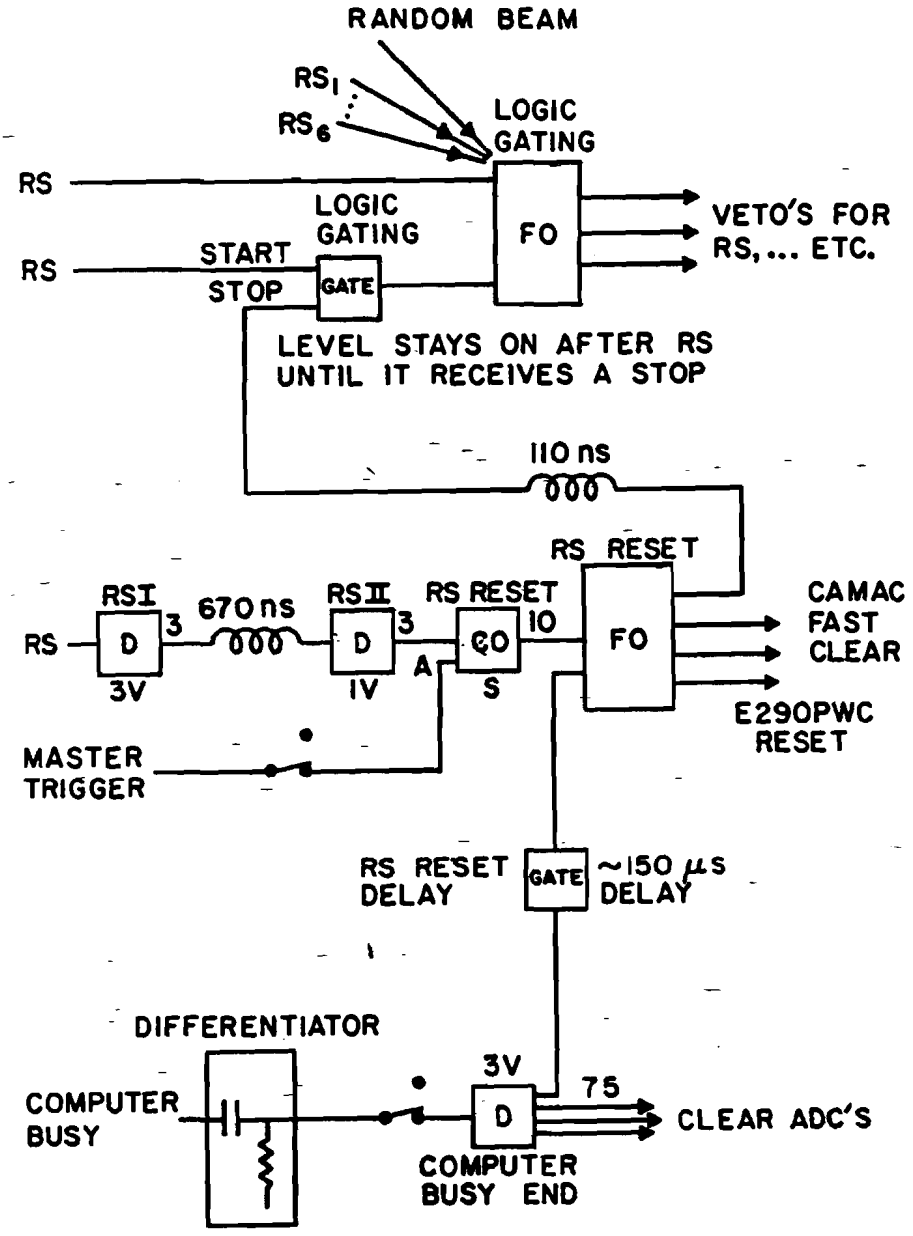

Figure IV-4. "Logic gating" (see text). (Figure drawn by R. Rubinstein, used here with his permission.)

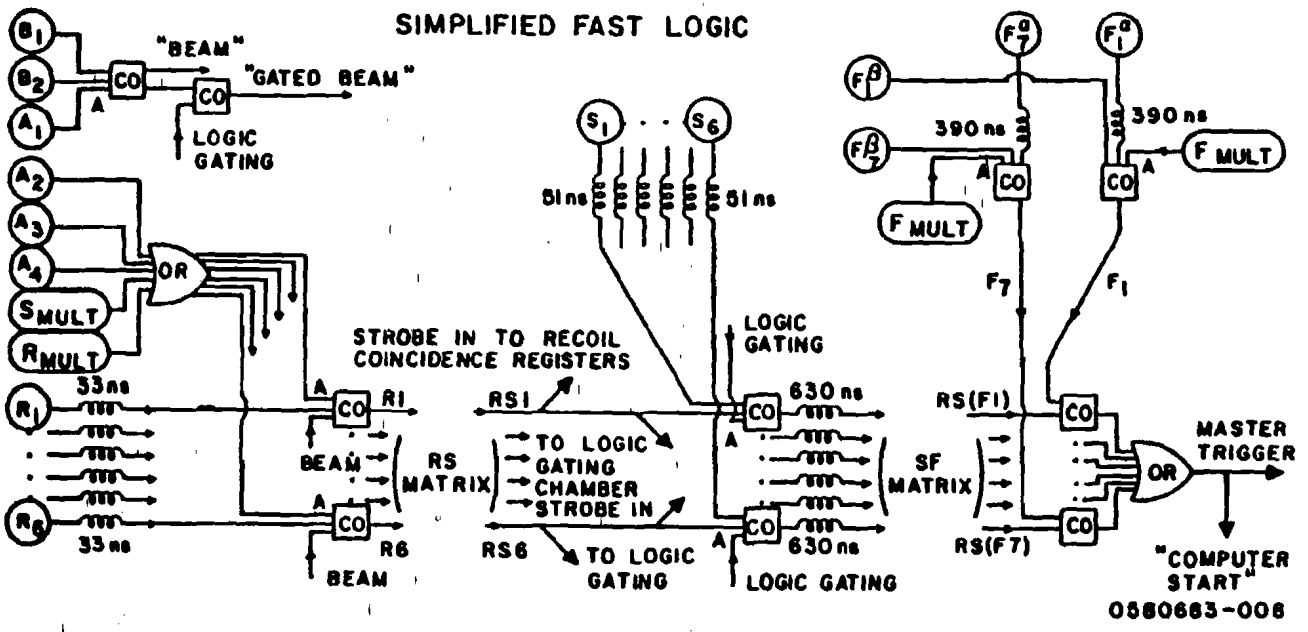

Figure IV-5. Simplified fast logic. (X) indicates output of discriminator corresponding to scintillation counter x. S,R,F MULT correspond to present of multiplicity signals (explained in test) from F^{α}, F^{B}, R, or S hodoscope. Logic gating is shown in Fig. IV-4.
~~~~ indicates (xxx) nanoseconds of delay cable. [CO] indicates a coincident unit, "A" indicates a "veto" input to coincidence unit. The name of the output signal is given on top of the arrow leaving the unit RSi for i=1,2,...,6 indicates the signal corresponding to the OR of any of the R counters for which counter S_i is required for an "RS matrix coincidence". RS(F_i) indicates the signal corresponding to the RS combinations needed for an "FS" coincidence with F_i.
~~~~

case, 150 master triggers gives a dead time of about half a second, i.e., about half the spill. So our original "guess" that the PDP11 could not handle much more than about 100 triggers per second was reasonable.

As we mentioned, at +100 GeV/c the trigger rate was about half that at -200 GeV/c. The "RS logic gating" (see above) dead time at +100 GeV/c (based on about 2400 RS "pretriggers" per ("10^7") spill) was negligible. Hence we expect a dead time of about half of 13.5% ≈ 7%. Experimentally it was about 8.5%.

V. SELECTING "TRUE" ELASTIC EVENTS FROM TRIGGERS

In this chapter we describe the further reduction of the sample of triggers to the final satisfactory sample of "true" general elastic events. This was done by off-line computer analysis of the MWPC information recorded on magnetic tape by the on-line PDP11 computer. In Section A the MWPC systems and the information from them recorded on tape are described in only slight detail. In Section B the off-line software is described in varying amounts of detail.

A. Multiwire Proportional Chamber Systems, Readouts, and Method of Recording Track Information on Tape

In this subsection we describe some of the hardware used to record positional information of sufficient accuracy about tracks so that the event separation could proceed.

1. Introductory Generalities and Classification

In all we had 31 Multiwire Proportional Chambers (PWC's) at our disposal for use in the experiment. These chambers were of three types:

i) Twenty "Fermilab" chambers. These chambers had been built at Fermilab and used successfully in Fermilab experiment #290. They had a sense wire spacing of 2mm and used a gas mixture that was 80% Argon, 19.9% Carbon Dioxide, and 0.1% Freon 13B1. They were read out by a parallel system somewhat similar to that first constructed by Cunitz and Sippach et al. These chambers and their associated readout system will be discussed in a bit more detail shortly.

ii) Seven "CLASP" chambers and four "CBUG" chambers. Since these chambers were all built at Cornell University, they will often be

collectively referred to as the "Cornell" chambers. The CLASP chambers had been previously used by the collaboration of the same name[109] at Cornell. These had twenty sense wires to the inch and an active area of two feet by three feet. The smaller CBUG chambers had 16 wires to the inch and an active area of about 12"×21". They had been used successfully in Fermilab experiment #177.[110] All of the Cornell chambers had "G10" frames and cathodes which were 1 mil thick aluminum (foil) planes 1/4 inch on either side of the anode plane (sense wires). The two large faces of each chamber (both Cornell and Fermilab) were covered with mylar (5 mils thick) to provide an effective seal for the circulating gas.

The Cornell chambers used a gas mixture consisting approximately of 75.5% Argon, 20% Isobutane, 4% Methylal and 0.5% Freon 13B1, this gas mixture having been found by Bouchlier et al.[111] at CERN to give simultaneously maximal gain and chamber efficiency.

For a variety of practical reasons, the Cornell chambers were read out by a different system than the Fermilab chambers.

2. Readout System for Cornell Chambers

The Cornell chambers were read out by a serial type system. "Hits" detected by wires during a "gate open" period of about 100 ns were stored in shift registers located on cards mounted on chamber edges. Each shift register handled 16 wires ("channels"). With the presence of a Master Trigger, a strobe was sent to the chambers initiating the readout into a special CAMAC module. Within about a millisecond of the strobe the data in this module was in a form ready for the computer. As this readout system will undoubtedly be described in considerable detail in Sean McHugh's thesis[112], we do not describe it further here except for one

comment in the next section.

3. Overview of Readout System for Fermilab Chambers

The Fermilab readout system was (unnecessarily) complicated in its details. Therefore we limit ourselves to giving the reader an overview of this system.

a. Some Generalities and Further Comment on Dead Time

The Fermilab chambers had a total of about 5000 wires. For each event, the identities of all the "hit" wires had to be written onto magnetic tape by our "on-line" PDP11 computer. One can imagine complementing this by assigning each wire a "binary" address. This would involve about 14 bits per address. DEC (Digital Equipment Corporation) PDP11 computers, however, have sixteen data lines. Therefore, it is obvious that addressses of hit wires had to be communicated one-by-one, i.e., serially, to the computer.

If the serial reading of wire chamber information for an event takes a long time compared to the mean period between Master triggers, it is clear that an advantage in decreasing dead-time would be gained by storing in buffers backed-up data waiting to get into the computer. In that case, the address generating parts of the system (and the wire chambers themselves) could be freed to work on new data while the previous data is waiting in the buffer.

With considerations of this sort in mind, our system was designed to obtain a readout time of about 200 ns per track (as compared, e.g., to the Cornell "readout time" of about 1 millisecond). This might be important for an experiment with extremely high Master Trigger rates. We, however, expected ≤50 Master Triggers per one-second spill. In that case,

even the Cornell system's millisecond of readout induced dead-time per trigger would lead to only about 2% total "readout" deadtime with a large enough data buffer. So, for us the extreme speed of the readout system was unnecessary.

Suppose we had aimed to design a simple system with a "buffer" for storage that would allow us to achieve this $\lesssim$2% deadtime. How big a buffer would this have required? Fifty Master Triggers per spill implies an average of about one trigger every twenty milliseconds. We have seen that the PDP11 apparently took about 3 milliseconds to read and process each trigger (see Chapter IV). So, on the average, data would have been leaving the buffer almost seven times as fast as it would have been entering. Thus it is clear that only a few events' worth of storage would have been sufficient.

Now, as we mentioned, there were twenty Fermilab chambers. Most of the time, chambers in an experiment such as ours do not have more than about 3 hit wires per event. So 20 chambers $\times$ 30 hits per chamber per event $\times$ say 3 events gives about 180 words of storage. For the Cornell system, 11 chambers similar implies a need for about 100 words of storage.

Neither the Fermilab nor the Cornell system had a sufficiently large buffer. For example, the Fermilab system had only <u>two words</u> of storage.

This being the case, both readout systems were "shut off" completely (with the Logic Gating signal discussed in Section II.D.5) during the entire $\sim$3 millisecond period it took for the computer to process each event. <u>Therefore, in this manner the "superfast" Fermilab readout system actually helped slow down the readout. This was directly responsible for the, e.g., 15% deadtime observed at -200 GeV/c</u>. Had the intensities

been higher the situation would have been worse. For example, had we run at the intensity mentioned in our original proposal ($\sim 5\times10^8$ per spill) the deadtime caused by the Fermilab system would have been intolerable.

"Because we had two different readout systems", we had two distinct almost identical sets of Fast Logic, one for each system. In order to have an event written on tape both sets of logic had to register "Master Triggers". This was unfortunate because the two sets of logic agreed with each other only about 85% of the time. This probably caused an additional 15% loss of events.

b. Simplified Overview of the Readout Process

i) Generalities

As we have mentioned previously, the layout of the experiment was such that the equipment in the recoil arm was much closer to the fast logic and readout electronics than that in the forward arm. For the purposes of making fast logic coincidences, therefore, scintillator signals from the recoil arm were delayed in appropriate lengths of "delay cable" (see Chapter IV). We did not do the same with the wire chamber information because the nature of the readout system allowed us not to.

What was needed then was a set of "stations" to store information from the recoil arm chambers until either (whichever came first)

a) Master Trigger came, in which case the stations had to release the wire chamber information upon demand to be sent to the computer, or

b) after a suitable delay (about 800 ns--roughly the speed of light travel time down the forward arm and back) Master Trigger had

still not come in which case the stations had to be readied to accept new information from the recoil arm.

In the case of the Cornell readout system, these "stations" were simple TTL RS latches which were on the cards mounted on the chamber edges. In the case of the Fermilab readout system the stations were RS latches made by using positive feedback with operational amplifiers. These latches were mounted on special cards called "coincidence registers" located in crates in our electronics trailer.

In the Fermilab readout system, amplifier cards were mounted on chamber edges. These cards used MECL (Motorola Emitter Coupled Logic) - "II" series circuitry for maximum sensitivity and good noise rejection. Each amplifier card handled 8 wires ("channels"). The outputs of these cards were sent to the coincidence registers via ribbon cable stripline, each stripline and coincidence register handling 32 channels.

ii) Simplified Interplay of Control Signals with Coincidence Register (see Figure V-1)

The positive and negative output pulses from the amplifier card were received differentially on the left, the resistor providing line termination and the value of C chosen to be about 1 μs so that amplifier output pulses passed through (the input from the amplifier was ∿50 ns wide with a rise time ∿ half this) and low frequency (e.g., 60 cps) noise was rejected. Differential receiving is used for low noise and high sensitivity. This sensitivity is determined by the "Th+" and "Th+" voltages, which were adjustable, input from outside, and set about 100 mV apart (which was somewhat less than the height of a typical pulse coming in from the stripline). The "Strobe In" signal originated from the fast

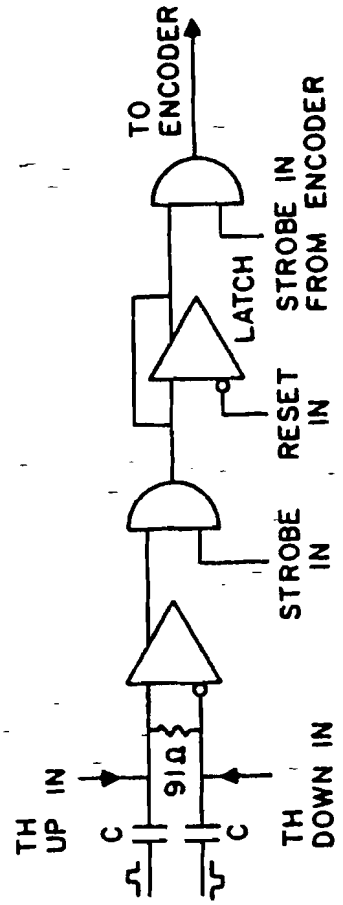

Figure V-1. A simplified channel of a coincidence register card (system designed by R. Cavanaugh after Sippach and Cuniltz (see text)).

logic (see Figure IV-4) upon the generation of, e.g., an RS coincidence. With the presence of this signal, the "hit bit" (high if hit, low if not) was stored in the latch. The Strobe In signal passed the hit bit on to the next level of readout logic, the encoder. (When the encoder was ready for information it generated the Strobe In.) "Reset In" was generated by the fast logic upon generation of a Master Trigger or about 800 ns after Strobe In if no Master Trigger comes (this is clear from Figure IV-5).

"Reset In" was also generated upon receipt of the trailing edge of the "Computer Busy Signal" (see Figure IV-4 again). This Computer Busy signal was a level raised by the computer for the entire length of time it was busy "digesting an event"--about 3 milliseconds, as we've seen.

As the chambers in the forward arm were at varying distances from the readout electronics, the same scheme was used there--the hit bits were latched up in Coincidence Registers until complete Master Trigger information was present.

In addition to passing on the "hit bit" the Coincidence Registers also performed part of the address generation. The coincidence registers (each handling 32 channels) were arranged into nine crates, each crate having 16 registers. The address of a hit was broken up into four pieces:

- the crate address (i.e., which crate) - 1-9 (4 bits)
- the coincidence register address within a crate (i.e., which register) - 4 bits
- the "group address" (which of four groups of 8 channels each) within a register - 2 bits

- the wire address within a group (1-8) - 4 bits

for a total of 14 bits

The coincidence register address within the crate was set by hand on each coincidence register itself with switches. This address was passed on to the encoder upon demand.

iii) Purposes of the Encoder and a Bit More on Its Interaction with Coincidence Register

As we remarked, addresses of hit wires ultimately had to be sent to the computer serially. To accomplish this, the encoder (there was one encoder per crate) considered a group of eight wires at once, scanned it for hits, generated and sent the addresses of them on if it found any, then moved to the next group of eight wires, scanned it, etc. When an entire coincidence register had had its four groups read the encoder immediately generated a "Reset" signal, sent it to that coincidence register, then moved on to the next register, etc. This sequential reading of coincidence registers was accomplished with a "Carry" signal, which propagated from register to register. All 32 "hit bit" (defined previously) outputs of each register were OR'D together ("FAST OR"). If a register had a "high" OR output upon receipt of the CARRY signal the data from that register was sent to the encoder. The encoder then handshook with the Reset for that register.

The outputs of the amplifier cards were also OR'D together. This feature could have been used to replace the entire scintillation hodoscope fast logic system. (That is, the experimental trigger could have been generated by requiring proper combinations of tracks in different chamber arrays, a "track" being defined by proper coincidences of the

OR's.) In an experiment with high information rates this would theoretically be a distinct advantage over using scintillation counters for the trigger as the effective segmentation could be made much finer, thus improving selectivity. However, there is an advantage to using scintillation counters in terms of reliability. Also, scintillation counters triggers had worked for elastic scattering in the past, and so it was chosen to stick with that scheme. At trigger rates like ours it doesn't make much difference except in expense.

In addition to scanning the registers for bits the encoder also encoded the create address (set by switches on the encoder; recall each crate had its own encoder), generated the group address and generated the "wire address" within a group. All of this information was sent to the next element of the Readout system, the "MIXER", upon demand. As the internal circuitry of the encoders were very complicated (in fact, over-complicated) we do not feel that this thesis is the appropriate place to describe any of it, even in simplification.

iv) The Mixer

The MIXER translated encoder signals from MECL levels to TTL level CAMAC convention commands so that communication with the computer would be possible. Likewise, it translated CAMAC convention commands originating from the computer onto MECL level signals usable to the encoder. As such it served as an interface. Also, it had a small buffer capable of storing two words (i.e., two addresses) at a time.

v) The System in Operation--the Readout Cycle

In this subsection we briefly describe the "dynamics" of the Fermilab Readout System with a list of temporarily ordered steps:

1 Quiescent state--no Master Triggers have come yet this spill. Data is being latched into coincidence registers and then released. The encoders are "off". The PDP11 is typically working on same program it has been given--e.g., making on-line plots of previous data, etc.

2 A Master Trigger is generated. Almost instantly the "Computer Start" (see Figure VI-4) is generated by the fast logic.

3 A computer "Interrupt" is generated which instructs the computer to drop what it was previously doing and begin a new "Readout Cycle". The computer immediately generates a "busy" level which remains on until the end of the readout cycle. The presence of this level leads to the generation of the logic gating signal, thus vetoing further $\overline{RS}$ coincidences.

4 The computer instructs the branch driver to send some commands the mixer. This step takes ~100 μs.

5 Mixer "translates" these commands into MECL standard and communicates them to the encoders. The encoders are turned on and begin reading coincidence registers.

6 Within about 150 ns, the encoder sends the first two addresses to the mixer, filling it. The mixer sends a signal to the computer indicating that its buffers are filled.

7 The computer terminates the write instruction and sends a "Read" command to the mixer. This step takes ≥100 μs.

8 The computer then reads words out of the mixer at a rate of about one per μs (the typical "read speed" of DEC computers). Several hundred words must be read.

9 The computer has "read" and stored all the data pertaining to this event (including scintillator latches, ADC's, etc.) in memory. The trailing edge of computer busy comes.

10 This trailing edge is differentiated by the fast logic (see Figure IV-4). After about 160 μs the reset signals for the chambers are generated. After another ~110 μs the Logic Gating signal is turned off, thus freeing the fast logic to make more RS coincidences, etc.

In all, about 3 ms have gone by since the start of the Readout cycle. This directly causes the, e.g., ~15% deadtime at 200 GeV/c referred to earlier.

B. Data Analysis Methods

[As we remarked in the introduction to this chapter, in this section off-line software methods are described in varying amounts of detail. The reason for this variation is to avoid extensive overlap with the thesis of P. Karchin.[24] To get the full view the reader should consult that also.]

The purpose of all of the experimental instrumentation and the "on-line" computing system was to make a "semi-permanent" record on magnetic tape of data about "candidate events" that had passed the trigger requirements. This data consisted of the addresses of all the "hit" wires in the event, hodoscope information, etc.

The next job was, of course, to separate true elastic events from mere candidate events. To give the reader some idea of the process, we mention here that in a typical run of several hours' duration at -200 GeV/c there were (recall that we had about 40 triggers per spill) about 48,000 triggers, only about 2,100 of which were "satisfactorily" elastic

events (mostly πp elastics)--i.e., the "elastic yield" was only about 4.3%. (At -100 GeV/c, on the other hand, elastic events comprised about 47% of the triggers (mostly because at -100 GeV/c the acceptance began near $-t \approx 0.4$ $(GeV/c)^2$ rather than $-t \approx 0.8$ $(GeV/c)^2$ as it did at -200 GeV/c, and at lower -t the cross sections are bigger).

As mentioned in the experimental overview section, this was done off-line" over a relatively long time interval (compared to the actual running time) using the Fermilab Cyber 175 computing system. In this section we describe how this was done.

1. Pattern Recognition

In order to decide if a candidate event was elastic one had to "reconstruct" the event--that is, determine "sufficiently precisely" the paths in space of the incoming beam particle and the outgoing final state particles associated with the event.

A given final state particle left a partial record of its path in a series of "hits" in successive proportional wire chambers spaced at intervals along the floor of the experimental area. The "best" straight line (see below) that could be fit to the pattern of hits associated with the passage of a particle was called the "track" of the particle. Thus, it was necessary to find the tracks of all the particles associated with an event, and algorithms were written to do this.

a. Arrays of Chambers

Once the chambers were aligned they were used for pattern recognition or "track finding". The first step in this program was the arrangement of the chambers (both physically and conceptually) in groups or "analysis arrays". These arrays are listed in Table V.1, along with

Table V.1. Characteristics of wire chambers and chamber arrays used for track reconstruction in elastic events. The angular resolution (in radians) is an estimate based on wire spacing and chamber separation. [Adapted from ref. 24, page 55]

Chamber array	Chamber name	Type	Wire spacing	Number of wires	z-coord inches	Low edge inches	High edge inches	Angular resolution of array	Min. no. chambers required
forward	FOXX	FNAL	2 mm	96	501.4	1.63	9.19	3.62×10^{-5}	
upstrm	FOX	FNAL	2 mm	96	512.1	1.68	9.24		
x-view	CF1X	CBUG	1/16"	256	1123.4	5.56	21.50		2
	F1X	FNAL	2 mm	192	1143.6	4.68	19.80		
forward	FOYY	FNAL	2 mm	64	496.9	-2.79	2.25	1.06×10^{-5}	
y-view	FOY	FNAL	2 mm	64	507.3	-2.74	2.30		
	CF1Y	CBUG	1/16"	144	1127.5	-4.66	4.28		
	F1Y	FNAL	2 mm	96	1147.7	-3.86	3.70		3
	CF2Y	CBUG	1/16"	144	1365.5	-4.80	4.14		
	CF3Y	CLASP	1/20"	320	2631.0	-8.21	7.74		
forward	CF2X	CBUG	1/16"	320	1361.4	5.31	25.25	1.54×10^{-5}	
dnstrm	F2X	FNAL	2 mm	256	1370.4	4.82	24.98		
x-view	CF3X	CLASP	1/20"	720	2627.0	-2.22	33.74		2
	F3X	FNAL	2 mm	448	2638.1	-3.46	31.82		
recoil	RB1X	FNAL	2 mm	448	26.36	-24.19	11.09	1.43×10^{-3}	
upstrm	RB2X	FNAL	2 mm	512	42.25	-32.05	8.26		1
x-view									
recoil	RB1Y	FNAL	2 mm	96	27.48	-4.16	3.40	1.43×10^{-3}	
upstrm	RB3Y	FNAL	2 mm	96	34.14	-3.68	3.88		--
y-view	RB2Y	FNAL	2 mm	128	43.37	-4.58	5.50		
recoil	RB4B	FNAL	4 mm	320	85.63	-43.07	7.33	6.45×10^{-4}	
down-	RB4A	FNAL	4 mm	320	91.33	-43.26	7.14		
stream	CRB5D	CLASP	1/20"	304	112.44	-58.23	-43.08		2
x-view	RB5A	FNAL	4 mm	320	114.85	-36.92	13.47		
	RB5C	FNAL	4 mm	128	120.88	-62.12	-41.96		
	RB5B	FNAL	4 mm	320	123.49	-37.46	12.94		

some characteristics of the chambers within them. The angular resolution of each array as listed is calculated from

$$\text{ang. res.} \approx \frac{\text{W.S.}}{\sqrt{12}\ D}$$

where D is the distance (in z) between the chambers at the extreme ends of the array and W.S. is the wire spacing.*

b. Alignment of Chambers

i) General Definitions

The first step in track finding involved the "alignment of chambers". What is meant by this phrase is the following: Each wire of a chamber corresponded to a given line in real space. In order to reconstruct events properly, the position in real space of each wire of a chamber had to be known with sufficient (see later) accuracy.

Thus, associated with each chamber were two constants--the position of the first wire in real space and the wire spacing. If these constants were not known with sufficient precision, elastic events would be lost and "false" events would be "found". The process of determining the constants that were the positions of all the first wires for an "array" of chambers was called "aligning the array". The two examples in Figure V-2 illustrate the concept. Note that we have defined two types of alignment--"relative alignment" (of the chambers within an array) and "absolute alignment".

---

*Note, for example, that the two forward arm x-arrays each have two pairs of chambers, the chambers within a pair having essentially the same z-coordinate. As the angular resolution of an array of four chambers is better with the chambers evenly spaced in z, the reader may wonder why the spacings in the table were used. The reason is "historical",

RB5C FNAL 4 mm 128 120.88 -62.12 -41.96
RB5B FNAL 4 mm 320 123.49 -37.46 12.94

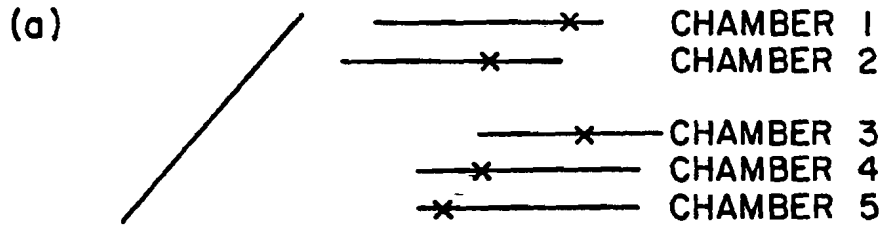

(a) The real space particle path is shown on the left. On the right are the real space positions of hits corresponding to the particle path at left as determined fron alignment constants. As shown here, chambers 2 and 3 are "out of alignment".

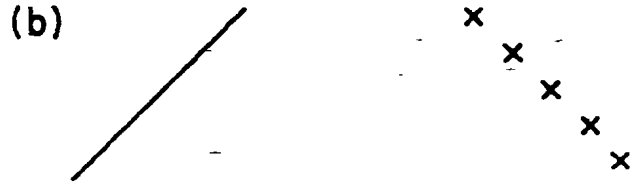

(b) The real space particle path is shown on the left. On the right are the real space positions of hits corresponding to the particle path at left. "Relative alignment" of chambers within array is satisfactory but "absolute alignment" is not.

Figure V-2. Illustrating the alignment procedure.

ii) Alignment Arrays

For the purpose of alignment the chambers were divided into groups or "alignment arrays", each array being aligned separately. The two chambers that were most separated in an array (i.e., the "end chambers") we shall call the "anchor point chambers" (for reasons that will shortly become obvious). It will become clear (if it is not already so) from the discussion in Subsection c that the greatest accuracy in alignment could be obtained by having the anchor chambers as far apart as possible--by having as many chambers as possible in an array. Clearly, this requirement could be achieved by aligning with tracks obtained during special runs when the bending magnets were off. The four alignment arrays were thus (1) all forward arm x-chambers, (2) all forward arm y-chambers, (3) all recoil arm x-chambers, and (4) all recoil arm y-chambers.

iii) General Method of Relative Alignment

The method of alignment that had been used previously (on Fermilab experiment #290) was something like the following: A particle passes through an array of n chambers. The "best line" is fit (lowest χ^2) to all the hits. For each chamber in the array the "residual" to the fitted line (distance between position of hit as measured using existing chamber alignment constant) is calculated and histogrammed. Procedure is repeated for many particle paths. Alignment constants for all chambers are adjusted ("chambers are moved") until peaks of residual histograms for all chambers are centered.

This is not a very efficient method of aligning chambers because it causes the alignment constants of all of the chambers in the array to be

"coupled" to each other during the alignment process. Thus the relative alignment of a nine chamber array becomes a fairly time consuming nine-dimensional problem. Therefore, the author did not use this method of alignment.

The method of alignment used by the author* was the following: For a given event a particle's path goes through all (or most) of the chambers in the array being (relatively) aligned. Only those events in which there is one and only one hit in each of the anchor (end) chambers are considered. For each such event a line is drawn connecting the hits in the anchor chambers (and thus intersecting all the other chamber planes in the array). (Note: This already streamlines the computing algorithm considerably in that a line does not have to be "fit", chi-squared does not have to be calculated, etc.). The point where this line intersects the plane defined by an intermediate chamber is called the "predicted position" (for a hit) in the intermediate chamber.

One then considers all of the actual hits in each of the intermediate chambers. The "residual" of a given intermediate chamber for an event is defined as the absolute value of the difference (in real space) between the predicted position and the actual position of the hit in the given chamber closest to the predicted position. The residuals are histogrammed for each chamber for all of the considered events, and each residual peak is then "zeroed" separately.

The main advantage of this method is that each chamber can be "moved"

---

*The author thanks John Klinger for helpful advice on this.

individually without affecting the residuals of any of the other chambers (since no fit lines are used)--the chambers are now uncoupled from each other. A complicated nine-dimensional problem has been reduced to nine simple one-dimensional problems. Thus, instead of the relative alignment of a sizeable array taking, e.g., a month, it can typically be done in a day.

iv) Sequence of Alignments. Absolute Alignment of the Experiment

Note that performing the relative alignment does not guarantee absolute alignment of the array. Indeed, after relative alignment the absolute alignment may be "off" by a rotation through some angle, by translation, or by combination of both.

TRIVIAL THEOREM: Purely translational misalignment may be ignored.

PROOF: As far as is known, the interactions of particles are translation invariant ("isotropy of space").

α) "Beam Tracks". Absolute Alignment of Forward Arm

In practice, in the forward arm it was found to be advantageous to perform the absolute rotational alignment before doing the relative alignment. This was accomplished by having the unscattered* beam pass through several special "beam chambers" in the forward arm. These chambers were "B1X", "CF1XL", "CF3X" and "F3X".

These "beam chambers" could not, of course, take the full intensity of our "normal running conditions" beam. Therefore, to perform the absolute alignment of the forward arm it was necessary to use special

*The beam did pass through the full target; however, after leaving the target the centroid of the beam still corresponds, of course, to the "no scattering" direction.

"beam track runs" which differed from our usual runs in three ways:

i) the intensity was much less--typically only 1×10^6 particles per pulse,

ii) in order to help cut down the intensity the beam was more collimated than usual--hence the "spot size" was smaller,

iii) the "AVB" magnets were typically off. Hence a priori the angular beam divergence may have been different than under normal running conditions.

With the existing alignment constants one could then calculate the apparent x (or y) "slope" of a particular beam track. In order to do this accurately, one uses two "end chambers" (e.g., B1X and F3X) separated by enough distance Δz.* When the apparent x (or y) slopes of many beam tracks are histogrammed, one expects (for a normal beam) to see a Gaussian distribution whose width is determined by the beam divergence.

One could then adjust the alignment constant of either of the end chambers so that the Gaussian distribution of slopes is "zeroed". When this is done the slope of a particular beam track as measured with the alignment constants is the actual slope relative to the average (over the run) beam direction. With this scheme, then, the z-axis in the forward arm is defined to be the average (over a run) beam track direction. The

---

*E.g., with one method of calculation the "apparent x slope", $\left.\frac{dx}{dz}\right|_{app}$ would be given by $\left.\frac{dx}{dz}\right|_{app} = \frac{\Delta x}{\Delta z}$ where Δx is the change in apparent x (y) coordinate associated with the track as measured by two chambers separated by a distance Δz. For accurate measurement of the slope it is clearly advantageous to a pair of chambers such that Δz is as large as possible--e.g., B1X and F3X.

intermediate beam chambers are then aligned relative to the end chambers using the method of residuals outlined above. When this is done all of the beam chambers are then aligned to within an uninteresting translation.

Another method of alignment, however, eliminates even this translation freedom. This is simply the following: One histograms the (x or y) coordinate where each beam track intercepts a chamber plane and then centers the resulting distributions. The result is that each beam chamber is "absolutely aligned" with respect to rotations and translations. Due to experimental inaccuracies, however, both methods should (and were) used to check each other. Agreement between the two methods was usually very good.

The rest of the forward arm was aligned relative to the then "absolutely aligned" beam chambers by the method of residuals mentioned above using "straight through" tracks obtained by inserting a lead brick in the beam path and turning the magnets.

β) Alignment of Recoil Arm*

The alignment of the recoil arm could be done by several methods; we mention only one:

The lab recoil angle θ_r was measured using chambers RB1X and RB2X (since these were the only chambers in the recoil arm upstream of the magnet). The absolute angular alignment of these two chambers could be made using the elastic signal: for each of a sample of elastic events one simply measured, e.g., θ_f (lab scattering angle of forward particle) and used it to predict θ_r for the recoil particle in that event. $\delta\theta_r$

*For simplicity we discuss only the x-alignment of the recoil arm. The y alignment was very similar.

(the measured value of θ_r minus the predicted value of θ_r) was then determined and histogrammed for each event. The center of the resulting Gaussian distribution was then zeroed.

The alignment of the other chambers in the recoil arm could then be done using "straight through" tracks. This was complicated slightly because the downstream part of the recoil arm was "split"; however, for this thesis we do not both with such detail.

v) Required Accuracy of Alignment

α) Recoil Arm

The resolution in measurement of θ_r, $\Delta\theta_r$, was determined by the separation of RB1X and RB2X and their wire spacings. This separation was about 16 inches and the wire spacing was 78 mils. The angular resolution is then the (wire spacing over $\sqrt{12}$) divided by the chamber $\approx \frac{.078}{\sqrt{12}\ (16)} = 1.4\times10^{-3}$ radians.

Thus we wished to be able to absolutely align the recoil angle to an accuracy better than this. Unfortunately, this could not be done. It is not too difficult to see that the expected experimental width of $\delta\theta_r$ was of order 10 mr (this was borne out experimentally (see reference 24, page 79). It is possible to center a the peak of a distribution to better accuracy than its width, though; however, typically not to a factor of 10 better. Thus, from this effect we estimate about a 2 mr error in the absolute alignment of the recoil arm. This, of course, affected the accuracy with which we could determine -t for an elastic event (recall that $\frac{1}{\sin^2\theta_r} \approx 1 - \frac{t}{4M^2}$; however, this was a systematic and not a random error).

The accuracy of the relative alignment of recoil chambers varied with

the chamber but could typically be done to an accuracy of better than a wire spacing. Clearly this was sufficiently accurate.

β) Forward Arm

In the forward arm the resolution in θ, $\Delta\theta_3$, was clearly dominated by the beam divergence (since B1X and F3X were so far apart wire spacing effects were unimportant). Since the beam track slope histogram could be zeroed to better than its width, the systematic error in forward angular alignment was less than the beam divergence. From beam-track slope histograms we estimate it as about 5×10^{-5} radians.

We will see shortly that the angular resolution in the forward arm was better than this; however, again, alignment errors are systematic rather than random.

c. Overview of the Track Finding Problem

Nowadays track finding is common to many high energy physics experiments. Some of the features of our track finding are discussed in great detail in Paul Karchin's thesis. Accordingly here we merely comment on some of the general features we think are interesting physically and important in the general philosophy of the analysis.

i) Don't Require All Chambers for a Track

Wire chambers are, unfortunately, not 100% efficient in detecting charged particles. Therefore it is usually unwise to require "hits" in all of the chambers in an array (e.g., for four chambers, each of 95% efficiency gives an array efficiency of $(.95)^4 \approx 0.81$--about 19% of tracks would be "lost" by requiring hits in all four chambers).

[One has two choices--boost cross sections by a relatively large correction factor or do not require all chambers in array to fire. The

former possibility involves loss of statistics (serious for rare events) and requires accurate knowledge of chamber efficiencies. The latter involves the possibility of introducing "spurious" tracks. However, these spurious tracks could usually be removed by careful subsequent data analysis. Therefore we chose the latter option. The number of chambers required to fire in each array is listed in Table V.1.]

ii) Comment on "Spurious Tracks"

As we have just mentioned, not requiring all of the chambers in an array to fire introduced the possibility of finding spurious tracks. The reader may wonder why this is true; it is because in a typical event there were chambers with more than one "cluster" of hits*, the clusters being nonadjacent to each other.**

One would like to be able to simply throw out those events with more than one cluster per chamber, reasoning that such situations correspond to inelastic contamination of the trigger. Although such contamination was undoubtedly peresent, such an approach is naive. Other causes of the effect include electronic noise in the chamber readout system (producing a random distribution of spurious hits in an array) and the remembrance of events

---

*By the phrase "cluster of hits" we mean a situation in which two or more adjacent wires "went off". The effect becomes more pronounced as the angle between the particle path and the normal to the given chamber becomes larger. Hence, in the forward arm most clusters had only one hit, while the recoil arm, being close to the target, had a large number of tracks at substantial angles relative to the chamber "normals" and hence a large number of clusters with more than one hit.

**Since adjacent clusters, by definition, form a single larger cluster.

from previous RF buckets (since wire chambers typically have a resolving time of order 200 ns).

This remembrance of previous buckets produces a situation in which even elastic events occur together with "non-elastic entire" tracks.

When the number of chambers required to fire in an array becomes small, the electronic noise problem alluded to above becomes substantial. For example, in the recoil upstream x-array there were only two chambers. If each of these chambers had three clusters, then there would have been nine possible "two point" tracks, most of them "spurious". Complicating matters, one sometimes finds several tracks that share hits.

iii) Procedure for Track Finding

[For elastic events the tracks were found by P. Karchin.]

The general procedure is to drop a line between hits in two of the different chambers in an array and use this line to predict the positions of hits in the other chambers. One typically looks within a "window" for the hits in these chambers. The size of the window was 1"--typically more than ten wire spacings.

[In view of the fact that the relative alignment was generally accurate to within a wire spacing, the reader may be wondering why such a liberal window size was used. Put another way, ultimately only tracks with chi-square per degree of freedom greater than 20 were rejected. The reason for this liberal cut was that that was the way things were done on earlier Fermilab experiment #290.]

2. Geometric Cuts

These cuts were applied by P. Karchin and are described in great detail in his thesis. They were all used to minimize the spurious track problem.

Here we simply list these cuts.

a. Hodoscope cut: The segmented hodoscopes were used by requiring the hodoscope element that a track intersected to "fire".

b. Target cut: The center of the target was defined to be at $z = 0$. The beam spot size at the target was less than 1" in radius. The x and y intercepts ($z = 0$) where required to be <2" in absolute value. The y intercept of the recoil y track had to be <4" in absolute value. The z-intercept ($x = 0$) of the recoil x-z track had to be within 23" of $z = 0$.

c. Shared cluster cut: If two or more tracks shared three or more clusters, only the track with the smallest chi-square per degree of freedom was retained. However, regardless of the chi squares, if two tracks shared at least three clusters the track with the lesser number of clusters was eliminated.

d. Paired chamber cut: In the forward arm (x only) chambers were frequently in pairs. Where this was true, two cluster tracks were required to have a hit from each pair.

e. Downstream recoil y: If any fitted recoil y-track passed within 1" of a cluster in chambers CRB6A or CRB6B, then all candidate recoil y-tracks were required to.

f. Matching of upstream and downstream tracks: Each "real" track should have had one upstream (of the magnet) and one downstream (likewise) segment. To be considered as a complete track, an upstream and a downstream segment had to have an x separation of less than 6" (3") for the recoil (forward) arm at the z-position of the magnet center.

g. Momenta as determined by magnets: In the forward arm the measured value of the momentum of the scattered particle had to be within 10% of the beam momentum. In the recoil arm it merely needed have the right sign.

h. Target vertex cuts: The vertex of forward and recoil tracks at the target had to satisfy $|x_v| \leq 1.2"$, $|y_v| < 1.2"$, $|z_v| < 20.5"$, where x_v = x coordinate at intersection of forward and recoil tracks in x-z plane, etc. In addition, $|y_{vf}-y_{vr}| < 0.35"$ had to be satisfied, where $y_{vf(r)}$ was the y coordinate coordinate of the target vertex determined from the forward (recoil) track candidate.

i. Kinematic track cut: If, after the application of all the above cuts there were still more than one segment in one or more arrays, the combinations were chosen that fit the constraints of elastic kinematics best.

3. Elastic Kinematic Cuts

There were five "kinematic variables" used--θ_f, p_f, θ_r, p_r and δ_ϕ. δ_ϕ ("acoplanarity") is defined by[24]

$$\delta_\phi = \tan^{-1}\left(\frac{m_y}{m_x}\right)_f + \tan^{-1}\left(\frac{m_y}{m_x}\right)_r ,$$

where $m_{x(y)} \equiv p_x(p_y)/p_z$ and where $f(r) \equiv$ "forward (recoil)". Let

$$\delta k \equiv k(\text{measured}) - k(\text{predicted from measured value of } \theta_f)$$

where k is any of p_f, θ_r or p_r. If the experimental resolutions were perfect δ_ϕ and all δk would be zero for all elastic events. Due to non-perfect resolutions events were generally distributed in an approximately Gaussian fashion around $\delta k = 0$ and $\delta_\phi = 0$.

For an event to be considered elastic it had to have all δk and δ_ϕ within 3 standard deviations of zero, the standard deviation of each distribution having been determined experimentally. The experimental widths of the distributions (for many events) for all δk and δ_ϕ were checked against theoretical expectations of these widths (expected resolutions) by P. Karchin; agreement was found to be good in all cases. Detail and pictures are given in his thesis.

4. Geometrical Acceptance

We refer the reader to pages 78-85 of P. Karchin's thesis.[24]

VI. RESULTS OF SPECIES IDENTIFICATION OF ELASTIC SCATTERING EVENTS

Introduction

Having determined from the track-finding and kinematic cuts that an event was indeed elastic, it was then necessary to determine the event type. Specifically, since we were interested in measuring the p-p and $\bar{p}p$ cross sections, it was necessary to "separate" pp and $\bar{p}p$ elastic events from other elastic events so that they could be counted. For this we had to use the Cerenkov counters.

As we remarked earlier, our original intent was to use the differential counter to tag kaons and the threshold counter to separate pions from protons or antiprotons. In order to accomplish the $\pi p^{\pm}$ separation in this scheme one would need a clear "$p^{\pm}$ peak" at the low pulse height end of a histogram of elastic event pulse heights in the threshold counter (since mean pulse height is proportional to mean number of photoelectrons).

However, in Chapter III we pointed out that by itself the threshold counter did not have the capability to separate baryons from mesons effectively for all of our beams. (For example, we expected that at -200 GeV/c meson contamination of antiprotons would be intolerable. This was indeed the case experimentally. If one looked at a histogram of the pulse heights of -200 GeV/c elastic events of "all" types, no $\bar{p}$ peak could be seen!)

(The reader may be wondering why antiprotons would be expected to register any non-zero pulse height at all in such a histogram. The reason is that the pulse heights were converted to digital form by a combination amplifier and analog to digital converter (the combination

being loosely referred to as "the ADC") before being recorded on tape. Uncontrollable noise in the amplifier section gave the (anti)protons their non-zero (and infrequently fairly large) pulse heights on the histograms.)

Thus, for certain beams it was necessary to use the differential counter in conjunction with the threshold counter to tag (anti)protons (i.e., require the differential counter to be set at the proton mass and fire (a condition referred to from now on as "CB on p and fire")), while for other beams it was not. So we consider the cases separately.

A. Elastically Scattered Antiprotons at 100 GeV/c

1. Threshold Counter Alone

At ~100 GeV/c, the pulse height separation between antiprotons and mesons was good enough so that one could see clear low pulse height peaks even when ignoring the differential counter. In Figure VI-1 an example of this is shown. (The sample was all -100 GeV/c elastics from our 1980 data run.) The large broad roughly Gaussian (actually Poisson) distribution that peaks around pulse height channel 570 corresponds almost completely to elastically scattered pions and indicates a mean of about 12 photoelectrons for these pions.

Although one does not see a clear kaon peak in the figure, it is known from making a similar histogram with "C_B required to be on K and fire" that the K peak occurs in the region near channel 150 and is simply buried under the mass of pions.

In any case, however, it is clear that the situation ignoring C_B is not optimal--extrapolating the "π peak" back in a smooth way indicates

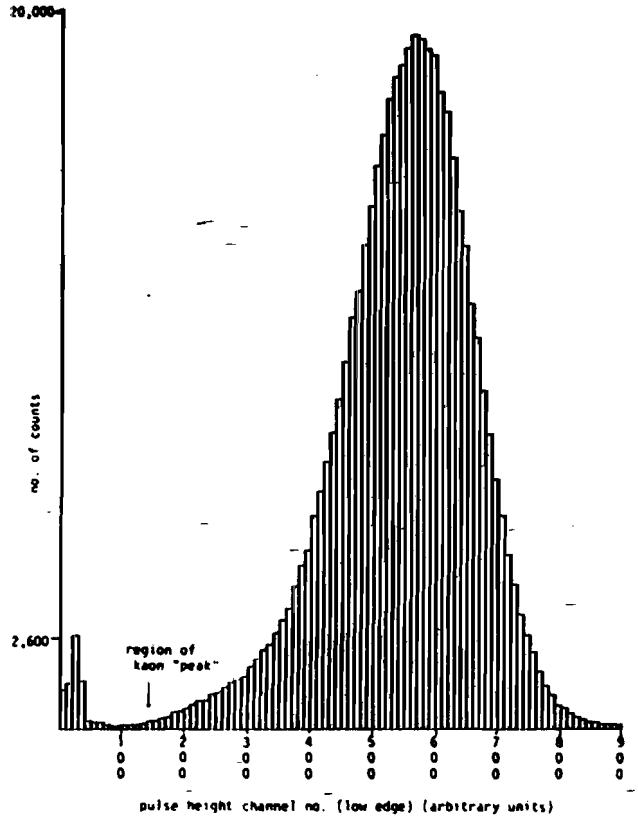

Figure VI-1. Threshold Cerenkov counter pulse height distribution for all ~100 GeV/c elastic events from 1981 running period. Differential Cerenkov counter was ignored in this histogram; so was "latch" (see text). Tall central peak is mostly pions; "pedestal peak" below channel 40 corresponds mostly to antiprotons.

of order 10% contamination even below channel 40. "Cutting" at channel 40 (calling everything below channel 40 a $\bar{p}$ and everything above channel 40 a meson) would also have lost us about 10% of the $\bar{p}$'s. We could have lived with these problems at this energy, but we didn't have to.

2. "C_B on $\bar{p}$ and Required to Fire"

a. General Features

The situation became much cleaner when one looked only at events for which the differential counter was set to give a signal "on the proton mass" and did indeed give such a signal ("C_B on $\bar{p}$ and required to fire"). We show an example of a pulse height distribution corresponding to this in Figure VI-2. The pi peak remains in the same place but is of course now much suppressed.

(The reader may wonder why there are any pions at all in such a plot. Most are due to the "two particles in a bucket" effect (pion and antiproton incident on the target within the same RF bucket and pion scatters, usually inelastically, into the threshold counter). We could have restricted the usable data sample to "one in a bucket" events only, but this would have depleted our data sample by about 30% and was unnecessary--if one was willing to pay the price of a usually small contamination of the antiprotons.)

b. Determination of Probable Total Number of Antiprotons in the C_B Sample

i) "Number Cut"

To this point we have alluded to pion contamination of the (anti)-proton signal in the lowest pulse height channels. However, the inverse effect also existed--some (anti)protons had relatively high pulse heights

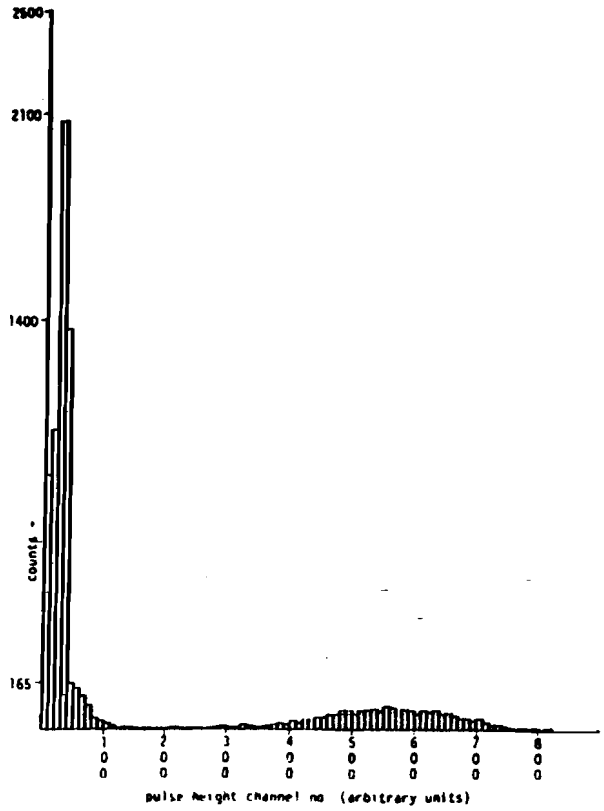

Figure VI-2. Pulse height distributions for -100 GeV/c "1981 sample" of elastic events of all types for which differential counter was "set on $\bar{p}$ and fired" (see text). "Latch" was ignored.

and were mixed in with the pions.*

The exact distribution of proton pulse heights could be determined by histogramming pulse heights of "one-per-bucket" protons only, and this was indeed done. Using the information gained from this one then had a method of determining statistically the expected total number of (anti) protons in a mixed π and p pulse height histogram. This method was, indeed, especially easy to apply to the positive beams.

However, the results of this procedure always agreed to within a percent or so with the results of the following simpler (for the negative beams) procedure:

The probable total number of antiprotons in the C_B sample could be determined by noting the channel number corresponding to the "deepest part of the valley between the (π and p) hills". (The kaons are largely removed already.) We shall call this channel the "number cut channel". For simplicity it was assumed that the number of antiprotons with pulse heights above the number cut was about equal to the number of pions with pulse heights below the number cut.

Both methods were always used to check each other. For simplicity we refer only to the "number cut" method from now on.

It should be noted that the antiproton peak shapes varied from year to year. Hence the number cut channel was determined separately for each year.

---

*This was largely because the ADC "gate" was typically "open" for a relatively long time (about 60 ns). Sometimes integration of noise was sizeable during this period.

ii) "Latch Bar"

As mentioned, noise in the ADC was largely responsible for non-zero (anti) proton pulse heights. We had reason to expect that there was another minor problem with the ADC, though--a low level failure rate which would cause some pions to register abnormally (and falsely) low pulse heights on the plots. Though this problem probably would have added only ~3% to the pion contamination of the antiprotons there was a simple check against it--there was also a "latch" which was (presumably) set whenever a signal came from the Cerenkov counter. So the combination of a low pulse height from the ADC and the absence of a signal from the latch ("latch bar") was required for a final state particle to be labelled a(n) (anti)proton.

The method, then, of determining the total number of (anti)protons scattered elastically during a set of "runs" was the following: First the pulse heights of all elastics from those runs were histogrammed ignoring the latch. From this histogram the number cut channel was determined. Then another histogram was made containing only events for which the latch did not fire. The total number of (anti)protons in this histogram was deemed to be equal to the notal number of counts in this "latch bar" histogram with pulse height below the number cut value number cut as determined from the "ignore latch" histogram. The number cut channel could not be determined directly from the "latch bar histogram" as the pions were "artifically" suppressed in it.

When this was done there were found 5816 total $\bar{p}$'s in the "latch bar" histogram for data taken during 1981 and 1411 total $\bar{p}$'s in the latch

bar histogram for 1980. These numbers should be taken as $\pm \lesssim 1\%$.

3. "C_B on K" Antiprotons at -100 GeV/c

As mentioned, there were many runs for which the differential counter was set "on the K mass" ("C_B on K"). This brought to mind the possibility of using the differential counter to eliminate kaons and then using the threshold counter to separate π and $\bar{p}$ at 100 GeV/c. If all of the kaons could be eliminated in this way very little contamination of antiprotons with pions could be expected.

However, it must be recalled that the differential counter was only about 25% efficient in tagging kaons. This meant that if we histogrammed pulse heights of elastics requiring "C_B to be on K and not fire" about 75% of the kaons would remain in the histogram. Would the resulting antiproton signal be too severely contaminated? There was only one way to tell. Experimental results for this are shown in Figure VI-3. There we show the "latch ignored" histogram. From this histogram we see that the meson contamination of the antiproton peak is probably less than 10% below channel 30. From the corresponding "latch bar" histogram (not shown), one sees that cutting at channel 30 gains us about 650 antiprotons --an increase of almost 10% in the data sample. Because of the relatively higher contamination of these antiprotons, however, they were used only to determine relative and not absolute cross sections, as we shall explain in Chapter VII.

4. Other 100 GeV/c Antiprotons

There were other ways in which the differential counter could be used to help the threshold counter identify antiprotons. However, methods not already mentioned at this energy yielded too small and too

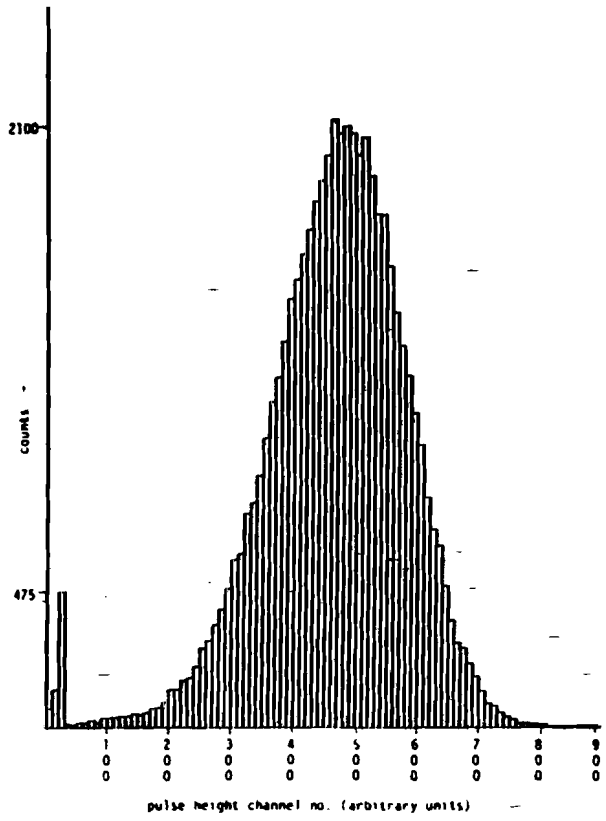

Figure VI-3. Total sample of elastic events of all types for which differential counter was set on kaon mass and did not fire (see text). "Latch" ignored.

contaminated an antiproton signal to bother with.

B. Elastically Scattered Antiprotons at 200 GeV/c

Here it was necessary to require "C_B to be on $\bar{p}$ and fire", as we have already pointed out. The data divides into three classes:

1. Antiprotons at 200 GeV/c from Runs During 1980

There were thirteen such antiprotons from the 1980 run. Expected pion contamination of these was negligible. Because of acceptance fluctuations below $|t| = 0.9$ (GeV/c)^2, only antiprotons with $-t \geq 0.9$ (GeV/c)^2 were considered at this energy. Seven of the thirteen satisfied $|t| > 0.9$ (GeV/c)^2.

2. 200 GeV/c Antiprotons from Runs During 1981

Unfortunately, during most of the 1981 running period the gas in the threshold counter was set at a higher pressure than we had planned for it to be at--during these "high pressure runs" antiprotons were well above Cerenkov threshold. There were a few "normal pressure runs" also. We consider the cases separately:

a. 1981 "Normal Pressure" 200 GeV/c Antiprotons

There were 20, 15 of which had $|t| > 0.9$ (GeV/c)^2.

b. 1981 "High Pressure" 200 GeV/c Antiprotons

This data gain divides up into two classes:

α) runs 314-368--somewhat variable high pressure

β) runs 369-374--more variable high pressure

i) Runs 314-368

Figures VI-4 & VI-5 show some histograms of the situation. Figure VI-4 is an "ignore latch" histogram with "C_B on $\bar{p}$ and required to fire" and

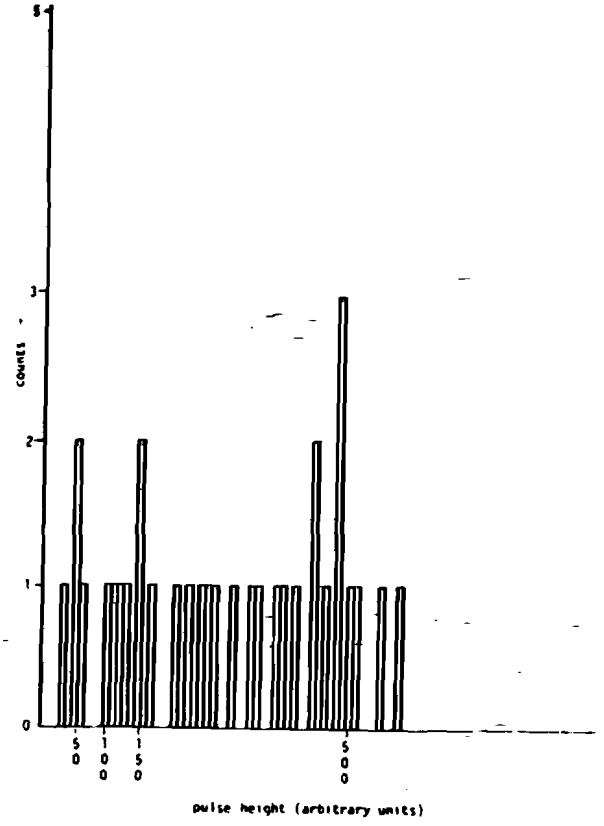

Figure VI-4. Pulse height distributions for elastic events of all types, Runs 314-368, "C_8 on $\bar{p}$ and required to fire", "any no. per bucket" (see text).

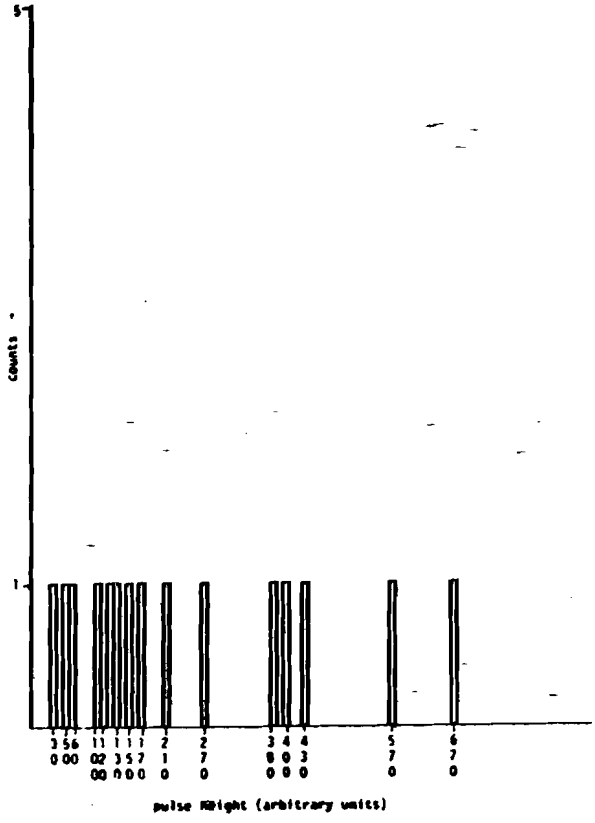

Figure VI-5. Same as Figure VI-4, but sample restricted to "one per bucket" only (see text).

with no restriction on the number of particles "in a bucket". At first sight the situation looks somewhat daunting.

Unfortunately, we had so few other antiprotons at this energy that we needed to salvage as many $\bar{p}$'s as possible from this data to be able to determine relative cross sections with any respectable degree of accuracy.

In Figure VI-4 the reader will notice a slight hint of a "pion peak" near channel 470. A better fix on the "theoretical" position of this peak was obtained by looking at pulse heights for the same runs but requiring "C_B to be set on $\bar{p}$ and <u>not</u> fire". (This will be called the "high statistics" histogram. For brevity it is not shown here. It had about 25,000 pions in it.) This shows the expected pion peak position to be near pulse height channel 420. Upon approximating the pion distribution by a Gaussian (mean number of photoelectrons $\approx$ 14--high enough to make this a good approximation except in the tails) we found that the half-width of the pi peak in a high statistics situation was about 130 chennels. We also found that only about 1% of these pions fell below channel 180, for example, and that about 12% fell below channel 300.

Thus, returning to our low-statistics situation (Figure VI-4) we statistically expected 1% of the pions to have pulse heights pushing them below channel 180. We did not have to worry much about variations of pressure affecting this result since both the low statistics histogram and the high statistics histogram of pions include the same pressure variations.

One could get a fix on the expected antiproton peak position in the following way. We recall that the positive 200 GeV/c beam had a much

higher percentage of protons than the negative beam had of antiprotons. Therefore, by running one short run at "high pressure" and at +200 GeV/c, we could quickly accumulate enough protons on a pulse height histogram to indicate where the antiproton peak should theoretically be. This was done, but somewhat too quickly (we did not have enough protons to get a really good fix). But it seemed that the proton peak was somewhere near channel 190 with a half width somewhere between 50 and 100 pulse height channels.

To determine the relative cross sections, however, we of course need as uncontaminated a sample as possible. So, for this, look at Figure VI-5 ("one-per-bucket" histogram). There are still some pions in this histogram. That is because the one-per-bucket condition is not perfectly applied with our hardware. But only about 5 or 6. Now recall that only 1% of the pis are expected to fall below channel 180. Therefore, even if there were forty pions in the low statistics plot we'd expect less than 0.5 of them below channel 180. So anyone in the one-per-bucket plot below channel 180 is almost definitely a $\bar{p}$. Unfortunately, there are only 8 such fellows.

ii) Runs 369-374

A similar procedure applied to these runs yields three "definite" protons for the relative cross section calculation.

C. Elastic Protons at 100 GeV/c

Relatively little running was done at +100 GeV/c; however, because protons comprised such a large fraction of the beam we were able to get a fair amount of data.

1. "C_B on p" Data

In all there were only four runs with "C_B on p", three of which comprised the total 1981 100 GeV/c pp sample, and one of which was in 1980. We need to consider data samples from each year separately, as the normalization will a priori vary.

a. 1981 Sample

A histogram of pulse heights was made (not shown here) ignoring the latch and ignoring C_B (i.e., using the threshold counter only). It was found that the pion-proton separation was excellent and that the meson contamination of the proton signal was probably less than 1%. However, for the purposes of normalization we got an even more pristine sample by using the differential counter ("C_B on p and required to fire"). The relevant histogram with the "latch ignored" was made for this. After the proper background subtraction of mesons was made it was estimated that there were about 3229 total protons in this "latch bar histogram".

b. 1980 C_B on p and Required to Fire Sample

By the same procedure we estimated 1130 protons in the "latch bar required" histogram. For brevity we omit the relevant histograms here; however we comment that they were very clean.

2. "C_B on K" Protons

During 1980 there were three runs at +100 GeV/c for which the differential counter was set for kaons. However, because of the ubiquity of protons in this beam and because of the relatively good π-p separation at this energy, it was not at all difficult to obtain a sufficiently clean sample of protons from these runs to use in cross section determination

by histogramming pulse heights of elastics in the threshold counter under the condition that the differential counter be set for kaons and not fire. In fact, the bulk of the elastic proton signal at this energy came from these conditions! In Figure VI-6 we show the histogram made under these conditions ignoring the latch. We see that there were about 11,000 protons to be gained.

ii) A Comment on Contaminations

So far we have been making light of the issue of contamination (by mesons under the proton peak) by showing the reader, in the appropriate cases, that the fractional contaminations were very small. But due to the differences in the meson and baryon differential cross sections, this was not good enough. We shall say something about this here and illustrate with the +100 GeV/c "C_B on K" data, but the method is general and should be understood to have been applied to each of the cross sections where appropriate.

In simplest terms the problem is the following. Consider the 11,000 odd protons we just found in the +100 GeV/c "pedestal". Suppose that for the purposes of calculating relative cross sections we demand a very pristine sample, so we only use those protons whose pulse height falls below channel 30. That's still almost 11,000 protons. Looking at a magnified version of Figure VI-6, we crudely (by eyeball extrapolation back of the "pi peak") guess, say, 60 mesons whose pulse heights put them below channel 30. So the "contamination" is crudely 60,11,000 < 1%. [This crude estimate of the contamination was checked in two ways:

i) In the histogram of Figure VI-6 we see about 30,300 events. It was known from DISC pressure curves that the beam was about 5% kaons.

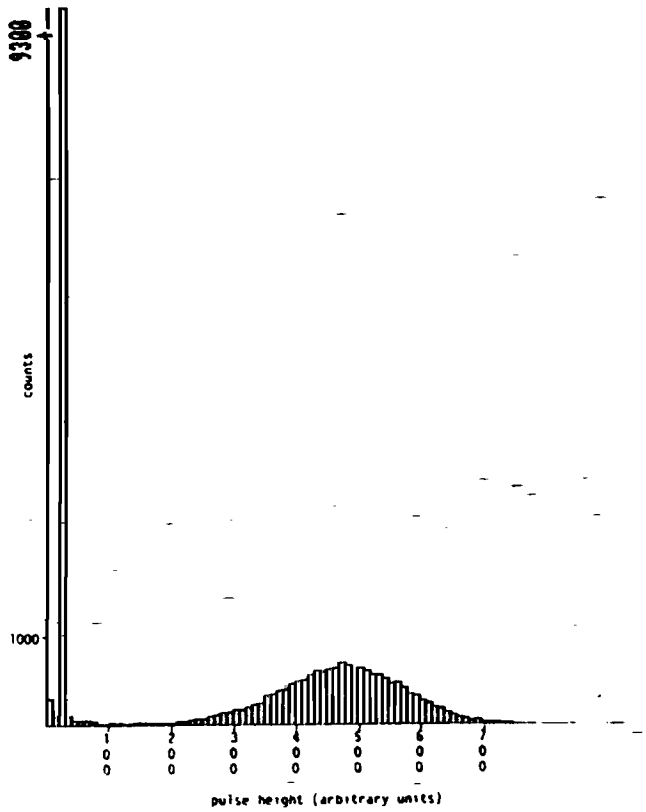

Figure VI-6. Pulse height distribution for +100 GeV/c elastics, "C_B on K and no fire" (see text).

So we expect about 1500 kaons, three fourths of which should be in the histogram of Figure VI-6 (since the DISC was known to be only about 25% efficient at tagging kaons). So there should be about 1,200 kaons in that histogram.

ii) When a histogram of pulse heights for a fairly clean sample of "one-per-bucket" kaons at this energy was made, it was found that less-than 4% of these "kaons" fall below channel 30.

In fact, this 4% figure is probably too high because the "one-per-bucket" condition cannot be perfectly applied--some low pulse height "kaons" are really protons (probably most, in fact). But let us keep this 4% figure as an upper limit. Then there are probably at most $(.04)(1200) \approx 50$ kaons falling below channel 30 in the histogram of Figure VI-6.

We also claim that there are probably not more than five pions below channel 30 in that histogram. That can be seen as follows: first note that the pion peak is centered near channel 480. In the vicinity of channel 880 (400 channels above the peak) we see about 1 pion every ten channels. But the pi distribution is Poisson, and Poisson distributions have "longer right tails than left tails". So in the vicinity of channel 80 (480-400) we expect at most 1 pion every ten channels. Thus it would be very surprising if there were more than five pions below channel 30. So we expect about 50 mesons at most under channel 30, a number not in disagreement with our original upper limit guess of 60.]

But suppose that the p-p cross section is "small" in a restricted range of $|t|$ (e.g., has a deep dip there, or worse--a shallow dip there) where the meson-p cross section is relatively large. Then if some of the 60

mesons fell right in that range they could completely have dominated the protons there. It is true that this may only involve a limited region of -t, but regions with structure (like dips) are frequently the most interesting regions! Even two mesons in a shallow "p-p dip" might completely wash it out.

At +100 GeV/c for p-p the situation was particularly interesting becasue it was not at all clear whether to expect a dip near $-t = 1.4$ $(GeV/c)^2$ or not. At 200 (GeV/c) there is one. At 50 GeV/c there apparently isn't one. At 100 GeV/c other experimenters have presented evidence for "no dip", but we believe that evidence is poor. In fact, in this thesis we will claim that there is a shallow dip at 100 GeV/c for p-p elastic scattering. So we had to get rid of contamination carefully. The question is, of course, how the contamination mesons distribute themselves in $|t|$. The answer to this was found by the histogramming -t for a large mixed sample of pions and kaons. Assuming roughly equal differential elastic cross sections for pions and kaons, it was found that for a total of 50 contaminating kaons, one expects less than one of them to have $-t < 1.4$ $(GeV/c)^2$ and only about 0.5 mesons to fall into the hypothetical $-t = 1.4$ to $-t = 1.6$ $(GeV/c)^2$ "dip" region. We see that we are not in danger of "losing dips".

D. Elastic Protons at 200 GeV/c

For +200 GeV/c, all of the 1981 runs were "C_B on p" and all the 1980 runs were "C_B on K". The techniques used to separate protons from mesons were very similar to those used for 100 GeV/c. Hence we simply state results:

1. The data obtained with "C_B on p and required to fire" was used

(see Chapter VII) for the normalization of the absolute cross section. There was an estimated total of 795 protons under these conditions, 787 of which fell below pulse height channel 40 and which were used for the |t| distributions.

2. 200 GeV/c Protons from "C_B on K and No Fire". 4026 protons were found that were considered negligibly contaminated (cut at channel 40).

3. Other 200 GeV/c Protons. With this beam it was also possible to salvage the protons that did not cause "C_B to fire" during the runs for which C_B was set on the proton mass (the existence of this class of data is due, of course, to the inefficiency of the differential counter). These protons were the "dirtiest", but even here the contamination was not bad at all. In fact it was expected to be only slightly worse than that of the "C_B on K and no fire" sample--since C_B misses 3/4 of the kaons! Anyway, there was another indirect method of checking the contamination--differential cross sections for pp elastic scattering at this energy were already known to show dip at $-t \approx 1.4$ $(GeV/c)^2$. When one histogrammed the t distribution of events in this class one saw that dip!

There were about 757 total protons in this sample whose pulse heights put them below channel 40 (and hence were used for calculating relative cross sections). Summarizing,

Estimate of total number of protons used in normalization: 795

Estimate of total number of protons used to determine -t distributions:

787 + 4026 + 757 = 5570

VII. DETERMINATION AND NORMALIZATION OF DIFFERENTIAL CROSS SECTIONS, METHOD AND RESULTS

A. Normalization*

1. Introductory Remarks

In order to calculate a cross section it is necessary to know the ratio [scattered particles of the type desired leaving the target/incident particles of the proper type] for the time period during which data is collected. We shall write this ratio symbolically as "elastics/no. incident", where the meaning of the terms is self-explanatory.

It was originally thought that the numbers of elastics found in Chapter VI, divided up into $|t|$ bins, would provide the numerators of these ratios. Likewise, it was expected that the denominators would be had by simply counting the number of "gated beam dot C_B" coincidences made during the relevant time period. [By "gated beam dot C_B" is meant a coincidence of fast-logic signals B_1, B_2, $\overline{A_i}$ (i=1,2,3,4) and C_B, where $\overline{A_i}$ (i=1,2,3,4) indicates the absence of a signal from any of the anti-counters and C_B indicates the presence of a signal from the differential Cerenkov counter in the beam.]

But life was not so simple as it was found experimentally that the ratio "elastics/no. incident" was a decreasing function of instantaneous beam intensity ("flux"). The causes of this effect and the general method of resolving the problems that were caused by it will be outlined briefly in Section A. In Section B we present the calculations of $d\sigma/dt$.

---

*I thank Paul Karchin for some very helpful discussions on this.

2. Intensity Effects

There were several causes of the intensity effect alluded to above. One was that the level of saturation (i.e., dead time) of the electronics associated with the beam scintillation counters increased with intensity. As a result the beam counters undercounted the number of incident particles, the undercounting getting worse as the intensity increased. This was partly due to our operating the discriminators for these counters in the "burst-guard" mode. Phototube pulses frequently extended over several RF buckets, the result being that effects like "two particles in a bucket" tended to dead-time out the counters.

If this were the only effect, the ratio of elastics to "gated beam·C_B" would have risen as a function of incident flux. However, since the "gated beam" coincidence was required for the experimental trigger, the numerator of the ratio also fell with intensity.

The reader might then argue that the two effects should have cancelled out leaving a constant ratio as a function of intensity. But this was not the case for the following reason: Part of the intensity "problem" was due to "two particles in a bucket" and part was due to consecutive buckets being occupied. For "two in a bucket" Gated Beam undercounted but the trigger essentially did not (due to the relative infrequency of elastic events). However, for "consecutive buckets" both undercounted. The result of these effects was nonlinearity in the apparent number of elastics per gated beam ("EL/GB") as a function of incident intensity. The same was true for "elastics per gated beam dot CB" ("EL/GB·CB").

Then there were other effects. For example, there were complicated intensity dependent effects in the veto counters surrounding the target. [Presumably much of this was due to inelastic scattering occurring in the same RF bucket as elastic scattering. However, some of the inelastic scattering that set off the veto counters apparently even occurred during the RF bucket previous to that of the elastic scattering event (in this case the vetos were perhaps set off by slow recoil protons from the inelastic scatter that didn't hit the anticounters until the bucket after that during which they were produced). Other elastic events were missed due to beam halo setting off the anticounters.]

As a result, the methods of Chapter VI undercounted the true number of elastically scattered protons and antiprotons for these reasons also. The upshot, then, was that the ratio EL/GB•CB fell with intensity--and in a nonlinear way. Since ideally this ratio would be independent of intensity, it was incumbent upon us to determine the value of the ratio at zero intensity--"(EL/GB•CB)".

3. A True Measure of Incident Flux

Luckily, a three element scintillation counter hodoscope (called "the N hodoscope") had been installed near the target. This hodoscope responded largely to hadrons produced by the inelastic scattering of beam and target particles. Since the target was only about 10% of an interaction length long one did not have to worry about "sagging" in the N counters. Thus it was expected that the N counters would provide a true measure of the incident flux.

In order to "calibrate" the N counters, a number of plots of gated N (coincidence of signal from an N counter with the absence of the logic

gating signal) counts per spill versus gated beam counts per spill were made. In the low intensity region (only) these plots were linear, and the linear region was large enough to determine the slope of such a plot at zero intensity to within a typical accuracy of a few percent. (For an example of such a plot, see page 90 of Paul Karchin's thesis.) We shall call this zero intensity slope "$(GB/GN)_0$". [GN stands for counts of gated N, GB for counts of gated beam.]

4. Choice of Variables

In order to determine $(EL/GB)_0$ one would at first suppose that he or she could extrapolate "backward" on a plot of (EL/GB) [no. of elastics per GB] versus GN per pulse. However, we remind the reader of the non-linearity in such plots. On the other hand, it seemed that plots of "elastics per gated N" ("EL.GN") vs. GN were tolerably linear. This linearity was, of course, easier to verify for elastic π-p scattering than, e.g., elastic $\bar{p}p$ scattering, due to the relative number of events. An example of the linearity of (EL/GN) vs. GN for pions is shown on page 88 of P. Karchin's thesis, where it is claimed that typical accuracy in the determination of "$(EL\pi/GN)_0$" (elastic pions per gated N in the limit of zero intensity) was a few percent. Then one could get $(EL/GB)_0$ for pions by noting that

$$\left(\frac{EL}{GB}\right)_0 = \left(\frac{EL}{GN}\right)_0 \times \left(\frac{GN}{GB}\right)_0$$

(where subscript zero refers to "zero intensity limit").

5. Normalization for Protons--General Method

The reader may wonder why we are talking at all about elastic pions per gated beam at zero intensity when what we want is the ratio

[elastic (anti)protons per gated beam] at zero intensity. However, we assert that the (anti)proton normalization could be obtained from the pion normalization. For the negative beams there were many more elastically scattered pions than elastically scattered protons. Thus $(\frac{EL}{GB})_0$ was in general much more accurately known for pions than for protons. We wished to take advantage of this fact.

Before explaining the method, let us illustrate the problem with an example. As the reader has seen, at -200 GeV/c there were only about 50 elastically scattered antiprotons. Most of these antiprotons were collected "at high intensity". Suppose that they all fall in the box in the plot in Figure VII-1. How does one extrapolate back to zero intensity? One makes use of the pion normalization, recalling that at -200 GeV/c there were many thousands of pions obtained during the runs that these antiprotons were obtained.

We now assert that <u>if</u> $f_{\bar{p}}$ (the fraction of the beam that is (anti)protons) and ϵ (the efficiency of the differential counter for tagging (anti)protons) are independent of intensity, the the following formula is valid for data collected during a given set of runs <u>with varying intensities</u>:

$$\left(\frac{EL\ \bar{p}}{GB \cdot CB}\right)_0 = \left(\frac{EL\ \pi}{GB}\right)_0 \times \frac{TOT\ EL\ \bar{p}}{TOT\ EL} \times \frac{TOT\ GB}{TOT\ BG \cdot CB} \qquad \text{(VII.1)}$$

where "TOT EL π ($\bar{p}$) $\equiv$ the total no. of elastically scattered π's ($\bar{p}$'s) in the data sample (taken at varying intensities), and where TOT GB (GB CB) $\equiv$ the total number of GB (GB·CB) counts for the runs for which the same data sample was taken.

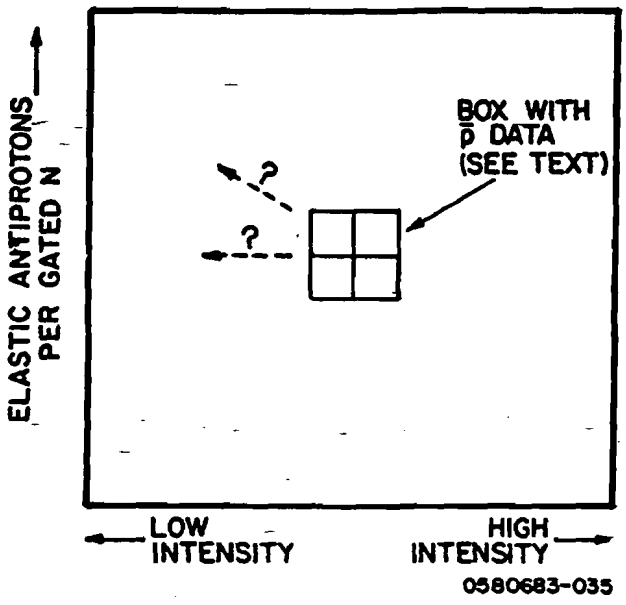

Figure VII-1. Illustration of the problem of extrapolating back to zero intensity.

Proof:

Let $\frac{d\sigma}{dt}(\pi(\bar{p}))$ denote the differential elastic $\pi p \to \pi p$ ($\bar{p}p \to \bar{p}p$) cross section. Let $\sigma_\pi(\bar{p}) \equiv \int_{\Delta t} \frac{d\sigma}{dt}(\pi(\bar{p}))\, dt$, where $\int_{\Delta t}$ indicates an integration over the range of experimental acceptance. Then $\sigma_\pi = k\,(\frac{EL\ \pi}{GB})_0$ and $\sigma_{\bar{p}} = k\,(\frac{EL\ \bar{p}}{GB \cdot CB})_0$, where k is a constant independent of particle species.

Now, suppose the entire data collecting was done at very low intensity. Then it is clearly true that

$$\left(\frac{EL\ \bar{p}}{GB \cdot CB}\right)_0 = \left(\frac{EL\ \pi}{GB}\right)_0 \left(\frac{TOT\ EL\ \bar{p}}{TOT\ EL\ \pi}\right)_0 \left(\frac{TOT\ GB}{TOT\ GB \cdot CB}\right)_0 .$$

But, if ϵ and f_p are independent of intensity, so is the last factor

$$\left(\frac{TOT\ GB}{TOT\ GB \cdot CB}\right)_I = \left(\frac{TOT\ GB}{TOT\ GB \cdot CB}\right)_0 \qquad \text{(subscript I indicates intensity I)} .$$

The factor

$$\left(\frac{TOT\ EL\ \bar{p}}{TOT\ EL\ \pi}\right)$$

is also independent of intensity. This is true for the following reason. The intensity dependence of the number of elastic protons detected is, we recall, caused by inelastic scattering "accompanying" elastic scattering, by beam halo, and by "sagging" of the beam counters. But these effects are exactly the same for the undercounting of elastic protons as for the undercounting of elastic pions. So the ratio is independent of intensity and hence equation (¥II.1) is proved.

Let us define

$$\frac{EL\ \bar{p}}{GB \cdot CB} \equiv \text{average of } \frac{EL\ \bar{p}}{GB \cdot CB} = \frac{TOT\ EL\ \bar{p}}{TOT\ GB \cdot CB}$$

$$\frac{EL\ \pi}{GB} \equiv \frac{TOT\ EL\ \pi}{TOT\ GB}$$

$$C \equiv \left(\frac{EL\ \pi}{GB}\right)_0 \Big/ \frac{EL\ \pi}{GB}$$

Then we can rewrite (VII.1)

$$\left(\frac{EL\ \bar{p}}{GB \cdot CB}\right)_0 = \left\langle \frac{EL\ \bar{p}}{GB \cdot CB} \right\rangle \times C$$

We see what this means physically: It means that the entire curve of $\frac{EL\ \bar{p}}{GB}$ versus intensity is a constant multiple of the curve of $\frac{EL\ \pi}{GB}$ versus intensity (see Figure VII-2).

In particular then, both curves go through their average values at the same abscissa and both curves go to zero together. (Just another way of saying that intensity effects are independent of particle type.)

6. The Intensity Dependence of "εf_p"

Now there is one possible flaw in all this. That is the possibility that εf_p depends on intensity. Then curves of ($EL\pi/GB$) vs. GN/spill and ($EL\bar{p}/GB \cdot CB$) vs. GN/spill would no longer be constant multiples of each other. We must now face this possibility.

First we ask, "In what situations could εf_p have depended on intensity?" It is clear that poor aiming of the proton beam on the beryllium "meson target", synchrotron main ring problems, etc., could have had no effect on ε or f_p. Also, since $\bar{p}$'s were so rare in the beam the differential counter did not "dead-time out" at high intensity. It

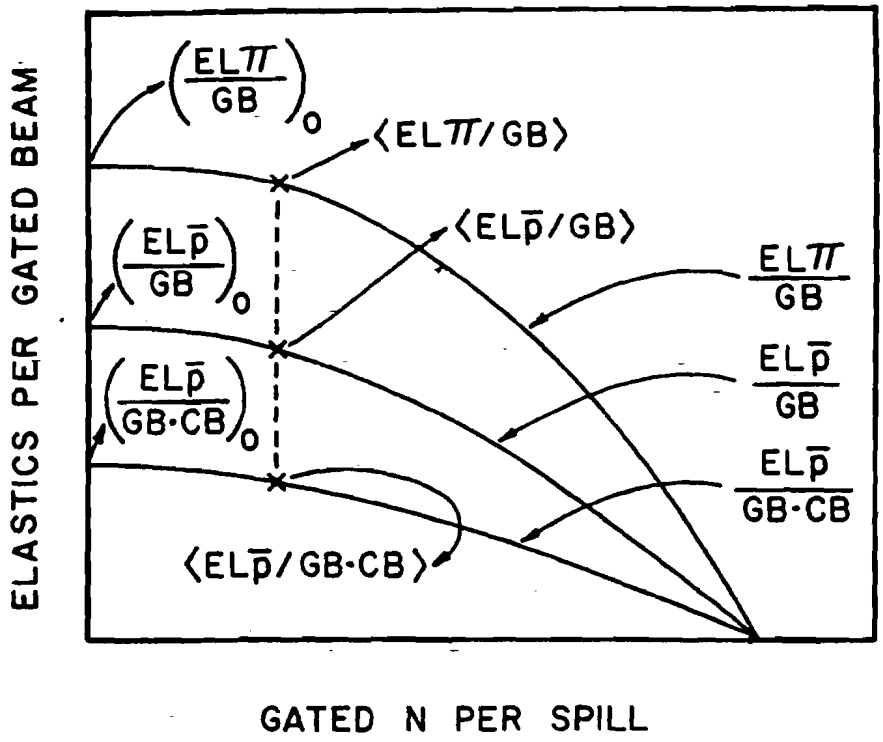

Figure VII-2. Proportionality of elastic/flux curves – (see text).

is only when the AVB magnet* currents or the collimator settings were changed that f_p and ε were affected.

However, there was only a very weak correlation between intensity and $f_p\varepsilon$. This is because, e.g., when the main ring intensity was low or the "meson targeting" was bad, the AVB magnet currents were turned up. At high main ring intensities the AVB currents were often turned down.

The result was that almost all of the intensities had the complete range of $f_{\bar{p}}$'s. Therefore, the curve of EL$\bar{p}$/GBCB vs. intensity was proportional to the curve of ELπ/GB vs. intensity; however, the constant of proportionality involved $\langle f_{\bar{p}}\varepsilon$ (AVB current)$\rangle$ ($\langle\ \rangle \equiv$ average) rather than $f_{\bar{p}}\varepsilon$ (zero current).

We are not interested in knowing this $\langle f_{\bar{p}}\varepsilon\rangle$. We merely point out that it differs from $\varepsilon f_{\bar{p}}$ (no current). This is an advantage to using other forms for the proton normalization--it does not contain $f_{\bar{p}}\varepsilon$ explicitly. That is helpful because, e.g., if $f_{\bar{p}}$ is gotten from the DISC curves it is obtained from a highly artificial beam and differs from the "true" $f_{\bar{p}}$. Because $f_{\bar{p}}$ was so small to begin with, it was not insensitive to these changes!

*The AVB magnets were dipole magnets immediately downstream of the beryllium target that were used to select the production angle of the particles that went into our "M6" experimental beam line.

B. Calculation of Differential Cross Sections

1. Introduction

In general the formula for calculating $\frac{d\sigma}{dt}$ for a particular bin labelled by the value t_o is

$$\frac{d\sigma}{dt}(t_o) = \frac{1}{\rho L \Delta t A_o R T} \left[\frac{\text{TOT EL}}{\text{GB}\cdot\text{CB}}\right]_0 \times \frac{n(t_o)}{n_{tot}} \times f_{cut} \times f_{kb}$$

where

ρL = no. of protons per square centimeter in the target. (for us ρL was $4.31 \times 10^{24} cm^{-2}$),

Δt = width in $|t|$ of the bin under consideration,

A_o = fractional geometrical acceptance of the apparatus at t_o,

R = "reconstruction efficiency" (includes effects of wire chamber efficiency),

T = "transmission factor". Includes effects of absorption in target, Cerenkov tank, etc., and δ-rays on veto counters, radiative correction, etc.,

f_{cut} = "cut correction factor"--associated with particle identification cut,

f_{kb} = kinematic background correction factor, and

$\left[\frac{\text{TOT EL}}{\text{GB}\cdot\text{CB}}\right]_0$ = the "zero intensity limit" of the ratio of the "total" (i.e., integrated over the -t range of the acceptance) no. of elastic $\bar{p}$'s (p's) obtained during a given period of data collection, divided by the total number of "GB·CB" counts recorded during this same time period.

The exact meaning of all these factors will become clear in the ensuing discussion.

2. Transmission Factor

a. Absorption in the Target

We correct for this by realizing that every particle that travelled through the forward arm after undergoing scattering in the target had, in fact, travelled through the entire target. Therefore, to calculate the fraction of elastics that were absorbed in the target, we used

$$\frac{\text{"absorbed"}}{\text{in}} = \sigma \rho L ,$$

where L is the entire target length, and where the rest of the notation is obvious except for "σ". That is, for "σ" should one use the total cross section or just the inelastic cross section? I.e., if elastic scattering occurs twice in the target, is the event missed? The answer is "yes" (one should use the total cross section).

[To pass the elastic cuts, θ_f had to be "correct" to within a tolerance on the order of its resolution. This resolution was defined by the beam divergence and was of order 10^{-4} radians. But, for example, for 100 GeV/c elastic scattering, a scattering angle of 10^{-4} radians corresponds to momentum transfer $q \sim (10^{-4})(100) = .01$ GeV/c, i.e. $-t \equiv q^2 = 10^{-4}$ $(\text{GeV/c})^2$. If q^2 of the "second" elastic scattering had been much larger than this, the event would have failed the kinematic cuts. But the elastic cross section at $P_L = 100$ GeV/c and $q^2 = 10^{-4}$ $(\text{GeV/c})^2$ has dropped less than 1% from its value at the optical point [i.e., over 99% of elastic pp scattering at this energy has $q^2 > 10^{-4}$ $(\text{GeV/c})^2$]. So elastic scattering had to be included in the absorption correction.]

At 100 GeV/c the total $\bar{p}p$ cross section is about 42 mb. At 200 GeV/c

it is about 41.4 mb. $\rho L = 4.31 \times 10^{24}$ cm^{-2} then implies that the "transmission factor" for $\bar{p}p$ scattering is about 82% for both 100 and 200 GeV/c, and about 83% for pp scattering, again at either energy, where "transmission factor" $\approx 1 - \sigma\rho L$ = "1-absorption".

b. Correction for Production of δ-Rays in the Target

The problem here is the following: "knock-on" electrons were produced by Coulomb scattering in the liquid hydrogen target. The target was surrounded, on 3 of its 4 faces (assuming a rectangular target, for ease of discussion) by aluminum plate an inch and a half thick. Outside of the plate were the "veto" counters. Could δ-rays have penetrated the plate and set off the veto counters?

The answer is technically "yes", but only a negligibly small number of δ-rays had enough energy to do so.

$$\frac{dN}{dx}(T > T_o) = \frac{D\rho}{2}\int_{T_o}^{\infty}\frac{dT}{T^2} = \frac{D\rho}{2T_o} = \frac{1.1}{T_o\ (\text{MeV})}\ (\delta\text{-rays per meter})$$

for the number of δ-rays produced per meter of target with kinetic energy $T > T_o$. (This formula is obtained by integrating the formula[113] for $\frac{dN}{dTdx}$. Here $D = .31$ MeV-cm^2/gram and $\rho = .071$ g/cm^3 for liquid hydrogen. Using the density of aluminum $\rho = 2.70$ gm/cm^3, 1.5 inches of Al implies a column density of about 10.3 gm/cm^2, which would imply $T_o \approx 20$ MeV.

Now, at our beam energies δ-rays are overwhelmingly produced at small with respect to the "primary hadron" travel direction that causes their production.* Let θ represent this angle for a given δ-ray. Then for the

*I thank Professor J. Orear, my thesis advisor, for reminding me of this fact.

cases when the primary hadron is either the incident beam hadron or the forward elastically scattered hadron, the "path length" of the δ-ray in the aluminum is essentially 1.5"/sinθ if sinθ is large enough that the knock-on electron even encounters the Al. Since sinθ is essentially always so small, the δ-ray correction due to incident or forward elastically scattered hadronic primaries is negligible.

Delta rays penetrating the aluminum that were produced from the elastically scattered particles that headed for the recoil arm were also negligible--in this case although most of these δ-rays "saw" about 1.5" of Al, the production length in the target was at most only 3". This gives an upper limit of about a 0.4% correction.

c. Other Absorption Corrections

(i) "Empty Target Rate" ≈ 0.7%

(ii) Correction for muons and electrons - 0% (since C_B was "on p and had to fire" for normalized sections

(iii) Absorption in forward arm scintillators and Cerenkov mirror ≈ 0% (C not required in track finding)

(iv) Absorption in R counter ≤ 1% (for plastic scintillator, a collision length is about 55 cm. For 1/4" inch thick scintillator, .25×2.54 cm/inch ≈ .6 cm)

(v) Combined absorption in air and helium [the scattered particles had to pass through air before being positively detected. The forward scattered particle also had to pass through 100' of S.T.P. helium in two helium bags we installed to minimize multiple scattering and absorption. (No absorption affecting our results

occurred in the He in the threshold Cerenkov counter or in the differential counter)] ≈ 4%.

d. Radiative Correction

Based on a study of radiative corrections applied to π-p scattering with the same equipment and beams[24] we conclude that the radiative correction is ≤1% for $t \leq 5$ GeV/c. So we apply a 1% "correction" to all cross sections (there were so few events with $-t \geq 5$ GeV/c that the added inaccuracy there didn't matter much). We include this radiative correction as an "absorption correction" in the transmission factor "T". Adding together the results of all these effects, we find that

T = .77 for both negative beams, and

T = .78 for both positive beams.

3. Kinematic Background Subtraction

The factor "f_{kb}" depends both upon the reaction and q^2. Due to the relative paucity of $\bar{p}p$ elastic scatters, f_{kb} was determined from the pion data (see Paul Karchin's thesis) and then applied to the anti-proton (and proton) data. These numbers are given in tables later under the heading "f_{kb}".

4. Reconstruction Efficiency Factor R

The overall reconstruction efficiency was determined by Monte Carlo methods and included the effects of chamber efficiencies that varied with time. This factor "R" was a function, then, of both time and q^2. As a result we generally consider R separately for each year in which data was taken.

The general method for obtaining the "chamber efficiency piece" of

R was as follows--chambers were grouped into arrays that had as many members as possible, coincident with the requirement that particle tracks through the arrays be essentially straight lines. (Thus, usually, an array could not have chambers both upstream and downstream of either analysis magnet (exception--see below).) If possible the array included as "members" hodoscope elements which particle paths would intersect. The efficiency of a given chamber in an array was then defined as the fraction of "suitable events" for which the given chamber registered a "hit" at a "proper position", coincident with the requirement that all other members of the array also register a hit, each at "proper position".

In order for the results of this scheme to truly represent chamber efficiencies we had to limit the definition of "suitable events" as follows: a) the event had to have, as well as could be determined, a bona fide particle track (as opposed to random hits due to electronic noise, etc.) in each array (x and y) of the arm of the experiment which the chamber being tested belonged to; b) track segments had to meet in the magnets, tracks had to originate from the target, etc.; and c) there was required to be one and only one track in an array.

By the phrase "proper position" we mean the following: having found a bona fide track exciting each "other" member of an array, it was then possible to predict (assuming good chamber alignment) the expected position for the hit in the chamber being tested. For the chamber to be considered efficient for the event in question it typically had to have a hit within a window 0.5" wide on each side of the "expected position" (sometimes a chi-squared test was applied instead).

The reader may imagine that this procedure presented a problem for

determining the efficiencies of the x-chambers in the recoil arm upstream of the analysis magnet there, since there were only two such chambers. (One "other" chamber cannot define the slope of a track to predict a hit position in the chamber being tested.) This problem was solved by enlarging the array to include the entire span in "z" of the recoil arm and then tracing rays through the magnet. (Given an x or y position and a slope on "side one" and a slope on "side two" of a homogeneous field magnet it is possible to predict an x or y position on "side two".) This was accomplished by using a Newton-Rapheson iteration technique.

For most chambers two different samples of tracks were used to find efficiencies--tracks from elastic events that were included in cross section calculations (typically πp elastics (Paul Karchin) and general inelastic tracks (myself). Wherever feasible the efficiencies obtained with these two test samples were compared to each other and always agreed to within about 2%. However, certain chambers in the recoil arm were positioned so that the only elastic rays they could receive were those of relatively high -t. As these rays were rare, these chambers were not illuminated sufficiently with them to allow determination of efficiencies using elastics. Thus, their efficiencies were found essentially only by using the inelastics.

5. Calculation of Normalization

a. Some Additional Notation

$p\phi$ Fermilab main ring beam intensity. 400 GeV/c during 1980 data run and 350 GeV/c during 1981 data run

$\left[\frac{GN}{GB}\right]_0$ The ratio of "gated N" counts to "gated beam" counts, extrapolated to the limit of zero intensity

$\left(\frac{EL\pi}{GN}\right)_0$ The ratio of the observed number of elastic pions to gated N counts, extrapolated to the limit of zero intensity

$\left(\frac{EL\pi}{GB}\right)_0$ The ratio of the observed number of elastic pions to gated beam counts, extrapolated to the limit of zero intensity. Recall $\left(\frac{EL\pi}{GB}\right)_0 = \left(\frac{EL\pi}{GN}\right)_0 \times \left(\frac{GN}{GB}\right)_0$

$\frac{TOT\ EL\bar{p}(p),\ |t| > \bar{t}}{TOT\ GB \cdot CB}$ The ratio of the total no. of elastic $\bar{p}$'s (p's) observed during a running period for which $|t| > \bar{t}$ to the total number of "gated beam dot C_B" counts for the same period. The reader will recall that this has essentially previously been defined as the average $\left\langle \frac{EL\bar{p}(p)}{GB \cdot CB} \right\rangle$.

f_{cut} The reader will recall that the estimated total no. of elastics obtained from a given reaction with "given conditions" was determined either by the "number cut" technique or by studying the "pedestal shape". For example, for $\bar{p}p$ scattering at 100 GeV/c, the reader will recall that we estimated 1411 total elastic antiprotons under the condition that "C_B be on $\bar{p}$ and fire". But, to minimize contamination, a much more severe pulse height cut (call it "PCUT2") was made.

$\left(\frac{TOT\ EL\pi}{TOT\ GB}\right)$ The ratio of the total number of elastic pions observed during a period of time to the total number of gated beam counts observed during the same period. The

reader will recall that this was defined also as the average $\left\langle \frac{EL\pi}{GB} \right\rangle$

C — The "intensity correction factor" determined from pions. Recall

$$C \equiv \left(\frac{EL\pi}{GB}\right)_0 \Big/ \left\langle \frac{EL\pi}{GB} \right\rangle$$

From following data the reader will note that C can be as large as about 1.45.

t_o — For a given reaction, the lowest -t bin for which the geometrical acceptance factor was judged to be stable with time (i.e., away from steep "edge effects"). The absolutely normalized cross section $d\sigma(t_o)/dt$ was calculated for this bin in this section.

$\bar{t}$ (generally, $-\bar{t} \leq -t_o$). — A particular "t" bin under consideration. Usually defined in the same way as "t_o" but with a somewhat more liberal criterion for "stability with time". Usually used instead of the generally more conservative "t_o" to improve statistics in determination of "N" (see later) before calling a particle an anti-proton (i.e., including its measured value of q^2 in the determination of $d\sigma/dt$). Then,

$$f_{cut} \equiv \frac{\text{total elastic (anti)protons}}{\text{total elastic (anti)protons with pulse hgt.} < \text{PCUT2}} ,$$

In the example alluded to above, (-100 GeV/c $\bar{p}p$),

$$f_{cut} = \frac{1411}{1399} .$$

$n(t_o)$ — The number of elastic $\bar{p}$'s or p's that had pulse height less than PCUT2 and -t in the "t-bin" labelled by "t_o")

N The "normalization number".

$$N \equiv C \times \frac{TOT\ EL\bar{p},\ |t| > t_o}{TOT\ GB \cdot CB} \times f_{cut} \times \frac{1}{R}$$

N was generally calculated separately for each year. Values were then compared. Theoretically independent of year. Deviation of values in N (called "Δ") obtained from year to year with the "same" beam were used to help estimate the "error" in N.

b. Calculation of "N" Values

On the next few pages we indicate the calculation of "N" values. Note--the only (anti)protons included in the calculation of N values were those for which "C_B was on p and required to fire". It will be noted that there are several "binnings" for +100 GeV/c. The reason for this will become clear later when "relative" cross sections are discussed.

Also, for +200 GeV/c, only "1981" data is used to determine N since that was the only "CB on p and required to fire" data.

Table VII-I. Determination of "C" Values

Beam	Pϕ (GeV/c)	$\left(\frac{GN}{GB}\right)_0 \times 10^{-3}$	$\times \left(\frac{EL\pi}{GN}\right)_0 \times 10^{-3}$	$= \left(\frac{EL\pi}{GB}\right)_0 \times 10^{-6}$	$\div \frac{TOT\ EL\pi}{TOT\ GB} \cdot 10^{-6}$	= "C"
-100 GeV/c	400	.190	5.65	1.07	0.740	1.45
	350	.182	5.81	1.06	0.782	1.35
+200 GeV/c	350+	.303	.248	7.51	0.0549	1.37
+100 GeV/c	400	.230	4.50	1.04	0.752	1.37
	350	.194	5.25	1.02	0.792	1.29
-200 GeV/c	400	.253	.788	.199	0.168	1.18
	350(a)*	.231	.996	.230	0.171	1.35
	350(b)*	.230	.996	.229	0.164	1.40

*Conditions between (a) and (b) slightly different--a priori N values will differ, so calculate separately.

+$p\phi$ = 400 GeV/c for +200 GeV/c scattering not included since no running done with "C_B on p".

Table VII-2. Determination of "N" Values, Comparison of Years

Beam	p_ϕ (GeV/c)	"C" × $\left[\frac{\text{TOT EL}\bar{p}\text{ (or p)}, \lvert t\rvert \geq \bar{t}}{\text{TOT GB·CB}}\right]^*$		"f_{cut}"	÷"R" =	"N"×10^{-7}	Δ
-100 GeV/c	400	1.45	$\frac{443\pm4.8\%}{2.70\times10^9}$ ++,**	$\frac{1411}{1399}$	.969	2.47	6.5%
	350	1.35	$\frac{1509\pm2.6\%}{9.30\times10^9}$ ++	$\frac{5816}{5757}$	.955	2.32	
+200 GeV/c	350	1.37	$\frac{547\pm4.3\%}{2.20\times10^{10}}$ +++	$\frac{795}{788}$	.941	.365	
+100 GeV/c Binning A only	400	1.37	$\frac{312\pm5.7\%}{1.37\times10^9}$ ++	$(.973)^{-1}$	.990	3.24	5.9%
	350	1.29	$\frac{871\pm3.4\%}{3.53\times10^9}$ ++	$(.965)^{-1}$	.963	3.43	
-200 GeV/c	400	1.18	$\frac{13\pm28\%}{0.304\times10^9}$ +++	1.0	.933	0.54	~25%
	350(a)+	1.35	$\frac{11\pm30\%}{0.292\times10^9}$ +++	1.0	.916	0.55	
	350(b)+	1.40	$\frac{8\pm35\%}{0.260\times10^9}$ +++	1.0	.946	0.44	
+100 GeV/c Binnings B,C,D	400	1.37	$\frac{461\pm5\%}{1.37\times10^9}$	$(.973)^{-1}$	.99	4.79	agree within statistical error
	350	1.29	$\frac{1200\pm2.9\%}{3.53\times10^9}$	$(.965)^{-1}$	.96	4.73	

Footnotes for Table VII.2:

* Error listed in numerator is "statistical error" in number of events

\+ Conditions between (a) and (b) slightly different--a priori N values will differ, so calculate separately.

** I.e., 443 out of 1399 $\bar{p}$'s had $-t \geq 0.6$ (GeV/c)^2 = $\bar{t}$

++ $\bar{t} = 0.6$ (GeV/c)^2

+++ $\bar{t} = 0.9$ (GeV/c)^2

Δ % deviation in "N" values indicated, defined as [(the greatest N over the least N) - 1]/100.

Table VII.3. Calculation of $\frac{d\sigma}{dt}(t_o)$ (absolute normalization)

Beam	"N"$\times 10^{-\gamma}$	$\times\ n(t_o)/TOT\ EL\bar{p},\|t\|>\bar{t}^{\Delta}$	$\div A(t_o)$	$\div T$	$\times (\rho L\Delta t)^{-1}$	$\div f_{kb}$	$= \frac{d\sigma}{dt}(t=t_o)$ $(cm^2)^{\nabla}$
-100 GeV/c	2.32±4%	$(\frac{376}{1509})\pm 5\%^{*,+}$	.0048	.77	2.32×10^{-24}	.996	$(3.60\pm7\%)\times10^{-29}$
+100 GeV/c, (binning "A" only)	3.38^{**} ±4%	$\frac{543^{++,o}}{1183^{++}}$ ±4%	.0035	.78	2.32×10^{-24}	.995	$(1.34\pm6\%)\times10^{-28}$
+200 GeV/c	.365±4%	$\frac{220^{\theta}}{547}$ ±7%	.0064	.78	2.32×10^{-24}	.988	$(6.96\pm8\%)\times10^{-30}$
-200 GeV/c	$.52^{**}$ ±12%	$\frac{10^{\theta,++}}{32}$ ±32% ***	.0072	.77	2.32×10^{-24}	.988	$(6.9\pm34\%)\times10^{-30}$
+100 GeV/c (binnings "B","C", and "D")	4.75^{**} 4%	$\frac{428\pm5\%^{+++,++}}{1661^{++}}$	.0042	.78	2.32×10^{-24}	.995	$(8.71\pm7\%)\times10^{-29}$

Footnotes for Table VII.3:

* "t_o" is 0.7-0.8 $(GeV/c)^2$ bin.

\+ Only 1981 data included in this--accuracy of that "sufficient".

** Weighted average (by number of events observed) of the yearly values.

++ Total, both years.

Δ Error quoted is from numerator only, since error in denominator is already included in determination of "N".

o "t_o" is 0.6-0.7 $(GeV/c)^2$ bin.

θ "t_o" is 0.9-1.0 $(GeV/c)^2$ bin.

*** No "high pressure events", no "non-normalizable events" in either numerator or denominator.

+++ "t_o" is 0.65-0.75 $(GeV/c)^2$ bin.

∇ In all cases except +200 GeV/c, error in "N" is estimated from value of Δ on page 228. Error in $[n(t_o)/TOT \ldots]$ is then determined from statistical error in numerator only, since error in denominator is already included in determination of "N". Final fractional error on $\frac{d\sigma}{dt}(t_o)$ is then obtained as quadrature addition of fractional errors in N, $[n(t_o)/TOT \ldots]$, $A(t_o)$, T, $(\rho L \Delta t)^{-1}$, $f_{kb}(t_o)$. The author realizes this is a conservative procedure.

For +200 GeV/c, error in N is estimated to be ±4%, then same procedure is applied.

Estimates of errors in factors $A(t_o)$, T, $(\rho L \Delta t)^{-1}$, $f_{kb}(t_o)$ are assumed to be ±2%, ±1%, ±1%, ±1%, respectively, for all "t_o" values used.

Comment on Errors and Accuracy of the Normalization:

We have already remarked that the typical accuracy in the determination of factors like $(GN/GB)_0$ and $(EL\pi/GN)_0$ was a few percent. Therefore the normalization "N" values cannot, of course, be accurate to more than "a few percent" no matter how many elastic $\bar{p}$'s (p's) are used.

It is noticed that the agreement between "N" values for, e.g., -100 GeV/c is good--($\Delta \approx 6.5\%$ is within expected statistical error). Since there were more total elastic $\bar{p}p$ events in 1981, the weighted average was very near the 1981 value--therefore, for simplicity we normalized using only the 1981 data for -100 GeV/c. For other data a weighted average of the "N" values for the two years was used. In general the agreement of the "N" values for different years and the "same" beam was as good as could be expected.

A moment's reflection about previously existing data and statistical accuracy of this data will convince the reader that there was no point in "normalizing" to better than 10% accuracy anyway. That being so, we were then free to choose the normalization bin "t_o" with a somewhat more conservative attitude toward acceptance fluctuations "near the edge" than we had in choosing "t" previously--here we merely needed the highest -t bin with more than about a hundred events. With this in mind the calculation of $\frac{d\sigma\ (t=t_o)}{dt}$ is completed on the next page for all cases.

6. Calculation of $d\sigma/dt$ for the Entire -t Range and Results

a. Formula and Notation

Once the "absolutely normalized" cross section is known for any -t bin, it is possible to calculate the cross section for all other bins simply by comparing relative numbers of events, relative geometrical acceptance factors, etc. In particular, for "bin t'",

$$\frac{d\sigma(t')}{dt} = \frac{d\sigma(t_o)}{dt} \times \frac{n(t')}{n(t_o)} \times \frac{E(t_o)}{E(t')} \times \frac{f_{kb}(t')}{f_{kb}(t_o)} \times \frac{f_{rc}(t')}{f_{rc}(t_o)} \times \frac{\Delta t_o}{\Delta t'}$$

Here,

$\frac{d\sigma(t_o)}{dt}$ = "absolutely normalized" cross section for bin centered on $|t| = t_o$

$n(t')$ = "total" number of events observed in -t bin labelled by the value t'. By "total number of events" we mean all elastic $\bar{p}p$ or pp events obtained under any operating condition of the differential Cerenkov counter that were considered (Chapter VI) to be "sufficiently" free of contamination (e.g., include "C_B on K and no fire" events if they were deemed okay in Chapter VI).

$n(t_o)$ = "total" number of events in -t bin labelled by the value t_o. Note that this is different than the "$n(t_o)$" defined previously--that involved a more restricted sample.

$\frac{E(t_o)}{E(t')}$ = ratio of product of geometrical acceptance factor and reconstruction efficiency for bin labelled by "t_o" to that for bin labelled by "t'".

$f_{kb}(t',t_o)$ = kinematic background correction factor for bin labelled by ("t'", "t_o")

$f_{rc}(t',t_o)$ = radiative correction factor for bin labelled by ("t'", "t_o")

$\frac{\Delta t_o}{\Delta t'}$ = ratio of "bin width" (in -t) for bin labelled by "t_o" to that for bin labelled by t'

b. Results

On the following pages we give the calculations and results. In the tables, by the phrase "stat err" we shall mean "statistical error". (The fractional statistical error was calculated as $1/\sqrt{n(t)}$, where n(t) was the "total" number of events in the bin (this time after slight background subtraction).

In the columns "Other 1" and/or "Other 2" we list values of cross section for the same process and same bin obtained by "others". The identities of the "others" can be found in the references.

Table VII.4. Calculation of $\frac{d\sigma}{dt}$ for $\bar{p}p \to \bar{p}p$ at 100 GeV/c, Sample "A"*,**

-t	$\frac{n(t)}{n(t_o)}$ †	× $\frac{E(t_o)}{E(t)}$	× $\frac{f_{kb}(t')}{f_{kb}(t_o)}$	× $\frac{d\sigma(t_o)}{dt}$	× $\frac{\Delta t_o}{\Delta t'}$	= $\frac{d\sigma(t)}{dt}$ ± stat err (cm^2) ††	Other ‡ ‡‡
0.55	1696/471	2.05	.995/.995	$(3.60\pm7\%)\times10^{-29}cm^2$	1.	$(2.66\pm0.06)\times10^{-28}$	$(2.5\pm0.5)\times10^{-28}$
0.65	940/471	1.38	.995/.995		1.	$(9.91\pm0.32)\times10^{-29}$	$(6.9\pm3.\ )\times10^{-29}$
0.75	471/471	1.00	.995/.995		1.	$(3.60\pm0.17)\times10^{-29}$	$(5.4\pm1.6)\times10^{-29}$
0.85	287/471	.793	.996/.995		1.	$(1.74\pm0.10)\times10^{-29}$	$(9.0\pm8.4)\times10^{-30}$
0.95	138/471	.643	.996/.995		1.	$(6.76\pm0.57)\times10^{-30}$	$(4.6\pm6.4)\times10^{-30}$
1.05	59/471	.542	.996/.995		1.	$(2.44\pm0.31)\times10^{-30}$	
1.15	17/471	.469	.996/.995		1.	$(6.07\pm1.5)\times10^{-31}$	
1.25	4/471	.410	.996/.995		1.	$(1.25\pm0.62)\times10^{-31}$	
1.35	2/471	.379	.996/.995		1.	$(5.77\pm4.0)\times10^{-32}$	
1.50	0/471	.339	.996/.995		.5	$UL^{(\dagger)} = 1.29\times10^{-32}$	
1.70	3/471	.282	.996/.995		.5	$(3.22\pm1.8)\times10^{-32}$	
1.90	3/471	.243	.995/.995		.5	$(2.78\pm1.6)\times10^{-32}$	
2.10	4/471	.214	.994/.995		.5	$(3.26\pm1.6)\times10^{-32}$	
2.30	4/471	.189	.990/.995		.5	$(2.88\pm1.4)\times10^{-32}$	
2.40	1/471	.175	.987/.995		1.	$(1.33\pm1.3)\times10^{-32}$	

Footnotes for Table VII.4:

* Sample "A" includes only "C_B on $\bar{p}$ and fire" events.

† "UL" means "upper limit"

** "t_0" is $-t = 0.7\text{-}0.8\ (\text{GeV}/c)^2$ bin

†† % statistical error is determined as $1/\sqrt{n(t)}$. The reader should realize that there is an additional systematic "normalization" error of up to ±7% from determination of $d\sigma/dt\ (t_0)$.

‡ C. W. Akerlof et al., Phys. Rev. D14, 1 (1976). Some of the cross sections and errors listed in this column were obtained by logarithmic interpolation of Akerlof's numbers. Errors listed are statistical only. There is an additional systematic normalization error not listed.

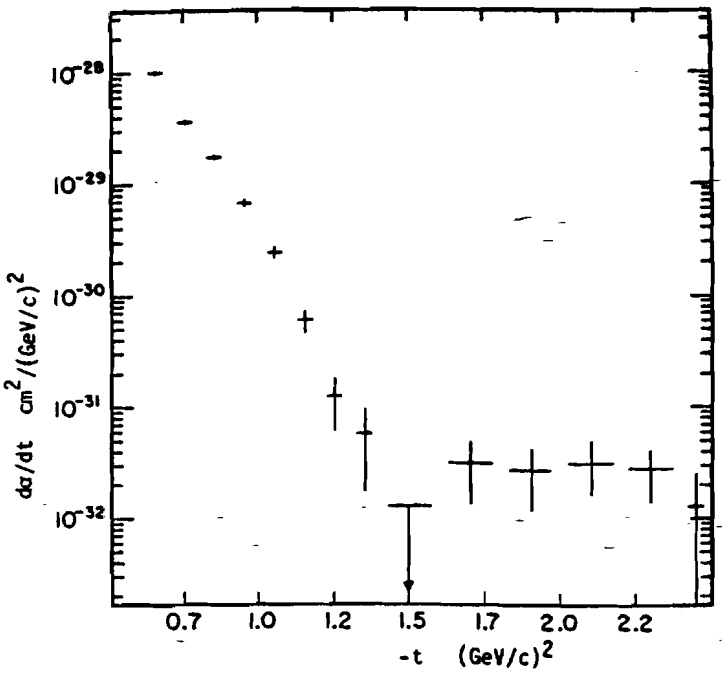

Figure VII-3. Results for $\frac{d\sigma}{dt}$ ($\bar{p}p \to \bar{p}p$) at 100 GeV/c, Sample "A" (see text and Table VII.4).

Table VII.5. Calculation of $\frac{d\sigma}{dt}$ for $\bar{p}p \to \bar{p}p$ at 100 GeV/c, Sample "B" *,**

-t	$\frac{n(t)}{n(t_o)}$	× $\frac{E(t_o)}{E(t)}$	× $\frac{f_{kb}(t')}{f_{kb}(t_o)}$	× $\frac{d\sigma(t_o)}{dt}$	× $\frac{\Delta t_o}{\Delta t'}$ = $\frac{d\sigma(t)}{dt}$ ± stat err (cm^2) ††	Other ‡
0.65	1021/522	1.38	.995/.995	$3.60 \pm 7\% \times 10^{-29}$ cm^2	1. $(9.72 \pm 0.3) \times 10^{-29}$	$(6.9 \pm 3.) \times 10^{-29}$
0.75	522/522	1.00	.995/.995		1. $(3.60 \pm 0.16) \times 10^{-29}$	$(5.4 \pm 1.6) \times 10^{-29}$
0.85	323/522	.793	.996/.995		1. $(1.76 \pm 0.10) \times 10^{-29}$	$(9.0 \pm 8.4) \times 10^{-30}$
0.95	154/522	.643	.996/.995		1. $(6.81 \pm 0.55) \times 10^{-30}$	$(4.6 \pm 6.4) \times 10^{-30}$
1.05	67/522	.542	.996/.995		1. $(2.50 \pm 0.30) \times 10^{-30}$	
1.15	22/522	.469	.996/.995		1. $(7.09 \pm 1.49) \times 10^{-31}$	
1.25	5/522	.410	.996/.995		1. $(1.41 \pm 0.63) \times 10^{-31}$	
1.35	2/522	.379	.996/.995		1. $(5.21 \pm 3.70) \times 10^{-32}$	
1.50	1/522	.339	.996/.995		.5 $(1.16 \pm 1.16) \times 10^{-32}$	
1.70	3/522	.282	.996/.995		.5 $(2.91 \pm 1.69) \times 10^{-32}$	
1.90	4/522	.243	.995/.995		.5 $(3.34 \pm 1.67) \times 10^{-32}$	
2.10	5/522	.214	.994/.995		.5 $(3.68 \pm 1.65) \times 10^{-32}$	
2.30	5/522	.189	.990/.995		.5 $(3.25 \pm 1.46) \times 10^{-32}$	
2.40	1/522	.175	.987/.995		1. $(1.20 \pm 1.20) \times 10^{-32}$	

Footnotes for Table VII.5:

* Sample "B" includes "C_B on K and no fire" events as well as the "C_B on $\bar{p}$ and fire" events included in Sample "A" (as per Section IV).

** "t_o" is $-t = 0.7\text{-}0.8$ $(GeV/c)^2$ bin.

†† % statistical error is determined as $1/\sqrt{n(t)}$. The reader should realize that there is an additional systematic "normalization" error of up to ±7% from determination of $d\sigma/dt$ (t_o).

‡ C. W. Akerlof et al., Phys. Rev. D14, 1 (1976). Some of the cross sections and errors listed in this column were obtained by logarithmic interpolation of Akerlof's numbers. Errors listed are statistical only. There is an additional systematic normalization error not listed.

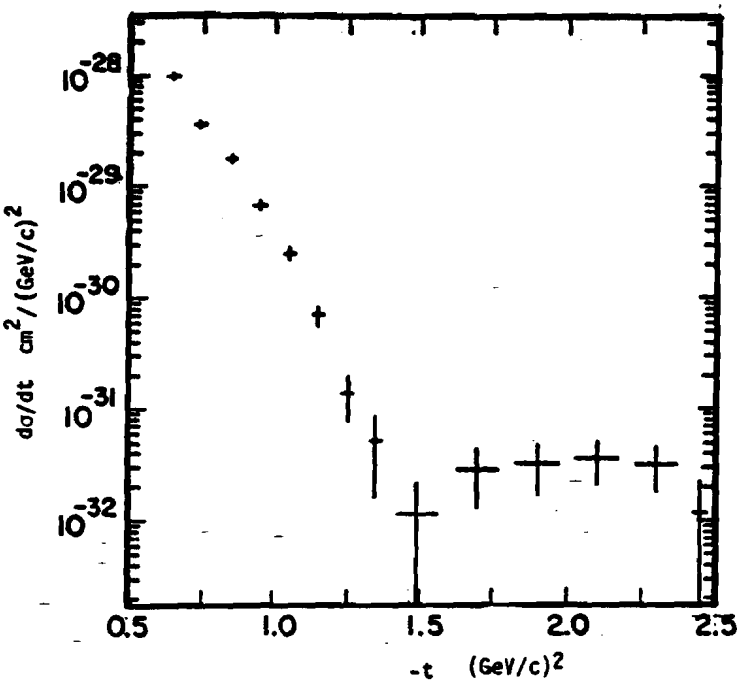

Figure VII-4. Results for $\frac{d\sigma}{dt}(\bar{p}p \to \bar{p}p)$ at 100 GeV/c, Sample "B" (see text and Table VII.5).

Table VII.6. Calculation of $\frac{d\sigma}{dt}$ for pp→pp at 200 GeV/c

$-t$	$\frac{n(t)}{n(t_o)}$ ×	$\frac{E(t_o)}{E(t)}$ ×	$\frac{f_{kb}(t')}{f_{kb}(t_o)}$ ×	$\frac{d\sigma(t_o)}{dt}$ ×	$\frac{\Delta t_o}{\Delta t'}$ =	$\frac{d\sigma}{dt} \pm$ stat err $(cm^2)^{++}$
.95	1424/1424	1.	.988/.988	$(6.96\pm8\%)\times10^{-30}cm^2$	1	$(6.96\pm0.18)\times10^{-30}$
1.05	801/1424	.766	.988/.988		1	$(3.00\pm0.11)\times10^{-30}$
1.15	330/1424	.631	.988/.988		1	$(1.02\pm0.05)\times10^{-30}$
1.25	124/1424	.551	.988/.988		1	$(3.34\pm0.29)\times10^{-31}$
1.35	425/1424	.491	.988/.988		1	$(1.02\pm0.15)\times10^{-31}$
1.45	16.7/1424	.453	.988/.988		1	$(3.70\pm0.86)\times10^{-32}$
1.55	15.8/1424	.418	.987/.988		1	$(3.22\pm0.78)\times10^{-32}$
1.65	10.9/1424	.390	.987/.988		1	$(2.08\pm0.59)\times10^{-32}$
1.75	17/1424	.355	.986/.988		1	$(2.94\pm0.70)\times10^{-32}$
1.85	32/1424	.330	.984/.988		1	$(5.14\pm0.86)\times10^{-32}$
1.95	27/1424	.307	.982/.988		1	$(4.03\pm0.76)\times10^{-32}$
2.05	36/1424	.291	.980/.988		1	$(5.08\pm0.81)\times10^{-32}$
2.15	33/1424	.274	.977/.988		1	$(4.37\pm0.74)\times10^{-32}$
2.25	16/1424	.261	.973/.988		1	$(2.01\pm0.48)\times10^{-32}$
2.35	23/1424	.241	.967/.988		1	$(2.65\pm0.53)\times10^{-32}$
2.45	27/1424	.232	.959/.988		1	$(2.97\pm0.57)\times10^{-32}$
2.55	17/1424	.223	.947/.988		1	$(1.78\pm0.43)\times10^{-32}$
2.65	16/1424	.213	.930/.988		1	$(1.57\pm0.39)\times10^{-32}$
2.75	19/1424	.202	.905/.988		1	$(1.72\pm0.40)\times10^{-32}$
2.85	18/1424	.197	.867/.988		1	$(1.52\pm0.36)\times10^{-32}$

Table VII.6 (continued)

$-t$	$\frac{n(t)}{n(t_o)}$	$\times \frac{E(t_o)}{E(t)}$	$\times \frac{f_{kb}(t')}{f_{kb}(t_o)}$	$\times \frac{d\sigma(t_o)}{dt}$	$\times \frac{\Delta t_o}{\Delta t'}$	$= \frac{d\sigma}{dt} \pm$ stat err (cm^2) ††
2.95	11/1424	.193	.807/.988	$(6.96\pm8\%) \times 10^{-30} cm^2$	1	$(8.48\pm2.6) \times 10^{-33}$
3.05	9/1424	.189	.807/.988(Δ)		1	$(6.79\pm2.3) \times 10^{-33}$(Δ)
3.15	5/1424	.185	.750/.988(Δ)		1	$(3.43\pm1.5) \times 10^{-33}$(Δ)
3.25	12/1424	.182	.707/.988		1	$(7.64\pm2.2) \times 10^{-33}$
3.35	6/1424	.179	.707/.988		1	$(3.76\pm1.5) \times 10^{-33}$
3.45	7/1424	.177	.707/.988		1	$(4.33\pm1.6) \times 10^{-33}$
3.55	7/1424	.175	.85/.988(Δ)		1	$(5.15\pm1.9) \times 10^{-33}$
3.65	5/1424	.173	.917/.988		1	$(3.92\pm1.8) \times 10^{-33}$
3.75	3/1424	.170	.917/.988		1	$(2.31\pm1.3) \times 10^{-33}$
4.0	4/1424	.167	.917/.988		1/4	$(7.6 \pm3.8) \times 10^{-34}$
4.55	4/1424	.159	.917/.988		1/7	$(4.1 \pm2.1) \times 10^{-34}$
5.45	3/1424	.147	.917/.988		1/11	$(1.8 \pm1.0) \times 10^{-34}$
6.55	1/1424	.135	.917/.988		1/11	$(5.6 \pm5.6) \times 10^{-35}$
8.15	1/1424	.126	.917/.988		1/21	$(2.7 \pm2.7) \times 10^{-35}$
10.25	0/1424	.136	.917/.988		1/21	upper limit = 2.9×10^{-35}

(Δ) may be inaccurate by ±7% due to guess of $f_{kb}(t')/f_{kb}(t_o)$

†† % statistical error is determined as $1/\sqrt{n(t)}$. The reader should realize that there is an additional systematic "normalization" error of up to ±7% from determination of $d\sigma/dt\ (t_o)$

due to guess of $f_{kb}(t')/f_{kb}(t_o)$

++ % statistical error is determined) $1/\sqrt{n(t)}$. The reader should realize that there is an additional systematic "normalizat) error of up to ±7% from determination of $d\sigma/dt\ (t_o)$

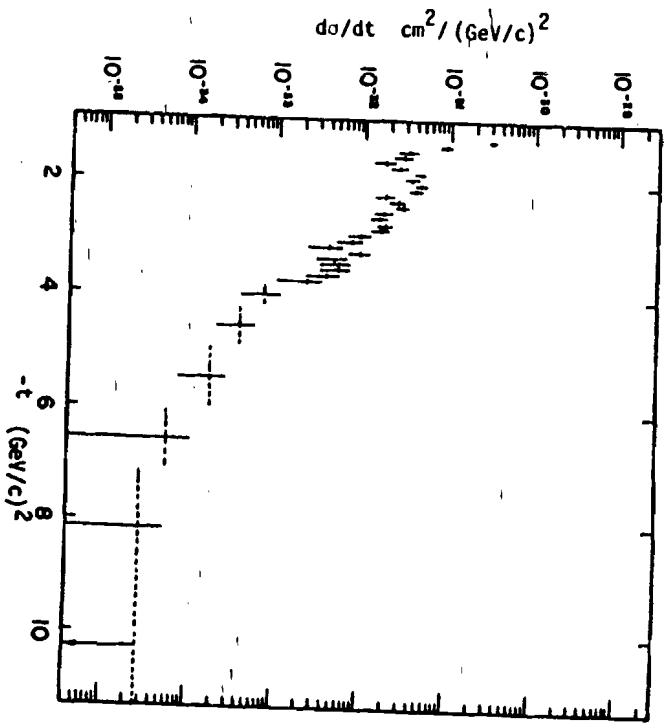

Figure VII-5. Results for $\frac{d\sigma}{dt}$ (pp → pp) at 200 GeV/c) (see text and Table VII.6).

Table VII.7. Calculation of $\frac{d\sigma}{dt}$ for pp→pp at 100 GeV/c, Binning "A"*

-t	$\frac{n(t)}{n(t_o)}$ ×	$\frac{E(t_o)}{E(t)}$ ×	$\frac{f_{kb}(t')}{f_{kb}(t_o)}$ ×	$\frac{d\sigma(t_o)}{dt}$ ×	$\frac{\Delta t_o}{\Delta t'}$ = $\frac{d\sigma}{dt}$ ± stat err (cm^2)††
.55	4103/2091	1.47	.995/.995	(1.34±6%) ×10^{-28}	1.0	(3.87±0.06)×10^{-28}
.65	2091/2091	1.00	.995/.995		1.0	(1.34±0.03)×10^{-28}
.75	1140/2091	.729	.995/.995		1.0	(5.35±0.15)×10^{-29}
.85	637/2091	.567	.995/.995		1.0	(2.32±0.09)×10^{-29}
.95	277/2091	.466	.995/.995		1.0	(8.27±0.48)×10^{-30}
1.05	122/2091	.386	.995/.995		1.0	(3.02±0.28)×10^{-30}
1.15	56.7/2091	.331	.995/.995		1.0	(1.21±0.16)×10^{-30}
1.25	27.1/2091	.294	.995/.995		1.0	(5.15±0.96)×10^{-31}
1.35	11.5/2091	.266	.995/.995		1.0	(1.98±0.6) ×10^{-31}
1.45	3.7/2091	.241	.995/.995		1.0	(5.6 ±2.9) ×10^{-32}
1.55	4.8/2091	.222	.995/.995		1.0	(6.7 ±3.0) ×10^{-32}
1.65	6.8/2091	.204	.995/.995		1.0	(8.8 ±3.3) ×10^{-32}
1.75	6.9/2091	.188	.995/.995		1.0	(8.2 ±3.1) ×10^{-32}
1.85	10.9/2091	.174	.995/.995		1.0	(1.22±0.36)×10^{-31}
1.95	4/2091	.162	.995/.995		1.0	(4.15±2.01)×10^{-32}
2.05	6/2091	.154	.994/.995		1.0	(5.92±2.3) ×10^{-32}
2.15	5/2091	.145	.993/.995		1.0	(4.64±2.0) ×10^{-32}
2.25	4/2091	.136	.991/.995		1.0	(3.5 ±1.7) ×10^{-32}
2.35	4/2091	.127	.989/.995		1.0	(3.2 ±1.6) ×10^{-32}
2.50	3/2091	.121	.986/.995		0.5	(1.2 ±0.66)×10^{-32}

* includes all +100 GeV/c protons from Sec. IV except "C_B on P and no fire".

†† % statistical error is determined as $1/\sqrt{n(t)}$. The reader should realize that there is an additional systematic "normalization" error of up to ±7% from determination of $d\sigma/dt\ (t_o)$

2.50	3/2091	.121	.986/.995	0.5	$(1.2 \pm 0.66) \times 10^{-32}$

* includes all +100 GeV/c protons from Sec. IV except "C_B on P and no fire".
†† % statistical error is determined as $1/\sqrt{n(t)}$. The reader should realize that there is an additional systematic "normalization" error of up to ±7% from determination of $d\sigma/dt$ (t_o)

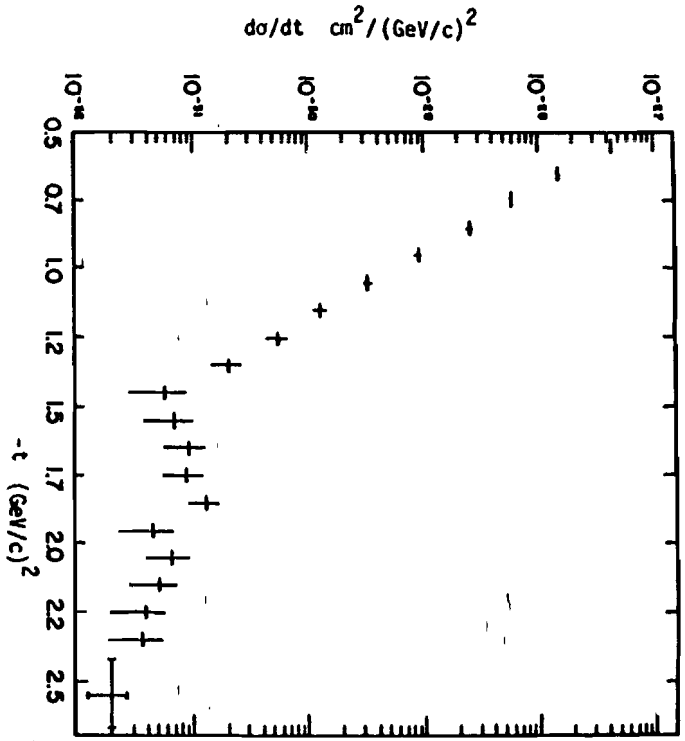

Figure VII-6. Results for $\frac{d\sigma}{dt}(pp_- + pp)$ at 100 GeV/c, Binning "A" (see text and Table VII.7).

Table VII.8. Calculation of $\frac{d\sigma}{dt}$ for pp→pp at 100 GeV/c, Binning "B"*

-t	$\frac{n(t)}{n(t_o)}$ ×	$\frac{E(t_o)}{E(t)}$ ×	$\frac{f_{kb}(t')}{f_{kb}(t_o)}$ ×	$\frac{d\sigma(t_o)}{dt}$ * ×	$\frac{\Delta t_o}{\Delta t'}$ =	$\frac{d\sigma}{dt}$ ± stat err (cm^2)††
.60	2961/1596	1.41	.995/.995	(8.71±7%)	1.0	$(2.27\pm0.04)\times10^{-28}$
.70	1596/1596	1.00	.995/.995	$\times10^{-29}cm^{-2}$	1.0	$(8.71\pm0.21)\times10^{-29}$
.80	847/1596	.756	.995/.995		1.0	$(3.48\pm0.12)\times10^{-29}$
.90	433/1596	.670	.995/.995		1.0	$(1.42\pm0.07)\times10^{-29}$
1.0	174/1596	.501	.995/.995		1.0	$(4.73\pm0.35)\times10^{-30}$
1.1	86/1596	.423	.995/.995		1.0	$(1.98\pm0.21)\times10^{-30}$
1.2	42/1596	.369	.995/.995		1.0	$(8.42\pm1.25)\times10^{-31}$
1.3	17.3/1596	.331	.995/.995		1.0	$(3.11\pm0.74)\times10^{-31}$
1.4	4.6/1596	.300	.995/.995		1.0	$(7.49\pm3.41)\times10^{-32}$
1.5	2.7/1596	.274	.995/.995		1.0	$(4.02\pm2.39)\times10^{-32}$
1.6	7.8/1596	.252	.995/.995		1.0	$(1.07\pm0.37)\times10^{-31}$
1.7	719/1596	.232	.995/.995		1.0	$(9.95\pm3.45)\times10^{-32}$
1.8	3.9/1596	.214	.995/.995		1.0	$(4.5\pm2.3)\times10^{-32}$
1.9	10/1596	.199	.995/.995		1.0	$(1.08\pm0.33)\times10^{-31}$
2.0	7/1596	.187	.994/.995		1.0	$(7.12\pm2.61)\times10^{-32}$
2.1	1/1596	.177	.993/.995		1.0	$(9.61\pm9.6)\times10^{-33}$
2.2	5/1596	.167	.992/.995		1.0	$(4.53\pm2.0)\times10^{-32}$
2.3	8/1596	.156	.990/.995		1.0	$(6.75\pm2.4)\times10^{-32}$
2.45	2/1596	.146	.986/.995		0.5	$(7.95\pm6.)\times10^{-33}$

* rebinned. No "C_B on P and no fire" data.
"t_o" = -t = 0.7-0.8 bin

†† % statistical error is determined as $1/\sqrt{n(t)}$. The reader should realize that there is an additional systematic "normalization" error of up to ±7% from determination of $d\sigma/dt\ (t_o)$

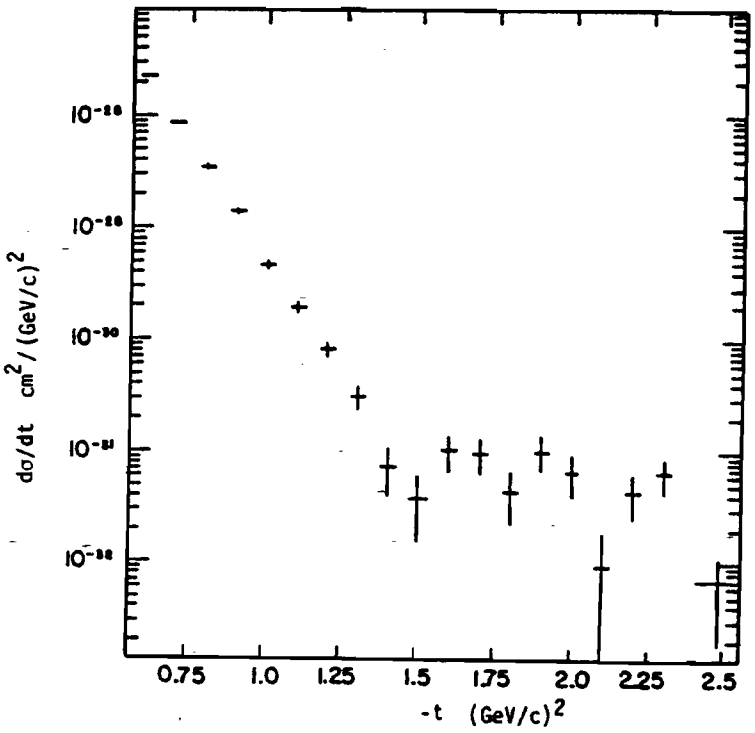

Figure VII-7. Results for $\frac{d\sigma}{dt}$ (pp → pp) at 100 GeV/c, Binning "B" (see text and Table VII.8).

* rebinned. No "C_8 on P and no fire" data.
"t_o" = -t = 0.7-0.8 bin
++ % statistical error is determined as $1/\sqrt{n(t)}$. The reader should realize that there is an additional systematic "normalization" error of up to ±7% from determination of $d\sigma/dt$ (t_o)

Table VII.9. "Event Types", -200 GeV/c

$-t, (\frac{GeV}{c})^2$	1980 "normal pressure", nnn *	1981 n.p., nnn *	n.p., n.n.‡	hi-pres,** 314-368	hi-pres,†† 369-374	total ± stat err
0.9-1.0	5	5	0	1	3	14±27%
1.0-1.1	1	4	0	2	0	7±38%
1.1-1.2	1	1	0	1	0	3±58%
1.2-1.7	0	0	0	0	0	0
Δ 1.7-1.8		1				1±100%
1.8-2.1	0	0	0	0	0	0
2.1-2.2	1					1±100%
2.2-2.3		1				1±100%
2.3-2.5	0	0	0	0	0	0
2.5-2.6	0	0	1	0	0	1±100%
2.6-2.7	0	0	0	0	0	0
2.7-2.8	0	1	0	0	0	1±100%
2.8-3.2	0	0	0	0	0	0
3.2-3.3	0	0	0	1	0	1±100%
3.3-3.4	0	0	0	0	0	0
3.4-3.8	0	0	0	0	0	0
3.8-3.9	1	0	0	0	0	1±100%
3.9-4.0	0	1	0	0	0	1±100%

Grand Total = 32 events, $t > 0.9$ $(GeV/c)^2$

Footnotes for Table VII.9:

Δ brackets indicate binning used in this thesis for calculation of $\frac{dσ}{dt}$

* events gathered during 1980 (1981) "normal" Cerenkov tank pressure running. No runs with attenuator problems, etc. (i.e., nnn - "no non-normalizable" data)

† events gathered during "normal pressure" period but "non-normalizable"--due to attenuator problems during these runs, slightly different trigger conditions, no multiplicity veto, etc.

** data gathered during "high Cerenkov pressure" period - runs 314-368

†† data gathered during uncertain Cerenkov pressure period - runs 369-374

Table VII.10. Calculation of $\frac{d\sigma}{dt}$ ($\bar{p}p \to \bar{p}p$) at 200 GeV/c.

$-t$ $(GeV/c)^2$	$\frac{n(t)}{n(t_o)} \times \frac{E(t_o)}{E(t)} \times \frac{f_{kb}(t')}{f_{kb}(t_o)} \times \frac{d\sigma(t_o)}{dt} \times \frac{\Delta t_o}{\Delta t'} = \frac{d\sigma(t)}{dt} \pm$ stat err ++ (cm^2)	
0.95	14/14	1. .988/.988 $(6.9\pm34\%) \times 10^{-30}\ cm^2$ 1. $(6.9\pm2.8)\times10^{-30}$
1.05	7/14	.78 .988/.988 1. $(2.7\pm1.0)\times10^{-30}$
1.15	3/14	.65 .988/.988 1. $(9.6\pm5.5)\times10^{-31}$
1.45	0/14	.48 .988/.988 0.2 Upper limit = (4.7×10^{-32})
1.95	2/14	.33 .982/.988 0.2 $(6.5\pm4.6)\times10^{-32}$
2.45	2/14	.24 .959/.988 0.2 $(4.6\pm3.3)\times10^{-32}$
3.05	2/14	.20 .85*/.988 0.14 $(2.2\pm1.6)\times10^{-32}$
3.75	2/14	.17 .85*/.988 0.14 $(2.0\pm1.4)\times10^{-32}$
4.45	0/14	.16 .917/.988 0.14 Upper limit = (1.02×10^{-32})

* Estimate ±10%

++ % statistical error is determined as $1/\sqrt{n(t)}$. The reader should realize that there is an additional systematic "normalization" error of up to ±7% from determination of $d\sigma/dt\ (t_o)$

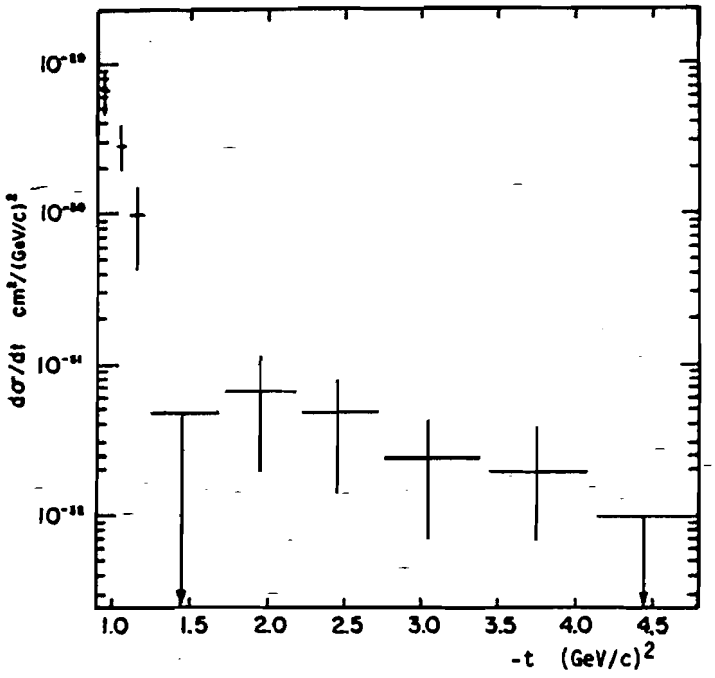

Figure VII-8. Results for $\frac{d\sigma}{dt}$ ($\bar{p}p \to \bar{p}p$) at 200 GeV/c (see text and Table VII.10).

C. Discussion of Results

(i) +200 GeV/c - Checking the Experiment

The existence of the $-t \approx 1.4$ $(GeV/c)^2$ dip in pp scattering has, of course, been known for some time. In Figure VII-9 we compare a preliminary version of our +200 GeV/c data with earlier pp data obtained at the same energy by Faissler et al.[115] and by Fidecaro et al.[116] The agreement is good, and with this important check satisfied we have confidence in our other results.

(ii) -100 GeV/c - New Result

As we have mentioned, in 1980 a dip in $\bar{p}p$ elastic scattering was first reported, also near $-t = 1.4$ GeV/c, with 50 GeV/c incident antiprotons. The reader will note from our data that the dip is also present, at about the same value of -t, with 100 GeV/c incident antiprotons.

We note that the papers of Asa'd et al.[18] and Fearnley[117] constitute the only other published indications of a $\bar{p}p$ dip at high energy; however, we recall that dips were seen in much lower energy $\bar{p}p$ scattering near $-t = 0.8$ $(GeV/c)^2$ and $-t = 2.2$ $(GeV/c)^2$. (We remind the reader that according to the Chou-Yang model the $-t = 1.4$ $(GeV/c)^2$ dip is the older $-t = 0.8$ $(GeV/c)^2$ dip moved out to larger -t because of the decrease of the $\bar{p}p$ total cross section. [However, recently (June 1983) news[117] has been announced of a dip in $\bar{p}p$ scattering at 30 GeV/c near $-t = 1.7$ GeV/c, contrary to expectations in the Chou-Yang model.]

As far as the position of the $\bar{p}p$ dip in -t at our energies, the similarity of $\sigma_{tot}(pp)$ and $\sigma_{tot}(\bar{p}p)$ predict (again, Chou-Yang model) nearly the same position for the $\bar{p}p$ dip at 100 GeV/c as the pp dip at ISR energies. Indeed, within our statistical accuracy we

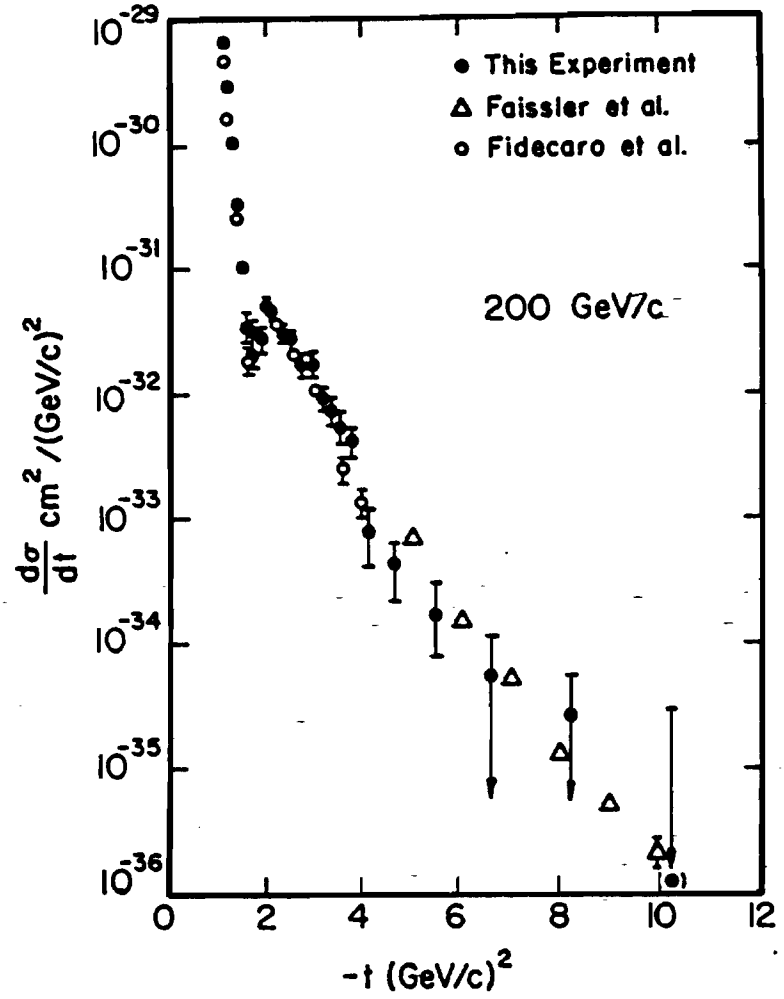

Figure VII-9. Comparison of preliminary +200 GeV/c data with those of Faissler et al. (ref. 115) and Fidecaro et al. (ref. 116) [from ref. 101].

cannot discern any difference in the position of the dip between -100 GeV/c $\bar{p}p$ scattering and +200 GeV/c pp scattering or between -100 GeV/c $\bar{p}p$ scattering and -50 GeV/c $\bar{p}p$ scattering. In Figure VII-10 we show a comparison of a preliminary version of our -100 GeV/c data with that of Asa'd et al. (50 GeV/c).

(iii) -200 GeV/c - New Result

Although our 200 GeV/c $\bar{p}p$ data is of poorer statistical accuracy than our 100 GeV/c data, they are also consistent with a dip in the same region of -t. As with -100 GeV/c, no previous data has been published at this energy for this range of -t.

In Figure VII-11 we show a comparison of preliminary versions of the data presented in this thesis for $\bar{p}p$ elastic scattering at 100 GeV/c, $\bar{p}p$ elastic scattering at 200 GeV/c, and pp elastic scattering at 200 GeV/c. There is no statistically significant difference between any of these cross sections in our range of -t.

(iv) +100 GeV/c - Possible New Feature

Previous measurements of elastic p-p scattering for our range of momentum transfer have been made at 100 GeV/c. But none show any evidence of a dip near $-t = 1.4$ GeV/c. For example, an experiment done at Fermilab by a Rochester-Imperial College-Fermilab collaboration[13] showed no dip near $-t = 1.4$ GeV/c up to an incident energy of about 150 GeV/c. But our data may show some evidence for such a dip.

The issue is potentially important as it may hint as to where an energy threshold for "new physics" beings. Certainly within the context of several of the models mentioned in Chapter I it is very interesting.

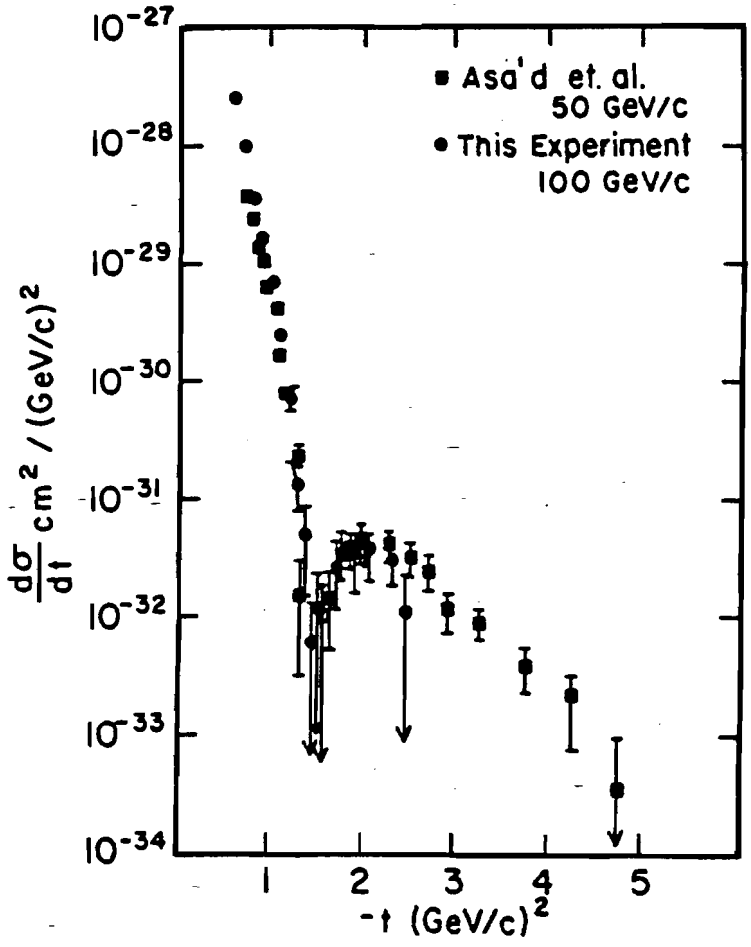

Figure VII-10. Comparison of 50 GeV/c $\bar{p}p$ data of Asa'd et al. (reference 18) with preliminary version of our 100 GeV/c $\bar{p}p$ data. (From reference 101.)

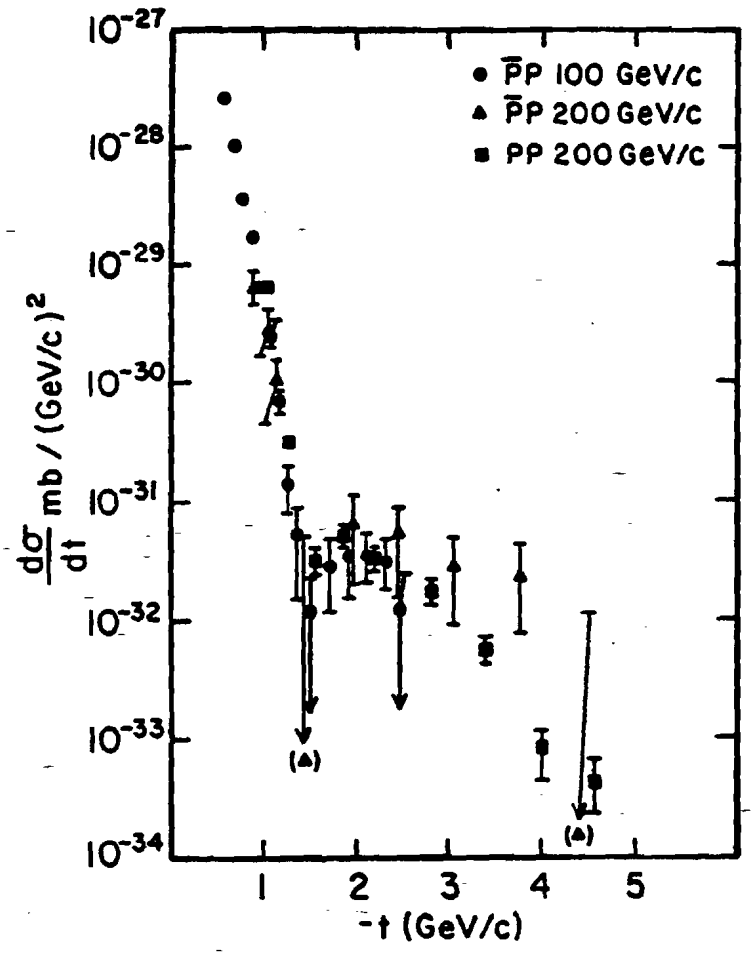

Figure VII-11. Comparison of preliminary versions of data presented in this thesis for cases indicated. (From reference 101.)

For example, it sets the energy scale for the onset of geometrical (not Chou-Yang) scaling. It also says something interesting about the ratio of the real part to the imaginary part of the scattering amplitude. This provides a check, e.g., on both conventional and "derivative" dispersion relations. We feel that it also has something interesting to say about the energy dependence of the absorptivity of the quark-quark scattering amplitude. But for here and now we refrain from speculation on this.

In Figure VII-12 we show a comparison of a preliminary version of our 100 GeV/c pp data with that of Akerlof et al.[12] Note the "dip region".

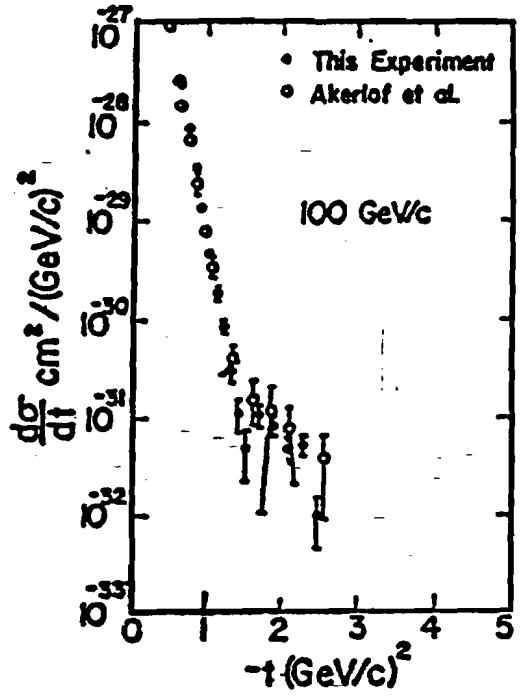

Figure VII-12. Comparison of preliminary version of +100 GeV/c data presented in this thesis with that of Akerlof et al. (reference 12). (From reference 101.)

Bibliography

1. J. Orear, Phys. Rev. Lett. 12, 112 (1964).
2. H. Frauenfelder and E. Henley, Subatomic Physics (Prentice-Hall, Englewood Cliffs, N.J., 1974), p. 141.
3. D. H. Perkins Introduction to High Energy Physics (Addison-Wesley, Reading, Mass., 1982), 2nd ed., p. 172.
4. Alan R. White, "The Pomeron and Hadrons Through Infrared Analysis of QCD", Ref. TH.3058-CERN, 1981.
5. Alan R. White, "Confinement Through Regge Limit Infra-Red Analysis of QCD", Ref. TH.3115-CERN, 1981.
6. U. Amaldi et al., Ann. Rev. Nucl. Sci. 26, 385 (1976).
7. F. Zachariasen, in Lectures in Theoretical Physics XIIB, Univ. of Colorado, 1971.
8. T. T. Wu and C. N. Yang, Phys. Rev. B137, 708 (1965).
9. V. V. Anisovich, E. M. Levin and M. G. Ryskin, Yad. Fiz. 29, 1311 (1979).
10. A. Böhm et al., Phys. Lett. B49, 491 (1974).
11. G. Giacommelli, Physics Reports 23C, 2, 125 (1976).
12. C. W. Akerlof et al., Phys. Lett. B59, 197 (1975).
13. D. Gross et al., Univ. of Rochester preprint 78-79 (1978).
14. E. Nagy et al., Nucl. Phys. B150, 221 (1979).
15. R. Phillips and V. Barger, Phys. Lett. 46B, 412 (1973).
16. J. L. Hartmann et al., Phys. Rev. Lett. 39, 975 (1977).
17. S. Connetti et al., Phys. Rev. Lett. 41, 924 (1978).
18. Z. Asa'd et al., CERN preprint CERN-EP/81-26 (1981)
19. P.D.B. Collins and F. D. Gault, Phys. Lett. 73B, 330 (1978).
20. T. T. Chou and C. N. Yang, Phys. Rev. 170, 5 (1968).
21. Maxwell Kac, Nucl. Phys. B62, 402 (1973).

22. G. Shaw, Phys. Lett. 39B, 255 (1972).

23. Nina Byers, in Proceedings of XIth School of Subnuclear Physics, Erice, Sicily (1973).

24. P. Karchin, Ph.D. thesis, Cornell University, May 1982.

25. E.g., U. P. Sukhatme, Phys. Rev. Lett. 38, 124 (1977).

26. W. Bartel et al., Nucl. Phys. B58, 429 (1973).

27. T. T. Chou and C. N. Yang, preprint "Dip Movement in $p\bar{p}$ and pp Elastic Collisions", (1981).

28. L. A. Fajardo et al., Phys. Rev. D24, 46 (1981).

29. N. Khuri and T. Kinoshita, Phys. Rev. 137B, 720 (1965).

30. W. F. Baker et al., Phys. Rev. Lett. 47, 24 (1981).

31. R. de L. Krönig and H. A. Kramers, Z. Phys. 48, 174 (1928). For a modern proof in the context of quantum field theory, see M. Goldberger, in Relations de Dispersion et Particules Elementaires (10th Les Houche Conf.), 1960.

32. L. Backsay et al., Nucl. Phys. B141, 1 (1978).

33. J. B. Bronzan, G. L. Kane and U. P. Sukhatme, Phys. Lett. 49B, 3 (1974).

34. Hannu Miettenen, Proc. 19th Recontre de Moriond, Méribel-les-Allues, 1974.

35. S. Y. Lo, Nucl. Phys. B19, 286 (1970).

36. D. J. Clarke and S. Y. Lo, Univ. of Melbourne preprint (1979).

37. L. Van Hove, Nuovo Cimento 28, 798 (1963).

38. Hannu Miettenen, Proc. 19th Recontre de Moriond, Méribel-les-Allues, 1974.

39. E. Predazzi, "A Review of High Energy Strong Interaction Physics", lecture delived at Basko Polje Summer School (1975).

40. E. H. Groot and H. I. Miettinen, Proc. 18th Recontre de Moriond, Méribel-les-Allues, 1973, Vol. II, p. 193.

41. W. Grein, R. Guigas and P. Kroll, Nucl. Phys. B89, 93 (1975).

42. U. Amaldi and K. R. Schubert, Nucl. Phys. B166, 301 (1980).

43. D. S. Ayres et al., Phys. Rev. D14, 3092 (1976).

44. I. V. Andreev and I. M. Dremin, Sov. J. Nucl. Phys. 8, 473 (1969).

45. M. T. Nazirov and A. V. Chernov, Sov. J. Nucl. Phys. 31, 6 (1980).

46. F. Zachariesen, Phys. Reports 2C (1971).

47. J. Dias de Deus, Nucl. Phys. B59, 231 (1973).

48. A. J. Buras and J. Dias de Deus, Nucl. Phys. B71, 481 (1974).

49. Clark De Haven, Jr., Ph.D. thesis, Univ. of Michigan (1978), unpublished.

50. J. Dias de Deus, Nuovo Cimento. 28A, 1 (1975).

51. J. Dias de Deus and P. Kroll, Acta Phys. Pol. B9-2 (1978).

52. P. Kroll, Univ. of Wuppertal preprint, March 1982.

53. V. Barger, J. Luthe and R. Phillips, Nucl. Phys. B88, 237 (1975).

54. J. Dias de Deus, "Things to Come in Strong Interactions at Very High Energies", talk at Ronda, Spain, 1980.

55. W. Grein, Nucl. Phys. B131, 255 (1977).

56. R. J. Glauber, Phys. Rev. 100, 252 (1955).

57. E. Schrauner, L. Benofy and D. W. Cho, Phys. Rev. 177, 5 (1969).

58. D. R. Harrington and A. Pagnamenta, Phys. Rev. 173, 1599 (1968) and A. Pagnamenta, Wayne State Univ. Conference, June 1969. Many of the quantitative conclusions of these references should be viewed with caution.

59. S. Wakaizumi, Prog. Theor. Phys. 42, 4 (1969).

60. A. Schiz et al., Phys. Rev. D24, 26 (1981).

61. E. M. Levin and V. M. Shekter, undecipherable source Russian preprint #442, October 1978.

62. A. Bialis et al., Acta Phys. Pol. B8, 10 (1977).

63. W. Slominski and M. Zielinski, Acta Phys. Pol. B9, 10 (1978).

64. L. Van Hove and K. Fialkowski, Nucl. Phys. B107, 211 (1976).

65. Seiichi Wakaizumi, Prog. Theor. Phys. 60, 4, 1040 (1978).

66. S. Wakaizumi, Phys. Lett. 70B, (1977), last paragraph.

67. J. L. Hartmann et al., Phys. Rev. Lett. 39, 975 (1977).

68. H. De Kerret et al., Phys. Lett. 62B, 363 (1976); 68B, 374 (1977)

69. Seiichi Wakaizumi, Hiroshima Univ. preprint, March 1982.

70. See, e.g., R. P. Feynman, M. Kisslinger and F. Ravndahl, Phys. Rev. D3, 2706 (1971).

71. K. Fujimura, T. Kobayashi and M. Namiki, Prog. Theor. Phys. 43, 1, 73 (1970).

72. S. B. Goloskokov et al., Sov. J. Nucl. Phys. 33, 5, 722 (1981).

73. S. P. Kuleshov et al., Dubna preprint (1981).

74. See, e.g., O. Köfoed-Hansen, Nuovo Cimento LXA, 4, 621 (1969).

75. W. C. Thacker, Phys. Rev. D3, 2774 (1971).

76. Jay Orear, Phys. Rev. D18, 2484 (1978).

77. G. W. Heines and M. M. Islam, Nuovo Cimento 61A, 3, 149 (1981).

78. R. P. Feynman, R. D. Field and G. C. Fox, Nucl. Phys. B128, 1 (1977).

79. John B. Kogut and Leonard Susskind, Phys. Reports 8, 75 (1973).

80. See, e.g., A. Chodos et al., Phys. Rev. 10, 2599 (1974).

81. G. E. Brown and M. Rho, Phys. Lett. 82B, 2 (1979).

82. G. C. Callan, Jr., R. F. Dashen and D. J. Gross, Phys. Rev. D19, 1826 (1979).

83. M. M. Islam, Lett. Nuovo Cimento 14, 627 (1955).

84. T. Gerrity and A. Pagnamenta, Univ. of Illinois at Chicago Circle preprint (1977).

85. M. Miettinen and G. Thomas, Nucl. Phys. B166, 365 (1980).

86. N. P. Zotov et al., Sov. J. Particles and Nuclei 11, 5, 462 (1980).

87. M. Zralek et al., Phys. Rev. D19, 820 (1979).

88. M. Ida and R. Kobayashi, Prog. Theor. Phys. 36, 846 (1966).

89. D. B. Lichtenberg, L. J. Tassie, P. J. Keleman, Phys. Rev. 167, 1535 (1968).

90. R.P. Feynman, Photon-Hadron Interactions (Benjamin, New York, 1972).

91. J. F. Gunion and D. E. Soper, Phys. Lett. 73B, 189 (1978).

92. Z. Dziembowski, W. J. Metzger, R. T. Van de Walle, Z. Phys. C 10, 231 (1981).

93. D. B. Lichtenberg, W.Namgung, E. Predazzi, and J. G. Wills, Phys. Rev. Lett. 48, 24 (1982).

94. S. D. Drell, H. Quinn, and M. Weinstein, SLAC report mentioned in Ref. 92 (to be published).

95. R. D. Carlitz and B. D. Creamer, Phys. Lett. 84B, 215 (1979).

96. R. D. Carlitz, S. D. Ellis, and R. Savit, Phys. Lett. 68B, 443 (1977).

97. R. Shanker and C. S. Warke, Z. Phys. C 6, 17 (1980).

98. J. Ribeiro, Z. Phys. C 5, 27 (1980).

99. J. Orr and A. L. Read, "Meson Laboratory Design Report", Fermi National Accel. Lab. (1971).

100. K. Krueger, Ph.D. thesis, Univ. of Arizona (expected 1983).

101. D. H. Kaplan et al., Phys. Rev. D26, 723 (1982).

102. P. Cornillon et al., Phys. Rev. Lett. 30, 403 (1973).

103. D. D. Yovanovitch et al., Nucl. Inst. and Methods 94, 477 (1971).

104. J. Litt and R. Mennier, Ann. Rev. Nucl. Sci. 23, 9 (1979).

105. M. Benot et al., Nucl. Inst. Meth. 105, 431 (1972).

106. J. Allaby et al., Phys. Lett. 34B, 431 (1971).

107. J. Orear, private communication.

108. J. Allaby et al., Phys. Lett. 34B, 431 (1971).

109. R. Galik, Ph.D. thesis, Cornell University (1977).

110. J. Vrieslander, Ph.D. thesis, Cornell University (1981), results published in Ref. 16.

111. R. Bouchlier et al., Nucl. Inst. Meth. 88, 149 (1970).

112. S. McHugh, Ph.D. thesis, University of California, San Diego (expected 1983).

113. Particle Data Group, Rev. Mod. Phys. 52, 2 (1972).

114. G. Alberi and G. Gaggi, Phys. Reports C74, 1 (1981).

115. W. Faissler et al., Phys. Rev. D23, 33 (1981).

116. G. Fidecaro et al., Phys. Lett. 105B, 4 (1981).

117. Tom Fearnley, contribution to the XVIIIth Recontre de Moriond on Antiproton-Proton Physics, LaPlagne, France, 1983.